DISSERTATION

Submitted to the

Combined Faculties for the Natural Sciences and for Mathematics

of the Ruperto-Carola University of Heidelberg, Germany

for the degree of

Doctor of Natural Sciences

presented by

Diplom-Molekularmedizinerin Julia Caroline Wolanski

Born in Kassel, Germany

Oral-examination: 22.09.2017

Regulatory Functions of the DAP Kinase Family in Antiviral RIG-I Signalling

Referees:

Prof. Dr. Ralf Bartenschlager

Prof. Dr. Alexander Dalpke

The applicant, Julia Caroline Wolanski, declares that she is the sole author of the submitted dissertation and no other sources or help from those specifically referred to have been used. Additionally, the applicant declares that she has not applied for permission to enter an examination procedure at any other institution and that this dissertation has not been presented to any other faculty and has not been used in its current or in any other form in another examination.

.....	.....
Date	Signature

Ich kann mir kein seligeres Wissen denken,
als dieses Eine:
dass man ein Beginner werden muss.
Einer der das erste Wort schreibt hinter einen
jahrhundertelangen
Gedankenstrich.

- Rainer Maria Rilke

Acknowledgements

The first big Thank You goes to my supervisor, Dr. Marco Binder, for accepting me as the second PhD student in his back then newly-established group and for giving me the opportunity to work on my project. I appreciate the help and discussions, especially towards the end, and I am glad to have worked in your lab which you made sure provided a very pleasant environment for every group member.

Furthermore, I would like to thank Prof. Dr. Ralf Bartenschlager for discussions and suggestions in the Friday seminar and for being my first referee and member of my thesis advisory committee.

I would also like to thank Prof. Dr. Alexander Dalpke for being my second referee and thesis advisory committee member. I really benefited from your input to the discussions during the thesis advisory committee meetings.

Furthermore, I would like to thank Dr. Ann-Kristin Müller for being my third thesis advisory committee member and her contributions to discussions. I would also like to thank her and Dr. Annika Guse for being part of my defence committee.

Another big Thank You goes to Pascal, Antje, Shariq, and Jan for proofreading the different parts of this dissertation. Thank you, Pascal and Antje, for fruitful discussions and your advice throughout the course of my project.

I would like to point out that I would not have been able to complete this dissertation without the help of my fellow lab members. Thank you, Joschka, for great scientific discussions on the project and for helping me with your expertise. Thank you, Jamie, Sandra, Christopher, and Aparna for being not only amazing colleagues, but also friends. It was a lot of fun working with you guys, as well as spending time outside of the lab. Thanks for making my PhD such an enjoyable one.

Moreover, I would like to thank every member of F170 who I got to work with in the IIC and everyone in the molecular virology unit for generating such an excellent working atmosphere, for the coffee breaks, birthday cakes, and for all other social activities.

I am extremely grateful for the support I received from my friends during the four years I worked on my PhD thesis. Thank you for your time, your energy, for the awesome parties, all the laughter, for everything.

Zuletzt möchte ich mich bei meiner Familie bedanken. Ihr seid immer für mich da und ihr steht mir in jeder Lebenslage bei. Ihr ermuntert mich, meinen eigenen Weg zu gehen.
Danke.

Summary

Cytosolic recognition of viral replication intermediates by RIG-I, the founding member of the RIG-I-like receptor (RLR) family, initiates a signalling cascade which culminates in the activation of latent transcription factors IRF3 and IRF7, inducing the expression of type I and type III interferons (IFNs) and interferon-stimulated genes (ISGs). These work in concert to combat viral infection. Thus, regulation of RIG-I activity is crucial in mounting a balanced antiviral response strong enough to ward off infection, but strictly transient in order to avoid tissue damage. Initially, death-associated protein kinases (DAPKs) were described as initiators of cell death. Since then, they have been found to mediate a variety of cellular processes, such as cell growth and survival, cytoskeletal remodelling and inflammatory responses, but had not been linked to the regulation of innate antiviral signalling.

We identified death-associated protein kinase 1 (DAPK1) as a negative feedback-regulator of RIG-I activity. The present study confirms that a minimal DAPK1 construct, DAPK1^{KCA}, comprising only the kinase, calmodulin (CaM)-binding and Ankyrin repeats domains, inhibits RIG-I in a kinase-dependent manner. DAPK1^{KCA} harbours residues targeted by growth factor signalling-related kinases. We could demonstrate, however, that inhibition of RIG-I signalling mediated by DAPK1 happened independently of its role in growth factor signalling. Nevertheless, DAPK1 expression was strongly influenced by cell growth and division.

Since the kinase domains of the different DAPKs are homologous and share some substrate specificity, we investigated if, in addition to DAPK1, other DAPK family members would interfere with RIG-I signalling. Upon over-expression, all DAPK family members inhibited RIG-I signalling, except DRAK2 which, in our hands, was kinase-inactive. Reciprocally, siRNA-mediated knockdown of DAPK1 and DAPK3 resulted in increased antiviral signalling activity. Moreover, silencing of DAPK1 and DAPK3 reduced the replication of two different RNA viruses, emphasizing the physiological relevance of these kinases in the regulation of RIG-I signalling.

Similar to what was observed for DAPK1, we found DAPK2 to inhibit RIG-I signalling in a kinase activity-dependent fashion. Moreover, the kinase domain of DAPK3 alone inhibited RIG-I signalling. While all DAPK family members phosphorylated RIG-I *in vitro*, interaction with RIG-I could only be shown for DAPK1 and DAPK2. Although we found DAPKs to physically interact with each other, we observed no interdependence of the kinases regarding their inhibitory function in RIG-I signalling. In order to further study DAPK functions in RIG-I signalling, we created single and combined knockout cell lines for DAPK1, DAPK2, and DAPK3. However, there was no change in the antiviral response in these cells, possibly due to up-regulation of other proteins compensating for loss of the DAPKs.

We observed that inhibition of RIG-I signalling by DAPKs happened independently of their well-studied role in apoptotic as well as autophagic cell death induction. In fact, we did not detect any induction of autophagy upon DAPK expression.

Ultimately, we discovered that regulation of antiviral signalling by DAPKs is not limited to an inhibition of RIG-I, but that they also inhibited MDA5-mediated signalling. Moreover, we found evidence that DAPKs additionally inhibit antiviral signalling at the level or downstream of IRF3-mediated gene transcription.

In summary, the present study identifies a conserved role for DAPKs in the regulation of antiviral RLR signalling independent of known DAPK functions in cell death and survival.

Zusammenfassung

Die Erkennung von viralen Replikationsintermediaten durch das zytosolische Rezeptorprotein RIG-I löst eine Signalkaskade aus, die in der Aktivierung der Transkriptionsfaktoren IRF3 und IRF7 mündet und damit die Expression von Typ I- und Typ III-Interferonen sowie von Interferon-stimulierten Genen (ISGs) auslöst. RIG-I ist namensgebend für die Familie der RIG-I-like Rezeptoren (RLRs). Interferone und ISGs tragen grundlegend zur Bekämpfung von Virusinfektionen bei. Deshalb ist es besonders wichtig, dass RIG-I kontrolliert aktiviert wird, sodass die antivirale Antwort stark genug ist, um eine Infektion zu bekämpfen, aber nicht ausufert und damit Gewebeschäden verursacht. Death-associated protein kinases (DAPKs) wurden initial lediglich als Verursacher von Zelltod beschrieben. Inzwischen ist bekannt, dass sie verschiedene zelluläre Prozesse wie Wachstum, Überleben, Umbau des Zytoskeletts und Entzündungsreaktionen beeinflussen. Dennoch wurden die Kinasen bisher nicht im Zusammenhang mit der antiviralen angeborenen Immunantwort untersucht.

Unsere Gruppe identifizierte death-associated protein kinase 1 (DAPK1) als Teil eines negativen Rückkopplungsmechanismus, welcher in einer Hemmung von RIG-I resultiert. Innerhalb der vorliegenden Dissertation wurde bestätigt, dass ein kleinstmögliches DAPK1-Konstrukt, $DAPK1^{KCA}$, bestehend aus der Kinase-, der Calmodulin-Binde- und der Ankyrin-Repeats-Domäne, RIG-I Kinase-abhängig inhibiert. $DAPK1^{KCA}$ enthält Aminosäurereste, die von Kinasen des Wachstumsfaktor-aktivierten Signalwegs phosphoryliert werden, welches die Aktivität von DAPK1 beeinflusst. Dennoch konnten wir zeigen, dass DAPK1 den RIG-I-Signalweg unabhängig von seiner Funktion im Wachstumsfaktor-aktivierten Signalweg beeinflusst.

Da die Kinasedomänen der DAPKs eine ausgeprägte Homologie aufweisen und die Kinasen zum Teil ähnliche Proteinsubstrate phosphorylieren, wurde untersucht, ob, zusätzlich zu DAPK1, noch andere Mitglieder der DAPK Kinasefamilie den RIG-I-Signalweg hemmen. Tatsächlich wurde dieser durch Überexpression alle Mitglieder der Kinasefamilie inhibiert. Umgekehrt war die Aktivität des RIG-I-Signalwegs erhöht, wenn die Expression von DAPK1 und DAPK3 durch siRNA-Transfektion vermindert wurde. Dies resultierte außerdem in einer niedrigeren Replikationsrate zweier RNA-Viren wodurch die physiologische Relevanz der DAPKs in der Regulation des RIG-I-Signalwegs bestätigt werden konnte.

Ähnlich wie im Falle von DAPK1 inhibierte DAPK2 den RIG-I-Signalweg abhängig von seiner Kinaseaktivität. Außerdem konnten wir beobachten, dass alleinige Überexpression der Kinasedomäne von DAPK3 ausreichte, um den RIG-I-Signalweg zu inhibieren. Obwohl alle DAPKs RIG-I *in vitro* phosphorylierten, konnten wir eine Interaktion mit demselbigen nur für DAPK1 und DAPK2 zeigen. Wir stellten zwar fest, dass die DAPKs einander binden, konnten aber bezüglich der Hemmung des RIG-I-Signalwegs keine gegenseitige Abhängigkeit der Kinasen untereinander feststellen. Um die Funktion der DAPKs in der antiviralen Immunantwort weiter untersuchen zu können, generierten wir Einzel- sowie kombinierte Knockout-Zelllinien für DAPK1, DAPK2 und DAPK3, konnten in diesen aber keine Änderung in Bezug auf die antivirale Immunantwort beobachten. Der Grund hierfür könnte eine kompensatorische Heraufregulation eines anderen Proteins sein, welches im Falle des Verlusts der Kinasen ihre Funktion übernimmt.

Unsere Ergebnisse zeigen, dass die DAPK-abhängige Inhibition des RIG-I-Signalwegs unabhängig von den bisher beschriebenen Funktionen der DAPKs als Zelltod-Initiatoren geschieht. Tatsächlich konnten wir nach Überexpression der DAPKs keine vermehrte Induktion von Autophagie feststellen.

Schlussendlich zeigen unsere Beobachtungen, dass die DAPKs nicht die RIG-I- sondern auch die MDA5-abhängige Signalantwort hemmen. Zudem inhibierten die DAPKs die antivirale Signalantwort auf der Ebene der Aktivierung von IRF3 und/oder der IRF3-abhängigen Gentranskription.

Zusammenfassend beschreibt die vorliegende Dissertation eine konservierte Funktion der DAPKs als Regulatoren der antiviralen RLR-abhängigen Immunantwort. Dies geschieht dabei unabhängig von der DAPK-abhängigen Regulation von Zelltod und –überleben.

Table of Contents

Figures

Tables

Protocols

Abbreviations

µ	micro
µM	micromolar
^{32}P	Phosphorus 32 (radioisotope)
A	Alanine
AIM2	Absent in melanoma 2
AMP	Ampicillin
ATF	Cyclic AMP-dependent transcription factor
ATG	Autophagy-related protein
ATP	Adenosine triphosphate
Bak	Bcl-2 homologous antagonist/killer
BAX	Bcl-2 associated X protein
Bcl	B cell lymphoma
bp	Base pairs
CaM	Calmodulin
CANX	Calnexin
CARD	Caspase-activation and recruitment domain
CBP	CREB-binding protein
cdc14A	cell division cycle 14A
cGAS	Cyclic GMP-AMP synthase
CHIP	Carboxyl terminus of HSC70-interacting protein
cIAP	Cellular inhibitor of apoptosis
CID	Central-interacting domain
CK2	Casein kinase II
c-PARP	Cleaved PARP
CTD	C-terminal domain
D	Aspartic acid
Da	Dalton
DAI	DNA-dependent activator or IRFs
DAPK	Death-associated protein kinase
DC	Dendritic cell
dd	double distilled
DD	Death domain
DI	Defective-interfering
DKO	double knockout
DNA	Deoxyribonucleic acid
DRAK	DAPK-related apoptosis inducing kinase
dsRNA	Double-stranded RNA
E	Glutamic acid
EGF	Epidermal growth factor
EGFR	Epithelial growth factor receptor
eIF2α	Eukaryotic translation initiation factor 2 α
EMCV	Encephalomyocarditis virus
EST	expressed sequence tag
FF	Firefly (luciferase)
FluA(V)	Influenza A (virus)
FLuc	Firefly luciferase
GAPDH	Glycerinaldehyde-3-phosphate dehydrogenase
Genta	Gentamicin
HA	Hemagglutinin
HBV	Hepatitis B virus
HCV	Hepatitis C virus
HIV	Human immunodeficiency virus
HSP	Heat Shock Protein
HSV	Herpes simplex virus
IFI16	Interferon-γ-inducible protein 16
IFIT1	Interferon-induced protein with tetratricopeptide repeats 1
IFLR	Interferon lambda receptor
IFN	Interferon
IFNAR	Interferon alpha receptor
IKK	Inhibitor of nuclear factor κ–B kinase
IL	Interleukin
IL10R2	Interleukin 10 receptor chain 2
IRF	Interferon-regulatory factor
ISG	Interferon-stimulated gene
ISGF3	Interferon-stimulated gene factor 3
ISRE	Interferon-stimulated response element
IκBα	Inhibitor of NFκB α
Jak	Janus kinase
k	kilo
K	Lysine
Kana	Kanamycin
kb	kilobases
KCA	Kinase-CaM-Ank
KLHL20	Kelch-like protein 20
KO	Knockout
KSHV	Kaposi's sarcoma-associated herpesvirus
LGP2	Laboratory of genetics and physiology 2
Luc	Luciferase
m	milli

MAM	Mitochondria-associated membrane
MAP1LC3B	Microtubule-associated protein 1 light chain 3 B
MAPK1/ERK	Mitogen-activated protein kinase 1
MARCH5	Membrane-associated RING finger protein 5
MAVS	Mitochondrial antiviral signalling
MBL	Mannose-binding lectin
MDA5	Melanoma-differentiation associated protein 5
MIB1	Mindbomb 1
MLC	Myosin light chain
MLCK	Myosin light chain kinase
mM	millimolar
MOI	Multiplicity of infection
mRNA	Messenger RNA
mTORc1	Mammalian target of rapamycin complex 1
Mx	Myxovirus resistance protein
NEMO	NFκB essential modifier
NFκB	Nuclear factor κ B
NK cell	Natural killer cell
NLR	NOD-like receptor
NLS	Nuclear localisation signal
NS	Non-structural
OAS	Oligoadenylate synthase
p-	phospho-
p.i.	post infection
PAMP	Pathogen-associated molecular pattern
Par4	pro-apoptotic PRKC apoptosis WT1 regulator protein
PARP	Poly(ADP-ribose) polymerase
PCR	Polymerase chain reaction
PE	Phosphatidylethanolamine
PFA	Paraformaldehyde
PI3P	Phosphatidylinositol 3-phosphate
PI4Kα	Phosphatidylinositol 4 kinase α
Pin1	Peptidyl-prolyl cis/trans isomerase NIMA-interacting 1
PKC	Protein kinase C
PKD	Protein kinase D
PKR	Protein kinase R
PLK1	Polo-like kinase 1
Poly(I:C)	Polyinosinic:polycytidylic acid
PP1/2	Phospho-protein phosphatase 1/2
PRR	Pattern recognition receptor
PTM	Post-translational modification
qPCR	Quantitative Real-time PCR
Ren	Renilla (luciferase)
RIG-I	Retinoic acid-inducible gene I
RIG-I CA	RIG-I CARD domains
RIOK3	Rio kinase 3
RLR	RIG-I-like receptor
Rluc	Renilla luciferase
RNA	Ribonucleic acid
RoV	Rotavirus
RSK/p90S6K	Ribosomal S6 kinase
RVFV	Rift Valley Fever virus
S	Serine
SARS CoV	SARS-associated coronavirus
SeV	Sendai virus
sgRNA	Small guide RNA
siRNA	Small interfering RNA
Spec	Spectinomycin
ssRNA	Single-stranded RNA
STAT	Signal transducers and activators
stim	stimulated
STING	Stimulator of interferon gene
STK	Serine threonine kinase
strep-	Strep-Tag® used for Strep-Tactin purifcation
T	Threonine
TBK1	TANK-binding kinase 1
TFIIH	Transcription factor II H
TGF	Transforming growth factor
TLR	Toll-like receptor
TRAF	TNF receptor associated factor
TRAIL	Tumor necrosis factor ligand superfamily member 10
TRIM	Tripartite motif-containing protein
TSC	Tuberous sclerosis
unstim	unstimulated
USP18	Ubl carboxyl-terminal hydrolase 18
VPS	Vacuolar protein sorting
WNV	West Nile virus
ZIPK	Zipper-interacting kinase

1 Introduction

Every higher organism has to fight infections on a daily basis. In order to prevent disease, the immune system (lat. "*immunis*", "unspoilt" or "pure") has evolved, a combination of different mechanisms and processes acting in concert to fight pathogens. In mammals the immune system consists of two major parts, the innate and the adaptive immune system. These two components are tightly interconnected, working together in preventing infection.

This study deals with an important part of innate immunity, the RIG-I signalling pathway and how it is activated and modulated in response to viral infections. Further introduction is, therefore, mainly focused on composition and function of the innate immune system.

1.1 The innate immune system

As a first line of defence against invading pathogens, the innate immune system takes action which is usually very fast (activation takes place within seconds to minutes). There are several mechanisms which ward off infection. First in line are physical barriers, e.g. epithelial layers, which separate the outside from the inside of an organism. Furthermore, these barriers are often covered in mucus (e.g. epithelial layers of the respiratory or the digestive tract) or secrete fluids (e.g. tear ducts) which not only make it difficult for pathogens to attach, but also often contain antimicrobial substances (such as lysozyme in tear fluid) which help to kill or attenuate pathogens even before they might invade a cell. Pathogens which manage to defy cellular barriers are recognised upon entering cells or interstitial space. In the blood stream, the complement system acts as an important part of innate immunity in that it "complements" other anti-microbial mechanisms, marking infiltrating microbes for destruction by phagocytic cells which are also part of the innate immune system. A successful mechanism of recognising basic microbial structures as foreign is the recognition by so-called "pattern recognition receptors" (PRRs). PRRs recognise "pathogen-associated molecular patterns" (PAMPs), such as parts of bacterial or fungal cell walls or nucleic acids from genomes of incoming viruses. Activated PRRs trigger an innate immune response which ultimately results in the secretion of soluble factors. These induce an anti-microbial state not only in the infected, but also in neighbouring cells, thereby preventing spread of infections. Moreover, soluble factors will attract specialised cells of the innate immune system whose activation will, eventually, prime adaptive immunity.

Although it requires up to several weeks to be fully efficient, only the adaptive immune system allows recognition of a multitude of microbial structures much more complicated

than regular PAMPs. These will be recognised not only as antigens by B-cell secreted antibodies, but also as peptides recognised by T-cell receptors. Also, initiation of an adaptive immune response results in formation of an immunologic memory as it gives rise to long-lived memory lymphocytes crucial for permanent immunity to certain pathogens. This is the working principle of vaccines. Without adequate priming by innate immunity, no effective adaptive immune response will be generated. The innate immune response as a first line of defence is, therefore, crucial for proper establishment of long-term immunity.

1.1.1 Specialised cells of the innate immune system

All cells of the immune system originate from precursor cells in the bone marrow, pluripotent hematopoietic stem cells. Early in their differentiation, these cells give rise to two distinct lineages, the lymphoid and the myeloid lineage. An overview of all immune cell types and their origin is shown in figure 1. Most specialised cells of the innate immune system belong to the myeloid lineage and originate from a common myeloid progenitor cell. These progenitors not only give rise to blood-building cells like megakaryocytes or erythroblasts, but also granulocytes, mast cells, monocytes, and dendritic cells. Granulocytes are, based on staining properties of the granules to which they owe their name, divided into neutrophils, eosinophils, and basophils. These have distinct functions such as phagocytosis of invading pathogens and killing of parasites too large to endocytose. Mast cells are potent inducers of inflammatory responses which are thought to have originally developed to fight helminthic infections, but were found to be especially important in the context of allergic reactions. Monocytes cycle the blood and mature into macrophages. These phagocytic, tissue-resident cells not only take up microbes, but also engulf dead cells and cellular debris. Moreover, activated macrophages will recruit other specialised immune cells by cytokine secretion. Another tissue-resident type of phagocytic cells are dendritic cells (DCs). Phagocytosed microbial components are presented on the surface of DCs, making them the most prevalent form of antigen-presenting cells essential for the maturation of T lymphocytes.

Interestingly, natural killer (NK) cells, another important cell type of the innate immune system, originate from the lymphoid lineage. These cells recognise abnormal cells such as tumour cells or virus-infected cells. Upon recognition, NK cells will release contents of their cytoplasmic granules (e.g. perforin and granzymes) leading to target cell lysis.

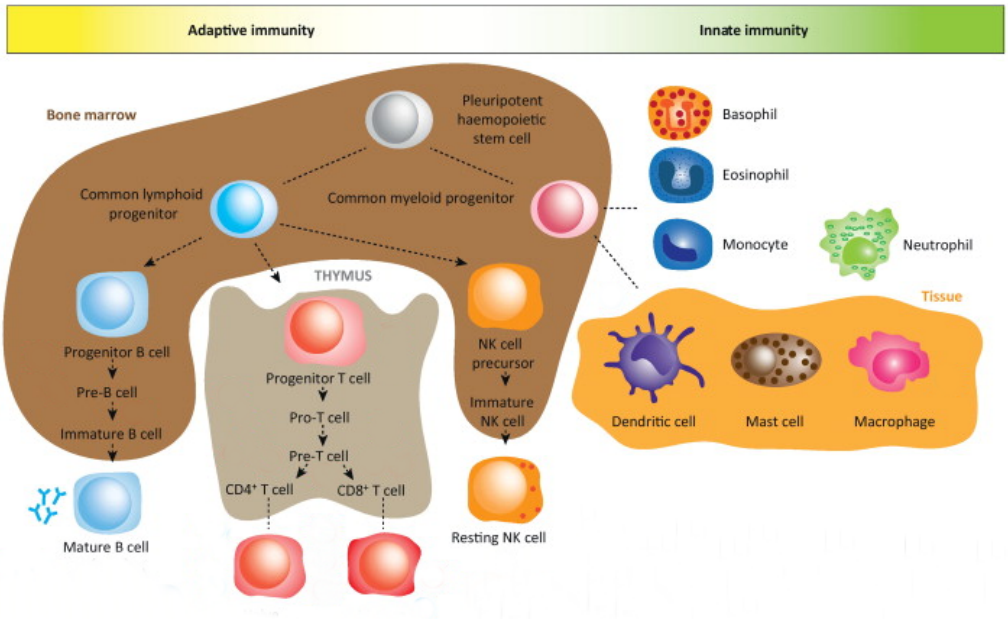

Figure 1 **Overview of cell types of adaptive and innate immunity**

All immune cells originate from a common precursor in the bone marrow. Whereas B- and T-cells, the major effectors of adaptive immunity, stem from a common lymphoid progenitor, most cells of the innate immune system belong to the myeloid lineage. Natural killer (NK) cells are effectors of innate immunity, based on their invariant receptors, but develop along the lymphoid lineage. Adapted from [1].

1.1.2 Pattern recognition receptors

As mentioned above, pattern recognition receptors (PRRs) recognise conserved molecular structures, so-called PAMPs. PAMPs are found in a variety of pathogens but do not occur in the host. Therefore, they can be identified as foreign and potentially harmful. As pathogens present a diversity of structures, different classes of PRRs have evolved. They recognise microbial proteins, peptidoglycans, protein-lipid structures, and nucleic acids, respectively. A common feature of PRRs is the activation of a signalling cascade which, ultimately, establishes an anti-microbial state in the infected cell and results in the secretion of soluble factors such as interferons, cytokines and chemokines. On top of activating a paracrine immune response in surrounding cells, these factors also attract phagocytes and, eventually, cells which are necessary for the initiation of adaptive immunity.

A class of PRRs which recognise carbohydrate residues on microbial surfaces are lectins, more specifically mannose-binding lectin (MBL) and calcium-dependent (C-type) lectins. MBL binds mannose and fucose residues only when they are presented in a defined spatial orientation, e.g. on bacterial surfaces, thereby marking pathogens for phagocytosis. C-type lectins expressed on antigen-presenting cells comprise a large group of different receptors. They recognise a variety of glycan structures which, again, stimulates phagocytosis of the pathogen. However, viruses may exploit binding to these

receptors, as in the case of HIV-1 which interacts with C-type lectin DC-SIGN, promoting infection and spread among T-cells [2].

Toll-like receptors (TLRs) are trans-membrane PRRs located either on cell surfaces or in endosomal compartments. In humans 10 different TLRs have been identified of which TLR1/TLR2, TLR2/TLR6 (both signal as heterodimers), TLR4 and -5 recognise bacterial PAMPs, such as flagellin for TLR5. TLR3, -7, -8, and -9 recognise foreign, often viral, nucleic acids, more specifically single stranded RNA (ssRNA), double stranded RNA (dsRNA), and unmethylated CpG DNA.

In addition to these free or membrane bound receptors, there are a number of cytosolic PRRs.

NOD-like receptors (NLRs) are cytosolic PRRs which bind bacterial proteoglycans. To date, 23 NLRs are known which are categorised based on their domain structure. Signalling initiated by NLRs results in the activation of pro-inflammatory genes (through inflammasome activation [3]) and cytokines. Inept activation of NLRs, however, may result in excessive inflammation causing tissue damage such as in inflammatory bowel disease [4].

In addition to cytosolic PRRs which sense bacterial or fungal surface components, there are also sensors recognising foreign nucleic acids, especially those stemming from viral genomes and replication intermediates [5].

As DNA is only located in the nucleus and in mitochondria of healthy mammalian cells, cytosolic DNA activates sensors such as Absent in melanoma 2 (AIM2), DNA-dependent activator of IRFs (DAI), and cyclic GMP-AMP synthase (cGAS). While AIM2, similar to NLRs, activates an inflammatory response [6], DAI and cGAS will, via the adaptor molecule Stimulator of interferon gene (STING), engage signalling cascades culminating in an activation of interferon signalling and expression of interferon-stimulated genes (ISGs) [7]–[9]. Interestingly, with interferon-γ-inducible protein 16 (IFI16), a sensor of dsDNA was discovered which can be localised both in the cytosol and in the nucleus, where it acts as a sensor of viral DNA, such as in case of herpesviruses [10], [11]. It is, therefore, unlikely that differentiation between host and viral DNA is based solely on spatial separation.

1.1.3 RIG-I-like receptors

The family of RIG-I-like receptors (RLRs) consists of three members: retinoic acid-inducible gene I (RIG-I, also called DDX58), melanoma-differentiation associated protein 5 (MDA5, also called IFIH1) and laboratory of genetics and physiology 2 (LGP2, also called DHX58). RLRs sense viral RNAs in the cytoplasm and are expressed in most cell types.

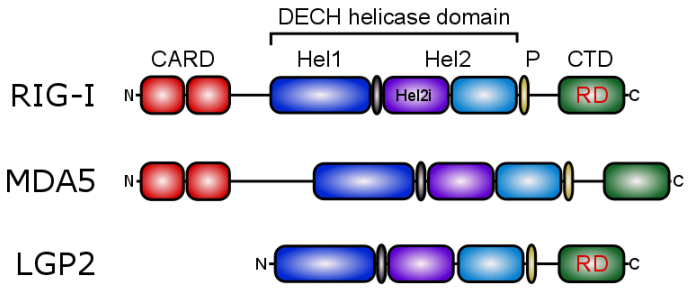

Figure 2 **Overview of the RIG-I-like receptor family domain structure**

All RLRs comprise a central DECH helicase domain consisting of two tandem helicase domains (Hel1 and Hel2) and an interspersed helicase insertion domain (Hel2i). Furthermore, they contain a pincer domain (P) and a C-terminal domain (CTD). Unlike RIG-I and MDA5, LGP2 does not contain the N-terminal tandem caspase activation and recruitment domains (CARD). The repressor domains (RD) in the CTD of RIG-I and LGP2 may interact. In an inactive state RIG-I RD interacts with its CARDs, masking them from other interaction partners.

As they contain a central DECH helicase domain (figure 2), RLRs are grouped into the DExD/H helicase family (superfamily 2). All RLRs contain a pincer domain which not only connects helicase domain 2 to the C-terminal domain (CTD), but also stabilises the ATPase core of the helicase domain, thereby regulating enzymatic activity [12]. The CTD contributes to substrate specificity of RLRs. RIG-I and MDA5 contain two N-terminal tandem caspase activation and recruitment (CARD) domains necessary for signal transmission. RLR CARDs interact with and activate mitochondrial antiviral signalling (MAVS, also called IPS-1, Cardif or VISA). This interaction takes place after activation of RIG-I and MDA5 by recognition of their ligands, different species of dsRNA. It results in the expression of type I and III interferons (IFNs), some ISGs, and, to a smaller extent, pro-inflammatory cytokines and chemokines. Since LGP2 does not harbour CARD domains it cannot initiate downstream signalling and is, therefore, thought to modulate RIG-I and MDA5 function [13], [14].

RLRs are essential for the recognition of intracellular viral replication. Their activation is crucial for the establishment of an antiviral response in infected and surrounding cells.

1.1.3.1 Structure and substrate specificity of RIG-I

RIG-I is the founding member of the RLR receptor family. It was initially described to be activated by the presence of dsRNA in the cytoplasm, triggering IFN expression by signalling through its tandem CARD domains [15]. Since then, intensive research on the mechanism of substrate recognition by RIG-I has revealed that it is particularly well activated by 5'-triphosphorylated dsRNAs [16]–[18], which were shown to be natural ligands of RIG-I in viral infection, for instance in influenza A virus (FluAV) infection [19]. RIG-I was also found to be essential for the recognition of RNA viruses belonging to the family of *paramyxoviridae* and *flaviviridae* such as Japanese encephalitis virus [20]. Although it was first proposed that RIG-I relies on a 5'-triphosphate for substrate recognition and mostly recognises short (< 25 bp) dsRNA, it was later shown that, depending on substrate length, RIG-I will also bind long (> 200 bp) dsRNA independently of the presence of the 5'-triphosphate moiety [21], [22]. Furthermore, 5'-diphosphorylated RNAs, which are generated in reovirus infection, were found to potently activate RIG-I [23], further challenging the view that RIG-I relies on a 5'-triphosphate for substrate binding. Upon substrate recognition, RIG-I will oligomerise along RNA strands, a process which has been shown to be ATP-dependent [24]. Recently, this ATP-dependency was shown to be a mechanism of discrimination between self and non-self RNA structures [25].

Substrate binding by RIG-I is mediated through its CTD which was shown to interact with dsRNA 5'-triphosphates [26]. Interestingly, the groove in which this binding happens is distinct in LGP2 and MDA5 which suggests it confers some degree of substrate specificity. Binding of RNA promotes a conformational change of RIG-I which exposes its CARD domains and enables interaction with downstream signalling adaptor MAVS.

1.1.3.2 Structure and substrate specificity of MDA5

The domain structure of MDA5 is similar to that of RIG-I with 23% amino acid sequence homology in the CARD and 35% sequence homology in the helicase domains, respectively (figure 2 and [27]). Originally, MDA5 was identified as a negative regulator of growth and differentiation in melanoma cells in which it is increasingly expressed in response to IFN and TNFα stimulation [28]. Although it is a well-characterised ISG, MDA5 is induced independently of cytokine signalling, but in an interferon-regulatory factor 3 (IRF3)-dependent manner in mature DCs infected with Sendai virus C (SeV-C) [29] and is essential for the recognition of defective interfering particles generated during paramyxovirus replication [30]. MDA5 was found to preferentially recognise long RNA

templates [21], which can be, as in the case of encephalomyocarditis virus (EMCV, a picornavirus), 5'-capped. In fact, MDA5 was shown to be essential for proper immune induction to picornavirus infection [31], [32] and in paramyxovirus infection [33]. Upon recognition of long dsRNAs, MDA5 oligomerises, forming filaments along an RNA template, a process which has been described to be regulated by MDA5 ATPase activity [34]–[36]. Similar to RIG-I, the CTD of MDA5 contains a positively charged region which preferentially recognises blunt-ended dsRNA, but, compared to RIG-I and LGP2, binds this RNA with lower affinity [37]. Formation of MDA5 filaments along RNA will expose MDA5 CARD domains and allow interaction with MAVS.

Interestingly, not only (long) viral RNAs will activate type I IFN and ISG expression, but also small duplex self-RNAs generated by RNase L activity, a process which is initiated upon viral infection and depends on RIG-I and MDA5 activity [38].

1.1.3.3 The role of LGP2

The most obvious difference between LGP2 and the other two RLRs, RIG-I and MDA5, is the absence of the tandem CARD domains (figure 2), which does not allow interaction with MAVS, thereby rendering LGP2 incapable of signal transmission. Nevertheless, the CTD of LGP2 recognises dsRNAs [39], [40] and binds them with the highest affinity of all RLRs [37]. Because of this, it was concluded that LGP2 must have a regulatory function in antiviral signalling, binding dsRNA and "competing" with RIG-I and MDA5. The mechanism by which LGP2 influences antiviral signalling, however, seems to be more complicated. Early reports suggested an inhibitory role of LGP2 in RIG-I-mediated signalling [41]. LGP2 was thought to interact with RIG-I by a shared repressor domain which would maintain RIG-I in an inactive state [42]. In line with this, a first study using LGP2 knockout mice found that mice lacking LGP2 were particularly resistant to infection with RIG-I-dependent viruses, but at the same time were extremely sensitive to MDA5-dependent virus infection [43]. In contrast to this, a later study using different LGP2 knockout mice found a positive regulatory effect of LGP2 on both RIG-I and MDA5 [44]. It is yet to be determined how exactly LGP2 regulates RIG-I-mediated signalling.

It is accepted that LGP2 acts as a positive regulator of MDA5 in antiviral signalling. This view is supported by the fact that viral proteins which inhibit MDA5 often display the same behaviour towards LGP2 [45], [46]. Furthermore, LGP2 enhances MDA5 binding to RNA and regulates filament assembly [47].

Another mechanism of LGP2-mediated inhibition of antiviral signalling downstream of RLR activation was described. It was proposed that LGP2 competes with inhibitor of

nuclear factor kappa-B kinase ε (IKKε) for a binding site on MAVS, thereby inhibiting IFN production [14].

1.1.4 Induction of type I and III IFNs by RLRs

As described above, RIG-I and MDA5 undergo conformational changes upon substrate recognition which exposes their CARD domains. RLR CARDs will interact with MAVS, a signalling adaptor which is, other than its name suggests, not only localised to mitochondria, but is also found on peroxisomes and mitochondria-associated membranes of the ER (MAMs). Although different localisation of MAVS was initially thought to influence signalling kinetics with peroxisomal MAVS inducing a quick, initial IFN response and mitochondrial MAVS establishing stable, amplified IFN induction [48], later studies could not confirm this assumption. As a matter of fact, there are no major differences between IFN induction by mitochondrial or peroxisomal MAVS in hepatocytes [49]. Upon binding of RLR CARDs, MAVS CARD domains will oligomerise, leading to an accumulation of MAVS on the mitochondrial surface, a process which has been compared to the aggregation of prions, especially since filamentous MAVS will promote aggregation of non-activated MAVS [50]. MAVS aggregates form highly ordered, α-helical structures [51] depending on lysine 63 (K63)-linked polyubiqutinylation. Only recently E3-ubiquitin ligase tripartite motif-containing protein 31 (TRIM31) was identified as the effector important for initiation and modulation of MAVS aggregation [52].

MAVS aggregates provide a platform for the recruitment of additional signalling factors. RLR signalling will induce two pathways which result in the initiation of an antiviral response. On the one hand, transcription factors IRF3 and IRF7 are phosphorylated and activated by effector kinases TANK-binding kinase 1 (TBK1) and IKKε. These kinases are activated by E3 ubiquitin ligase TNF receptor associated factor (TRAF) 3 which is engaged by clustering and self-ubiquitinylation within the MAVS signalosome [53], [54]. On the other hand, nuclear factor κ B (NFκB) is activated by RLR signalling. This is achieved by TRAF6 activation which results in the recruitment of IKKα, IKKβ and IKKγ/NEMO [55]. Additionally, TRAF6 signals trough TGFβ-activated kinase 1 (TAK1) and induces the mitogen-activated protein kinase (MAPK) pathway [56]. Upon phosphorylation of the inhibitor of NFκB α (IκBα) by the IKKα/β/NEMO complex, NFκB is released and translocates to the nucleus.

Transcription factors IRF3, IRF7, and NFκB will activate type I and III IFNs, pro-inflammatory cytokines and some ISGs. Other than their name suggests, ISGs are not only induced by IFN signalling, but are also expressed in response to IRF3 and IRF7

activation. An ISG which is strongly induced by activated IRF3 is Interferon-induced protein with tetratricopeptide repeats 1 (IFIT1), also called ISG56 [57]. Because of this, IFIT1 expression is often used as a direct readout for IRF3 activity. An overview of the RLR signalling pathway and its main effectors is given in figure 3.

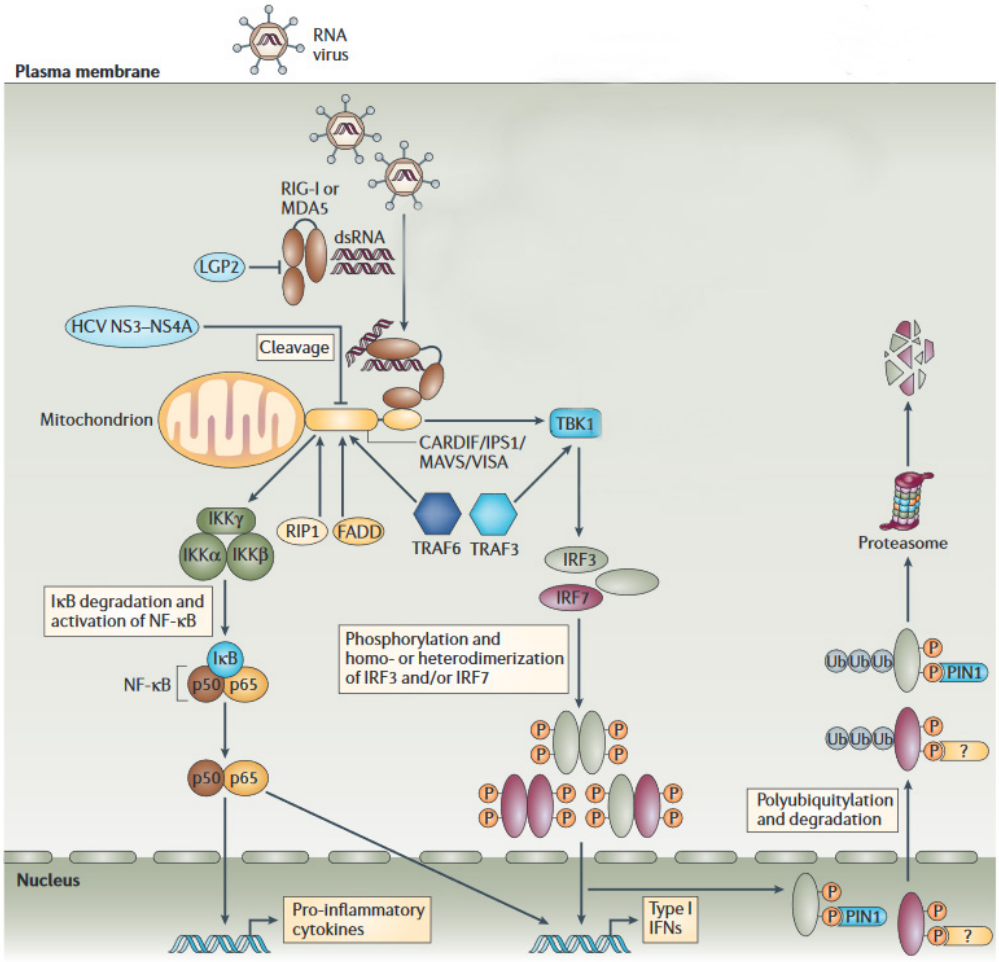

Figure 3 **Overview of the RLR signalling pathway**

Activation of RIG-I and MDA5 by their respective ligands results in a conformational change exposing the CARD domains which interact with and activate MAVS. (Note that LGP2 was described to inhibit RIG-I but promote MDA5 activity [13], [41].) MAVS oligomerisation provides a signalling platform which recruits TRAF3 and TRAF6 leading either to the activation of IRF3 by phosphorylation through TBK1 (or IKKε, not displayed), or NFκB activation by recruitment of IKKα and IKKβ. Phosphorylation of IκBα (IκB) by these kinases marks the inhibitor for degradation. Highlighting the importance of MAVS as an central signalling adaptor, it is targeted by NS3-NS4A protease of hepatitis C virus (HCV) which cleaves and thereby inactivates MAVS. Both IRFs and NFκB activation results in expression of type I and III IFNs, pro-inflammatory cytokines and some ISGs. Activated IRFs are recognised by effectors of the ubiquitinylation pathway and labelled for degradation. Adapted from [58].

1.1.5 Interferons and the interferon signalling pathway

Interferons were named after their ability to interfere with viral replication when they are added to cells in culture prior to infection. They are a group of cytokines which are commonly induced in response to viral infection and which will, ideally, help to clear an infection by induction of an antiviral state. Based on their amino acid sequence, they are grouped into three classes: Type I, type II, and type III IFNs. While there are several type I and III IFNs, there is only one type II interferon, IFNγ. Since IFNγ is not directly secreted in response to viral infection, but rather by activated T and NK cells in the course of adaptive immunity, further introduction is going to focus on type I and III IFNs only.

1.1.5.1 Type I interferons

Type I IFNs were first described 60 years ago by Isaacs & Lindemann [59]. While there are at least seven different type I IFNs in mammals, only IFNα (which comprises a group of 13 genes in humans) and IFNβ (monogenic in humans) are induced in response to viral infection. The role of the other type I IFNs, IFNω, ε, τ, δ, and κ, is less well-defined, but some were found to have distinct roles, such as IFNω and IFNτ which act at the placental interface and are important for maternal recognition of pregnancy [60], [61].

All type I IFNs bind to a common receptor which is a heterodimeric complex consisting of the interferon alpha receptor (IFNAR) 1 and 2 proteins. IFNs induce classical Janus kinase/signal transducers and activators (Jak/STAT) signalling pathways (figure 4 and [62]). Binding of IFNs to IFNAR1 and 2 induces oligomerisation which brings both receptors into close proximity. This causes receptor-associated kinases Tyk2 (bound to IFNAR1) and JAK1 (bound to IFNAR2) to cross-phosphorylate not only the cytoplasmic tails of the IFNARs, but also STAT2 and STAT1. These are weakly associated with the IFNARs prior to stimulation but associate more strongly to phosphorylated receptors [63]. Phosphorylated STATs form a stable heterodimer which, together with IRF9, forms the interferon-stimulated gene factor 3 (ISGF3) complex capable of binding interferon-stimulated response elements (ISRE) present in the promoter regions of most ISGs (figure 4 and [64]).

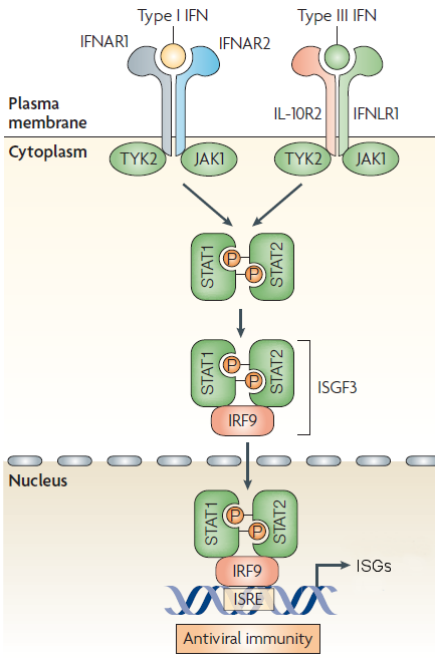

Figure 4 **Classical Jak/STAT pathway induction by type I and type III IFNs**

Binding of type I IFNs induces dimerisation of IFNAR receptor proteins 1 and 2 which results in cross-phosphorylation of cytoplasmic receptor chains as well as subsequent interaction with and phosphorylation of STAT1 and STAT2. Phosphorylated STATs heterodimerise and translocate to the nucleus where they induce transcription of antiviral ISGs. While they bind a heterodimeric receptor consisting of IFNLR1 and IL10R2 proteins, intracellular signalling induced by type III IFNs is very similar to that in response to type I IFNs. Adapted from [62].

Interestingly, it was found that ISGF3 complexes are formed directly at the level of IFNARs by recruitment of cytoplasmic CREB-binding protein (CBP) which acetylates IFNAR2, thereby inducing IRF9 association. Furthermore, IRF9, STAT1, and STAT2 require acetylation by CBP for proper ISGF3 complex activation [65]. All components of the ISGF3 complex are IFN-inducible themselves which not only facilitates signal amplification, but may also reduce the requirement of STAT1 phosphorylation in the phase after initial pathway activation [66], [67].

As IFNAR1 and 2 are ubiquitously expressed, type I IFNs are the main inducers of antiviral responses in most cell types and tissues. Moreover, ubiquitous expression of IFNARs results in a systemic response to type I IFNs. An overshooting systemic immune reaction might be detrimental which is probably the reason why type I IFNs usually induce a strong but short expression of ISGs [68], [69].

1.1.5.2 Type III interferons

Type III IFNs were discovered much later than type I IFNs with first reports published by two independent groups in 2002/2003 [70], [71]. So far, four different type III IFN genes have been identified, encoding for IFNλ1/IL-29, IFNλ2/IL-28A, IFNλ3/IL-28B, and IFNλ4. Similar to type I IFNs, λ-IFNs signal through a heterodimeric receptor complex which is composed of the interferon lambda receptor 1 (IFNLR1, also called IL28RA) and the interleukin 10 receptor chain 2 (IL10R2). Interestingly, this receptor chain is shared with the receptor complexes binding IL-10, IL-22, and IL-26. The downstream signalling

cascade induced by type III IFNs is almost identical with that induced by type I IFNs in that it culminates in ISGF3 complex formation and nuclear translocation (figure 4). In contrast to type I IFN signalling in which JAK1 is an effector kinase, JAK2 was reported to be implicated in type III IFN signalling [72], although another group observed normal STAT activation in JAK2-deficient cells [73].

Type III IFN expression and effects are limited to mucosal surfaces due to the selective expression of IFNLR1 in cells of epithelial origin [74], [75]. Sure enough, epithelial cells in the respiratory and gastrointestinal tract frequently encounter different viruses. It was found that especially type III IFNs contribute to resistance against viruses which commonly infect these cells while they were less efficient against viruses with different tropism, e.g. hepatotropic viruses [76], [77]. Moreover, type III IFNs act with different kinetics than type I IFNs in that λ-IFNs induce a delayed but prolonged ISG response [68], [78].

Both type I and type III IFNs are induced upon antiviral signalling initiated by RLRs and have similar effects when they bind their respective receptors on target cells. However, differential expression of IFN receptors allows fine-tuning of the IFN response, just as certain modulators of the IFN signalling pathway may have an effect on one, but not the other signalling pathway. For example, Ubl carboxyl-terminal hydrolase 18 (USP18) is involved in negative feedback regulation of IFN signalling and is induced in response to type I and type III IFN. Since it competes with JAK1 for its binding site on IFNAR2, however, it suppresses IFNα signalling much stronger than IFNλ responses [79]. This is only one of many mechanisms which modify IFN signalling and result in an adequate response to virus infections of different cells and tissues.

1.1.6 Interferon-stimulated genes and antiviral effectors

As mentioned above, IFN signalling results in the expression of many different ISGs and antiviral effectors. While some ISGs merely interfere with a specific step in a viral life cycle, others display greater potency in that they enhance further IFN production resulting in an even stronger ISG response. Because of this, many viruses have developed effective countermeasures and are capable of inhibiting certain classes of ISGs, some even using specific genes to their advantage. Remarkably, ISGs modulate a multitude of cellular processes such as cytoskeletal remodelling, apoptosis induction, regulation of RNA translation and post-translational modifications. As examples, two “classical” and well-studied ISGs will be discussed in this section. Lastly, some viral stress-induced genes will be introduced.

1.1.6.1 Mx GTPases

One important group of ISGs whose expression strongly depends on type I and type III IFNs are the Myxovirus resistance protein (Mx) family of GTPases [80]. There are two Mx proteins in humans, Mx1 and Mx2. While the antiviral activity of Mx1 has been thoroughly examined, it is not clear to which extent Mx2 restricts viral infection [81]. Mx proteins contain an N-terminal GTPase domain, a central interacting domain (CID) and a C-terminal leucine zipper domain. Their main targets seem to be viral nucleocapsids as shown for orthomyxoviruses [82]. Due to its localisation at the smooth ER [83], Mx1 recognises viral components early in the viral life cycle. Moreover, it was shown to effectively block viral gene transcription in influenza virus replication by binding and inhibiting the viral polymerase [84]. As Mx proteins effectively counteract viral replication and spread, several viruses have developed mechanisms to evade or overcome this inhibition. West Nile virus (WNV), for one, produces cytoplasmic membrane structures which hide viral components from Mx1 recognition [85], and Hepatitis B virus (HBV) core protein was shown to suppress Mx1 expression by binding the Mx1 promoter region [86].

1.1.6.2 ISG15

Another prominent ISG is ubiquitin homologue ISG15 which post-translationally conjugates to proteins [87]. This process is referred to as ISGylation. Similar to what is known for ubiquitinylation (compare section 1.3.1), ISGylation requires an E1-activating enzyme (E1-like ubiquitin-activating enzyme, UBE1L) as well as E2-conjugating enzymes (e.g. UBCH6 or UBCH8). Finally, an E3-ligase (e.g. HERC5 or TRIM25) mediates the transfer of ISG15 to its target protein [88]. Just as it is observed for ubiquitinylation, ISG15 may be removed from target proteins by deconjugating enzymes such as USP18 [89]. Unlike K48-linked (poly)ubiquitinylation, ISGylation does not mark proteins for degradation, but rather mirrors the activating effect of K63-linked ubiquitinylation. On the one hand, ISGylation can prevent the degradation of vital factors in antiviral signalling like IRF3 [90] and RIG-I [91]. On the other hand it is secreted from cells and may act as a cytokine [92]. Viral countermeasures against ISG15 include binding of viral factors to ISG15, like in the case of influenza B virus NS1 protein [93], and promotion of deISGylation by several other viruses such as SARS-associated coronavirus [94].

1.1.6.3 Viral stress-induced genes

Ultimately, some antiviral factors are directly induced in response to the presence of viral components in the cytoplasm without the necessity for IFN induction, although IFN

signalling often leads to an additional up-regulation of those genes. These viral stress-induced genes are activated upon sensing of viral genomes, glycoproteins and lipoproteins and effectively inhibit viral spread, often by shutting down cap-dependent translation. An important factor which senses dsRNA and inhibits cap-dependent translation by phosphorylation of eukaryotic translation initiation factor 2 α (eIF2α) is protein kinase R (PKR). PKR is usually ubiquitously expressed at low levels, but is up-regulated upon viral infection [95].

Another type of viral stress-induced genes are 2'-5' oligoadenylate synthases (OASs). Similar to PKR, these proteins are usually present at low levels in cells and are induced upon viral infection. OASs recognise dsRNA whose binding induces a conformational change, activating the enzyme. Activated OASs synthesize 2'-5'-linked oligoadenylates which facilitate homodimerisation of RNase L [96], activating its enzymatic function. Thereby, OASs induce degradation of viral RNAs.

1.2 RNA viruses

As mentioned in the previous sections, RLRs are the predominant cytosolic receptors for foreign RNAs, i.e. viral genomes. Hence, RLR signalling is strongly initiated after infection with viruses, especially those with RNA genomes since these will, at some point, give rise to replication intermediates recognised by RLRs. This section will introduce the different RNA viruses used to trigger RLR signalling in the present study.

1.2.1 Sendai virus

Sendai virus (SeV), also called murine parainfluenza virus type 1, is a negative sense, single-stranded RNA virus belonging to the family of *paramyxoviridae*. While the natural host of SeV has not been identified, the virus seems to infect mostly rodents, although it was also isolated from humans. SeV causes mostly upper respiratory tract disease and was found to replicate with similar efficiency as human parainfluenza virus type 1 in the respiratory tract of nonhuman primates [97]. SeV infection in humans is usually asymptomatic, whereas it can be fatal in mice [98]. Replication of SeV genomes results in the formation of double-stranded intermediates which are recognised by RIG-I [20] and induce a strong IFN response. Interestingly, in addition to viral particles containing full-length viral genomes, Sendai virus infection also produces so-called defective interfering (DI) particles containing smaller fragments of the viral genome which do not support replication and, therefore, do not enhance viral spread [99]. Moreover, probably because they are 5'-triphosphorylated, double-stranded, and relatively short, they are strong inducers of interferons [100], [101].

1.2.2 Rift Valley Fever Virus

Belonging to the family of *bunyaviridae*, Rift Valley Fever virus (RVFV) has a segmented, single-stranded RNA genome of negative (L and M segment) and ambisense orientation (S segment). If transmitted from mosquito vectors to humans, RVFV causes mostly fevers, which in about 1% of all cases develop into severe haemorrhagic fever and meningoencephalitis [102]. Although RVFV replication does not produce large amounts of dsRNA, the 5'-triphosphorylated dsRNA panhandle structure of its genome is recognised by RIG-I and strongly induces IFN [103], [104] which RVFV is highly sensitive to. Consequently, mice are protected from disease when they are pre-treated with interferon-inducing agents [105]. In order to avoid and counteract recognition by RIG-I, the S segment of the RVFV genome encodes non-structural protein NSs, a potent inhibitor of IFN signalling. This is reflected in RVFV clone 13 which is attenuated due to a large in-frame deletion within the NSs gene [106]. Among other effects, NSs was found to shut off cellular translation by sequestration of transcription factor II H (TFIIH) [107]. Moreover, NSs induces proteasomal degradation of PKR [108] which, if not degraded, is a strong inhibitor of RVFV replication. Deletion of NSs does not only result in attenuation of RVFV virus and increased IFN sensitivity, but also allows the introduction of reporter genes in its place. A luciferase-tagged RVFV has been used to study the effect of IFN pre-treatment on viral replication [109] and is employed in RVFV replication assays within this study.

1.2.3 Influenza A virus

Influenza A virus (FluAV) belongs to the family of orthomyxoviruses, together with influenza B, C, and D virus. It is the most common and also the most virulent of the different types of influenza. FluAV has a negative-sense ssRNA genome which is divided into 8 segments. The best-characterised viral proteins are hemagglutinin (H) and neuraminidase (N) which are used to classify FluAV serotypes (e.g. H5N1, "bird flu"). FluAV causes annual epidemics which are characterised by slight changes in antigenicity, usually requiring a new round of vaccination each year to sustain protection [110]. Infection with FluAV leads to febrile disease accompanied by headache, weakness, cough, muscle and joint pain, and can become severe, resulting in viral pneumonia, secondary bacterial pneumonia and heart failure. Similar to RVFV, complementary regions in the 5' and 3' regions of the FluAV genome form a panhandle structure which is recognised by RIG-I [111]. Additionally, U/A-rich stretches in the untranslated region of the FluAV genome activate RIG-I independently of a 5'-triphosphate [112]. Induction of IFN is efficiently inhibited by FluAV NS1 protein, which

was shown to interact with a multitude of cellular proteins (e.g. RIG-I or TRIM25 [18], [113]) thereby repressing the RIG-I signalling pathway [114]. Influenza A/WSN/(19)33 of serotype H1N1 replicates in many different cell lines [115] and is used in this study to examine RIG-I signalling in response to FluAV infection.

1.2.4 Hepatitis C virus

A member of the family of *flaviviridae*, Hepatitis C Virus (HCV) is a member of the genus *hepacivirus*. HCV is a positive-strand ssRNA virus which is hepatotropic and causes chronic hepatitis in the majority of infected individuals. Perpetual liver inflammation often leads to the development of liver cirrhosis and hepatocellular carcinoma. Spontaneous clearance within acute HCV is very rare and is usually associated with rapid induction of IFN and ISGs early in infection and a delayed onset of the adaptive immune response [116]. Both RIG-I and MDA5 have been reported to be involved in the sensing of HCV replication intermediates [42], [117] and will induce IFN in response to HCV infection. As an evasion mechanism HCV NS3-4A protease cleaves MAVS off the mitochondrial membrane and inhibits IFN induction (figure 3 and [118]). By tagging the viral genome with a reporter gene HCV replication can be monitored [119]. The present study made use of a HCV JCR2A, a genotype 2 reporter virus harbouring a renilla luciferase gene.

1.3 Post-transcriptional modifications modulating the RLR signalling pathway

Several different post-translational modifications (PTMs) are necessary for effective induction of antiviral signalling, be it on the level of IRF induction by RLRs or the IFN signalling pathway resulting in the expression of ISGs. ISGylation is an important PTM directly induced by IFN signalling, which influences RIG-I stability [91], and has been described in the previous section. Furthermore, acetylation of IFNARs was mentioned as another PTM which modulates IFN signalling [65]. There is a plethora of different PTMs many of which are involved in regulating the RLR signalling pathway, but the most prominent and well-studied ones are ubiquitinylation and phosphorylation, which the following sections will describe in more detail.

1.3.1 Ubiquitinylation

Section 1.1.4 already highlighted that ubiquitinylation is necessary for proper signalling induction by RLRs, e.g. for the activation of effector kinase TBK1 by E3-ubiquitin ligase TRAF3. Generally, ubiquitinylation can have several effects on a protein target. The best understood are K48-linked ubiquitinylation which targets a protein for proteasomal

degradation [120], and K63-linked ubiquitinylation which, in contrast, often activates the target [121]. Ubiquitinylation is carried out by three different enzymes, the ubiquitin-activating enzyme (E1), the ubiquitin-conjugating enzyme (E2), and an ubiquitin-ligase (E3) which transfers activated ubiquitin onto a target protein. There are over 600 E3-ubiquitin ligases encoded in the human genome which allows precise regulation of signalling pathways.

Already early in the initiation of antiviral signalling, on the level of receptor activation, the RLR signalling pathway is controlled by ubiquitinylation. K63-linked ubiquitinylation of the RIG-I CARD domains by TRIM25 and RING finger protein 135 (RNF135, also called Riplet) are necessary for tetramerisation and MAVS interaction [122], [123]. Only recently, a similar activating mechanism was found for MDA5 whose oligomerisation depends on TRIM65 K63-linked ubiquitinylation [124]. Interestingly, RIG-I is not only down-regulated by K48-linked ubiquitinylation by RNF125 [125], but its activity is also decreased by USP3 and ubiquitin C-terminal hydrolase [126], [127] which remove previously attached activating ubiquitin chains. Control of RLR activity is also carried out by enzymes like USP15. This deubiquitinylating enzyme has a dual role in RLR signalling. It removes inactivating K48-linked ubiquitin chains from TRIM25 on the one hand, but may also remove K63-linked ubiquitin chains from RIG-I [128], [129].

Ubiquitinylation further controls RLR signalling downstream of its RNA sensors. Central signalling adaptor MAVS itself is subject to activating ubiquitinylation by TRIM31 [52], but is, at the same time, also regulated through K48-linked ubiquitinylation by TRIM25, a mechanism which is thought to detach MAVS from its mitochondrial location, releasing the signalling complex to the cytosol [130]. Among many other negative regulators of MAVS activity, membrane-associated RING finger protein 5 (MARCH5), a mitochondrial membrane-bound E3 ligase, plays an important part in MAVS inactivation since it resolves MAVS aggregates at the mitochondria by marking them for proteasomal degradation [131].

E3-ubiquitin ligases TRAF3 and TRAF6 are mediators of RLR signalling directly downstream of MAVS. They are not only auto-ubiquitinylated but also activate their targets TBK1 and IKKs, engaging IRF3 and NFκB. At the same time, TRAF3 and TRAF6 activity is tightly regulated by enhancing ubiquitinylation, e.g. by RNF166 which targets both TRAFs [132], and inhibiting/down-regulating ubiquitinylation, such as that conferred by cellular inhibitor of apoptosis 2 (cIAP2) which mostly targets TRAF3 [133]. Interestingly, cIAP2 itself is activated by TRAF6 and can also increase TRAF3 activity, suggesting that, depending on the context, cIAP2 can serve as an activator or as an

inhibitor of antiviral signalling [134]. There are also a number of cellular deubiquitinases targeting TRAF3 and TRAF6, which will suppress RLR signalling.

Although TRAF-activated effector kinases TBK1 and IKKε are quite similar and often simultaneously induced upon viral infection, there are functional differences between the two. A mechanism which could confer a different means of regulation of IKKε and TBK1 could be K63-ubiquinitylation by mindbomb 1 (MIB1) which only targets TBK1 [135]. Additionally, there are a few ubiquitinylation events which target TBK1 for proteasomal degradation.

Lastly, activity of IRF3 and IRF7 is greatly influenced by ubiquitinylation. Only some of the multiform ubiquitinylation events which regulate the IRFs will be highlighted here.

Nuclear activated IRF3 quickly binds peptidyl-prolyl cis/trans isomerase NIMA-interacting 1 (Pin1) which promotes IRF3 degradation [136]. Among others, TRIM26 was found to K48-ubiquitinylate IRF3 [137]. Since down-regulation of IRF3 is undesirable in early stages of infection, there are several mechanisms which inhibit premature IRF3 degradation. Again, there are factors which have a dual role in IRF3 degradation, capable of either stabilising or degrading IRF3. One of these is TRIM21, which may on the one hand interrupt IRF3-Pin1 interaction, but can on the other hand also target IRF3 for proteasomal degradation [138], [139]. Importantly, TRIM21 also targets and down-regulates IRF7, although this mechanism was, so far, only studied in TLR-mediated signalling [140]. IRF3 activity is, furthermore, stabilised by HECT and RRC1-ilke domain-containing protein (HERC5) which ISGylates several residues on IRF3 so that it cannot bind to Pin1 [141]. This interplay between ISGylation and ubiquitinylation highlights that different PTMs are employed to fine-tune the RLR signalling pathway.

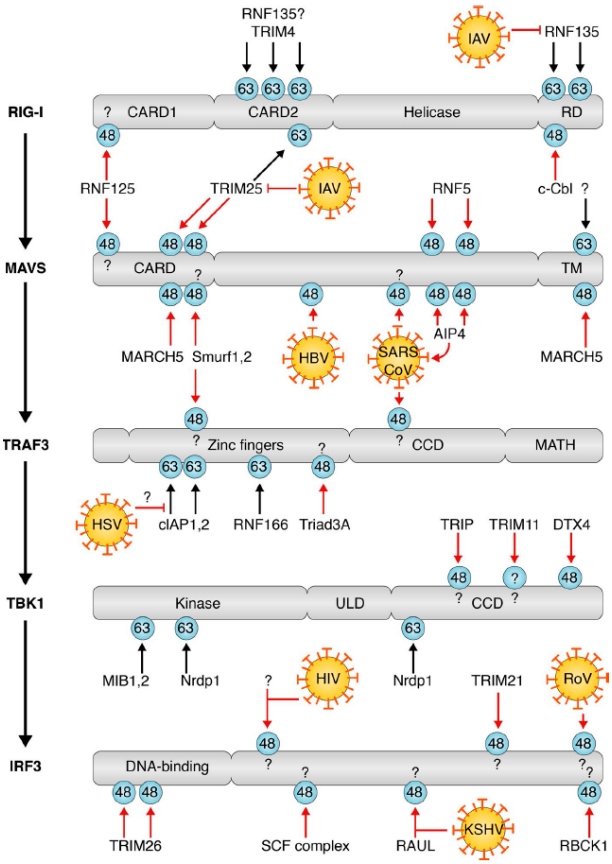

Figure 5 **RIG-I signalling is regulated by ubiquitinylation events which are targeted by viral effectors**

K63-linked ubiquitinylation may activate effectors of the RIG-I signalling network and happens on every level of pathway activation. At the same time, this is counteracted by K48-linked ubiquitinylation which targets RLR signalling effectors for proteasomal degradation. Examples for viruses which target ubiquitinylation events are shown. IAV, Influenza A virus. HBV, Hepatitis B virus, SARS CoV, SARS-associated corona virus. HSV, Herpes simplex virus. HIV, human immunodeficiency virus. RoV, Rotavirus. KSHV, Kaposi's sarcoma-associated herpesvirus. Adapted from [142].

In summary, ubiquitinylation is a major PTM which modulates the RLR signalling pathway and occurs on every level of pathway activation. It is used to target most effectors of the RLR signalling cascade and can have, based on the composition of ubiquitin chains, either negative or positive influence on effector activity. Consequently, many viruses encode proteins which counteract cellular ubiquitinylation events, an overview of which is given in figure 5.

1.3.2 Phosphorylation

Protein phosphorylation is one of the most common PTMs influencing protein activity. Often, phosphorylation of a protein by a kinase is directly counter-regulated by a phosphatase, creating a dynamic and flexible equilibrium in phosphorylation events.

As was mentioned in section 1.1.4, some of the main effector proteins in the RLR signalling pathway are kinases signalling downstream by their ability to phosphorylate the respective target, like TBK1 and IKKε, which are both capable of IRF3 and IRF7 phosphorylation. Similarly, NFκB activation requires phosphorylation of IκBα by the activated IKKα/IKKβ/NEMO complex. This section is not going to focus on those phosphorylation events which are employed to directly transfer the signal resulting in gene transcription, but rather highlight a few phosphorylation events which influence RLR signalling effector activities. With over 500 members [143], the human kinome provides a variety of candidates which are potentially capable of influencing RLR signalling, many of which might not have been studied in this context yet.

RIG-I and MDA5 activity is regulated by several (de)phosphorylation events. Firstly, dephosphorylation of both RLRs is necessary for IFN production in response to various RNA viruses. Phospho-protein phosphatases 1 α and γ (PP1α/γ) were identified to remove inhibiting phosphate moieties from the CARD domains of both RLRs [144]. Furthermore, RIG-I activity is inhibited by protein kinase C α and β (PKCα/β), as well as casein kinase II (CK2) which phosphorylate residues in its CARD, as well as its RD domain, respectively [145], [146]. In this context, phosphorylation of RIG-I CARD domains was shown to inhibit TRIM25-RIG-I interaction. For MDA5, RIO kinase 3 (RIOK3) was reported as a negative regulator, phosphorylating the C-terminus of MDA5 and blocking oligomerisation [147].

Although there are a few signalling pathways which result in TBK1 activation, not all of them culminate in an activation of IRF3 and subsequent expression of IFNs. Remarkably, it was recently discovered that phosphorylation of MAVS by TBK1 was required for IRF3 recruitment. Moreover, this mechanism was found to be conserved among all IRF3-mediated IFN-inducing signalling pathways, including the cGAS/STING pathway of DNA recognition and TRIF-mediated signalling after TLR stimulation [148]. There are indications that tyrosine phosphorylation of MAVS is not only increased after viral infection, but is even required for proper signal transmission [149]. Finally, there are also phosphorylation events limiting MAVS activity. One of these is conferred by polo-like kinase 1 (PLK1) which inhibits MAVS-TRAF3 interaction [150].

Downstream of MAVS, (de)phosphorylation controls not only TRAF3 and TRAF6 activity, but also TBK1 activity since it is recruited to active TRAF3. As a matter of fact, without CK1ε-mediated phosphorylation TRAF3 is not efficiently ubiquitinylated and therefore incapable of TBK1 recruitment [151]. Phosphorylation of TRAF6 by serine/threonine kinase 26, on the contrary, inhibits TRAF6 auto-ubiquitinylation and oligomerisation which inhibits an inflammatory response [152].

TBK1 itself undergoes auto-phosphorylation at serine 172 (S172) [153], an event which is facilitated by interaction with GSK3β. Remarkably, this happens independently of GSK3β kinase activity [154]. TBK1 phosphorylation by proto-oncogene tyrosine-protein kinase Src, however, is required for efficient auto-phosphorylation. Interestingly, Src does not directly interact with TBK1, but is instead recruited to signalling complexes by adaptors like MAVS or STING [155]. Based on these findings, it is not surprising that removal of the S172 phosphate moiety by protein phosphatase 1 β (PPM1B) reduces TBK1 activity, resulting in decreased IFN production in response to virus infection [156]. Similar mechanisms probably regulate IKKε activity which was, similar to TBK1, found to auto-phosphorylate at S172 [157], but has not been investigated as extensively.

Within the RLR signalling pathway, phosphorylation events for IRF3 and IRF7 were found to be mediated predominantly by TBK1 and IKKε. While these kinases phosphorylate several residues at the IRF3 and IRF7 C-terminus, thereby activating the transcription factors, protein phosphatase 2A (PP2A) counteracts this by IRF3 dephosphorylation, dependent on its adaptor Receptor of activated protein C kinase 1 (RACK1) [158].

As described in this section, protein (de)phosphorylation is one of the most important PTMs in RLR signalling and influences protein activity, stability and interaction on every level of signal transmission. Since its discovery, many kinases and phosphatases have been found to modulate the RLR signalling cascade. Hence, it is feasible that out of the hundreds of seemingly uninvolved kinases at least a few more are important regulators of antiviral signalling.

This study focuses on a family of kinases which influences RIG-I signalling, the death-associated protein kinases (DAPKs), which the next section is going to introduce.

1.4 Death-associated protein kinases

The death-associated protein kinase (DAPK) family consists of five members, namely DAPK1, DAPK2, DAPK3, serine threonine kinase 17A (STK17A)/DAPK-related apoptosis inducing kinase1 (DRAK1), and STK17B/DRAK2. An overview of the kinases is shown in figure 6. Only DAPK1 and DAPK2 are calmodulin (CaM)-dependent kinases and possess a CaM auto-regulatory domain. Both DAPK1 and DAPK2 undergo an auto-phosphorylation mechanism on serine 308/318 in their CaM domain (figure 6) which regulates their kinase activity. Both kinases attain full kinase activity when they are dephosphorylated [159], [160].

Based on the structure of their kinase domains DAPKs are related to myosin light chain kinases (MLCKs). Accordingly, they phosphorylate myosin light chain which results in membrane blebbing [159], [161]–[163]. All DAPKs are serine/threonine kinases and are, as their name suggests, involved in the induction of cell death. While DAPK1, DAPK2, and DAPK3 have been described to induce both type I (apoptotic) and type II (autophagic) cell death, DRAK1 and DRAK2 have, so far, only been linked to apoptotic cell death. DAPK1, DAPK2, and DAPK3 are, furthermore, considered tumour suppressors.

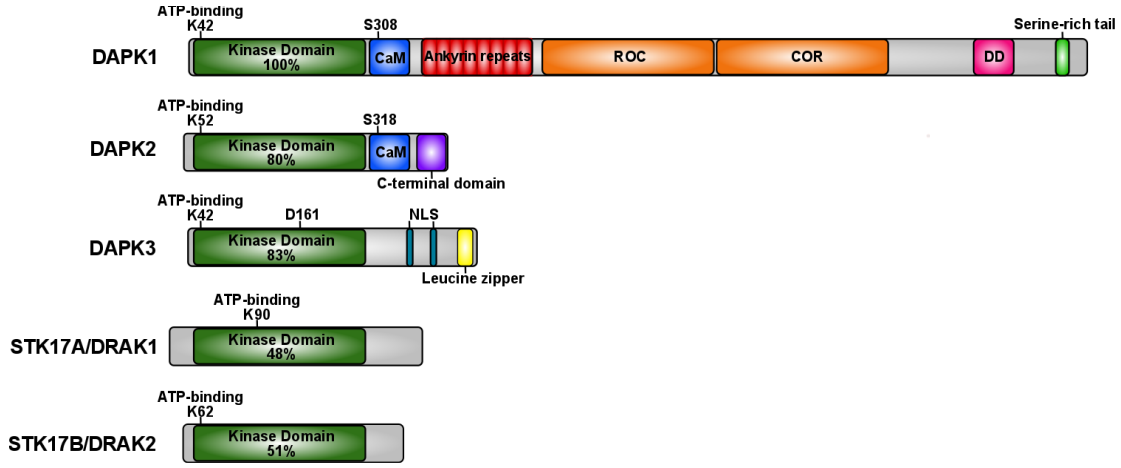

Figure 6 Overview of the family of death-associated protein kinases

The DAPK family comprises five kinases. DAPK1 is its founding member and the largest protein. In addition to its kinase and CaM domain, DAPK1 contains 8 Ankyrin repeats, a ROC-COR domain, and a death domain (DD). The kinase domains of DAPK2 and DAPK3 display 80% and 83% amino acid sequence homology to DAPK1. Like DAPK1, DAPK2 is a CaM-dependent kinase and contains a C-terminal domain with no homology to any known protein. DAPK3 contains several nuclear localisation signals (NLS) and a C-terminal leucine zipper domain. The kinase domains of DRAK1 and DRAK2 share less amino acid sequence homology to DAPK1, but are highly homologous to each other.

This section is going to introduce the DAPKs and key findings about their role in cellular metabolism, while section 1.5 focuses on the cell death pathways DAPKs have been found to influence.

1.4.1 DAPK1

In addition to its kinase and CaM domain, DAPK1 contains 8 Ankyrin repeats, a ROC-COR domain and a death domain (DD). It is the founding member of the DAPK family of protein kinases and was originally described as the main effector of IFNγ-induced cell death in HeLa cells [164]. Interestingly, it was later discovered that IFNγ-stimulation induced DAPK1 expression in an cyclic AMP-dependent transcription factor 6 (ATF6)/ERK-dependent fashion and resulted in the induction of autophagy dependent on apoptosis signal-regulating kinase 1 [165], [166].

As mentioned above, DAPK1 was first identified as a mediator of apoptosis induction, e.g. in response to transforming growth factor β (TGFβ) stimulation [167]. Furthermore, netrin receptor UNC5H2 induces apoptosis via DAPK1. UNC5H2 directly interacts with DAPK1 via its DD and recruits PP2A which dephosphorylates DAPK1 S308 and thereby increases its activity [168], [169]. DAPK1 does not only mediate type I (apoptotic) cell death, but also type II (autophagic) cell death. Autophagy induction by DAPK1 is achieved through either phosphorylation of Beclin1 or protein kinase D (PKD), which has similar outcomes. Phosphorylated Beclin1 is released from a complex with B cell lymphoma 2 (Bcl-2) or Bcl-X_L, allowing interaction with and activation of lipid kinase autophagy-promoting vacuolar protein sorting 34 (VPS34). Activation of PKD results in direct phosphorylation of VPS34, which, once activated, produces phosphatidylinositol 3 phosphate (PI3P) and thereby promotes autophagosome formation ([170]–[172]).

In addition to its cell death promoting function, DAPK1 influences a variety of other processes and pathways in the cell.

One of the main cellular functions of DAPK1 seems to be that of a tumour suppressor, which was first postulated based on the finding that its promoter region is frequently hyper-methylated in a variety of solid tumours [173]–[175] and in follicular lymphoma [176]. As a matter of fact, DAPK1 was not only found to activate p53 in a $p19^{ARF}$-dependent manner which suppresses oncogenic transformation [177], but was also found to control metastasis formation, most probably by inhibition of integrin-mediated cell polarity pathways [178], [179].

Additionally, DAPK1 is important in brain metabolism. DAPK1 not only mediates neuronal cell death by direct phosphorylation of p53 in ischemic tissue, but also binds and phosphorylates NMDA receptor NM2B which results in exacerbated brain damage after stroke due to increased Ca^{2+} influx [180], [181]. Moreover, DAPK1 contributes to the development of Alzheimer's disease. Direct phosphorylation of Pin1, which regulates tau protein stability, and tau itself by DAPK1 promote tau aggregation [182]–[184].

Interestingly, cell growth and survival, especially via ERK-mediated growth factor signalling, is positively and negatively regulated by DAPK1. Src, a kinase identified as a proto-oncogene, which signals downstream of the epithelial growth factor receptor (EGFR) phosphorylates residues located in the DAPK1 Ankyrin repeats resulting in DAPK1 inhibition. LAR phosphatase counteracts Src-mediated phosphorylation [185]. Unlike Src, its downstream effector ERK does not inhibit DAPK1, but promotes its apoptotic function, phosphorylating serine 735 within the DAPK1 DD. As ERK itself is a target of DAPK1, its phosphorylated form being retained in the nucleus, this describes a positive feedback mechanism, which, ultimately, results in cell death [186]. To make matters even more complex, DAPK1 targets the tuberous sclerosis 1 (TSC1)/TSC2 complex which results in activation of the mammalian target of rapamycin (mTOR) complex [187]. This promotes cell growth and survival by activation of ribosomal S6 kinase (RSK). RSK itself targets and inhibits DAPK1 which constitutes another feedback mechanism reinforcing cell survival [188]. Hence, depending on the activity and expression of different growth factor pathway members, DAPK1 can either promote or inhibit cell death.

Recently, the importance of recognising the role of DAPK1 in cell survival was highlighted as it was discovered that, other than previously assumed, DAPK1 does not always act as a tumour suppressor. On the contrary, it can promote tumour growth in cancers harbouring p53 mutations, since its cell death-inducing function is based on an activation of p53. In combination with its ability to enhance cell growth by activation of the mTOR signalling pathway, loss of cell death inducing properties of DAPK1 actually makes it an oncogene. This was demonstrated not only in p53 mutant breast cancer, but also ovarian cancer and pancreatic cancer [189].

Because of the manifold role of DAPK1 in both cell death and survival, its activity is tightly controlled. On the one hand, DAPK1 S308 needs to be dephosphorylated in order to allow interaction with CaM for full kinase activity, as was mentioned above. On the other hand, several other kinases phosphorylate and thereby activate or deactivate DAPK1, such as previously mentioned Src, ERK, and S6K. Another level of

intramolecular regulation of activity is provided by the ROC-COR domain of DAPK1 which has intrinsic GTPase activity [190]. Upon binding of GTP to DAPK1 ROC-COR S308 auto-phosphorylation is increased and DAPK1 activity is reduced [191].

DAPK1 protein stability is controlled by chaperone Heat Shock Protein 90 (HSP90). Upon inhibition of HSP90, activated DAPK1 is ubiquitinylated by E3 ligases carboxyl terminus of HSC70-interacting protein (CHIP) or MIB1 and degraded [192]–[194]. MIB1 has been described to regulate the innate immune response (section 1.3.1 and [135]), and could provide a link between DAPK1 and innate signalling. Another E3 ligase, kelch-like protein 20 (KLHL20), interacts with the DAPK1 DD and marks DAPK1 for degradation. KLHL20 is inhibited by IFNα and IFNγ treatment and DAPK1 levels are stabilised [195]. This is another finding that connects DAPK1 to immune signalling.

As a matter of fact, DAPK1 has been examined in the context of immune and inflammatory responses. It was found to inhibit NFκB activation after T cell receptor stimulation by promoting IKK sequestration in membrane rafts [196] and was identified as a crucial activator of NLRP3 inflammasome assembly, as loss of DAPK1 impaired IL-1β maturation [197]. Importantly, DAPK1 was initially described as an IRF3/IRF7-interacting protein based on a yeast two hybrid screen. In the respective study, DAPK1 promoted IFN signalling independently of its kinase activity [198]. In contrast to that, our group has very recently described DAPK1 to control RIG-I activity by inhibitory phosphorylation. We have established that DAPK1 is involved in a negative feedback loop which helps to control IFN induction after initial RIG-I activation [199]. Parts of the findings which contributed to that publication are presented in the results section of this study.

1.4.2 DAPK3

DAPK3 was first described three years after the discovery of DAPK1 as a 54 kDa large kinase similar to DAPK1 which mediates apoptosis induction and contains a leucine zipper domain [200]. Hence, it is also called zipper-interacting kinase (ZIPK). DAPK3 leucine zipper domains were found to mediate heterodimerisation [200] and might also mediate DAPK3 homodimerisation [201]. DAPK3 contains two nuclear localisation signals (NLS, figure 6). Thus, DAPK3 can translocate to the nucleus depending on the phosphorylation status of specific residues located close to its NLS sequences [202]. Generally, DAPK3 is highly phosphorylated which directly influences its kinase activity. A residue which was found to be especially important for full DAPK3 kinase activity is threonine 265 (T265), whose phosphorylation is induced in response to IL-6 stimulation

[203], [204]. Interestingly, DAPK3 is phosphorylated and activated by DAPK1, which demonstrates that DAPKs interact and might depend on each other in order to attain full activity [201].

DAPK3 induces apoptosis by phosphorylation of MDM2 and $p21^{WAF1}$ both of which are effectors of the p53 pathway [205]. Furthermore, DAPK3 interacts with pro-apoptotic PRKC apoptosis WT1 regulator protein (Par4) and induces mitochondrial cytochrome c release [206]. Just as DAPK1, DAPK3 is involved in autophagy induction. It phosphorylates myosin II, facilitating autophagosome formation [207], and Beclin1 [208]. Interestingly, DAPK3 does not target the same residues on Beclin1 as DAPK1, indicating a non-redundant role for DAPK3 in controlling autophagy induction. There are indications that DAPK3 is, additionally, involved in cell cycle control as it was not only shown to localise to centrosomes and the contractile ring during mitosis [209], but also interacts with cell division cycle 14A (cdc14A) phosphatase which is known to influence cell cycle progression [210].

Reminiscent of what has been reported for DAPK1, DAPK3 is thought to be a tumour suppressor as it often harbours loss of function mutations in different cancers [162], [211]. In prostate cancer DAPK3 is specifically inhibited. Thus, cancer cell survival is increased due to diminished autophagy induction [212], [213]. Remarkably, a recent study described DAPK3 to modify the ERK signalling pathway in non-small cell lung cancer, resulting in promotion of cell growth and division [214]. Hence, it is possible that, just like DAPK1, DAPK3 has a dual role in cell death and survival.

To this day, DAPK3 has not been linked to classical immune-modulatory signalling pathways, but has been described in the context of inflammation, albeit with conflicting results. DAPK3 promotes vascular inflammation in the context of hypertension by promoting p38 and Akt activity [215], but also represses inflammatory genes by phosphorylation of ribosomal protein L13a, a central regulator of inflammation [216].

This study describes DAPK3 as a potential regulator of RIG-I-mediated antiviral signalling.

1.4.3 DAPK2

DAPK2 is a 43 kDa protein and, therefore, significantly smaller than DAPK1 and slightly smaller than DAPK3 (figure 6). Its most common isoform, DAPK2α, contains, in addition to its kinase and CaM-regulatory domain, a C-terminal domain which is not homologous to any known protein [217]. Interestingly, an alternatively spliced isoform termed

DAPK2β was discovered in which the extra-catalytic part of the kinase is replaced with a sequence similar to the extra-catalytic region of DAPK3, harbouring a leucine zipper domain. DAPK2β apparently retains all of its kinase-related functions towards known DAPK2 substrates, but appears to have some DAPK3-related properties as well, such as binding of transcription factor ATF4 [218]. In this study, analyses focused on the more common DAPK2α, referred to as DAPK2 in the rest of this thesis.

As mentioned above, DAPK2 activity is increased by dephosphorylation at S318 which also enhances DAPK2 homodimerisation. Consequently, a S318D phospho-mimetic mutant is kinase inactive, whereas a S318A mutant displays increased kinase activity. The C-terminal domain of DAPK2 seems to be necessary for dimerisation and full DAPK2 activity [160], [217], [219].

Just like DAPK1 and DAPK3, DAPK2 acts as a tumour suppressor. Restoring DAPK2 expression in tumours induces apoptosis in malignant cells [220]. Additionally, DAPK2 expression is frequently reduced in hepatocellular carcinomas, but can be induced by thyroid hormone stimulation which suppresses carcinogenesis via autophagy induction [221].

Although DAPK2 can promote cell death, the extent to which it induces apoptosis is still not clear. It was reported that membrane blebbing and cell detachment after DAPK2 over-expression happened independently of caspase activation [219]. In line with this, another group showed inhibition of DAPK2 in granulocytes did not interfere with apoptosis induction and could not detect an increase in apoptotic cell death after DAPK2 over-expression [222]. DAPK2 inhibition in granulocytes, however, resulted in loss of migration due to improper polarisation. Furthermore, it was found that epithelial cancer cells were unaffected by DAPK2 over-expression as long as they were attached to the extracellular matrix (ECM), but induced apoptosis in response to DAPK2 expression when ECM attachment was lost [223]. Apoptosis induction by DAPK2 was further linked to cell polarity and cytoskeletal organisation by the finding that DAPK2 binds tubulin and promotes apoptosis after nocodazole treatment [224]. Importantly, DAPK2 activity is down-regulated by binding of anti-apoptotic 14-3-3 proteins, an interaction which is promoted by survival kinase Akt-mediated phosphorylation of DAPK2 [225], [226]. Thus, extra- and intracellular cues seem to determine if and to which extent DAPK2 promotes apoptosis. Interestingly, DAPK2 might behave similar to DAPK1 in that it might promote cell survival in some instances since tumor necrosis factor ligand superfamily member 10 (TRAIL)-induced apoptosis is increased after DAPK2 knockdown [227].

The role of DAPK2 in autophagy is less controversial. One of the first reports on DAPK2 already reported that it localised to autophagic vesicles [219], and it was later discovered that DAPK2 negatively regulates mTOR signalling by phosphorylation of raptor [228]. Moreover, a recent screening approach found that DAPK2 interacted with ATG14, a member of the Beclin1-VPS34 autophagy-promoting complex [225]. DAPK1, DAPK3, and DAPK2 seem to differently regulate cell death induction. These non-redundant mechanisms might confer increased control of cell death pathways, which, ultimately, ensures proper regulation of cellular metabolism and survival.

So far, DAPK2 has not been examined in the context of immune regulation. This study links DAPK2 activity to regulation of the RIG-I signalling pathway.

1.4.4 DRAK1 and DRAK2

DRAK1/STK17A and DRAK2/STK17B were identified by searching existing expressed sequence tag (EST) clone libraries for sequences homologous to DAPK1. Although their kinase domains display only ~50% amino acid homology to that of DAPK1, DRAKs behave similar to conventional DAPKs in that they are subject to auto-phosphorylation and phosphorylate MLC. They were also initially described to be inducers of apoptosis [163], although the exact mechanisms have not been investigated.

Interestingly, there is no DRAK1 orthologue in the mouse genome, but mouse DRAK2 was reported to behave similar to human DRAK1. Unlike DAPK1, which promotes apoptosis upstream of p53, DRAK1 seems to be a p53-induced protein which mediates cell death downstream of p53 activation [229]. However, DRAK1 can also have a dual function in that it promotes cell growth and survival, as was shown in glioblastoma where high DRAK1 expression correlates with poor prognosis [230]. Furthermore, high DRAK1 expression in head and neck cancers results in suppression of TGFβ signalling and, therefore, reduced expression of $p21^{WAF}$, leading to increased cell survival and growth [231].

Whether DRAK2, which is highly expressed in human T cells, influences TGFβ signalling is still debated. While one study described a negative feedback regulation of TGFβ signalling by DRAK2 in T cells [232], another study could not reproduce these findings using cells from DRAK2-deficient mice [233]. It seems clear, however, that DRAK2 is involved in T cell receptor signalling, most probably as a negative regulator [234], [235].

Unlike DRAK1, DRAK2 has been described in the context of viral infection. It was reported to contribute to lethal encephalitis in WNV infection as $DRAK2^{-/-}$ mice had

significantly reduced viral titres and lower numbers of T cells in the brain compared to WT mice [236]. Whether this is due a role of DRAK2 in T cell migration or pro-inflammatory responses which might influence the permeability of the blood brain barrier is not yet clear. In murine coronavirus infection DRAK2 deficiency results in increased T cell activation and memory [237].

It remains to be determined if and how DRAKs might influence innate immune signalling in response to viral infection. Some findings concerning RIG-I signalling regulation by DRAK1 are described in this study.

1.5 Cell death

To this day, several forms of programmed cell death have been identified, such as apoptosis, autophagy, necroptosis, and pyroptosis. As DAPKs have been described in the context of apoptosis and autophagy, this introduction is going to focus on these two best known and investigated types of cell death.

1.5.1 Apoptosis

The process of apoptosis has been studied extensively and is relatively well understood. It can be triggered either extrinsically, e.g. by growth factor withdrawal or ligand binding to death receptors, or intrinsically, e.g. by DNA damage. Extrinsic and intrinsic apoptotic pathways engage different effectors but both culminate in the activation of caspases, which are ubiquitously expressed as inactive zymogens. Initiator caspases, such as caspase 8 and 9, are usually activated by homodimerisation and subsequent proteolytic cleavage and will then activate effector caspases, such as caspase 3 or caspase 7 [238].

Activation of those culminates in proteolytic degradation of cellular components, resulting in membrane blebbing, cell shrinkage, chromatin condensation as well as nuclear fragmentation, all of which are typical signs of apoptosis. Apoptotic bodies produced during this process are taken up by phagocytic cells so that no intracellular molecules reach extracellular space where they could serve as inducers of inflammatory responses.

A main inducer of the intrinsic apoptotic pathway is p53 which is usually activated in response to DNA damage and will activate Bcl-2 associated X protein (BAX) or Bcl-2 homologous antagonist/killer (Bak) whose accumulation results in mitochondrial cytochrome C (cyt C) release and apoptosome formation (figure 7).

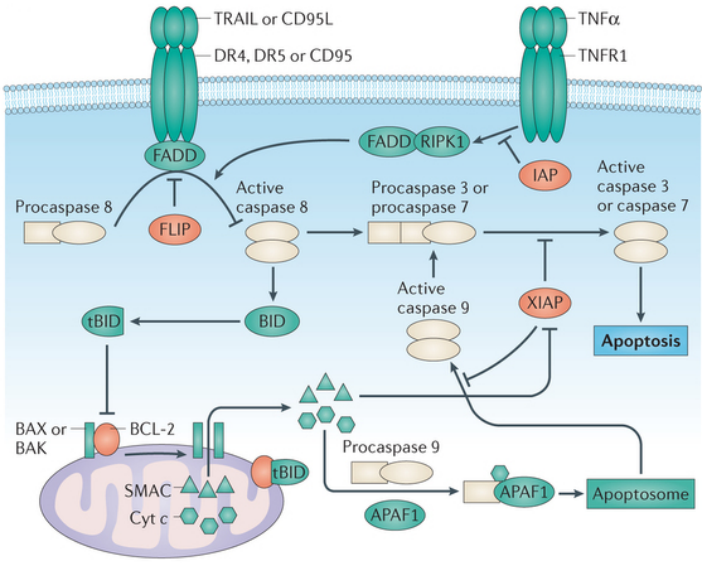

Figure 7 Overview of apoptotic pathways

Binding of ligands of cell surface receptors CD95 or tumor necrosis factor superfamily member 1A (TNFR1) activates an apoptotic cascade resulting in the activation of procaspase 8 whose activated form cleaves effector caspases 3 and 7. Intrinsic signals result in the inhibition of Bcl-2 (or Bcl-X_L) which releases Bax and Bak at the mitochondrial membranes. Pore formation by those two effectors releases cytochrome c (Cyt c) into the cytoplasm, contributing to apoptosome formation together with procaspase 9 and Apoptotic protease-activating factor 1 (APAF1). This again culminates in effector caspase activation which carry out the consecutive steps to apoptotic cell death. Inhibitors of apoptosis are highlighted in orange. Adapted from [239].

As described in the previous chapter, DAPKs promote apoptosis by different means, e.g. through interaction with p53 or promotion of cytochrome C release.

Apoptosis induction is usually measured in the extent of caspase activity. Early after its discovery, it was found that activated caspase-3 cleaves poly(ADP-ribose) polymerase (PARP) [241], a protein usually involved in sensing DNA damage and eliciting repair [242]. The accumulation of cleaved PARP (c-PARP) is, therefore, a direct measure of caspase activity and apoptosis induction.

1.5.2 Autophagy

(Macro)autophagy is a process in which proteins and organelles are degraded by engulfing them in double membrane vesicles, the autophagosomes, which later fuse with lysosomes.

Autophagy induction is inhibited by mTOR complex 1 (mTORc1) which restricts formation of the ULK1 complex necessary for isolation membrane formation, a step referred to as initiation. Consequently, inhibition of mTORc1, e.g. by small molecule inhibitors such as Torin-1 [243], will result in enhanced autophagy induction. After isolation membranes have been formed, nucleation leads to phagophore formation via a complex of activated Beclin1, VPS34, VPS15 and autophagy-related protein (ATG) 14L which locally induces phosphatidylinositol 3-phosphate (PI3P) production necessary for isolation membrane enlargement. Autophagy induction is, therefore, efficiently counteracted by inhibitors such as Spautin-1 which interfere with PI3P production [244]. In a final step, the isolation membranes are expanded by a complex consisting of ATG5,

ATG12, and ATG16, which facilitates the lipidation of microtubule-associated protein 1 light chain 3 B (MAP1LC3B or LC3B) forming phosphatidylethanolamine-conjugated LC3B-II (LC3-PE). In its unlipidated state LC3B is referred to as LC3B-I. Cleavage of LC3B by ATG4 and subsequent lipidation (figure 8) change its running behaviour in polyacrylamide gels and can, therefore, be observed on Western Blot level by a shift of LC3B to a lower molecular weight [245]. As described above, by phosphorylation of mTORc1 member Raptor, Beclin1, or ATG4, DAPKs have been shown to promote autophagy induction.

Ultimately, autophagosomes fuse with lysosomes, generating autolysosomes, in which their contents are degraded. Usually, autophagy precedes apoptosis and is detectable before phenotypic signs of apoptotic cell death are visible [246].

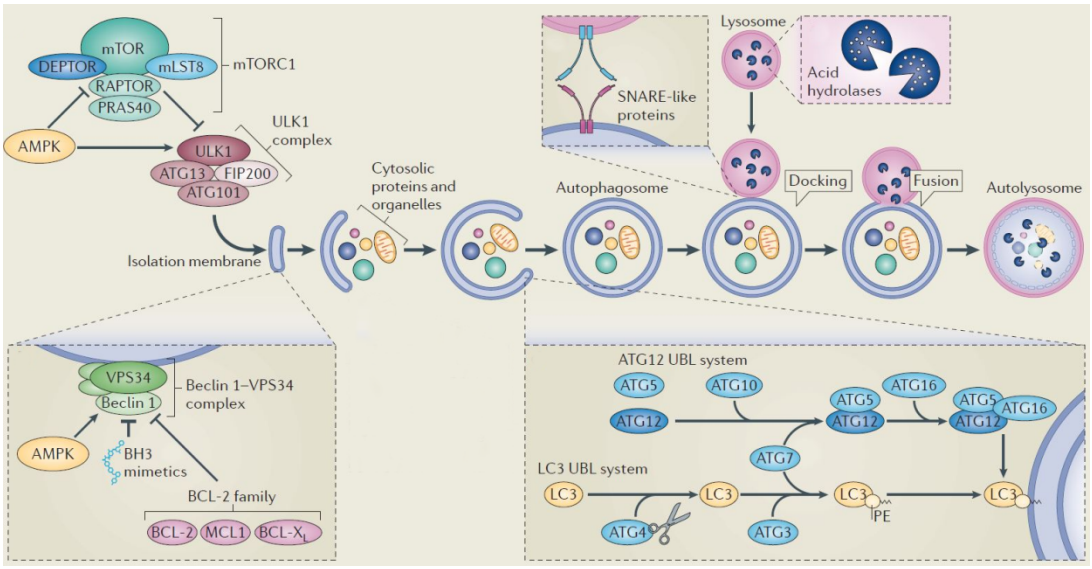

Figure 8 **Overview of autophagosome formation and degradation of cellular components in the lysosome**

Autophagosome formation starting with initiation of isolation membranes by ULK1 complex, nucleation by recruitment of PI3P-producing Beclin1-VPS34 complex, and expansion by LC3(B)-PE is shown. Active mTORc1 inhibits autophagosome formation, just as Bcl-2 family members inhibit PI3P production. Adapted from [246].

2 Material

2.1 General lab consumables

Table 1 General lab consumables

Name	Supplier
1,5 ml reaction tube	Sarstedt AG & Co., Germany
10 cm bacteria culture plate Falcon	Corning GmbH, Germany
12 well cell culture plate	Corning GmbH, Germany
15 ml Falcon	Corning GmbH, Germany
2 ml reaction tube	Sarstedt AG & Co., Germany
24 well cell culture plate	Corning GmbH, Germany
50 ml Falcon	Corning GmbH, Germany
6 well cell culture plate	Greiner Bio-One GmbH, Germany
96 well cell culture plate	Corning GmbH, Germany
96 well flat bottom plate	Corning GmbH, Germany
Cell scraper	Sarstedt AG & Co., Germany
CELLSTAR® Cell Culture Dishes 6cm	Greiner Bio-One GmbH, Germany
CELLSTAR® Cell Culture Dishes 10cm	Greiner Bio-One GmbH, Germany
CELLSTAR® Cell Culture Dishes 15cm	Greiner Bio-One GmbH, Germany
Cover slips	Glaswarenfabrik Karl Hecht GmbH, Germany
Cryo vials	Greiner Bio-One GmbH, Germany
Extra thick blotting paper	Bio-Rad Laboratories GmbH, Germany
Face mask	Rösner-Mautby Meditrade Holding GmbH, Germany
Filter 0,2 µm	GE Healthcare, USA
Filter 0,45 µm	GE Healthcare, USA
Glas slides Superfrost™	Thermo Fisher Scientific Inc., USA
Hard-Shell® 96-Well PCR Plates	Bio-Rad Laboratories GmbH, Germany
Neubauer counting chamber	Neolab, Germany
PVDF Western blot membrane	Bio-Rad Laboratories GmbH, Germany
Scalpel	B. Braun Melsungen AG, Germany
Sealing sheets PCR plates	Bio-Rad Laboratories GmbH, Germany
Stericup® 0,22 µm	Thermo Fisher Scientific Inc., USA
Stericup® 0,45 µm	Millipore, Germany
Stripetten 2, 5, 10, 25 and 50 ml	Corning GmbH, Germany
Syringe 5, 10, 20 ml	BD, Germany
Tips 10, 100 and 1000, filtered	STARLAB GmbH, Germany
Tips 10, 200 and 1000 µl, refill pack	Greiner Bio-One GmbH, Germany
Tips 10, 200 and 1000, Stecksystem	STARLAB GmbH, Germany
Whatman filter paper	GE Healthcare Life Sciences, UK
XCEED Nitrile Gloves, S	Barrier Safe Solutions International, Inc., USA

2.2 Kits

Table 2 Kits

Name	Supplier	Application
BD Cytofix/Cytoperm™	BD Biosciences, Germany	FACS stain
CalPhos™ Mammalian transfection kit	BD Biosciences, Germany	Lentiviral transduction
High-Capacity cDNA Reverse Transcription Kit with RNase Inhibitor	Thermo Fisher Scientific Inc., Germany	Reverse transcription/cDNA preparation
NucleoBond® PC 500	Macherey-Nagel GmBH & Co. KG, Germany	Plasmid purification
NucleoSpin® Gel and PCR Clean-up	Macherey-Nagel GmBH & Co. KG, Germany	Gel and PCR purification
NucleoSpin® Plasmid	Macherey-Nagel GmBH & Co. KG, Germany	Plasmid purification
NucleoSpin® RNA Plus	Macherey-Nagel GmBH & Co. KG, Germany	RNA extraction
Pierce™ BCA Protein Assay Kit	Thermo Fisher Scientic Inc., Germany	Determination of protein concentration

2.3 Chemicals and Reagents

Table 3 Chemicals and reagents

Name	Supplier
100 bp DNA ladder	Thermo Fisher Scientific Inc., USA
5x Q5® Reaction buffer	New England Biolabs GmbH, Germany
Aceton	Sigma Aldrich, Germany
Actinomycin D	Sigma Aldrich, Germany
Adenosine triphosphate	Roche, Germany
Agarose	Sigma Aldrich, Germany
Ammonium peroxydisulfate	Carl Roth GmbH & Co. KG, Germany
Anchored Oligo dT Primer	Thermo Fisher Scientific Inc, USA
Anti-HA, Agarose conjugate (beads)	Sigma Aldrich, Germany
Blasticidin S hydrochloride	AppliChem, Germany
BP clonase II Enzyme Mix	Life Technologies, Germany
BSA, IgG-free	Sigma Aldrich, Germany
BsmBI restriction enzyme	New England Biolabs GmbH, Germany
BsrGI restriction enzyme	New England Biolabs GmbH, Germany
BXT - biotin elution buffer	IBA Life Sciences, Germany
Calcium chloride dihydrate	AppliChem, Germany
Calf Intestinal Phosphatase	New England Biolabs, Germany
Calmodulin, bovine	Th Geyer, Germany
Calyculin A	Sigma Aldrich, Germany
Carbenicillin	Thermo Fisher Scientific Inc., USA
Clarity™ ECL Western Blotting Substrate	Bio-Rad Laboratories GmbH, Germany
Coelentarazine	PJK, Germany
Complete protease inhibitor cocktail	Roche, Germany
DEPC	Carl Roth GmbH & Co. KG, Germany
Dimethylsulfate	VWR International, Germany
Di-potassium phosphate	Carl Roth GmbH & Co. KG, Germany
D-Luciferin	PJK, Germany
DMEM, high glucose	Life Technologies, Germany
DMSO	Carl Roth GmbH & Co. KG, Germany
DNA Gel Loading Dye (6X)	Thermo Fisher Scientific Inc, USA
dNTPs	Peqlab, Germany
DTT	Sigma Aldrich, Germany
ECL Plus Western Blot Detection System	PerkinElmer, Germany
EDTA	AppliChem, Germany
Effectene transfection reagent	Qiagen, Germany
EGTA	AppliChem, Germany
Ethanol	Sigma Aldrich, Germany
Expand Reverse Transcriptase System	Roche, Mannheim
Fetal Calf serum (FCS)	PAA Laboratories, USA
FideliTaq	USB, USA
Gamma-32-ATP	PerkinElmer, Germany
Geneticin (G418) sulfate	Santa Cruz Biotechnology, Inc, USA
Gentamicin	Life Technologies, Germany
Gibson Assembly® Master Mix	New England Biolabs GmbH, Germany
Glycerol	Sigma Aldrich, Germany
HEPES	Carl Roth GmbH & Co. KG, Germany
Isopropanol	Sigma Aldrich, Germany
iTaq™ Universal SYBR® Green Supermix	Bio-Rad Laboratories GmbH, Germany
Kanamycin	Serva, Germany
Lambda DNA/Eco1301 (StyI) Marker	AppliChem, Germany
Lipofectamine 2000	Life Technologies, Germany
Lipofectamine RNAiMax	Life Technologies, Germany
LR clonase II Enzyme Mix	Life Technologies, Germany
Magnesium chloride hexahydrate	Merck Millipore, Germany
Magnesium sulfate heptahydrate	Merck Millipore, Germany
MagStrep "type3" XT Beads	IBA Life Sciences, Germany

MEM Non-essential amino acids	Life Technologies, Germany
Methanol	Sigma Aldrich, Germany
Midori Green	Nippon Genetics Europe GmbH, Germany
Milk powder, blotting grade	Carl Roth GmbH & Co. KG, Germany
NEBuffer Set 1.1, 2.1, 3.1 and Cutsmart	New England Biolabs GmbH, Germany
Nonidet P-40	AppliChem, Germany
OptiMEM	Life Technologies, Germany
Paraformaldehyde, ultrapure	Merck Millipore, Germany
Penicillin/Streptomycin	Life Technologies, Germany
Pepton	Sigma Aldrich, Germany
Poly(I:C)	Sigma Aldrich, Germany
Poly(I:C), HMW	InvivoGen, France
Potassium dihydrogen phosphate	AppliChem, Germany
Precision Plus Protein™ Dual Color Standard	Bio-Rad Laboratories GmbH, Germany
Purified recombinant RIG-I	Joseph Marcotrigiano, NIH, Bethesda, USA
Puromycin	Sigma Aldrich, Germany
Q5® High-Fidelity DNA Polymerase	New England Biolabs GmbH, Germany
Q-VD-OPh	Biomol GmbH, Germany
rNTPs	Roche, Germany
Rotiphorese® Gel 40 (29:1)	Carl Roth GmbH & Co. KG, Germany
Sodium chloride	Sigma Aldrich, Germany
Sodium fluoride	Sigma Aldrich, Germany
Spautin-1	Sigma Aldrich, Germany
Spectinomycin	Merck Millipore, Germany
Staurosporine	Biomol GmbH, Germany
Sulfuric acid	Carl Roth GmbH & Co. KG, Germany
T4 DNA-Ligase	Thermo Fisher Scientific Inc., USA
T4 Polynucleotide Kinase	Thermo Fisher Scientific Inc., USA
TEMED	AppliChem, Germany
Torin-1	Sigma Aldrich, Germany
Triton-X-100	AppliChem, Germany
Trypsin-EDTA (0.05%)	Thermo Fisher Scientific, Germany
Tween-20	AppliChem, Germany
Zeocin	Thermo Fisher Scientific Inc., Germany
β-mercapthoethanol	Sigma Aldrich, Germany

2.4 Instruments

Table 4 Instruments

Name	Supplier
Analytical balance LP-3102	VWR International GmbH, Germany
Analytical fine balance LA-124i	VWR International GmbH, Germany
BD Accuri™ C6 Flow cytometer	BD Biosciences, Germany
Biological safety cabinet Safe 2020	Thermo Fisher Scientific, Germany
C1000 Touch Termal Cycler	Bio-Rad Laboratories GmbH, Germany
Centrifuge 5424	Eppendorf AG, Germany
Centrifuge 5424 R	Eppendorf AG, Germany
Centrifuge 5810 R	Eppendorf AG, Germany
Centrifuge HeraeusMultifuge 3S-R	Thermo Fisher Scientific, Germany
Centrifuge Sorvall RC-5C plus	Sorvall, Germany
CFX Connect™ Real-Time PCR Detection System	Bio-Rad Laboratories GmbH, Germany
CO_2 Cell Incubator MCO-20AIC	Panasonic Healthcare Co., Ltd., Japan
Counting chambers	Brand, Germany
ECL ChemoCam imager 3.2	INTAS Science Imaging Instruments, Germany
Electric Power Supply EPI 500/400	Amersham Pharmacia Biotech, Germany
ELISA plate reader Multiskan Ex	Thermo Fisher Scientific, USA
Freezer Liebherr Premium	Liebherr-International Deutschland GmbH, Germany
Fridge Med Line	Liebherr-International Deutschland GmbH, Germany
Gel-iX-imager	Intas Science Imaging Instruments, Germany

Heidolph Duomax 1030	Heidolph Instruments GmbH & Co. KG, Germany
HI-2211 Bench Top pH & mV Meter	HANNA instruments Deutschland GmbH, Germany
Ikamag Reo Magnetic stirrer	IKA®-Werke GmbH & CO. KG, Germany
Immunofluorescence Microscope	Leica CTR MIC Leica, Germany
Microfuge B	Beckman, Germany
Microscope Primovert	Zeiss, Germany
MicrowaveOven	CLAtronic, Germany
Mini-PROTEAN® Tetra Handcast Systems	Bio-Rad Laboratories GmbH, Germany
Mini Trans-Blot® Cell	Bio-Rad Laboratories GmbH, Germany
Mini-PROTEAN® Tetra Vertical Electrophoresis Cell	Bio-Rad Laboratories GmbH, Germany
Mithras LB 940 Multimode Microplate Reader	Berthold Technologies, Germany
Mithras² LB 943 Multimode reader	Berthold Technologies, Germany
Multi-Axle Rotating mixer	NeoLab, Germany
Multi-channel pipette 10-100	Eppendorf, Germany
Multi-channel pipette 10-300	Eppendorf, Germany
NanoDrop NP-1000	Thermo Fisher Scientific, Germany
neoLab Mini Vacuum pump and compressor	NeoLab, Germany
PerfectBlue™ Gelsystem Mini S	VWR International, Germany
Pipetboy Acu 2	Integra Biosciences GmbH, Germany
Pipette P10	Eppendorf AG, Germany
Pipette P1000	Eppendorf AG, Germany
Pipette P20	Eppendorf AG, Germany
Pipette P200	Eppendorf AG, Germany
PowerPac™ Basic	Bio-Rad Laboratories GmbH, Germany
PowerPac™ Hc	Bio-Rad Laboratories GmbH, Germany
ThermoForma Incubator 3862	Labotect, Germany
Thermomixer Comfort 1.5 ml	Eppendorf AG, Germany
Thermomixer F1.5	Eppendorf AG, Germany
Trans-Blot® SD Cell	Bio-Rad Laboratories GmbH, Germany
Trans-Blot® Turbo™ System	Bio-Rad Laboratories GmbH, Germany
UV Transilluminator	VilberLourmat, Germany
Vacuubrand BVC professional	Vacuubrand GmbH & Co. KG, Germany
Vortex Genie 2	Scientific Industries Inc., USA
Waterbath GFL 1083	GFL, Germany

2.5 Software

Table 5 Software

Name	Supplier	Application
(Fiji Is Just) ImageJ	Wayne Rasband, NIH, USA (imagej.nih.gov/ij) [247]	Western Blot evaluation and figure generation
Bio-Rad CFX Manager	Bio-Rad Laboratories, Hercules, California, USA	qRT-PCR evaluation and quantification
FlowJo V10	FlowJo LLC, Ashland, Oregon, USA	Flow cytometry evaluation
GraphPad Prism 7	GraphPad Software, San Diego, California, USA	Generation of graphs and figures
Inkscape: Open Source Scalable Vector Graphics Editor, 0.91	Inkscape Community (Open Source, www.inkscape.org)	Generation of figures and vector graphics
INTAS Chemostar	INTAS Science Imaging, Göttingen, Germany	Western Blot picture acquisition
Labimage1D	INTAS Science Imaging, Göttingen, Germany	Western Blot quantification
Microsoft Office 2010	Microsoft, Redmond, USA	Documentation, Calculation, Data presentation
SnapGene	GSL Biotech LLC, Chicago, Illinois, USA	Plasmid design and *in silico* cloning
Zotero (Mozilla Firefox extension)	Roy Rosenzweig Center for History and New Media, George Mason University, Fairfax, Virginia, USA	Citation management and bibliography

2.6 Cells

2.6.1 Eukaryotic cells

Table 6 Eukaryotic cells

Name	Resistance	Description
293T DKFZ	-	Parental cell line for 293T^{RIG-I} and 293T^{MDA5}
293T MCB	-	Lentiviral particle production
293T^{RIG-I}	Blasticidin	-
293T^{MDA5}	Blasticidin	-
293T^{RIG-I} lenticrisp empty puro	Blasticidin, Puromycin	Empty vector control for CRISPR/Cas9 DAPK1 or DAPK3 single KO cells
293T^{RIG-I} lenticrisp empty puro/hygro	Blasticidin, Puromycin, Hygromycin	Empty vector control for CRISPR/Cas9 DAPK1/DAPK3 double KO cells
293T^{RIG-I} lenticrisp empty puro/hygro/zeo	Blasticidin, Puromycin, Hygromycin, Zeocin	Empty vector control for CRISPR/Cas9 DAPK1/DAPK3/DAPK2 triple KO cells
293T^{RIG-I} lenticrisp empty zeo	Blasticidin, Zeocin	Empty vector control for CRISPR/Cas9 DAPK2 single KO cells
293T^{RIG-I} DAPK1_crisp [*1-4*]	Puromycin	DAPK1 KO bulk [*sgRNA 1-4*]
293T^{RIG-I} DAPK1 [*clone number*]	Blasticidin, Puromycin	DAPK1 KO single cell clone [*number*]
293T^{RIG-I} DAPK3_crisp [*1-4*]	Puromycin	DAPK3 KO bulk [*sgRNA 1-4*]
293T^{RIG-I} DAPK3 [*clone number*]	Blasticidin, Puromycin	DAPK3 KO single cell clone [*number*]
293T^{RIG-I} DAPK2_crisp[*1-4*]	Blasticidin, Zeocin	DAPK2 KO bulk [*sgRNA 1-4*]
293T^{RIG-I} DAPK1/DAPK3_crisp [*1-4*]	Blasticidin, Puromycin, Hygromycin	DAPK1/DAPK3 KO bulk [*sgRNA 1-4*]
293T^{RIG-I} DAPK1/DAPK3 [*clone number*]	Blasticidin, Puromycin, Hygromycin	DAPK1/DAPK3 KO single cell clone [*number*]
293T^{RIG-I} DAPK1/DAPK3/DAPK2_crisp[*1-4*]	Blasticidin, Puromycin, Hygromycin, Zeocin	DAPK1/DAPK3/DAPK2 triple KO bulk [*sgRNA 1-4*]
Huh7 Lunet CD81^{high}	G418	HCV replication assays
Huh7 Lunet CD81^{high} MAVS-GFP$_{NLS}$	G418, Blasticidin	HCV replication assays, localisation of GFP to nucleus after infection
A549	-	-
A549 lenticrisp empty puro	Puromycin	Empty vector control for CRISPR/Cas9 DAPK1 or DAPK3 single knockout cells
A549 lenticrisp empty puro/hygro	Puromycin, Hygromycin	Empty vector control for CRISPR/Cas9 DAPK1/DAPK3 double knockout cells
A549 lenticrisp empty puro/hygro/zeo	Puromycin, Hygromycin, Zeocin	Empty vector control for CRISPR/Cas9 DAPK1/DAPK3/DAPK2 triple knockout cells
A549 lenticrisp empty zeo	Zeocin	Empty vector control for CRISPR/Cas9 DAPK2 single knockout cells
A549 DAPK1_crisp [*1-4*]	Puromycin	DAPK1 KO bulk [*sgRNA 1-4*]
A549 DAPK1 [*clone number*]	Puromycin	DAPK1 KO single cell clone [*number*]
A549 DAPK3_crisp [*1-4*]	Puromycin	DAPK3 KO bulk [*sgRNA 1-4*]
A549 DAPK3 [*clone number*]	Puromycin	DAPK3 KO single cell clone [*number*]
A549 DAPK2_crisp[*1-4*]	Zeocin	DAPK2 KO bulk [*sgRNA 1-4*]
A549 DAPK1/DAPK3_crisp [*1-4*]	Puromycin, Hygromycin	DAPK1/DAPK3 KO bulk [*sgRNA 1-4*]
A549 DAPK1/DAPK3 [*clone number*]	Puromycin, Hygromycin	DAPK1/DAPK3 KO single cell clone [*number*]
A549 DAPK1/DAPK3/DAPK2_crisp[*1-4*]	Puromycin, Hygromycin, Zeocin	DAPK1/DAPK3/DAPK2 triple KO bulk [*sgRNA 1-4*]
HeLa	-	Provided by Felix Hoppe-Seyler, DKFZ Heidelberg

2.6.2 Bacteria

Gateway® destination and entry vectors harbouring the ccdB gene were amplified in One Shot® ccdB Survival™ 2 T1R Chemically Competent cells (Invitrogen).

For general cloning and retransformation *E. coli* strain DH5α was used.

2.7 Viruses

Table 7 Viruses

Name	Description	Origin
SeV	-	Rainer Zawatzky, DKFZ Heidelberg
Influenza A Virus	WSN/1933 (H1N1)	Georg Kochs, Albert-Ludwigs University Freiburg
RVFV	ΔNSs_Rluc, NSs was replaced with Renilla luciferase gene	Friedemann Weber (Justus-Liebig University Gießen)
HCV	JcR2A, genotype 2 harbouring a Renilla luciferase gene	-

2.8 DNA and RNA oligos

2.8.1 Primers for cloning

2.8.1.1 DAPK1 mutants

Table 8 Primers for DAPK1 mutants

Name	Sequence (5' – 3')	Description
DAPK1 FL fw	*GGGGACAAGTTTGTACAAAAAAGCAGGCTTC*ATG ACCGTGTTCAGGCAGG	$DAPK1^{KCA}$
DAPK1 Ank1 rev	*GGGGACCACTTTGTACAAGAAAGCTGGGTC*CTAC GCCTCAACGCTGGCTCCCATCAGAC	$DAPK1^{KCA}$
DAPK1 S308A fw	GAAAAAATGGAAACAAGCCGTTCGCTTGATATC	$DAPK1^{KCA\ S308A}$ overlap PCR
DAPK1 S308A rev	GATATCAAGCGAACGGCTTGTTTCCATTTTTT	$DAPK1^{KCA\ S308A}$ overlap PCR
DAPK1 S308D fw	GAAAAAATGGAAACAAGACGTTCGCTTGATATC	$DAPK1^{KCA\ S308D}$ overlap PCR
DAPK1 S308D rev	GATATCAAGCGAACGTCTTGTTTCCATTTTTTC	$DAPK1^{KCA\ S308D}$ overlap PCR
DAPK1 K42A fw	GCCTCCAGTATGCCGCCGCATTCATCAAAAAAG	$DAPK1^{KCA\ K42A}$ overlap PCR
DAPK1 K42A rev	CTTTTCTTGATGAATGCGGCGGCATACTGGAGGC	$DAPK1^{KCA\ K42A}$ overlap PCR
DAPK1 S289E fw	CAGGCACTTAGTAGAAAAGCAGAGGCAGTAAACA TGGAGAAATTC	$DAPK1^{S289E}$ overlap PCR
DAPK1 S289E rev	GAATTTCTCCATGTTTACTGCCTCTGCTTTTCTAC TAAGTGCCTG	$DAPK1^{S289E}$ overlap PCR
DAPK1 S289A fw	CAGGCACTTAGTAGAAAAGCAGCCGCAGTAAACA TGGAGAAATTC	$DAPK1^{S289A}$ overlap PCR
DAPK1 S289A rev	GAATTTCTCCATGTTTACTGCGGCTGCTTTTCTAC TAAGTGCCTG	$DAPK1^{S289A}$ overlap PCR
DAPK1 Y491F fw	CTGTGCTGCTTGGCACGGCTTCTACTCTGTGGCC AAAGCCCTTTG	$DAPK1^{Y491F}$ overlap PCR
DAPK1 Y491F rev	CAAAGGGCTTTGGCCACAGAGTAGAAGCCGTGC CAAGCAGCACAG	$DAPK1^{Y491F}$ overlap PCR
DAPK1 Y492F fw	GTGCTGCTTGGCACGGCTATTTCTCTGTGGCCAA AGCCCTTTGTG	$DAPK1^{Y492F}$ overlap PCR
DAPK1 Y492F rev	CACAAAGGGCTTTGGCCACAGAGAAATAGCCGTG CCAAGCAGCAC	$DAPK1^{Y492F}$ overlap PCR
DAPK1 Y491E fw	GCACTGTGCTGCTTGGCACGGCGAGTACTCTGTG GCCAAAGCCCTTTG	$DAPK1^{Y491E}$ overlap PCR
DAPK1 Y491E rev	CAAAGGGCTTTGGCCACAGAGTACTCGCCGTGC CAAGCAGCACAGTGC	$DAPK1^{Y491E}$ overlap PCR
DAPK1 Y492E fw	GTGCTGCTTGGCACGGCTATGAGTCTGTGGCCAA AGCCCTTTGTG	$DAPK1^{Y492E}$ overlap PCR

DAPK1 Y492E rev	CACAAAGGGCTTTGGCCACAGACTCATAGCCGTG CCAAGCAGCAC	DAPK1^{Y492E} overlap PCR
DAPK1 Y491F/Y492F fw	CCTGCACTGTGCTGCTTGGCACGGCTTCTTCTCT GTGGCCAAAGCCCTTTGTGAAG	DAPK1$^{Y491/492F}$ overlap PCR
DAPK1 Y491F/Y492F rev	CTTCACAAAGGGCTTTGGCCACAGAGAAGAAGCC GTGCCAAGCAGCACAGTGCAGG	DAPK1$^{Y491/492F}$ overlap PCR
DAPK1 Y491E/Y492E fw	CCCTGCACTGTGCTGCTTGGCACGGCGAGGAGT CTGTGGCCAAAGCCCTTTGTGAAGC	DAPK1$^{Y491/492E}$ overlap PCR
DAPK1 Y491E/Y492E rev	GCTTCACAAAGGGCTTTGGCCACAGACTCCTCGC CGTGCCAAGCAGCACAGTGCAGGG	DAPK1$^{Y491/492E}$ overlap PCR

2.8.1.2 DAPK2 cDNA and mutants

DAPK2 full-length coding sequence was cloned from A549 cDNA.

Table 9 Primers for DAPK2 mutants

Name	Sequence (5' – 3')	Description
DAPK2 fw	*GGGGACAAGTTTGTACAAAAAAGCAGGCTTC*ATG TTCCAGGCCTCAATGAGG	Gateway cloning of DAPK2 WT
DAPK2 rev	*GGGGACCACTTTGTACAAGAAAGCTGGGTC*TTAG GAGGTGCTGCTCCTCC	Gateway cloning of DAPK2 WT
DAPK2 KD fw	*GGGGACAAGTTTGTACAAAAAAGCAGGCTTC*ATG TATGACATCGGAGAGGAGCTGGGG	DAPK2^{Kinase}
DAPK2 KD rev	*GGGGACCACTTTGTACAAGAAAGCTGGGTC*TCAG ATCCAGGGGTGTCTGAGAGCC	DAPK2^{Kinase}
DAPK2 Kinase-CaM rev	*GGGGACCACTTTGTACAAGAAAGCTGGGTC*TCAC AGGTCCTCATCCGGCCTCAGG	DAPK2$^{Kinase-CaM}$
DAPK2 K52A fw	GGGGCTTGAGTATGCAGCCGCCTTCATCAAGAAG CGGCAG	DAPK2^{K52A} overlap PCR
DAPK2 K52A rev	CTGCCGCTTCTTGATGAAGGCGGCTGCATACTCA AGCCCC	DAPK2^{K52A} overlap PCR
DAPK2 S318A fw	GCAGGCGGTGGAAGCTTGCCTTCAGCATCGTGT CCCTGTGC	DAPK2^{S318A} overlap PCR
DAPK2 S318A rev	GCACAGGGACACGATGCTGAAGGCAAGCTTCCA CCGCCTGC	DAPK2^{S318A} overlap PCR
DAPK2 S318D fw	GCAGGCGGTGGAAGCTTGACTTCAGCATCGTGTC CCTGTGC	DAPK2^{S318D} overlap PCR
DAPK2 S318D rev	GCACAGGGACACGATGCTGAAGTCAAGCTTCCAC CGCCTGC	DAPK2^{S318D} overlap PCR

2.8.1.3 DAPK3 mutants

The pENTR223 plasmid harbouring the DAPK3 coding sequence (open conformation) was obtained from the DKFZ GPCF clone repository.

Table 10 Primers for DAPK3 mutants

Name	Sequence (5' – 3')	Description
ZIPK fw	*GGGGACAAGTTTGTACAAAAAAGCAGGCTTC*ATG TCCACGTTCAGGCAGGAGGAC	Gateway cloning of DAPK3 WT
ZIPK rev	*GGGGACCACTTTGTACAAGAAAGCTGGGTC*CTAG CGCAGCCCGCACTCC	Gateway cloning of DAPK3 WT
DAPK3 KD fw	*GGGGACAAGTTTGTACAAAAAAGCAGGCTTC*ATG TATGAGATGGGGGAGGAG	DAPK3^{Kinase}
DAPK3 KD rev	*GGGGACCACTTTGTACAAGAAAGCTGGGTC*TCAA ATCCAGGAATGTTCCAGGC	DAPK3^{Kinase}
DAPK3 delta KD fw	*GGGGACAAGTTTGTACAAAAAAGCAGGCTTC*ATG AAGGCGATCCGGCGGCGGAAC	DAPK3$^{delta\ Kinase}$
DAPK3 delta LZ rev	*GGGGACCACTTTGTACAAGAAAGCTGGGTC*TCAT TGCTTGGCCAGCGCCTCG	DAPK3$^{delta\ Leucine\ zipper}$

DAPK3 K42A fw	GCAAGGAGTACGCAGCCGCCTTCATCAAGAAGC GCCGCCT	DAPK3^{K42A} overlap PCR
DAPK3 K42A rev	AGGCGGCGCTTCTTGATGAAGGCGGCTGCGTAC TCCTTGC	DAPK3^{K42A} overlap PCR
DAPK3 D161A fw	CACGAATCAAGCTCATCGCCTTCGGCATCGCGCA CAAGATC	DAPK3^{D161A} overlap PCR
DAPK3 D161A rev	GATCTTGTGCGCGATGCCGAAGGCGATGAGCTT GATTCGTG	DAPK3^{D161A} overlap PCR

2.8.1.4 DRAK1 from cDNA

The pENTR221 plasmid harbouring the DRAK2/STK17B coding sequence (closed conformation) was obtained from the DKFZ GPCF clone repository. DRAK1 full-length coding sequence was cloned from A549 cDNA.

Table 11 Primers for DRAK1 cloning

Name	Sequence (5' – 3')	Description
DRAK1 fw	*GGGGACAAGTTTGTACAAAAAAGCAGGCTTC*ATG ATCCCTTTGGAGAAGCC	Gateway cloning of DRAK1
DRAK1 rev	*GGGGACCACTTTGTACAAGAAAGCTGGGTC*tcagta gataaattctcctggaatttcttg	Gateway cloning of DRAK1

2.8.1.5 Cloning of Lenticispr v2 with different antibiotic resistance

Different antibiotic resistance genes were cloned into Lenticrispr v2 plasmid using NEB Gibson Assembly®. Hygromycin resistance gene had to be codon adjusted due to BsmBI cleavage site within the resistance gene.

Table 12 Lenticrispr primer

Name	Sequence (5' – 3')	Description
Lenticrisp bb fw	ACGCGTTAAGTCGACAATC	Gibson assembly amplification of backbone
Lenticrisp bb rev	CGGTCCAGGATTCTCTTC	Gibson assembly amplification of backbone
Hygro fw	GAGAATCCTGGACCGAAAAAGCCTGAA CTCACC	Amplification of Hygromycin resistance gene
Hygro rev	TGTCGACTTAACGCGTCTATTCCTTTGC CCTCGG	Amplification of Hygromycin resistance gene
Val_mut_ovlp fw	CGAAAAGTTCGACAGCGTGTCCGACCT GATGCAGC	Elimination of BsmBI cleavage site
Val_mut_ovlp rev	GCTGCATCAGGTCGGACACGCTGTCG AACTTTTCG	Elimination of BsmBI cleavage site
Zeo fw	GAGAATCCTGGACCGGCCAAGTTGACC AGTGCC	Amplification of Zeocin resistance gene
Zeo rev	TGTCGACTTAACGCGTTTACGTACGGT CCTGCTC	Amplification of Zeocin resistance gene

2.8.2 CRISPR/Cas9 KO sgRNA oligos

Table 13 sgRNA oligos

Name	Sequence (5' – 3')	Description
DAPK1_crisp1 fw	CACCTGATTACTACGACACCGGCG	Generation of DAPK1 KO
DAPK1_crisp1 rev	AAACCGCCGGTGTCGTAGTAATCA	Generation of DAPK1 KO
DAPK1_crisp2 fw	CACCGTGGATGATTACTACGACAC	Generation of DAPK1 KO
DAPK1_crisp2 rev	AAACGTGTCGTAGTAATCATCCAC	Generation of DAPK1 KO
DAPK1_crisp3 fw	CACCTTACCTGCCAAGTTCCTCGC	Generation of DAPK1 KO
DAPK1_crisp3 rev	AAACGCGAGGAACTTGGCAGGTAA	Generation of DAPK1 KO

DAPK1_crisp4 fw	CACCCGTGTTCAGGCAGGAAAACG	Generation of DAPK1 KO
DAPK1_crisp4 rev	AAACCGTTTTCCTGCCTGAACACG	Generation of DAPK1 KO
DAPK2_crisp1 fw	CACCGGACTTTTATGACATCGGAG	Generation of DAPK2 KO
DAPK2_crisp1 rev	AAACCTCCGATGTCATAAAAGTCC	Generation of DAPK2 KO
DAPK2_crisp2 fw	CACCGTATGTTCCAGGCCTCAATG	Generation of DAPK2 KO
DAPK2_crisp2 rev	AAACCATTGAGGCCTGGAACATAC	Generation of DAPK2 KO
DAPK2_crisp3 fw	CACCGGAGCCATTCAAGCAGCAGA	Generation of DAPK2 KO
DAPK2_crisp3 rev	AAACTCTGCTGCTTGAATGGCTCC	Generation of DAPK2 KO
DAPK2_crisp4 fw	CACCGTGGAGGACTTTTATGACAT	Generation of DAPK2 KO
DAPK2_crisp4 rev	AAACATGTCATAAAAGTCCTCCAC	Generation of DAPK2 KO
DAPK3_crisp1 fw	CACCCCATGTCCACGTTCAGGCAG	Generation of DAPK3 KO
DAPK3_crisp1 rev	AAACCTGCCTGAACGTGGACATGG	Generation of DAPK3 KO
DAPK3_crisp2 fw	CACCCATGTCCACGTTCAGGCAGG	Generation of DAPK3 KO
DAPK3_crisp2 rev	AAACCCTGCCTGAACGTGGACATG	Generation of DAPK3 KO
DAPK3_crisp3 fw	CACCCGGCCGCCATGTCCACGTTC	Generation of DAPK3 KO
DAPK3_crisp3 rev	AAACGAACGTGGACATGGCGGCCG	Generation of DAPK3 KO
DAPK3_crisp4 fw	CACCCCGGCCGCCATGTCCACGTT	Generation of DAPK3 KO
DAPK3_crisp4 rev	AAACAACGTGGACATGGCGGCCGG	Generation of DAPK3 KO

2.8.3 Primers for qRT-PCR

Table 14 qRT-PCR primers

Name	Sequence (5' – 3')
DAPK1 fw	TGGCCATGCTGACGTGGCTC
DAPK1 rev	GGCTGTCAGGAGGGGCGTCT
DAPK2 fw	GGCTCACAATCCAAGAGGCT
DAPK2 rev	CTCACAGTTCCTCAGGTCCTC
DAPK3 fw	GTGGAGCATCGGTGTCATCA
DAPK3 rev	ATGGTCATTCTCCGCTTGGG
IFNβ fw	GACGCCGCATTGACCATCTA
IFNβ rev	GACATTAGCCAGGAGGTTCTC
ISG56 (IFIT1) fw	GAAGCAGGCAATCACAGAAA
ISG56 (IFIT1) rev	GAAACCGACCATAGTGGAA
GAPDH fw	GAAGGTGAAGGTCGGAGC
GAPDH rev	CAAGATGGTGATGGGATTTC

2.9 Plasmids

Table 15 Plasmids

Name	Tag	Backbone	Prokaryotic resistance	Eukaryotic resistance
DAPK1 (WT and mutants)	HA	pcDNA5	AMP	Hygromycin
DAPK1_crisp1	-	Lenticrispr v2	AMP	Puromycin
DAPK1_crisp2	-	Lenticrispr v2	AMP	Puromycin
DAPK1_crisp3	-	Lenticrispr v2	AMP	Puromycin
DAPK1_crisp4	-	Lenticrispr v2	AMP	Puromycin
DAPK2 (WT and mutants)	HA	pcDNA5	AMP	Hygromycin
DAPK2_crisp1	-	Lenticrispr v2	AMP	Zeocin
DAPK2_crisp2	-	Lenticrispr v2	AMP	Zeocin
DAPK2_crisp3	-	Lenticrispr v2	AMP	Zeocin
DAPK2_crisp4	-	Lenticrispr v2	AMP	Zeocin
DAPK3 (WT and mutants)	HA	pcDNA5	AMP	Hygromycin
DAPK3_crisp1	-	Lenticrispr v2	AMP	Hygromycin
DAPK3_crisp1	-	Lenticrispr v2	AMP	Puromycin
DAPK3_crisp2	-	Lenticrispr v2	AMP	Hygromycin
DAPK3_crisp2	-	Lenticrispr v2	AMP	Puromycin
DAPK3_crisp3	-	Lenticrispr v2	AMP	Hygromycin

DAPK3_crisp3	-	Lenticrispr v2	AMP	Puromycin
DAPK3_crisp4	-	Lenticrispr v2	AMP	Hygromycin
DAPK3_crisp4	-	Lenticrispr v2	AMP	Puromycin
IFIT1 Firefly	-	pGL3	AMP	-
IRF3 5D		pcDNA3.1	AMP	G418
Lenticrispr empty hygro	-	Lenticrispr v2	AMP	Hygromycin
Lenticrispr empty puro	-	Lenticrispr v2 (Addgene: 52961)	AMP	Puromycin
Lenticrispr empty zeo	-	Lenticrispr v2	AMP	Zeocin
MAVS	Lumio V5	pcDNA6.2	AMP	Blasticidin
NFκB Firefly	-	pGL4.32	AMP	-
pcDNA3.1 (mock)	-	pcDNA3.1	AMP	G418
psPAX2	-	-	AMP	-
pDONR207	-	pDONR207	Genta	-
pDONR221 STK17B closed		pDONR221	Kana	-
pDONR223 DAPK3 open	-	pDONR223	Spec	-
pMD2.G	-	-	AMP	-
Renilla CMV	-	pcDNA3.1	AMP	G418
Renilla SV40	-	pRL	AMP	-
RIG-I	Lumio V5	pcDNA6.2	AMP	Blasticidin
RIG-I CA	Lumio V5	pcDNA6.2	AMP	Blasticidin
DRAK2 WT in Gateway		pENTR221	Kana	
DAPK3 WT in Gateway		pENTR223	Spec	-

2.9.1 siRNAs

Table 16 siRNAs

Name	Target sequence (5' – 3')	Supplier
Hs_DAPK1_5	AAGCATGTAATGTTAATGTTA	Qiagen, Germany
Hs_DAPK1_6	CGGCTATTACTCTGTGGCCAA	Qiagen, Germany
DAPK1 sig1 (SASI_Hs01_00238227)	GAATTAAGCTCAAGCTGTT	Sigma Aldrich, Germany
DAPK1 sig2 (SASI_Hs01_00238226)	CAACTATGATGTTAACCAA	Sigma Aldrich, Germany
DAPK1 sig3 (SASI_Hs01_00238225)	GAGAATCGATGTCCAGGAT	Sigma Aldrich, Germany
DAPK2 sig1 (SASI_Hs01_00206406)	CTTTGGTCTGGCTCACGAA	Sigma Aldrich, Germany
DAPK2 sig2 (SASI_Hs01_00206405)	CGGAATTTGTTGCTCCAGA	Sigma Aldrich, Germany
DAPK2 sig3 (SASI_Hs01_00206404)	CAAAGCTCTTAATTCTCCA	Sigma Aldrich, Germany
Hs_DAPK3_3	CCCAGAGATTGTGAACTATGA	Qiagen, Germany
DAPK3 sig1 (SASI_Hs01_00020911)	GCTACGAGGCGCTGGCCAA	Sigma Aldrich, Germany
DAPK3 sig2 (SASI_Hs01_00020910)	CAGAGATTGTGAACTATGA	Sigma Aldrich, Germany
DAPK3 sig3 (SASI_Hs01_00020912)	CACGACATCTTCGAGAACA	Sigma Aldrich, Germany
Hs_PI4KCA_12	N/A	Qiagen, Germany

2.10 Buffers and solutions

Table 17 Buffers and solutions

Name	Recipe
1% Paraformaldehyde solution	4% paraformaldehyde solution diluted in PBS
4% Paraformaldehyde solution	4g paraformaldehyde dissolved with simultaneous stirring at 60°C in 100 ml PBS
6x Laemmli buffer	9,75 ml Tris 0,5M (pH6.8), 15 ml Glycerol, 15 ml 10% SDS, 3,75 ml β-mercaptoethanol, 30 mg Bromophenol blue, 6.5 ml H_2O
Ampicillin stock solution (100 mg/ml)	100 mg/ml Ampicillin in ddH2O, sterile-filtered and stored at -20 °C
Coelenterazine stock (1nM)	5 mg Coelenterazine in 11.8 ml Methanol
Co-IP lysis buffer (HA-IP)	20 mM Tris (pH 7.6), 100 mM NaCl, 1% NP-40, 50 mM NaF, protease inhibitor tablet (Roche)
Co-IP lysis buffer (Strep-IP)	20 mM Tris (pH 7.6), 300 mM NaCl, 1% NP-40, 50 mM NaF, protease inhibitor tablet (Roche)
Cryo freezing medium (20% DMSO)	40 ml FCS + 10 ml DMSO
D-Luciferine stock (1mM)	84.1mg D-luciferin in 300ml, 25mM Glycylglycine
DMEM standard cell culture medium	Dulbecco's Modified Eagle Medium (High Glucose) containing 1x nonessential amino acids, 1% Penicillin/Streptomycin, 10% (v/v) Fetal Calf Serum (heat inactivated at 56 °C for 30 min)
DMEM w/o Pen-Strep	Dulbecco's Modified Eagle Medium (High Glucose) containing 1x nonessential amino acids 10%, (v/v) Fetal Calf Serum (heat inactivated at 56 °C for 30 min)
Glycylglycine (0.5M) for Luciferase buffer	33.03 g Glycylglycine (132.12 g/mol) in 500 ml H_2O adjust pH to 7.8 using KOH
***In vitro* kinase assay buffer (2X)**	100 mM HEPES pH 7.5, 40 mM $MgCl_2$, 1 mM $CaCl_2$
K_2HPO_4 (0.2M) for Luciferase buffer	34.83 g (174,18 g/mol) in H_2O
Kanamycin stock solution (30µg/ml)	30 mg/ml Kanamycin sulfate in H_2O, sterile filtered and stored at -20°C
KH_2PO_4 (0.2M) for Luciferase buffer	27.21 g KH_2PO_4 (136,09 g/mol) in H_2O
KPO_4 (0.1M) pH7.8	17 ml KH_2PO_4 + 183 ml K_2HPO_4 in 200 ml H_2O
Luciferase Assay Buffer	For 200 ml: 10ml Glycylglycine (0.5M pH 7.8), 30ml KPO_4 (0.1M pH 7.8), 3 ml $MgSO_4$ (1 M), 4 ml EGTA (0,2 M pH 7.8) and 153 ml H_2O
Luciferase Lysis buffer	For 500 ml: 5 ml Triton-X100, 25 ml Glycylglycine (0.5 M pH 7.8), 7.5 ml $MgSO_4$ (1M), 10 ml EGTA (0,2M pH 7.8), 50 ml Glycerol, 402.5 H_2O
Lysogeny broth (LB) Agar	30 g Bacto-Trypton, 15 g Yeast extract, 15 g NaCl, 15 g Agar in 3 l ddH_2O and autoclaved
Lysogeny broth (LB) medium	50 g Bacto-Trypton, 25 g Yeast extract, 25 g NaCl in 5 l ddH_2O and autoclaved
$MgSO_4$ (1M) for Luciferase buffer	15.2 g EGTA (380.35 g/mol) in 200 ml H_2O, adjust pH to 7.8 using KOH.
PBS	80 mM Na2HPO4, 20 mM Na2HPO4, 1.4 M NaCl, 2.7 mM KCl, 1.76 mM KH2PO4
PBST	PBS (1x), 0.1% (v/v) Tween-20
Resolving gel buffer	1,5 M Tris Base 0,4 % SDS pH 8.8
Ripa protein extraction buffer	10 mM Tris HCl, pH 8.0; 150 mM NaCl, 1% (v/v) NP-40, 0.5% (w/v) sodium deoxycholate, 0.1% (w/v) SDS
Semi-dry blotting buffer	25 mM Tris Base (pH 8.3), 150 mM Glycine; 1x buffer: 100 ml 10x buffer, 800 ml H2O and 100 ml Methanol
Spectinomycin stock solution (50 mg/ml)	50 mg/ml Spectinomycin in H2O, sterile filtered and stored at -20°C
Stacking gel buffer	1 M Tris Base 0,8 % SDS pH 6.8
TAE (50x)	2 M Tris, 2 M Acetic Acid, and 50 mM EDTA, pH 8.3
TBS (10x), pH 7.5	20 mM Tris-Hcl, 150 mM NaCl, adjust pH to 7.5 with NaOH
TBST	TBS (1x), 0.1% (v/v) Tween-20
Tris-gylcin-sulfate (TGS), 10x	25 mM Tris Base, 150 mM Glycine, pH 8.3,
Western Blot blocking buffer	0.1% (v/v) of Tween-20, 5% milk powder in PBS
Wet blotting buffer	25 mM Tris Base (pH 8.3), 150 mM Glycine; 1x buffer: 100 ml 10x buffer, 700 ml H2O and 200 ml Methanol

2.11 Primary antibodies

Table 18 Primary antibodies

Antibody (anti-)	Specificity	Supplier	Clonality	Dilution (WB/FACS)
Calnexin	rabbit	Enzo Life Sciences, Inc., USA	polyclonal	1:1000 (WB)
cleaved PARP (Asp214)	rabbit	Cell Signaling Technology, Germany	polyclonal	1:1000 (WB)
DAPK1	mouse	BD Biosciences, Germany	monoclonal	1:500 (WB)
DAPK1	rabbit	Sigma Aldrich, Germany	polyclonal	1:1000 (WB)
DAPK1 p-S308	mouse	Sigma Aldrich, Germany	monoclonal	1:1000 (WB)
DAPK2	rabbit	Abcam, Germany	monoclonal	1:500 (WB)
DAPK3	rabbit	Bethyl Laboratories, Inc., Germany	polyclonal	1:1000 (WB)
DAPK3 p-T265	rabbit	tebu-bio GmbH, Germany	polyclonal	1:1000 (WB)
GAPDH	mouse	Santa Cruz Biotechnology, USA	monoclonal	1:2500 (WB)
HA	mouse	Sigma Aldrich, Germany	monoclonal	1:2000 (WB)
Influenza A NP (FITC)	mouse	Thermo Fisher Scientific, Germany	monoclonal	1:50 (FACS)
LC3B	rabbit	MBL International, Germany	polyclonal	1:1000 (WB)
MDA5	mouse	Enzo Life Sciences, Inc., USA	polyclonal	1:1000 (WB)
Mx1	mouse	Georg Kochs, Albert-Ludwigs University Freiburg, Germany	monoclonal	1:1000 (WB)
PI4Kα	rabbit	Cell Signaling Technology, Germany	polyclonal	1:1000 (WB)
p-p70S6K (Thr389) (108D2)	rabbit	Cell Signaling Technology, Germany	monoclonal	1:1000 (WB)
RIG-I (D14G6)	rabbit	Cell Signaling Technology, Germany	monoclonal	1:1000 (WB)
V5	rabbit	Cell Signaling Technology, Germany	monoclonal	1:1000 (WB)
V5	mouse	Thermo Fisher Scientific, Germany	monoclonal	1:1000 (WB)

2.12 Secondary antibodies

Table 19 Secondary antibodies

Antibody (anti-)	Specificity	Supplier	Clonality	Dilution (WB/FACS)
mouse-HRP	goat	Sigma Aldrich, Germany	polyclonal	1:10.000
Rabbit-HRP	goat	Sigma Aldrich, Germany	polyclonal	1:10.000

3 Methods

3.1 Cell culture

3.1.1 Culture and passaging of eukaryotic cells

All cell lines were cultured in DMEM standard cell culture medium and kept at 37 °C, 95% relative humidity and 5% CO_2. For passaging, medium was removed and cells were washed with 1xPBS. Cells were detached by adding Trypsin-EDTA and incubating for up to 5 min at 37°C. Detached cells were washed off the dish using standard cell culture medium, diluted to desired concentration and added to a new cell culture dish. Cells were passaged before confluency was reached.

Stably-transduced cell lines were grown in presence of 1 mg/ml G418, 1 µg/ml puromycin, 100 µg/ml zeocin and/or 5 µg/ml blasticidin, respectively.

3.1.2 Cryopreservation and revival

For cryopreservation a confluent 15 cm dish was detached as described above. Detached cells were spun down and resuspended in 9 ml fetal calf serum which was distributed to ten cryovials (900 µl per vial). 900 µl of 20% DMSO freezing medium were added to cryovials and contents were mixed by inverting cryovials several times before they were stored at -80°C for at least 48h. For long term storage cells were then transferred to liquid nitrogen.

Cells were revived by quickly thawing contents of cryovials. Cells were added to pre-warmed standard cell culture medium and incubated until they had attached to the plate. Medium was changed to remove DMSO.

3.1.3 Cell counting

From a cell suspension the number of cells per ml was determined by using a hemocytometer, i.e. Neubauer counting chamber. 10µl of single cell suspension were loaded to the chamber and living cells (determined by morphology) within the four large quadrants were counted using an inverted light microscope. The space over each large quarter has a defined volume of 0,1 µl. Hence, the number of counted cells multiplied by 10.000 and divided by 4 is the number of cells per ml in the cell suspension of interest.

3.1.4 Transfection of expression plasmids

3.1.4.1 Lipofectamine 2000 transfection

Expression plasmids were transfected into 293T^{RIG-I} using lipofectamine 2000 transfection reagent. For a 24 well 2µl lipofectamine were incubated in 50µl OptiMEM for 5 min and then added to 50µl OptiMEM containing 500 ng plasmid DNA. The DNA/lipofectamine mix was incubated for at least 20 min at RT. Medium was removed from target cells and replaced with 500 µl of DMEM w/o Pen-Strep. 100µl per 24 well of DNA/lipofectamine mix were added. 4-8h post transfection medium was changed to standard cell culture medium. Different amounts of DNA were transfected keeping a constant ratio between DNA and Lipofectamine. Within the same experiment DNA amounts were kept constant by adding empty vector DNA to reach the desired DNA amount.

Stimulatory RNA analogues (e.g. poly(I:C)) were transfected into 293T^{RIG-I} using lipofectamine 2000 transfection reagent. For a 24 well 1µl lipofectamine were incubated in 50µl OptiMEM for 5 min and then added to 50µl OptiMEM containing 0.4 µg/ml RNA. The RNA/lipofectamine mix was incubated for at least 20 min at RT. Medium was removed from target cells and replaced with 500 µl of DMEM w/o Pen-Strep. 100µl per 24 well of RNA/lipofectamine mix were added. In case less RNA was transfected the ratio between RNA and lipofectamine were kept constant. Within the same experiment the amount of RNA was always kept the same within one experiment by adding non stimulatory polyC to reach the desired RNA amount.

3.1.4.2 Effectene transfection

Luciferase reporter constructs were transfected into 293T^{RIG-I}, A549, or derived cell lines using Effectene transfection reagent. 150 ng firefly promoter reporter and 50 ng CMV/SV40 renilla plasmids were transfected following the protocol provided by the manufacturer. Medium was changed 4-8h post transfection.

3.1.5 siRNA transfection

For siRNA-based silencing 293T^{RIG-I}, A549, or derived cell lines were seeded into 24 well plates with a density of ~7x10^4 cells per well and were immediately transfected with desired siRNAs. 0.3 µl 20µM siRNA were added to 100 µl of OptiMEM containing 1µl of RNAiMAX. The mix was incubated for 10-15 min at RT before it was added to the freshly seeded cells, resulting in a final siRNA concentration of 10nM. Cells were reporter transfected 36h and stimulated 48h post siRNA transfection.

3.1.6 Lentiviral transduction

Stable ectopic expression of a gene or sgRNA (in case of CRISPR/Cas9) was achieved by lentiviral transduction of target cells. Lentiviral particles were produced by transfection of a lentiviral vector (.e.g pWPI) together with two packaging plasmids. Lentiviral particles were produced in 293T (MCB) cells, harvested, and used to infect target cells.

To produce lentiviral particles $1.2x10^6$ 293T cells were seeded in a 6cm dish. Medium was changed the next day and cells were transfected with pWPI lentiviral vector, gag-pol (psPAX2) and VSV-G expression plasmid (pMD2.G) using CalPhos™ Mammalian transfection kit. 6.4 µg pWPI, 6.4 µg psPAX2 and 2.1 µg pMD2.G were diluted in a final volume of 438 µl sterile H_2O and 62 µl 2M $CaCl_2$ were added on top. 500 µl 2X HBS were added drop wise to the mix while air was blown into the liquid to provide oxygen aiding precipitate formation. The transfection mix was added drop-wise to 293T cells. 8h post transfection medium was changed. 48h after transfection supernatants were collected and passed through a 0.45 µm-pore filter to prevent contamination with particle producing 293T cells. Filtered supernatants were added onto target cells which were seeded the day before ($4x10^4$ cells/ 12 well). Supernatants of transfected 293T cells were harvested again after 8 and 24h and handled the same way as described above. After three rounds of target cell infection the medium was replaced with standard cell culture medium containing the appropriate restriction antibiotic. Antibiotics were kept while passaging stable cell lines to ensure constitutive expression of the gene of interest, but were removed when experiments were performed.

3.2 Molecular biological methods

3.2.1.1 Transformation of competent bacteria

100 µl of chemically competent E.coli DH5α bacteria were thawed on ice and mixed with 100 - 500 ng plasmid DNA for retransformations, with 5 µl of ligation reaction, or with the total volume of LR/BP reaction. DNA was incubated with bacteria for 20 min on ice followed by 70 sec of heat shock at 42°C. After a recovery period of 2 min on ice, 200 µl of LB medium was added and bacteria were incubated on a shaker for 1h at 37°C. Bacteria were plated onto LB-agar plates containing restriction antibiotics (Ampicillin (0,1 mg/ml), Kanamycin (0,3mg/ml), Gentamicin (7µg/ml) or spectinomycin 50 (µg/mL)).

3.2.2 Plasmid amplification and purification

Plasmid DNA was amplified in *E.coli* DH5α. Clones were picked from plates and grown in LB medium supplemented with plasmid-specific restriction antibiotics overnight at 37°C while shaking.

3.2.2.1 Small scale plasmid purification

Transformed bacterial clones were incubated in 5 ml of LB medium containing the respective restriction antibiotics. Overnight cultures were spun down at 11.000 x g and LB medium was removed. DNA was purified from bacterial pellets using the Nucleospin® plasmid purification kit according to manufacturer's instructions. DNA pellets were resuspended in sterile ddH_2O and concentrations were determined using the Nanodrop photo spectrometer.

3.2.2.2 Large scale plasmid purification

Transformed bacterial clones were pre-cultured for 8h in 5 ml antibiotic-containing LB medium and then added to 250 ml of antibiotic-containing LB medium. Plasmid DNA was extracted from overnight cultures using the Nucleobond® PC 500 plasmid purification kit according to manufacturer's instructions. DNA pellets were resuspended in sterile ddH_2O and concentrations were determined using the Nanodrop photo spectrometer.

3.2.3 Polymerase chain reaction

Polymerase chain reactions (PCRs) were performed using the Q5® High-Fidelity DNA Polymerase and the appropriate buffer.

PCR mixes were prepared according to the following protocol.

Protocol 1 Q5 PCR reaction mix

Component	50 µl reaction
5x Q5® reaction buffer	10 µl
10 mM dNTPs	1 µl
10 µM Primer fw	2.5 µl
10 µM Primer rev	2.5 µl
Template DNA	variable (~ 100 – 500 ng)
Q5® High-Fidelity Polymerase	0.5 µl
5x Q5® GC Enhancer	10 µl
Nuclease-free ddH_2O	ad 50 µl

PCRs using the Q5® High-Fidelity polymerase were incubated according to the following protocol.

Protocol 2 Q5 PCR programme

Step	Temperature /°C	Time /sec	Number of cycles
Initial denaturing	98	30	1
Denaturing	98	5 – 10	25
Annealing	50 - 72	10 – 30	25
Elongation	72	20 – 30	25
Final elongation	72	120	1

3.2.3.1 Overlap PCR

In order to mutate a given sequence, overlap PCR was employed. Overlap primers were designed by choosing the desired mutation and including ~20 nucleotides up- and downstream of the target site so that a final overlap of ~40 nucleotides was achieved. This was done in fw and rev orientation. Overlap primers were combined with desired primers binding 5' and 3' of the mutation site and PCR fragments were generated. PCR fragments were separated on 1% agarose gels, purified and dissolved in 30 µl ddH_2O. In a last step, both PCR fragments were used as a template in a PCR reaction containing the respective 5' and 3' primers so that the full-length mutated PCR product was generated. The final PCR product was either ligated into a vector or used for BP recombination by Gateway® cloning technology.

3.2.4 Reverse transcription for cDNA cloning

In order to obtain a cDNA preparation which could be used for cloning of a specific gene, a reverse transcription using the Expand™ Reverse Transcriptase System and an anchored oligo(dT) primer and was applied. Whole cell RNA preparations were used as templates. Input RNA was generated from a confluent 24 well. 9 µl of RNA were mixed with 1 µl of anchored oligo(dT) primer.

2X Expand™ Reverse Transcriptase reaction mix was prepared according to the following protocol.

Protocol 3 Expand RT reaction mix

Component	10 µl reaction
5x Expand™ RT buffer	4 µl
100 mM DTT	2 µl
RNase inhibitor	0.5 µl
10 mM dNTPs	2 µl
Expand™ RT	1 µl
Nuclease-free ddH_2O	0.5 µl

Expand™ Reverse Transcriptase reaction mix was added to RNA-primer preparation. Reactions were incubated at 43°C for 1h and immediately transferred to ice.

3.2.5 Agarose gel electrophoresis

1% agarose gels were prepared by boiling 0.5 g agarose in 50 µl 1X TAE buffer. 2 µl of Midori Green gel dye was added to the slightly cooled down mixture and gels were cast in PerfectBlue™ Gelsystem Mini S gel slides. Appropriate combs were put into gel slide and gels were left until set. 6X DNA loading dye was added to DNA samples to a 1X final concentration and samples were loaded onto agarose gels. Gels were run until desired DNA separation was reached (~30 min) at 100 V. DNA was visualised using the Gel-iX-imager (INTAS Science Imaging Instruments).

3.2.6 PCR purification and gel extraction

DNA fragments of the desired size were cut out from agarose gels after visualisation on a UV Transilluminator (VilberLourmat). UV exposition was kept as short as possible to avoid DNA damage. DNA extraction and purification was performed using the NucleoSpin® Extract II kit following the manufacturer's instructions.

3.2.7 DNA digestion

PCR fragments or plasmid DNA were digested using recombinant restriction enzymes and the appropriate buffer system purchased from NEB. Analytic digestions were performed in a total volume 20 µl, preparative DNA digestions were performed in 50 µl. The amount of enzyme was adjusted according to amount of DNA.

A typical DNA digestion reaction was prepared according to the following protocol.

Protocol 4 DNA digestion mix

Component	20 µl reaction
10X digestion buffer	2 µl
Input DNA	1 µl (200 – 500 ng/µl)
Restriction enzyme	1 µl
ddH2O	ad 20 µl

3.2.8 DNA ligation

For ligations insert and backbone DNA were digested and the vector was additionally treated with calf intestine phosphatase (CIP) for 30min removing 5' phosphates thereby preventing religation. Purified DNA was subsequently mixed in a molar ratio of 3 insert to 1 backbone together with 1 µl 10X ligase buffer and 1 µl T4 ligase (Fermentas) in a total volume of 10µl. For control ligations ddH_2O was added instead of insert DNA. Control ligations were performed to estimate the amount of backbone re-ligations. Ligation reactions were incubated at 16°C for 2h or overnight and subsequently transformed into competent DH5α bacteria.

3.2.9 Gibson Assembly®

Gibson Assembly® uses a master mix which includes three different enzymatic activities that perform in a single buffer to enable quick plasmid generation from up to six DNA fragments. An exonuclease creates single-stranded 3' overhangs facilitating annealing of fragments that share complementary regions at one end (overlap). A polymerase then fills the gaps within the annealed fragments. A DNA ligase seals nicks in the assembled DNA.

DNA fragments were generated using overlapping primers which harboured the sequence of either the vector or another fragment the original fragment was to be joined with. By this, fragments and the vector backbone were "seamlessly" joined without interspacing DNA sequences. Primers were generated using the NEBuilder™ (New England Biolabs GmbH) online resource. Vector backbones were either linearised by restriction enzyme digestion or PCR amplified. After PCR amplification of fragments and vector backbone, all generated templates were separated on a 1% agarose gel and purified. Purified DNA was resuspended in 30 µl ddH_2O.

Gibson Assembly® mix was prepared according to the following protocol.

Protocol 5 Gibson assembly reaction mix

Component	2-3 fragment assembly
DNA ratio	Vector:insert = 1:2
Total amount of fragments	0.03 – 0.2 pmol
Gibson Assembly® Master Mix	10 µl
Nuclease-free ddH_2O	ad 20 µl

Gibson Assembly® mix was incubated at 50°C for 15 min and directly transformed into DH5α chemically competent bacteria.

3.2.10 Gateway™ cloning

Gateway™ cloning is based on site-specific recombination. The system is used to first shuttle a gene of interest into an entry vector. From this entry vector the gene of interest can be quickly shuttled into a variety of destination vectors harbouring different tags. The BP reaction mediates the recombination of PCR fragments flanked by attB sites into pDONR vectors harbouring attP sites. This reaction results in an entry (pENTR/pDONR) vector harbouring the gene of interest flanked by attL sites. As a side product a linear fragment is removed from the vector encoding for bacterial toxin ccdB. In case of a non-successful recombination bacteria transformed with non-recombined pDONR plasmids will express the ccdB gene and die, thereby selecting for positive colonies. pDONR vectors can be used in an LR reaction to shuttle the gene of interest into a destination

vector (pDEST) that again harbours the ccdB gene flanked by attR sites. Similarly to the pDONR vector non-recombined pDEST will be negatively selected by the expression of the ccdB gene. To differentiate between pDONR and pENTR vectors different selection markers are used (e.g. gentamicin vs ampicillin resistance).

3.2.10.1 Generation of entry clones (BP reaction)

Primers were designed which harboured the attB sites necessary for recombination. A start codon was added to the fw and a stop codon to the rev primer.

Table 20 BP recombination sites

Name	Sequence 5' – 3'
attB fw	GGGGACAAGTTTGTACAAAAAAGCAGGCTTC
attB rev	GGGGACCACTTTGTACAAGAAAGCTGGGTC

By PCR amplification attB-flanked inserts were generated, separated on a 1% agarose gel and purified. DNA inserts were resuspended in 30 µl ddH_2O. BP reactions were set up according to the following protocol.

Protocol 6 BP reaction mix

Component	10 µl reaction
pDONR/pENTR	150 ng
attB-flanked Insert	150 ng
BP clonase	1 µl
1x TE buffer	ad 10 µl

BP reactions were incubated for at least 2h at 25°C and subsequently transformed into competent DH5α bacteria. Successful BP cloning was visualised by digesting pDONR plasmids with BsrGI which, due to cutting both recombination sites and the vector backbone, generated three specific fragments. Plasmids were sequenced to ensure the desired sequence was amplified.

3.2.10.2 Generation of expression clones (LR reaction)

LR reactions were carried out by combining desired destination vectors with generated pDONR vectors. LR reactions were set up according to the following protocol.

Protocol 7 LR reaction mix

Component	10 µl reaction
pDONR/pENTR	150 ng
pDEST	150 ng
LR clonase	1 µl
1x TE buffer	ad 10 µl

LR reactions were incubated for at least 2h at 25°C and subsequently transformed into competent DH5α bacteria. Successful LR cloning was visualised by digesting pDEST plasmids with BsrGI which, due to cutting both recombination sites, generated two

specific fragments. Plasmids were sequenced to ensure the desired sequence was cloned.

3.2.11 Sequencing of plasmid DNA

All sequencing was performed by the GATC-Biotech service. 5 µl sequencing primer (5 µM) was mixed with 80 – 100 ng of plasmid DNA and filled up to 10 µl with nuclease-free ddH_2O. DNA was sent to the company and sequencing data was provided online 24 to 48 hours later.

3.2.12 RNA extraction and purification

RNA isolation was performed using the Nucleospin® RNA Plus kit according to the manufacturer's instructions. Cells were washed with 1X PBS prior to lysis in LBP buffer. Lysates were stored at -80°C until RNA extraction. Purified RNA was resuspended in nuclease-free ddH_2O and used for Expand^{TM} RT or cDNA preparation for quantitative Real-Time PCR.

3.2.13 cDNA preparation by reverse transcription

Reverse transcription was performed using the High Capacity cDNA Reverse Transcription kit (Applied Biosystems). Reaction mixes were prepared according to the following protocol.

Protocol 8 RT reaction mix

Component	6.6 µl reaction
10X reaction buffer	0.66 µl
100 mM dNTPs	0.25 µl
10X random hexamer primers	0.66 µl
RNase inhibitor	0.33 µl
Reverse Transcriptase	0.33 µl
Nuclease-free H_2O	1.07 µ
RNA	3.3 µl

Protocol 9 RT reaction programme

Temperature /°C	Time
25	10 min
37	2h
85	5 min

For each sample, a non-amplification control was included which contained ddH_2O instead of reverse transcriptase.

3.2.14 Quantitative Real-Time PCR

Quantitative Real-Time PCR (qPCR) was performed using the iTaq™ Universal SYBR® Green Supermix and a CFX Connect™ Real-Time PCR Detection System (Bio-Rad). Samples were measured in triplicates. Non-amplification and non-target controls were included to control for specific amplification.

qPCR reactions were prepared according to the following protocol.

Protocol 10 qPCR reaction mix

Component	15 µl reaction
2x iTaq SYBR® Green	7.5 µl
Primer fw	1.5 µl
Primer rev	1.5 µl
Nuclease-free H2O	1.5 µl
cDNA	3 µl

qPCR amplification reactions were carried out with the following programme.

Protocol 11 qPCR reaction programme

Step	Procedure	Description
1	95°C	3 min
2	95°C	10 sec
3	60°C	30 sec
4	measure	
5	Go back to 2	45 cycles
6	65°C to 95°C	0.05 sec / 0.5°C
7	Measure every 0.5°C	

qPCR data was analysed using the Bio-Rad CFX Manager software. Relative mRNA expression was calculated using the $2^{-\Delta\Delta Ct}$ method as described in [248].

3.3 Biochemical methods

3.3.1 Protein cross-linking

In order to cross-link cellular proteins in a 24 well, cells were washed with 1X PBS and 250 µl of 1% PFA/PBS solution was added. Cells were incubated for 10 min at RT before reaction was stopped adding 250 µl of ice-cold 1.25 M Glycine/PBS. Cells were washed once with ice-cold1.25 M Glycine/PBS. 50 µl of 1X Laemmli buffer were added and cells were scraped off the dish. Samples were heated to 65°C for 20 min and stored at -20°C until SDS PAGE. If necessary, samples were treated with Benzonase® (Merck) prior to gel loading.

3.3.2 Western Blot analysis

3.3.2.1 Determination of protein concentration

Protein concentrations were determined using the Pierce™ BCA Protein Assay Kit (Thermo Fisher Scientific) which allows protein quantification based on a colorimetric reaction. BCA solution was prepared according to manufacturer's instructions. 100 µl of BCA solution were mixed with 5 µl of protein lysate and incubated at 60°C for 20 min. In parallel, a serial dilution of the provided 2 mg/ml BSA standard in protein lysis buffer was prepared and incubated. 95 µl of BCA-standard and BCA-sample mix were transferred into a clear 96 well flat bottom plate and absorption at 570 nm was determined. Measurements of BSA standard were displayed in a standard curve. Protein concentrations were calculated according to BSA standard.

3.3.2.2 Polyacrylamide gel electrophoresis

SDS polyacrylamide gel electrophoresis (SDS PAGE) resolving gels containing 8% or 15% polyacrylamide (PAA) were prepared using 40% acrylamide/bisacrylamide (ratio 29:1) stock solution diluted in resolving gel buffer (section 2.10). 1:500 TEMED (Applichem) and 1:500 saturated ammonium peroxydisulfate (APS) (Roth) solution were added to initiate polymerisation reaction. Solution was immediately cast using the Mini-PROTEAN® Tetra Handcast System (Bio-Rad) and carefully overlaid with 100% isopropanol to insure plane polymerisation. 5% PAA stacking gel solution was prepared using 40% acrylamide/bisacrylamide (ratio 29:1) stock solution diluted in stacking gel buffer. TEMED and APS supplemented gel solution was cast on top of the resolving gel after residual isopropanol was removed.

Cells for protein samples were lysed in 1X Laemmli buffer or Ripa buffer supplemented with protease inhibitors. Samples in Ripa buffer were quick frozen, thawed and debris was pelleted by centrifugation at full speed for 10 min. Supernatants were mixed with 6X Laemmli to 1X concentration. Protein samples were denatured by boiling for 5 min at 95°C. If necessary, samples were treated with Benzonase® prior to gel loading. Equal amounts of samples were loaded onto gels. A lane with pre-stained protein marker was included to determine size of detected proteins. Gels were run in 1X TGS buffer for 30 min at 70V and 1 – 1.5h at 130V.

3.3.2.3 Protein blotting

After SDS PAGE separation, proteins were blotted onto PVDF membranes using the Trans-Blot® SD Cell or Trans-Blot® Turbo™ System for semidry transfer or the Mini

Trans-Blot® Cell for wet transfer (all systems by Bio-Rad). PVDF membranes were activated in 100% methanol for 30 seconds before equilibration in blotting buffer (10% methanol for semidry transfer, 20% methanol for wet transfer) for at least 5 min. Semidry transfer was performed for 1.5h at 1.5 mA/cm^2 of membrane. Wet transfer was performed for 1.5h at 350 mA/100V.

3.3.2.4 Antibody staining of Western Blot membranes

After blotting, membranes were incubated for at least 1h in 5% milk/PBST or TBST (for phospho-protein detection) to block unspecific antibody binding. Primary antibodies were diluted in blocking solution (section 2.10) and incubated on membranes overnight at 4°C or for at least 2h at RT. Primary antibodies were removed and membranes were washed three times 10 min in PBST/TBST before secondary antibodies diluted in blocking solution (section 2.10) were added. Membranes were incubated with secondary antibodies for at least 1h at RT. Secondary antibodies were removed and membranes were washed two times in PBST/TBST and a final wash was done in PBS/TBS to remove Tween. After addition of Clarity^{TM} ECL Western Blotting Substrate (Bio-Rad) or ECL Plus Western Blot Detection System (Amersham) signals were visualised using the ECL ChemoCam imager 3.2 (INTAS Science Imaging Instruments).

3.3.2.5 Western Blot quantification

Western Blot signals were quantified using the standard protocol of the Labimage1D software (INTAS). Densitometric signals of bands of interest were normalised to loading controls.

3.3.3 Co-immunoprecipitation

For co-immunoprecipitation experiments, 1x10^7 293T cells were seeded onto a 15 cm dish one day prior to transfection. 62 µg of tagged constructs were transfected using calcium phosphate transfection, reagents were scaled up according to dish size (section 3.1.6). Medium was changed 8h post transfection.

3.3.3.1 HA-tag co-immunoprecipitation

Co-immunoprecipitations of HA-tagged proteins were performed using anti-HA-coated agarose beads (Sigma Aldrich).

One day after transfection a confluent 15 cm dish was lysed with 1 ml HA-Co-IP lysis buffer (section 2.10) for 30 min on ice. Lysates were centrifuged for 30 min at 18500 x g at 4°C. 50 µl supernatant were taken as an input control. The remaining supernatant was

added to 20 µl HA beads which had been washed 3 times with pre-chilled HA-CoIP lysis buffer. Lysates were incubated with the beads for 4-16 h at 4°C on an overhead rotating device. Samples were centrifuged at 2000 x g for 1 min to carefully pellet beads. If required, supernatants were used as flow through control. Subsequently, beads were washed two times with 1 ml of ice cold HA-CoIP lysis buffer for 15 min and two washes with cold PBS for 5 min. Beads were either immediately mixed with 1x sample buffer or an SDS based elution followed by acetone precipitation was performed. In case of an SDS elution 100 µl 5% SDS/PBS was added to the washed beads and shaken for 5 min at 1100 rpm (shaking function of thermo block) at RT. Beads were pelleted by centrifugation at 18500 x g for 2 min. Supernatants were collected and pellets were washed adding 100 µl PBS. 5 min shaking at 1100 rpm and centrifugation at 18500 x g was repeated. Collected supernatants (~200 µl) were mixed with ~800 µl ice-cold acetone and protein was precipitated overnight at -20°C. Next morning precipitates were spun down at full speed for 30 min at 4°C. Pellets were resuspended in 50 µl 1x sample buffer and boiled for 5 min at 95°C.

3.3.3.2 Strep-tag co-immunoprecipitation

Co-immunoprecipitations of Strep-tagged proteins were performed using MagStrep "type3" XT Beads (IBA Life Sciences). Separation was achieved using a magnetic rack.

One day after transfection a confluent 15 cm dish was lysed with 1 ml Strep-Co-IP lysis buffer (section 2.10) for 30 min on ice. Lysates were centrifuged for 30 min at 18500 x g at 4°C. 50 µl supernatant were taken as an input control if needed. The remaining supernatant was added to 20 µl Strep beads which had been washed 3 times with pre-chilled NP40 lysis buffer. Lysates were incubated with the beads for 2 h at 4°C on an overhead rotating device. Beads were washed three times with 1 ml of ice cold Strep-Co-IP lysis buffer on the magnetic rack. Proteins were eluted from beads by addition of 75 – 100 µl BXT biotin elution buffer and shaking for 5 min at 1100 rpm (shaking function of thermo block) at RT. Collected supernatants were either quick frozen in liquid nitrogen or stored on ice until further use.

3.3.4 In Vitro Kinase Assay

In vitro kinase assay buffer was prepared adding 0.1 mg/ml BSA. Reactions were prepared on ice according to the following protocol.

Protocol 12 Kinase Assay reaction mix

Component	50 µl reaction
2x Kinase Assay Buffer	25 µl
1 µg/µl purified RIG-I	1 µl
100 µM CaM	0.5 µl
Eluted kinase	21 µl

Phosphorylation reactions were started by adding a mix of 1 µl 2.5 mM ATP and 1.5 µl ^{32}P-ATP (15 µCi). Samples were incubated at 30°C for 1h. Reactions were stopped by boiling samples for 5 min at 95°C. Samples were separated on an 8% polyacrylamide gel, transferred onto PVDF membranes and incubated on storage phosphor screens to detect incorporated ^{32}P-ATP.

3.4 Viral replication assays

3.4.1 Rift Valley Fever Virus replication assay

For RVFV replication assays a RVFV ΔNSs_Rluc (originally kindly provided by Friedemann Weber, Gießen) stock prepared by Pascal Mutz (titer: 2.24x10^2 /ml $TCID_{50}$ on HeLa cells) was used.

A549 (7x10^4 cells/24 well) cells were silenced for 48h with control and targeting siRNAs. Cells were infected with RVFV ΔNSs_Rluc diluted 1:100 in standard cell culture medium for 24h. Supernatants were removed and cells were lysed in 100 µl luciferase lysis buffer. Samples were stored at -80°C until measurement on the Mithras² LB 943 Multimode reader.

3.4.2 Influenza A Virus replication assay

For FluAV replication assays FluAV WSN/1933 stock (titer: 3.5x10^6/ml $TCID_{50}$ on A549 cells) prepared by Joschka Willemsen [249] was used.

A549 (7x10^4 cells/24 well) cells were silenced for 36h with control and targeting siRNAs. Cells were infected with an MOI of 0.01 in OptiMEM for 1h before the inoculum was removed and 500 µl of standard cell culture medium complete was added. 32h p.i. cells were analysed by flow cytometry.

3.4.3 Hepatitis C Virus replication assay

For HCV replication assays HCV JCR2A stock (4.85x10^3 /ml $TCID_{50}$ on Huh7 Lunet cells) prepared by Christopher Dächert was used.

Huh7 CD81^{high} or CD81^{high} MAVS-GFP$_{NLS}$ (5x10^4/24 well) cells were silenced for 24h with control and targeting siRNAs. Cells were infected with HCV JcR2A stock diluted 1:2 in standard cell culture medium. Samples were harvested at 24, 48, 72, and 96h p.i. by removing media, washing with 1X PBS, and adding 100 µl of luciferase lysis buffer. Samples were stored at -80°C until measurement on the Mithras² LB 943 Multimode reader.

3.5 Flow cytometry

Intracellular antigen staining was performed using Cytofix/Cytoperm™ (BD Biosciences). Influenza-infected A549 cells were washed with 1X PBS, detached with 0.05% trypsin/0.02% EDTA and washed again with PBS. Cell pellets were carefully resuspended in 100µl Cytofix/Cytoperm and incubated for 20 min on ice. Cells were washed twice with 1ml Perm/Wash solution and then stained in 50µl 1:50-diluted Anti-Influenza A NP FITC-coupled antibody in Perm/Wash for 30 min on ice. Cells were washed twice with 1ml Perm/Wash solution and transferred into PBS. Cells were filtered through gauze and kept on ice before analysis on an Accuri^{TM} C6 Flow Cytometer (BD Biosciences). Flow cytometry analysis was performed using the FlowJo V10 software (FlowJo LLC).

3.6 Luciferase reporter assay

In the morning, cells seeded the day before were transfected with firefly and renilla reporter plasmids either using lipofectamine 2000 or Effectene transfection reagent. In the evening of the same day cells were stimulated either by poly(I:C) or plasmid transfection or by SeV infection (MOI 5). If not indicated otherwise, cells were stimulated for 16h before medium removal and lysis in 100 µl/24 well luciferase lysis buffer. Until measurement cells were kept at -80°C.

Samples were measured using Mithras² LB 943 Multimode reader or Mithras LB 940 Multimode Microplate Reader. As firefly substrate assay buffer (see section 2.10) supplemented with 1:20 D-luciferin stock solution (section 2.10), 1:100 100 mM ATP and 1:1000 1 M DTT was prepared. As renilla substrate Coelenterazin was diluted 1:700 in assay buffer (section 2.10). Reactions were stopped using 10% SDS solution as samples were measured in clear 24 well plates.

24 well plates were measured using the following protocol.

Protocol 13 Luciferase assay programme

Action	Procedure
Dispense firefly substrate	4x100 µl
Shake	2 sec
Measure (No filter)	10 sec
Dispense renilla substrate	4x100 µl
Shake	2 sec
Measure (480m20BRET filter)	10 sec
Dispense 10% SDS	100 µl
Shake	2 sec

Luciferase samples were measured in triplicates.

3.7 Generation of CRISPR/Cas9 knockout cell lines

The CRISPR/Cas9 system which was introduced in 2012 [250] is now extensively used in genome editing. Originally, CRISPR/Cas9 is a bacterial defence mechanism against foreign nucleic acids. Today, it is frequently used to generate knockout cell lines, as was done within the course of this study. Briefly, specific guide RNAs (sgRNAs) lead the Cas9 to the target gene where Cas9 induces double strand breaks. This induces DNA repair mechanisms which, due to insertion/deletion of bases, often result in frameshift mutations. Occurrence of early stop codons results in nonsense-mediate decay of mRNA transcripts, thereby shutting down gene expression.

Four different sgRNAs for each targeted gene were designed using the standard settings of the DKFZ e-crisp tool (http://www.e-crisp.org). To enable cloning into lenticrispr v2 (Addgene: 52961), BsmBI digest-compatible overhangs were added:

Table 21 Overhangs for crispr cloning

Oligo	Overhang 5' – 3'
sense	CACC
antisense	AAAC

Oligos were annealed according to the following protocol.

Protocol 14 Crispr ligation mix

Component	10 µl reaction
sgRNA sense	1 µl
sgRNA antisense	1 µl
10X T4 ligation buffer	1 µl
T4 PNK	1 µl
Nuclease-free H_2O	ad 10 µl

Phosphorylation by PNK was carried out for 30 min at 37°C, followed by annealing starting at 95°C and ramping down to 25°C at 5°C/min.

3 µg of lenticrispr v2 plasmid were digested using BsmBI restriction enzyme (section 3.2.7) and de-phosphorylated using CIP (3.2.8). Linearised plasmid was gel-purified (section 3.2.6). Annealed oligos were diluted 1:200 and ligated into BsmBI-digested plasmid (section 3.2.8). Using the human U6 primer sgRNA insertions were sequenced to verify correct insertion. Using the generated crispr plasmids, lentiviral particles were produced (section 3.1.6) and target cells were infected. Successful transduction was ensured by antibiotic restriction. In order to allow targeting of multiple genes, lenticrispr v2 plasmids harbouring a hygromycin and a zeocin resistance gene were cloned employing Gibson® assembly (3.2.9). Generated knockout bulks were tested for protein expression. Lowest expressing bulks were chosen for single cell clone generation which were again tested for lack of target protein expression.

3.8 Data evaluation

Means and error bars were calculated using the GraphPad Prism 7 software. Number of biological replicates is indicated in the respective figure legends.

4 Results

Death associated protein kinase 1 (DAPK1) was recently identified as a negative regulator of RIG-I signalling using a kinome-wide siRNA screen [199]. In this screening approach, siRNAs were used to target over 700 cellular kinases in cells which were then stimulated by transfection of the dsRNA analogue poly(I:C). Effects on translocation of GFP-tagged IRF3 were analysed by automated fluorescence microscopy. Thereby, several positive and negative regulators of antiviral signalling were identified, one of them being DAPK1.

The present study focused on the mechanism how DAPK1 might execute its inhibitory function and how this ties in with its known roles in cellular homeostasis. Furthermore, DAPK1 is closely-related to the other members of its protein kinase family. Based on the fact that DAPKs often have similar functions in signalling pathways, it was investigated if and how other members of the DAPK family might be involved in innate antiviral signalling.

4.1 The role of DAPK1 as an inhibitor of RIG-I signalling depends on its kinase activity but is independent of known DAPK1 functions

4.1.1 A minimal kinase-active DAPK1 construct inhibits RIG-I signalling like full-length DAPK1

A minimal construct of DAPK1 comprising its kinase, calmodulin binding and Ankyrin repeats domains (termed DAPK1^{KCA}) was identified which was able to inhibit RIG-I signalling activation to the same extent as full-length DAPK1 when over-expressed in 293T^{RIG-I} cells [199]. DAPK1 undergoes unique auto-phosphorylation at serine residue 308 (S308) which decreases its kinase activity and it was shown that de-phosphorylation at S308 was necessary for full activity of DAPK1, as a phospho-mimetic mutant lost its apoptotic potential [251]. Extent of DAPK1 S308 phosphorylation can be observed on protein level using a specific antibody. In order to investigate whether DAPK1 kinase activity was necessary for the inhibitory effect on RIG-I signalling upon over-expression, several mutants of DAPK1^{KCA} were generated, namely a supposedly kinase-inactive K42A mutant, a phospho-mimetic S308D and a phospho-ablatant S308A mutant, as well as a mutant lacking the very N-terminus of the kinase (Δ1-73), incapable of ATP-binding and transfer (Figure 9A). These mutants were over-expressed in 293T cells which stably over-express RIG-I (293T^{RIG-I} cells) and may, therefore, activate IRF3 signalling when probed with a suitable stimulus, e.g. infection with ssRNA viruses such as Sendai virus

(SeV). Indeed, kinase-inactive DAPK1$^{KCA\ S308D}$ and DAPK1$^{KCA\ \Delta1\text{-}73}$ mutants did not inhibit IFIT1 promoter activity as efficiently as full-length DAPK1, DAPK1^{KCA} or DAPK1$^{KCA\ S308A}$ mutant (Figure 9B). The inhibitory effect of supposedly kinase-dead DAPK1$^{KCA\ K42A}$ mutant was only slightly reduced compared to DAPK1^{KCA} and did not reflect kinase-inactive DAPK1$^{KCA\ S308D}$ mutant (Figure 9B). Moreover, DAPK1$^{KCA\ K42A}$ retained capability of auto-phosphorylation at S308 which was not seen for DAPK1$^{KCA\ \Delta1\text{-}73}$ truncation mutant (Figure 9C).

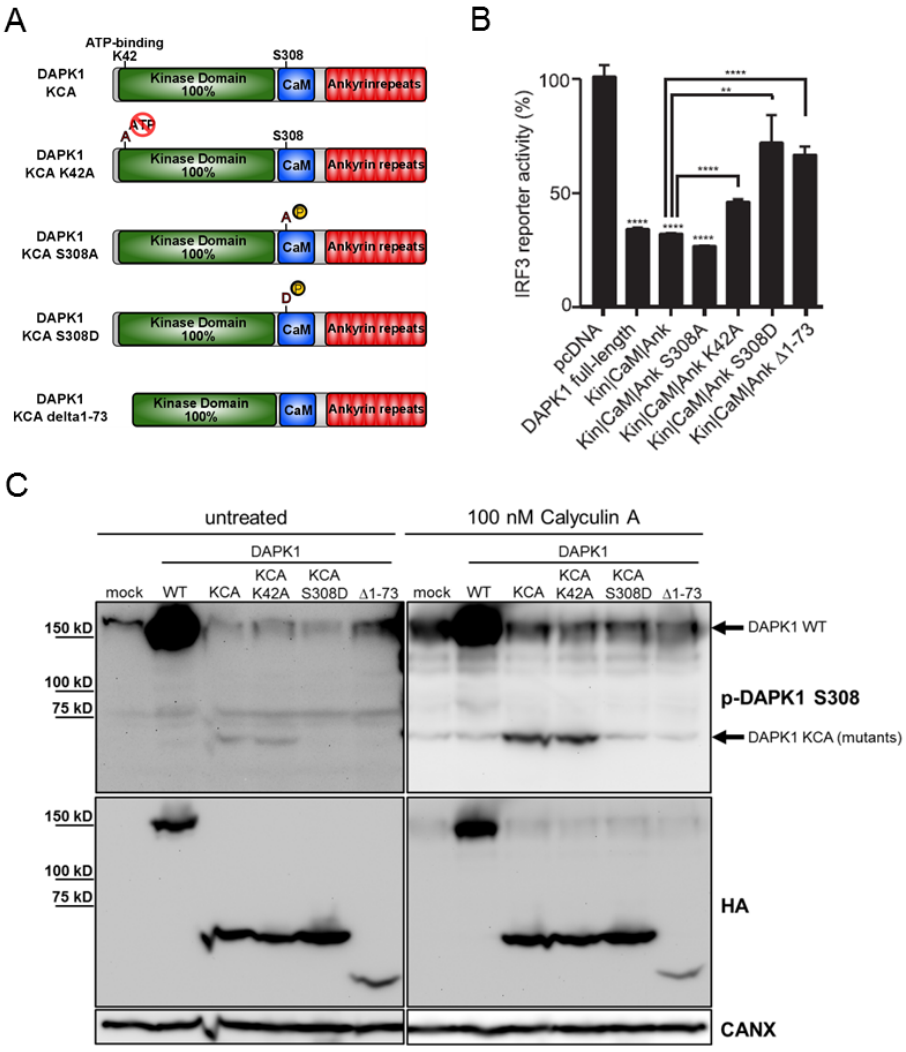

Figure 9 **Inhibition of RIG-I signalling by a minimal DAPK1 construct depends on DAPK1 kinase activity**

A) An overview of DAPK1 minimal construct KCA and its mutants is shown. Mutation of lysine 42 to alanine was shown to render DAPK1 kinase-inactive in *in vitro* [164], [251]. Phospho-ablatant (S308A) and phospho-mimetic (S308D) mutants were found to exhibit increased or decreased apoptotic activity, respectively [251]. DAPK1$^{KCA\ \Delta1\text{-}73}$ mutant does not harbour the ATP binding site in the active centre of the kinase domain and is expected to be kinase dead. **B)** Comparison of DAPK1^{KCA} mutants and full-length DAPK1 in an IFIT1 promoter activity assay. 293T$^{RIG\text{-}I}$ cells were transfected with DAPK1 constructs and stimulated with 0.4 µg/ml poly(I:C) for 16h. (modified from [199]), n = 3 **C)** Western Blot of DAPK1 p-S308 levels in cells over-expressing DAPK1 constructs left untreated or treated with phosphatase inhibitor calyculin A for 1h prior to lysis. Detection of HA-tagged constructs shows transfection efficiency. Arrows indicate full-length DAPK1 and KCA mutants. A representative of three independent experiments is shown.

A minimal DAPK1 construct comprising its kinase domain, CaM domain and Ankyrin repeats inhibited RIG-I signalling activation when over-expressed in $293T^{RIG-I}$ cells, given that it retains its kinase activity. Hence, DAPK1 kinase activity is necessary for the observed inhibitory effect on the RIG-I signaling pathway.

4.1.2 Limiting the function of DAPK1 in growth factor induced signalling does not interfere with its role in RIG-I signalling

The $DAPK1^{KCA}$ minimal variant behaved like full-length DAPK1 when over-expressed in $293T^{RIG-I}$ cells, but an even smaller construct, harbouring only the kinase domain and the CaM domain was not able to inhibit RIG-I signalling [199]. Hence, the Ankyrin repeats domain seems to be indispensable for the inhibitory effect of DAPK1 on RIG-I signalling. Ankyrin repeats are found in a variety of proteins and mostly mediate protein-protein interactions [252]. In case of DAPK1, the Ankyrin repeats are a target of several kinases of the growth factor signalling network, specifically ribosomal protein S6 kinase α (p90S6K/RSK) and proto-oncogene tyrosine-protein kinase Src, both of which act downstream of mitogen-activated protein kinase 1 (MAPK1), also called ERK. p90S6K/RSK phosphorylates DAPK1 on serine 289 (S289), resulting in decreased apoptotic activity and cell survival [188]. Moreover, DAPK1 activity is regulated by phosphorylation of tyrosine residues 491 and 492 (Y491 and Y492, respectively) by Src and de-phosphorylation of those residues by receptor-type tyrosine-protein phosphatase F (RTPRF)/LAR [185]. Y491/Y492 phosphorylation decreases DAPK1 activity. Thus, growth-factor signalling, resulting in Src activation and LAR suppression, will result in decreased apoptotic potential of DAPK1 and overall cell survival. Phospho-mutants of the above-mentioned residues were created in order to examine if the effect seen by over-expression of $DAPK1^{KCA}$ was mediated by a cross-talk with growth factor-induced signalling. In the case of S289, a phospho-mimetic S289E and -ablatant 289A mutant were generated, and in the case of Y491/Y492 phospho-mimetic Y491/492E and -ablatant Y491/492F mutants were generated (Figure 10A). These mutants were over-expressed in $293T^{RIG-I}$ cells and compared to full-length DAPK1 and $DAPK1^{KCA}$ in terms of RIG-I activation upon SeV infection. All generated mutants efficiently inhibited IFIT1 promoter activity after stimulation and behaved similar to $DAPK1^{WT}$ and $DAPK1^{KCA}$ (Figure 10B).

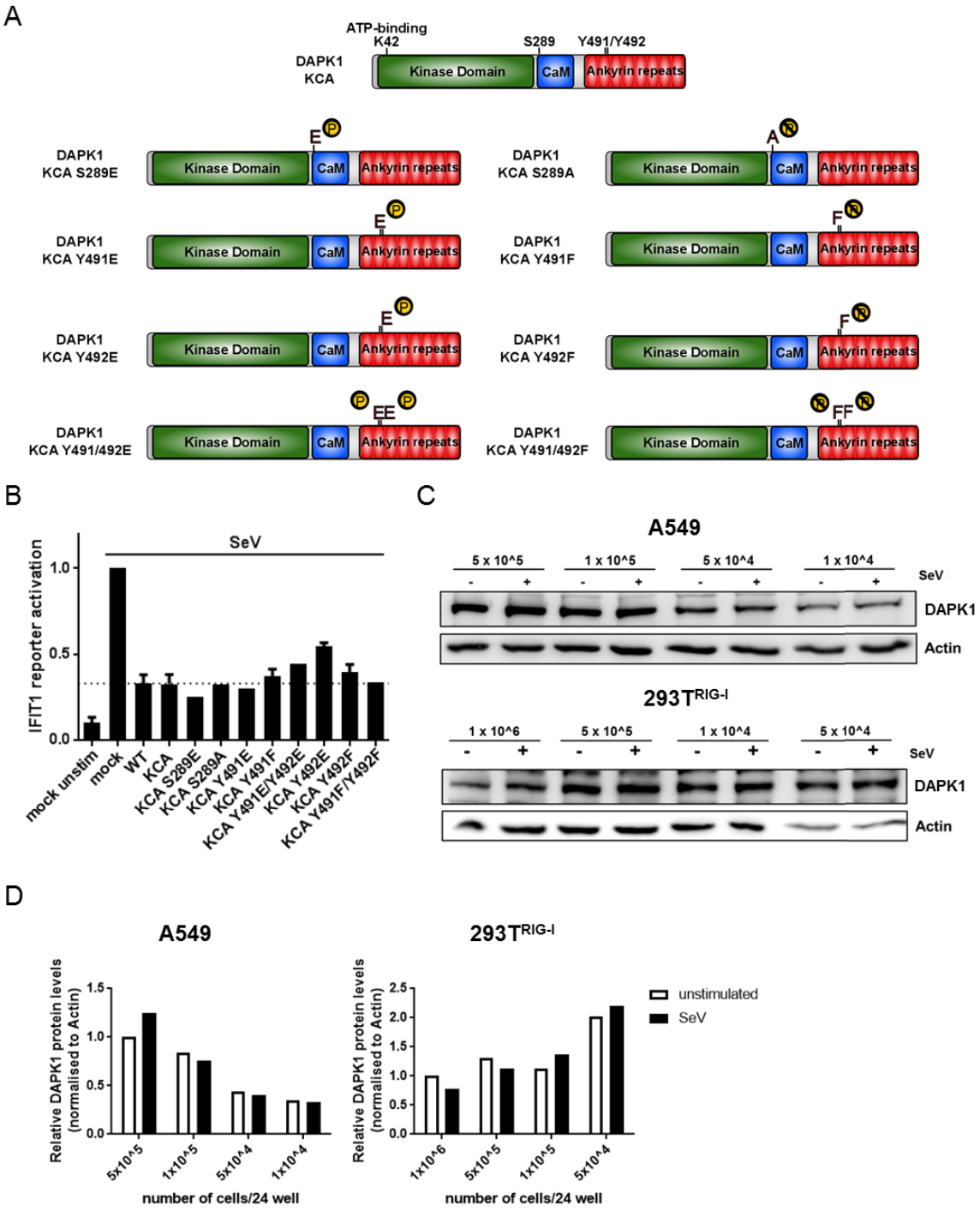

Figure 10 Limiting DAPK1 function in growth factor signalling does not abrogate its ability to inhibit RIG-I signaling

A) Overview over DAPK1 KCA phospho-mimetic and phospho-ablatant mutants of residues important for growth factor related signalling **B)** IFIT1 promoter reporter assay in 293T^{RIG-I} cells over-expressing DAPK1^{WT}, DAPK1^{KCA} and DAPK1^{KCA} variants stimulated with SeV (MOI 5) for 16h, error bars correspond to two independent experiments **C)** Western Blot analysis of DAPK1 levels in A549 and 293T^{RIG-I} cells seeded at different densities in 24 well plates, either unstimulated or infected with SeV (MOI 5) for 16h. 20 µg of protein were loaded per lane. **D)** Densitometric quantification of C)

293T^{RIG-I} cells, in which all over-expression assays were performed, express endogenous DAPK1. It has not been studied how DAPK1 behaves in 293T cells in response to growth factor signalling and mitotic stimuli. Contact inhibition of densely seeded cells normally leads to stagnation of cell growth and division in culture, whereas cells seeded at low densities will usually grow and undergo mitosis until they reach confluency. As growth factor signalling is needed for induction of cell division, it will be influenced by the number of cells seeded onto a defined area [253].

In order to determine if growth factor signalling affects DAPK1 protein levels in A549 and 293T^{RIG-I} cells, an assay was performed in which the cells were seeded at different densities onto a defined area. DAPK1 levels in cells either growing fast without contact inhibition (low densities, strong growth factor signalling) or growing slowly with increasing contact inhibition (high densities, weak growth factor signalling) was examined in 293T^{RIG-I} and A549 cells by immune staining.

In 293T^{RIG-I} cells DAPK1 levels were inversely correlated with cell density, whereas in A549 cells, DAPK1 levels rose proportionally with increasing numbers of cells per well (Figure 10C and 10D), resulting in a ~2-fold difference between highest and lowest concentration of cells for both cell types.

DAPK1 expression and probably its activity were influenced by cell growth in A549 and 293T^{RIG-I} cells, although growth-dependent regulation of endogenous DAPK1 levels differed between analysed cell types. Over-expression of DAPK1^{KCA} phospho-mutants mimicked regulatory phosphorylation by kinases involved in growth factor signalling. However, all over-expressed constructs inhibited RIG-I signalling to the same extent. Thus, inhibition of RIG-I signalling by DAPK1 does apparently not depend on regulation of DAPK1 activity by Src or RSK phosphorylation, both of which are downstream targets of ERK, activated upon induction of growth factor signalling.

4.2 DAPK family members are negative regulators of RIG-I signalling

DAPK1 is the founding member of the DAPK family of protein kinases. Its closest relatives are DAPK2 and DAPK3 whose kinase domains display high amino acid sequence homology to DAPK1 (Figure 6). The minimal DAPK1^{KCA} construct is significantly smaller than full-length DAPK1 and harbours only the kinase domain, CaM domain and Ankyrin repeats. In this, it is structurally similar to DAPK2 and DAPK3. It was established that DAPK1 negatively regulated RIG-I signalling in a feedback loop [199]. Since cells endogenously express not only DAPK1 but also other DAPK family members

it was investigated if and how these regulate antiviral signalling and might in turn be regulated in their activity.

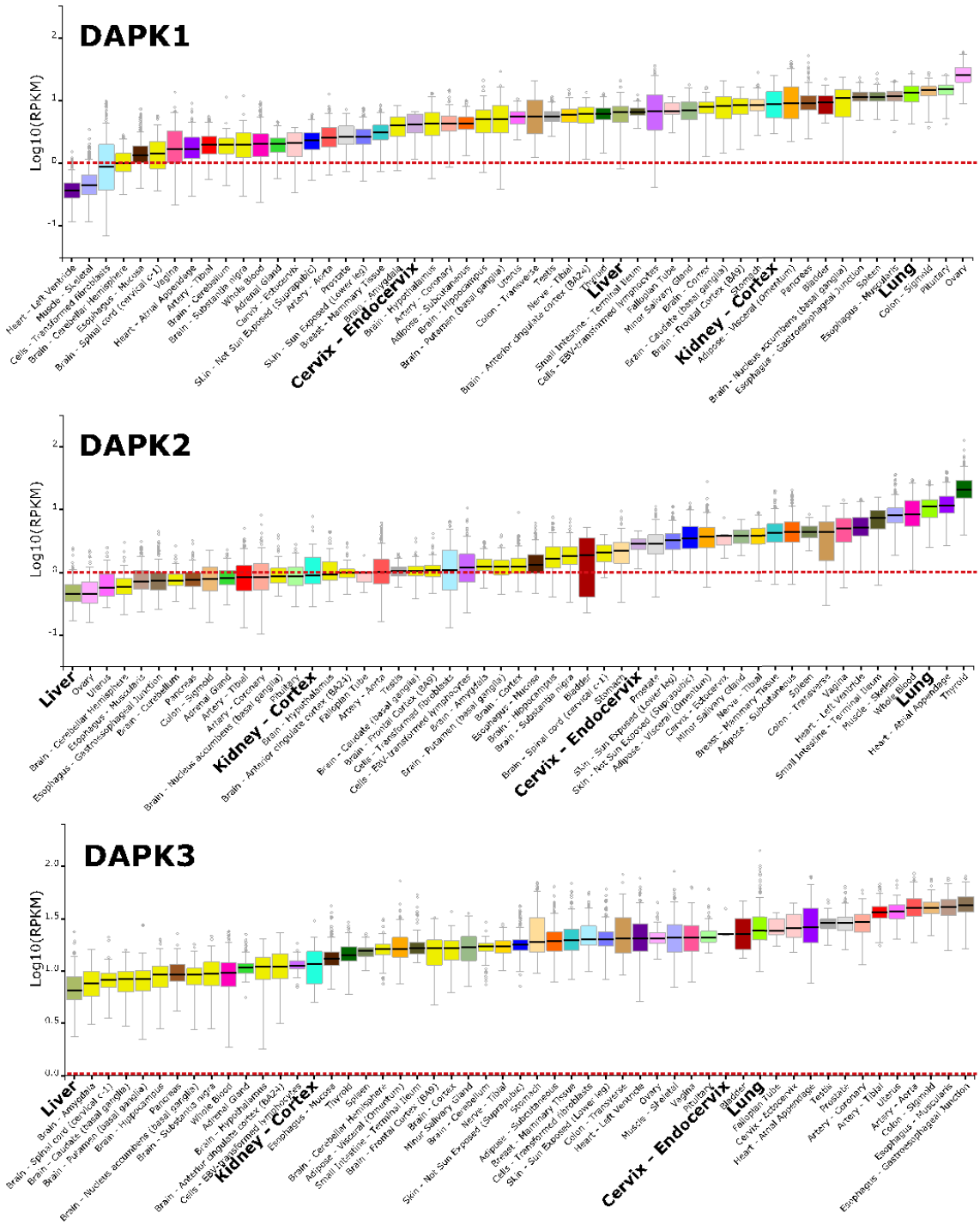

Figure 11 **Gene expression profiles of human DAPK1, DAPK2, and DAPK3**

Overview of DAPK1, DAPK2, and DAPK3 gene expression in different tissues from patient samples. Gene expression is shown in Reads Per Kilobase of transcript per Million mapped reads (RPKM) and dashed lines indicate a Log10(RPKM) of zero. Highlighted tissues correspond to origins of cell lines examined in Figure 6. Error bars indicate different sample numbers (for more information, visit the GTEx Portal). Displayed data were obtained from the GTEx Portal (gtexportal.org, GTEx Analysis Release V6p, dbGaP Accession phs000424.v6.p1) on 05/31/17.

4.2.1 DAPK2, DAPK3, and DRAK1 are inhibitors of RIG-I signalling

It is known that DAPKs can have similar functions in signalling pathways. For example, DAPK1 and DAPK3 both phosphorylate Beclin, but target different residues in order to allow tight, possibly tissue-specific regulation of the autophagic network [170], [208]. Hence, variable expression of DAPKs in different cell types allows flexible and tight regulation of not only cell death pathways, but also other signalling cascades DAPKs are involved in. As a matter of fact, DAPK gene expression varies considerably between different tissues (Figure 11). Whereas DAPK1 and DAPK3 are expressed in the liver, DAPK2 is not. Similarly, DAPK3 is the only of the three kinases which is expressed in endocervical tissue, while there is hardly any expression of DAPK1 and DAPK2. Thus, it is feasible that different DAPKs fulfil certain tasks in a specific cell type, based on their expression.

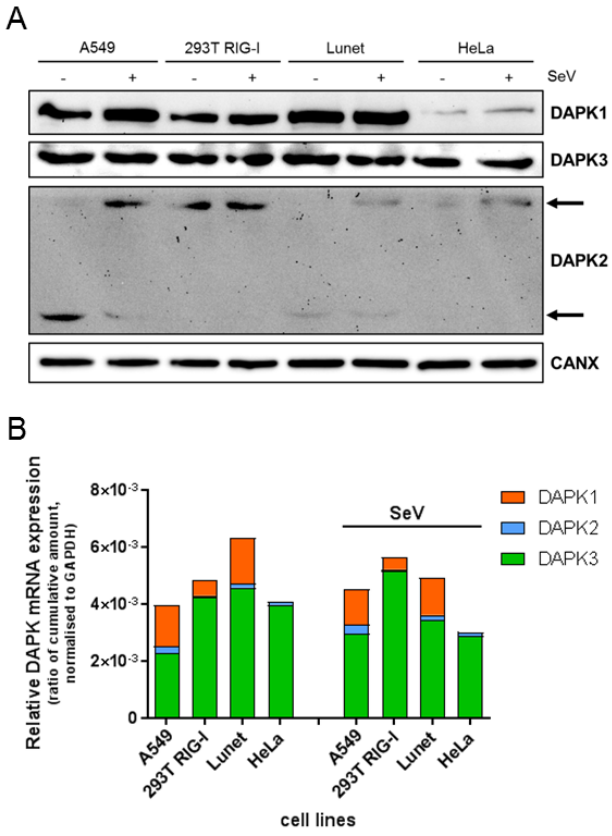

Figure 12 **DAPK expression in different cell lines**

A) Comparative Western Blot analysis of DAPK1, DAPK2, and DAPK3 protein expression in A549, 293T^{RIG-I}, (Huh7) Lunet, and HeLa cells. Cells were either left unstimulated or infected with SeV (MOI5) for 16h. Arrows indicate DAPK2 monomers and dimers. 20 µg of protein were loaded. **B)** DAPK mRNA expression in different cell lines. mRNA levels of DAPK1, DAPK2, and DAPK3 were measured by qPCR in A549, 293T^{RIG-I}, Huh7 Lunet, and HeLa cells. Cells were either left untreated or infected with SeV (MOI 5) for 16h.

In order to know if and how strong the three most closely related DAPKs, DAPK1, DAPK2, and DAPK3 were expressed in cells of different origin, their expression levels were assessed in four different human cell lines. Besides the transformed human embryonic kidney cell line (HEK)293T^{RIG-I}, cancer cell lines A549 (lung), Lunet (Huh7, hepatoma), and HeLa (endocervix) were examined. Protein levels were analysed in a comparative Western Blot and mRNA levels were measured via qPCR in uninfected versus SeV infected cells (Figure 12).

In general, protein levels corresponded to mRNA expression levels, emphasized by findings for HeLa cells which expressed very low amounts of DAPK1 and DAPK2 mRNA and correspondingly low amounts of protein independent of virus stimulation (Figure 12). DAPK1 mRNA and protein expression was highest in Lunet and A549 cells and was not significantly changed in response to virus infection. 293T^{RIG-I} cells expressed lower amounts of DAPK1 mRNA and protein than Lunet and A549 cells, while HeLa cells expressed virtually no DAPK1 mRNA or protein. DAPK2 mRNA and protein expression was highest in A549 cells, followed by Lunet and then 293T^{RIG-I} cells. HeLa cells expressed very low levels of DAPK2 mRNA. Interestingly, DAPK2 protein dimerised in response to virus infection in A549, Lunet, and to some extent in HeLa cells, but was exclusively detected in its dimerised form in 293T^{RIG-I} cells, independent of stimulation (Figure 12A, arrows). As a matter of fact, DAPK2 dimerisation is indicative of increased DAPK2 activity [160], which was examined in the course of this study (Figure 23). Overall DAPK3 mRNA and protein levels were similar between examined cell lines. While DAPK3 mRNA levels were increased in A549 and 293T^{RIG-I} cells in response to virus infection, Lunet and HeLa cells expressed less DAPK3 mRNA after stimulation (Figure 12B).

Taken together, DAPK1, DAPK2, and DAPK3 mRNA and protein were detectable in the four different cell lines, albeit expression differed considerably. While DAPK1 and DAPK3 were highly expressed in A549, 293T RIG-I, and Lunet cells, DAPK2 was best detectable in A549 cells with very low expression in the other cell lines. HeLa cells were found to be unsuitable for studies on endogenous DAPK functions and interactions as they only expressed detectable amounts of DAPK3 and hardly any DAPK1 or DAPK2. Interestingly, DAPK expression in the examined cell lines (Figure 12) reflected their gene expression profiles in human tissues (Figure 11) to a large extent. For example, HeLa cells, which are of endocervical origin, expressed well detectable amounts of DAPK3 mRNA and protein, but hardly any DAPK1 or DAPK2, which are also expressed in limited amounts only in endocervical tissue from patient samples (Figure 11).

4.2.1.1 Similar to DAPK1, DAPK2 and DAPK3 dose dependently inhibit RIG-I signalling

It was established DAPK1 was an inhibitor of RIG-I signalling and that this inhibitory effect was dose-dependent [199]. Therefore, it was analysed if the same could be observed for DAPK2 and DAPK3. To this end, different amounts of plasmid encoding for DAPK1, DAPK2, and DAPK3 were transfected into 293T^{RIG-I} cells, cells were stimulated by SeV infection and the respective amount of RIG-I signalling induction was compared.

Similar to DAPK1 (Figure 13A), DAPK2 and DAPK3 dose-dependently inhibited IFIT1 promoter activity, i.e. RIG-I signalling (Figure 13B and 13C). Transfection efficiency was monitored by Western Blot and showed increasing HA signal with increasing amounts of transfected plasmid (Figure 13D).

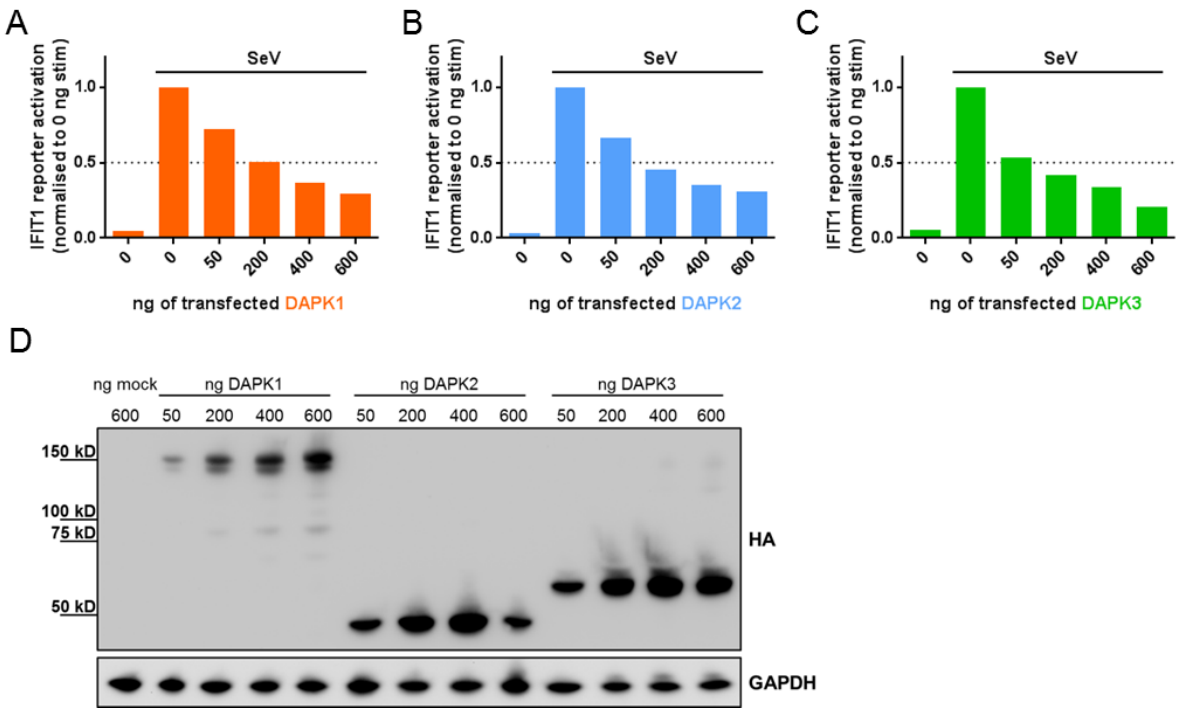

Figure 13 **Over-expressed DAPK1, DAPK2, and DAPK3 dose-dependently inhibit RIG-I signalling**

For IFIT1 promoter reporter activation assay increasing amounts of plasmid encoding HA-tagged DAPK1 **(A)**, DAPK2 **(B)**, and DAPK3 **(C)** were transfected into 293T^{RIG-I} cells. Cells were infected with SeV (MOI 5) for 16h before IFIT1 promoter activity was measured. Transfection efficiency was assessed in Western Blot analysis by staining for HA **(D)**.

In contrast to DAPK1 and DAPK2, which reached 50% reduction of IFIT1 promoter activity when 200 ng of plasmid were transfected, a 50% reduction in IFIT1 induction was reached transfecting only 50 ng of plasmid in the case of DAPK3. Since DAPK over-expression induced apoptosis in 293T^{RIG-I} cells, transfection of high amounts (> 500 ng) of the kinases lead to a dramatic increase in cell death as seen in a large percentage of

floating, detached cells (data not shown). Therefore, a maximum of 500 ng of plasmid was used for over-expression assays in this study.

As not only DAPK1 but also closely related DAPK2 and DAPK3 were found to be inhibitors of RIG-I signalling, the question remained whether this inhibitory role was a general trait of all members of the DAPK family. In order to investigate this, the effects of remaining DAPK family members DRAK1 and DRAK2 on RIG-I signalling were analysed. To this end, DRAK1 and DRAK2 were over-expressed in 293T^{RIG-I} cells and cells were infected with SeV.

When compared in the IFIT1 promoter activity assay, over-expressed DRAK1 inhibited signalling to a similar extent as DAPK1, whereas no change in IFIT1 promoter activity was observed upon over-expression of DRAK2 (Figure 14A). Compared to DRAK1 and DAPK1, expression of DRAK2 was less efficient and did not reach the same levels as the other DAPKs (Figure 14B).

Over-expression of four DAPK family members strongly inhibited IFIT1 promoter activity in response to SeV stimulation. Only DRAK2 over-expression did not influence the RIG-I signalling response.

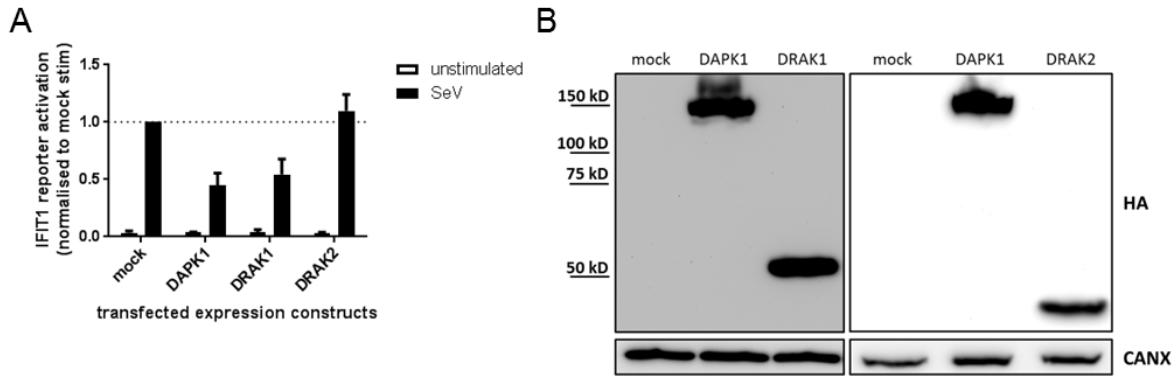

Figure 14 Over-expressed DRAK1 inhibits RIG-I signalling whereas DRAK2 does not

A) IFIT1 promoter activity assay in 293T^{RIG-I} cells over-expressing DAPK1, DRAK1, and DRAK2. Cells were infected with SeV for 16h. Error bars correspond to three independent experiments. **B)** Western Blot analysis. HA-tag was stained to assess expression levels of individual kinases.

4.2.1.2 Down-regulation of DAPK2 and DAPK3 increases RIG-I signalling

Up to this point, all analyses regarding the role of DAPKs in RIG-I signalling were performed in over-expression studies in 293T^{RIG-I} cells. Exogenous expression of proteins is an artificial situation and does not represent actual expression and function of a cellular protein. In order to assess how DAPKs might influence RIG-I signalling based on their natural expression levels a silencing approach was employed in which siRNAs

were transfected thereby depleting cells of endogenous DAPKs. Additionally, these silencing studies were carried out not only in 293T^{RIG-I} cells but also the lung carcinoma cell line A549. Due to low expression of vital components of the antiviral signalling machinery, antiviral IFN signalling is greatly impaired in 293T cells, requiring over-expression of RLRs to achieve ISG and IFN expression after RNA virus infection. A549 cells are naturally responsive to RNA virus infection and do not require additional expression of RLR signalling components. Silencing studies focused on DAPK1, DAPK2, and DAPK3, since these are the closest related DAPK family members, their expression could be validated in A549 and 293T^{RIG-I} cells (Figure 12), and they are the best studied DAPK family members regarding their activity and regulation.

Kinases were silenced in A549 and 293T^{RIG-I} cells and cells were infected with SeV. In the case of DAPK1, six individual siRNAs from two different suppliers were tested which all resulted in strong down-regulation of DAPK1 protein levels (Figure 15B). Down-regulation of DAPK1 by three siRNAs (namely siDAPK1_5, siDAPK1 sig1 and sig2) resulted in an increase in IFIT1 promoter activity which confirmed an inhibitory role for DAPK1 in RIG-I signalling (Figure 15A and [199]). Differences in remaining DAPK1 protein levels undetectable in Western Blot analyses and increased cytotoxicity probably account for a lack of effect on IFIT1 promoter activity by two siRNAs (siDAPK1_6, siDAPK1 sig3). SiRNA “siDAPK1 sig1” whose transfection resulted in the highest IFIT1 promoter activity after SeV infection was chosen for knockdown of DAPK1 in subsequent analyses and is referred to as “siDAPK1” throughout this study.

Subsequently, DAPK2 and DAPK3 were silenced in A549 and 293T^{RIG-I} cells and IFIT1 promoter activity after virus infection was analysed. DAPK2 protein levels in both cell lines were low, allowing detection only after exposure times of 30 to 60 minutes in Western Blot analysis, and were, in comparison, even lower in 293T^{RIG-I} cells than in A549 (Figure 12A and Figure 15E and 15F). Therefore, it was questionable whether depletion of such low protein amounts would have any effect on target cells. Accordingly, although three tested siRNAs resulted in down-regulation of DAPK2 protein levels, there was little to no change in IFIT1 promoter activity in response to DAPK2 knockdown (Figure 15 C). One siRNA, “siDAPK2 sig1” did result in a slight increase in IFIT1 promoter activity in 293T^{RIG-I} cells (Figure 15C right panel), but it also down-regulated DAPK1 levels when transfected in A549 and 293T^{RIG-I} cells (Figure 15 E), which probably resulted in the observed increase in IFIT1 promoter activity (compare Figure 15A).

DAPK3 was generally expressed to higher levels than DAPK2 in A549 and 293T^{RIG-I} cells. Three individual siRNAs targeting DAPK3 by two different suppliers resulted in up

to a three-fold increase in IFIT1 promoter activity after SeV infection in A549 and around a two-fold increase in 293T^{RIG-I} cells (Figure 15D) and all siRNAs efficiently down-regulated DAPK3 protein levels (Figure 15F).

These results confirm a role of DAPK3 as an inhibitor of RIG-I signalling. Importantly, siRNA “siDAPK3_3” lead to a down-regulation of DAPK2 levels in both A549 and 293T^{RIG-I} cells (Figure 9F). “siDAPK3 sig3” transfection resulted in highest IFIT1 promoter activity and high knock-down efficiency. It was, therefore, chosen for subsequent silencing analyses and is referred to as “siDAPK3” in this study.

Importantly, DAPK2 expression varied significantly in independent experiments (compare Figure 12, and Figure 15E and 15F), but was generally much lower than DAPK1 or DAPK3 expression (Figure 12). Additionally, DAPK2 silencing and additional stimulation by SeV infection often resulted in a dramatic increase in cell death, making it difficult to read out IFIT1 promoter activity assays in which signals were often close to background (data not shown). Based on these observations, subsequent analyses based on siRNA-mediated silencing were performed only for DAPK1 and DAPK3.

It had been established that DAPK1 silencing not only up-regulated IFIT1 promoter activity, but also resulted in increased IFIT1 and IFNβ mRNA levels after RIG-I stimulation [199]. In addition to DAPK1, DAPK3 also negatively regulated RIG-I signalling. This was observed in IFIT1 promoter activity assays after over-expression and was supported by results from siRNA-mediated silencing experiments. Since reporter-based promoter activity assays only reflect cellular responses to a stimulus to a certain extent but allow no conclusion on changes in endogenous protein or mRNA levels, endogenous levels of IFIT1 and IFNβ mRNA were analysed in response to SeV infection after DAPK3 depletion. These analyses were carried out in parallel to DAPK1 depletion to allow a comparison between both kinases. To this end, DAPK1 and DAPK3 were silenced in A549 and 293T^{RIG-I} cells and RIG-I signalling was stimulated by SeV infection. IFIT1 and IFNβ mRNA levels were determined by quantitative real-time PCR (qPCR). In parallel, knockdown efficiencies for DAPKs were determined measuring DAPK1, DAPK2, and DAPK3 mRNA levels. In analogy to results obtained in IFIT1 promoter activity assays, an overall increase in IFNβ and IFIT1 mRNA levels was observed after silencing of DAPK1 and DAPK3 (Figure 16).

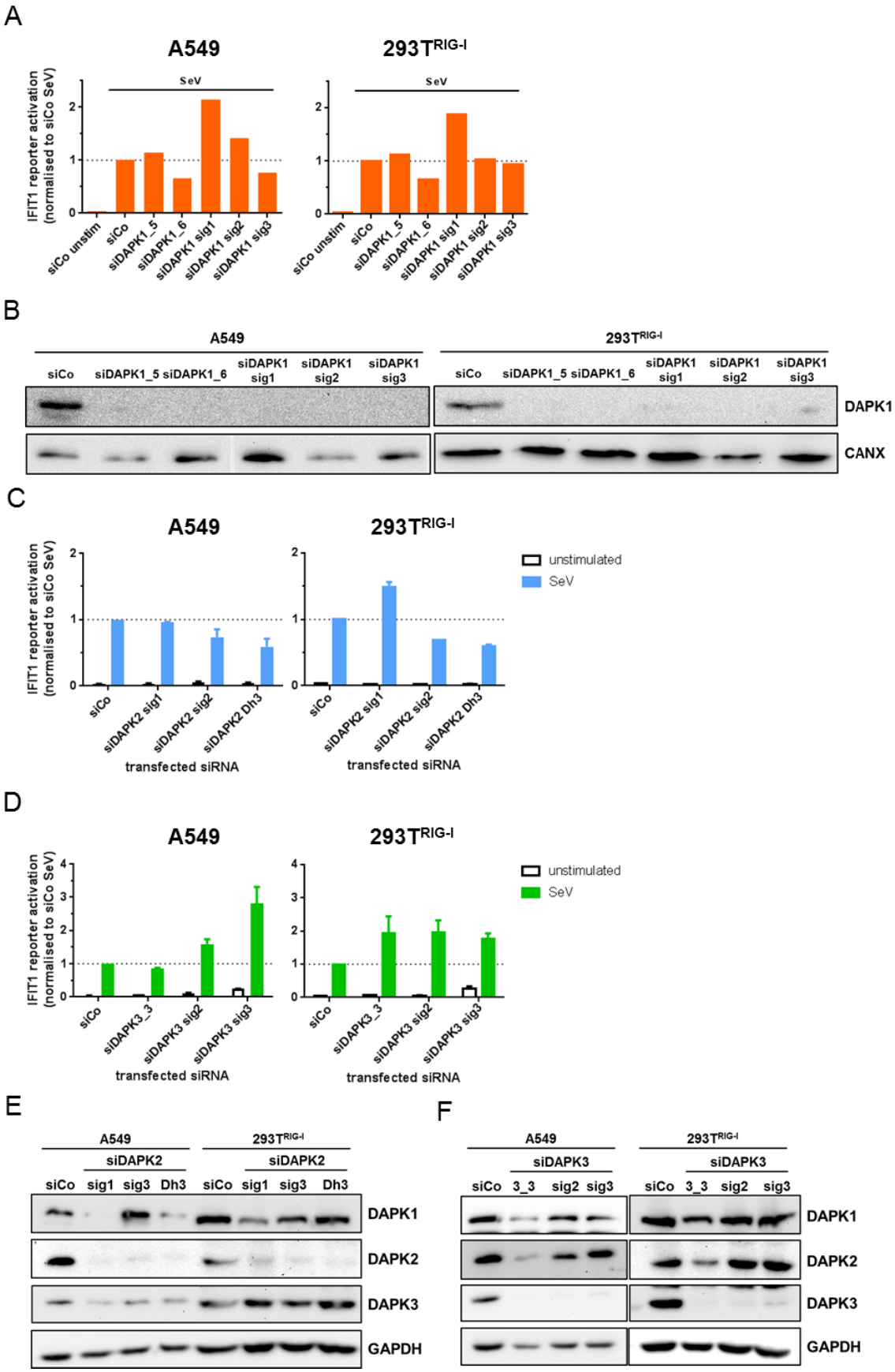

Figure 15 **Silencing of DAPK family members enhances IFIT1 promoter activity** (figure legend on the following page)

For IFIT1 promoter activity after silencing of DAPKs, siRNAs targeting the individual kinase were reverse transfected into A549 or 293T^{RIG-I} cells. 38h after siRNA transfection, reporter plasmids were transfected, and 48h after siRNA transfection cells were infected with SeV (MOI 5) for 16h. **A)** IFIT1 promoter activity after silencing of DAPK1 in A549 and 293T^{RIG-I} cells using six different siRNAs. **B)** Western Blots assessing silencing efficiency of DAPK1 corresponding to measurements in A). **C)** IFIT1 promoter activity assay after silencing of DAPK2 with **E)** corresponding Western Blot analysing silencing efficiency and expression of DAPK1, and DAPK3. **D)** IFIT1 promoter activity assay after silencing of DAPK3 with **F)** corresponding Western Blot analysing silencing efficiency and expression of DAPK1, and DAPK2. Mean of two **(C)** or three **(D)** independent experiments are shown. Western Blots show one representative result.

While IFNβ mRNA levels were increased around 6-fold in A549 and 4-fold in 293T^{RIG-I} cells after silencing of DAPK1 (Figure 16A and [199]), silencing of DAPK3 resulted in an average increase in IFNβ mRNA of 2-fold in A549 and 4-fold in 293T^{RIG-I} cells. Silencing of DAPK3 also resulted in a 2-fold increase in IFIT1 mRNA levels, while the increase in IFIT1 mRNA levels was slightly smaller in A549 cells (Figure 16B).

Notably, in analyses carried out in the present studies, silencing of DAPK1 had no effect on IFIT1 mRNA levels in either cell line, although it reproducibly up-regulated IFIT1 mRNA in previous experiments [199]. mRNA levels of both DAPK1 and DAPK3 were reduced up to 90% in A549 and 293T^{RIG-I} cells, while the knockdown of one DAPK did not have a strong influence on mRNA expression of the other examined kinases, with a mere 1.5-fold increase in DAPK2 mRNA levels after silencing of DAPK1 or DAPK3 in 293T^{RIG-I} cells (Figure 16C). DAPK3 mRNA levels were slightly increased in A549 cells in response to virus infection which is in agreement with previous findings stating that DAPK3 might be an ISG [205].

Silencing experiments lasted a total of four days. Therefore, seeding a low number of cells was required as cells continued to grow and divide throughout the experiment. As indicated above, DAPK1 protein levels were changed dramatically based on cell density and growth (Figure 10C and 10D) and it is not unlikely that this might be the case for DAPK2 and DAPK3 as well. It was observed that, probably due to varying cell growth and division, results of siRNA-based silencing assays, which lasted longer than over-expression assays, were subject to larger internal variation than over-expression experiments. This is also a likely explanation for the here observed lack of up-regulation of IFIT1 mRNA upon silencing of DAPK1.

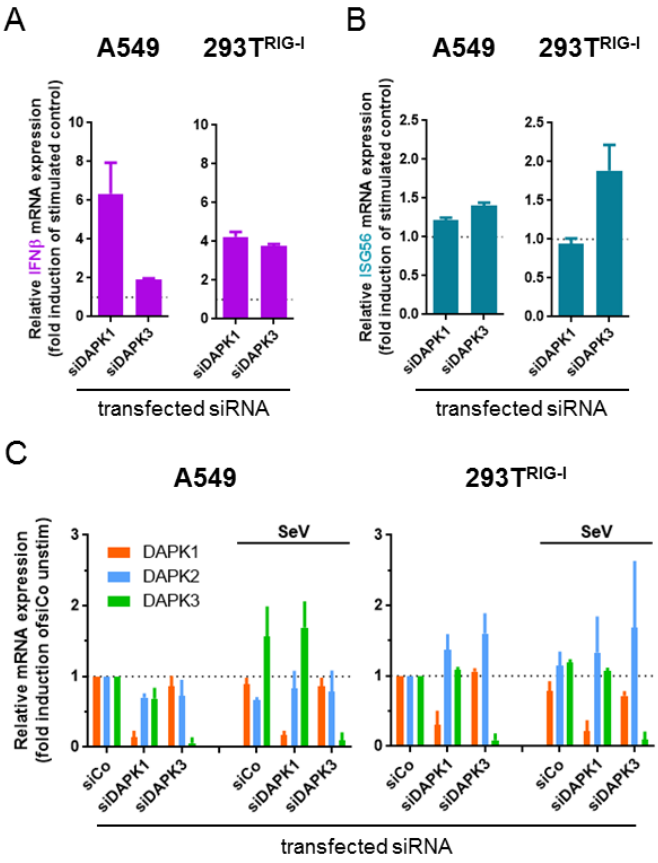

Figure 16 **Silencing of DAPK1 and DAPK3 increases IFNβ and IFIT1 mRNA levels**

For qPCR analyses DAPK1 or DAPK3 were silenced for 48h in A549 or 293T^{RIG-I} cells. Cells were stimulated with SeV (MOI 5) for 16h before mRNA levels of DAPK1, DAPK2, DAPK3, IFNβ and IFIT1 were measured.

A) IFNβ and **B)** IFIT1 mRNA levels in A549 and 293T^{RIG-I} cells silenced for either DAPK1 or DAPK3 are shown. **C)** mRNA levels of DAPK1, DAPK2, and DAPK3 in unstimulated and SeV infected A549 and 293T^{RIG-I} cells are shown. mRNA levels of target genes are normalised to GAPDH mRNA levels and shown as fold-induction of stimulated non-targeting siRNA control. Results are the mean of two independent experiments.

No conclusions could be drawn from silencing experiments with DAPK2 due to the lack of an effect in IFIT1 promoter activity assays and toxicity of siRNAs in combination with virus infection. However, silencing of DAPK3 resulted in an increase in RIG-I signalling activity after SeV infection in 293T^{RIG-I} and A549 cells as analysed by examination of IFIT1 promoter activity and qPCR, confirming its role as an inhibitor of the RIG-I signalling pathway.

4.3 Induction of cell death by DAPKs is independent of RIG-I signalling inhibition

4.3.1 Induction of apoptosis by DAPKs is not responsible for their inhibitory role in RIG-I signalling

As indicated by their name “death-associated protein kinases”, DAPKs are known and well-described inducers of cell death pathways such as apoptosis and autophagy [161], [164], [200], [207], [219], [228]. Hence, in order to assure cell survival, their activity is tightly regulated.

DAPK1, DAPK2, and DAPK3 induced cell death in $293T^{RIG\text{-}I}$ cells when over-expressed which could be observed by an increased amount of detached and floating cells compared to mock transfection (data not shown). Since cell death induction is one of the main cellular functions of DAPKs, it could not be ruled out that their effects on RIG-I signalling were mediated by an increase in apoptosis, especially after over-expression in $293T^{RIG\text{-}I}$ cells. In order to determine whether increased induction of apoptosis upon DAPK over-expression was responsible for reduced RIG-I signalling activity, cells were treated with small molecule inhibitors which potently inhibit apoptosis induction and effects on RIG-I signalling activation in response to SeV stimulation were observed.

First, in order to assess their inhibitory potential and find working concentrations, small molecule pan-caspase inhibitors Q-VD-OPh [254] and zVAD [255] were tested in $293T^{RIG\text{-}I}$ and A549 cells. To this end, cells were treated with apoptosis-inducing drugs staurosporine, which besides broadly inhibiting cellular kinases such as PKC [256] also directly enhances caspase-3 activity [257], and actinomycin D, an inhibitor of DNA transcription [258], [259]. After drug treatment, extent of Poly ADP ribose polymerase (PARP) cleavage was analysed by Western Blot quantification. PARP is an enzyme involved in DNA repair and a direct target of activated caspase-3 [240], [241]. Induction of apoptosis, i.e. caspase 3 activation, results in the proteolytic cleavage of full-length PARP in its 24 kDa DNA-binding and 89 kDa catalytic domain (cleaved PARP, c-PARP). The extent of caspase-3 activity and PARP cleavage is directly proportional, allowing a relative quantification of cell death induction by quantification of PARP cleavage.

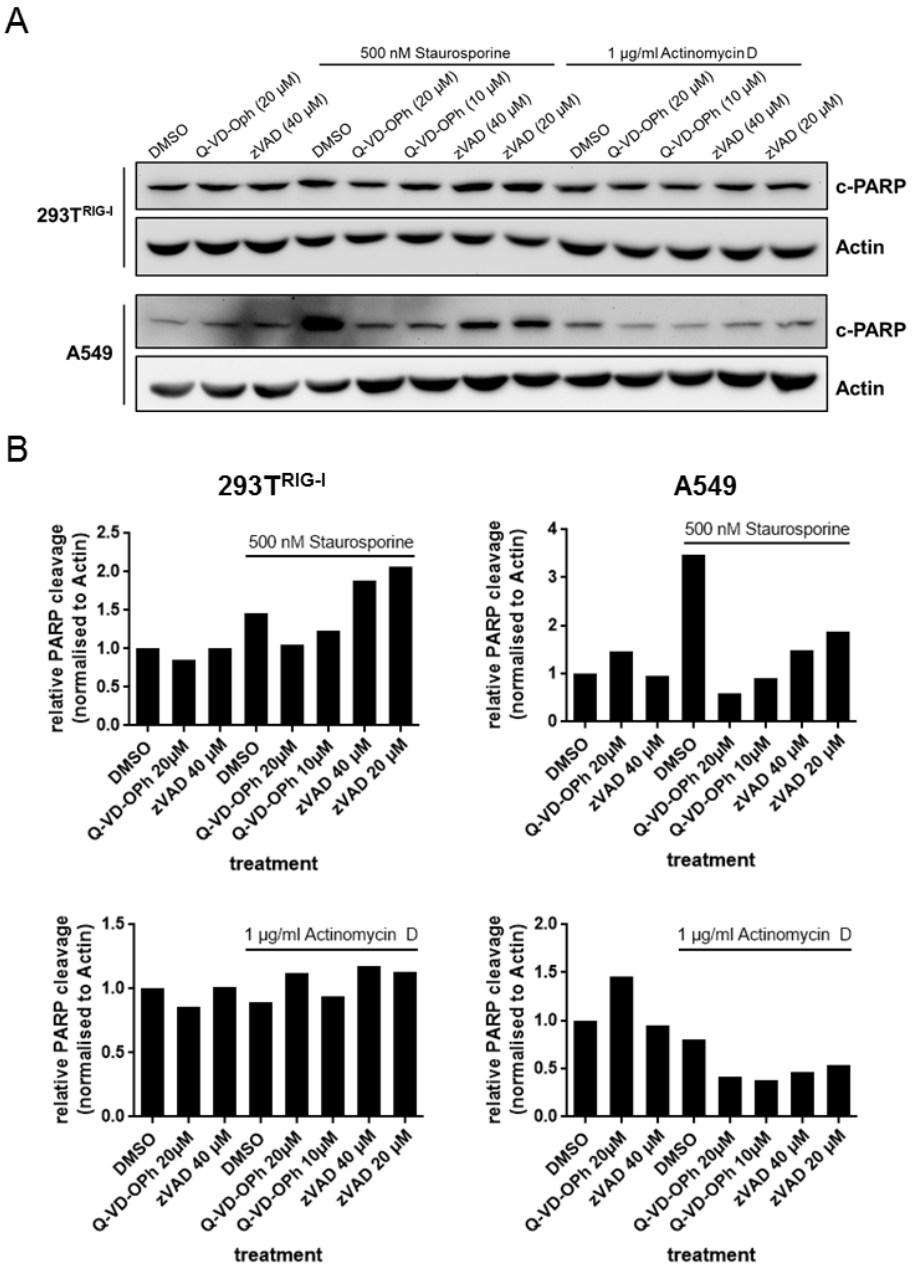

Figure 17 **Q-VD-OPh is a non-toxic apoptosis inhibitor**

Analysis of PARP cleavage after treatment of 293T^{RIG-I} or A549 cells with apoptosis inducers staurosporine and actinomycin D. Cells were treated with drugs for 4h (A549) or 8h (293T^{RIG-I}) either in the absence or presence of different concentrations of Q-VD-OPh or zVAD and PARP cleavage was observed. Western Blots **(A)** were quantified by densitometry **(B)**.

Whereas treatment with staurosporine induced strong (over 3 fold) PARP cleavage in A549 cells and weak (0.5 fold) PARP cleavage in 293T^{RIG-I} cells, treatment with actinomycin D did not lead to an increase in PARP cleavage (Figure 17B lower panels).

Generally, 293T^{RIG-I} cells displayed higher endogenous levels of cleaved PARP compared to A549 cells (Figure 17A). Although PARP cleavage, i.e. apoptosis induction, in 293T^{RIG-I} cells in response to staurosporine treatment was low (Figure 3B upper left panel), it was efficiently and dose-dependently inhibited by treatment with Q-VD-OPh, which also potently inhibited PARP cleavage in A549 cells. zVAD did not inhibit apoptosis induction in A549 cells (Figure 17B upper right panel) as efficiently as Q-VD-OPh, and, at least in tested concentrations, was toxic in 293T^{RIG-I} cells, in which PARP cleavage was increased after zVAD treatment.

Based on the above results Q-VD-OPh in a concentration of 20 µM was chosen as an inhibitor of apoptosis induction for subsequent assays.

To address whether inhibitory effects on RIG-I signalling by DAPKs were mediated by their cell death-inducing properties, 293T^{RIG-I} cell were transfected with DAPK family members all of which have been described to induce apoptosis [161], [200], [217]. Importantly, DRAK2 was excluded since it did not inhibit RIG-I signalling when over-expressed in 293T^{RIG-I} cells (Figure 14). Pre- and co-treatment with Q-VD-OPh was compared to vehicle control. Effects on RIG-I signalling were analysed assessing IFIT1 promoter activity, while apoptosis induction was monitored by Western Blot analysis for PARP cleavage.

Over-expression of all DAPK family members induced apoptosis in 293T^{RIG-I} cells as observed by an up to 2.5 fold increase in PARP cleavage (Figure 18A and 18B). Out of all DAPKs, DAPK3 showed highest levels of cleaved PARP both in unstimulated and infected cells. PARP cleavage induced by DAPK1 and DAPK2 was slightly increased in infected cells compared to the unstimulated control. PARP cleavage, i.e. apoptosis induction, was inhibited in cells expressing DAPK1, DAPK2 and DAPK3 which were pre- and co-treated with Q-VD-OPh. Notably, DRAK1 over-expression resulted in only a mild increase in PARP cleavage which could not be inhibited by Q-VD-OPh treatment (Figure 18B). Over-expression of all examined DAPK family members strongly inhibited IFIT1 promoter activity. However, neither in untreated nor in infected cells did inhibition of apoptosis induction by Q-VD-OPh treatment change RIG-I signalling induction or the inhibition of the former by DAPKs (Figure 18C). Based on these results it is unlikely that DAPKs mediate an inhibition of RIG-I signalling by induction of the apoptotic machinery. Instead, regulation of RIG-I signalling by DAPK family members seems to happen independently of their apoptosis-promoting function.

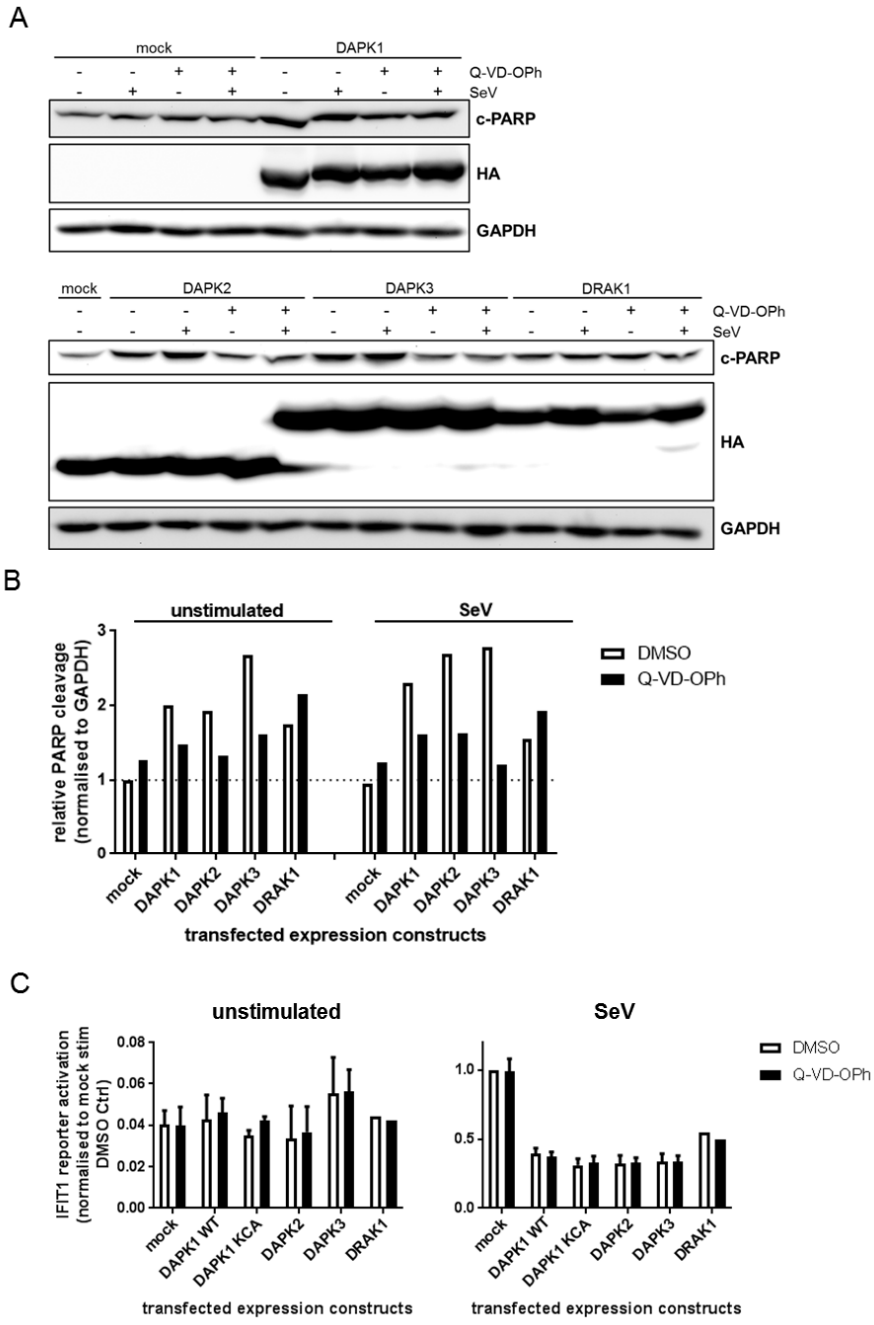

Figure 18 **Inhibition of RIG-I signalling by DAPKs is not due to cell death induction**

A) Western Blot for PARP cleavage in 293T^{RIG-I} cells expressing HA-tagged DAPK family members. Cells were infected with SeV (MOI 5) for 16h and either pre- and co-treated with 20 µM Q-VD-OPh or treated with vehicle control. Transfection efficiency was monitored by detection of the HA-tag. **B)** Quantification of c-PARP signal from A) in untreated compared to infected cells. **C)** IFIT1 promoter reporter assay of untreated and infected cells pre- and co-treated either with vehicle control or 20 µM Q-VD-OPh. Data is the mean of four independent experiments for DAPK1, DAPK2 and DAPK3 and one experiment for DRAK1.

4.3.2 Autophagy may influence RIG-I signalling, but is not induced by DAPK over-expression in 293T^{RIG-I} cells

DAPK1, DAPK2, and DAPK3 are not only involved in the induction of type I (apoptotic) cell death pathways, but also promote type II (autophagic) cell death by several mechanisms such as direct phosphorylation of beclin-1 [170], [171], [208], [228] and interaction with cytoskeletal components, promoting autophagic vesicle formation [260]. Autophagy was found to influence cellular antiviral responses. On the one hand, induction of autophagy helps degrading viral components which have entered the cytoplasm, as was shown in PKR-mediated clearance of herpes simplex virus type 1 [261]. On the other hand, proteins of the ATG family, whose activation is crucial for the autophagic machinery, may inhibit the RIG-I signalling pathway by direct interaction with either RIG-I or MAVS [262], [263]. Thus, it appears feasible that an induction of autophagy by over-expression of DAPK1, DAPK2, and DAPK3 will have an impact on antiviral signalling and could explain the observed inhibition of the RIG-I signalling pathway.

Autophagy induction relies on the formation of isolation membranes by the Beclin-VPS34-ATG14L complex inducing production of PI3P which is incorporated in the growing membranes. Another essential protein which is necessary for autophagosomal membrane expansion is lipidated LC3B. In its non-lipidated form LC3B is referred to as LC3B-I. In response to autophagy induction, LC3B is cleaved and lipidated and the generated product is referred to as LC3B-II. LC3B-II is characterised by distinct running behaviour in polyacrylamide gels and its relative amount is often used to quantify the amount of autophagy induction, e.g. after drug treatment of cells [245]. Hence, inhibition of autophagy by Spautin-1 which interferes with local PI3P production [244] can be observed as an increase in LC3B-I compared to LC3B-II levels. In contrast, induction of autophagy by mTOR inhibitor Torin-1 [243], [264] results in a decrease in LC3B-I levels as most LC3B will be lipidated.

In order to examine if the effect on RIG-I signalling mediated by DAPK1, DAPK2, and DAPK3 was due to an induction of autophagy, the three kinases were over-expressed in 293T^{RIG-I} cells. In parallel, cells were treated with Spautin-1 or with Torin-1. IFIT1 promoter activity was measured after stimulation. To assess changes in autophagy induction in transfected cells, immune staining for LC3B-I and LC3B-II was employed.

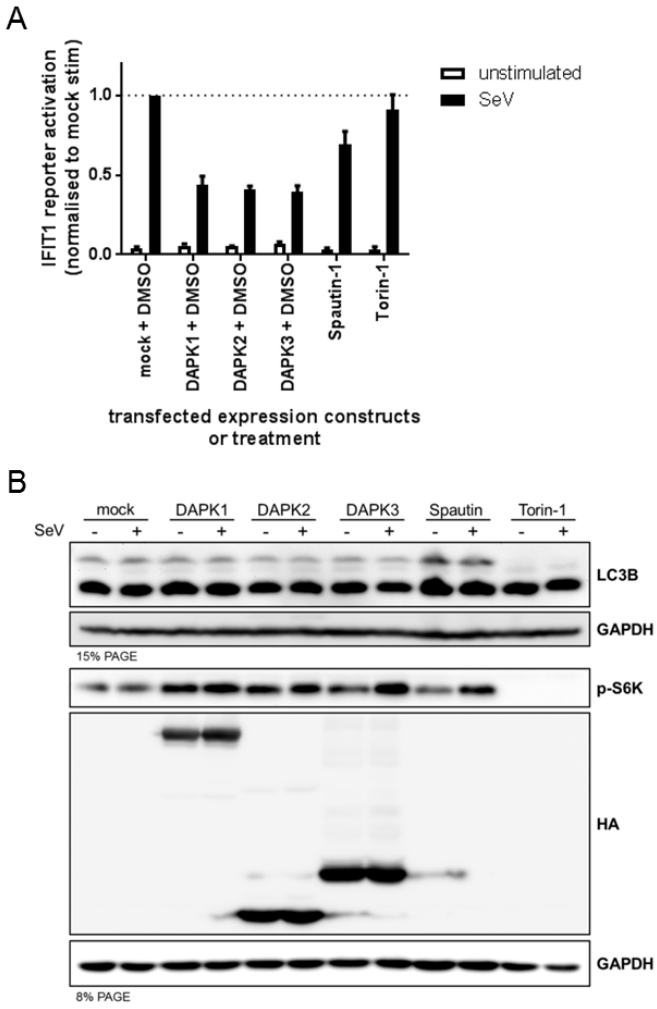

Figure 19 Autophagy may influence RIG-I signalling but is not induced by over-expression of DAPK family members

A) 293T^{RIG-I} cells over-expressing DAPKs were either left unstimulated or infected with SeV (MOI 5) for 16h. Additionally, cells were treated with 20 µM Spautin-1 or 250 nM Torin-1 for 16h, either without stimulation or in combination with SeV (MOI 5) infection. Data is the mean of three (DAPK2, DAPK3, Torin-1) or four (mock, DAPK2, Spautin-1) experiments. **B)** Western Blot analysis of LC3B levels under DAPK over-expression or drug treatment. P-S6K levels indicated state of mTOR inhibition. Expression of DAPK constructs was monitored by staining HA-tag. A representative of three independent experiments is shown.

While inhibition of autophagy by Spautin-1 treatment did result in a slight but reproducible decrease of IFIT1 promoter activity, induction of autophagy by Torin-1 treatment did not change IFIT1 promoter activity as compared to mock transfected, vehicle treated cells (Figure 19A). Efficiency of autophagy inhibition by Spautin-1 or induction by Torin-1 was assessed by observation of LC3B-I and –II levels on Western Blot. As expected, Spautin-1 treatment resulted in increased LC3B-I (Figure 19A, upper LC3B signal) levels, whereas Torin-1 treatment resulted in a strong decrease in LC3B-I levels (Figure 19B). This is in line with findings that the autophagic flux in mTOR inhibitor treated cells is strongly increased and most LC3B will be found as membrane-associated LC3B-II (Figure 19A, lower LC3B signal). Efficiency of mTOR inhibition by Torin-1 was

assessed by analysis of p70-S6 kinase (p-S6K) phosphorylation status, which was not found in its phosphorylated form after Torin-1 treatment (Figure 19B).

Over-expression of DAPK1, DAPK2, and DAPK3, significantly decreased IFIT1 promoter activity (Figure 19A) as observed previously (Figure 13A, 13B, 13C). Neither DAPK1, nor DAPK2 or DAPK3 over-expression resulted in a change in LC3B levels compared to mock transfected cells, indicating that, contrary to previous reports, DAPK over-expression does not induce autophagy in the $293T^{RIG-I}$ cells used in our study.

Although autophagy inhibition did result in a slight decrease in IFIT1 promoter activity, the observed effect was not as strong as the inhibition observed upon DAPK over-expression. Furthermore, autophagy was not detectably induced (nor inhibited) after DAPK over-expression, arguing that the observed inhibitory effect of DAPKs on RIG-I signalling is not linked to known DAPK functions in type II cell death, i.e. autophagic pathways.

4.4 The role of DAPK2 and DAPK3 in the RIG-I signalling pathway

4.4.1 Inhibition of RIG-I signalling by DAPK2 and DAPK3 is kinase-dependent

Similar to DAPK1, DAPK2 and DAPK3 were found to be negative regulators of RIG-I signalling. It was established that RIG-I signalling inhibition by DAPK1 was dependent on kinase activity as shown above (Figure 1) and in [199]. Hence, it was likely that DAPK2 and DAPK3 acted similarly and that their function as negative regulators of RIG-I signalling was also based on their kinase activity. Five different mutants of DAPK2 and DAPK3, respectively, were cloned which either included or lacked different known domains of the kinases (Figure 20). Apart from reportedly kinase-dead $DAPK2^{K52A}$ and $DAPK3^{K42A}$, additional mutants which were reported to have lost kinase activity were generated, namely $DAPK3^{D161A}$ which was reported to harbour a destabilised active centre of the kinase domain [160] and $DAPK3^{K42A\ D161A}$ double mutant. In analogy to S308 mutants generated for DAPK1 (Figure 1), $DAPK2^{S318D}$ (phospho-mimetic) and $DAPK2^{S318A}$ (phospho-ablatant) mutants were generated which have been studied and found to display either increased ($DAPK2^{S318A}$) or decreased ($DAPK2^{S318D}$) kinase activity [265]. Additionally, $DAPK2^{Kinase}$ and $DAPK3^{Kinase}$, kinase-only mutants, and $DAPK2^{Kinase-CaM}$, a mutant comprising kinase and CaM domain, and a mutant lacking the kinase domain of DAPK3 ($DAPK3^{deltaKinase}$) were generated.

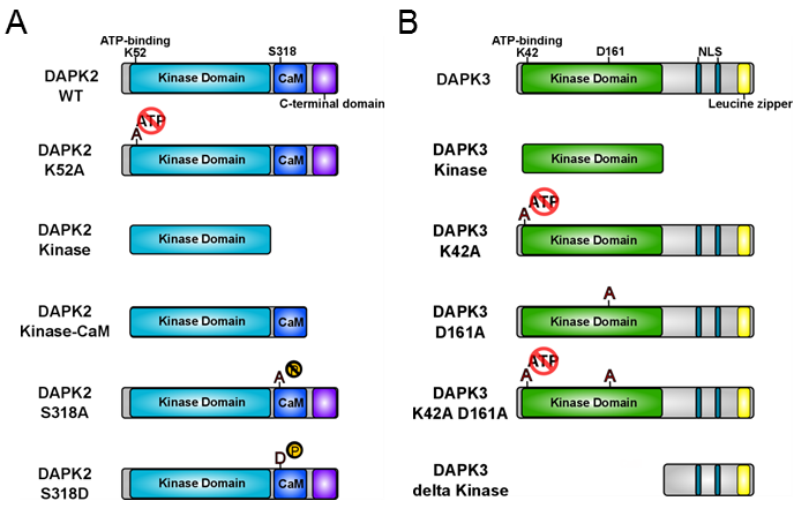

Figure 20 **DAPK2 and DAPK3 mutants**

A) Overview of DAPK2 mutants **B)** Overview of DAPK3 mutants

Unlike DAPK3, DAPK2 is a CaM-dependent kinase. Its C-terminal domain displays no homology to any other known protein domain. In addition to its nuclear localisation signals (NLS), the C-terminus of DAPK3 contains a Leucin zipper domain which mediates protein-protein interaction. A DAPK3 mutant lacking the Leucin zipper domain was generated. It generally behaved like full-length DAPK3 (compare appendix, figure 40) and is, therefore, omitted here.

DAPK2 and DAPK3 mutants were compared to full-length DAPK2 and DAPK3 by assessing changes in IFIT1 promoter activity.

DAPK2^{K52A} and DAPK2$^{Kinase-CaM}$ inhibited IFIT1 promoter activity to the same extent as full-length (WT) DAPK2, whereas DAPK2^{Kinase} lost part of its ability to inhibit RIG-I signalling (Figure 21A). Remarkably, there was a clear difference between constitutively kinase-active DAPK2^{S318A} and kinase-inactive DAPK2^{S318D} regarding their ability to inhibit IFIT1 promoter activity, with DAPK2^{S318A} behaving similar to DAPK2^{WT}. DAPK2 constructs were expressed to similar levels as shown in Western Blot staining for HA-tag (Figure 21C). DAPK3^{K42A}, DAPK3^{D161A}, DAPK3$^{K42A\ D161A}$, and DAPK3^{Kinase} inhibited RIG-I signalling to the same extent as full-length (WT) DAPK3 when over-expressed in 293T^{RIG-I} cells (Figure 21B). DAPK3^{deltaKinase}, however, did not reduce but rather enhanced IFIT1 promoter activity compared to mock transfection. DAPK3 constructs were expressed to similar levels when over-expressed in 293T^{RIG-I} cells (Figure 21D). For DAPK3^{K42A}, DAPK3^{Kinase} and DAPK3^{deltaKinase} similar results were obtained in a NFκB promoter activity assay, in which DAPK3^{K42A} and DAPK3^{Kinase} inhibited RIG-I signalling to the same extent as DAPK3^{WT}. DAPK3^{deltaKinase} mutant did not show any inhibitory effect (appendix, figure 40).

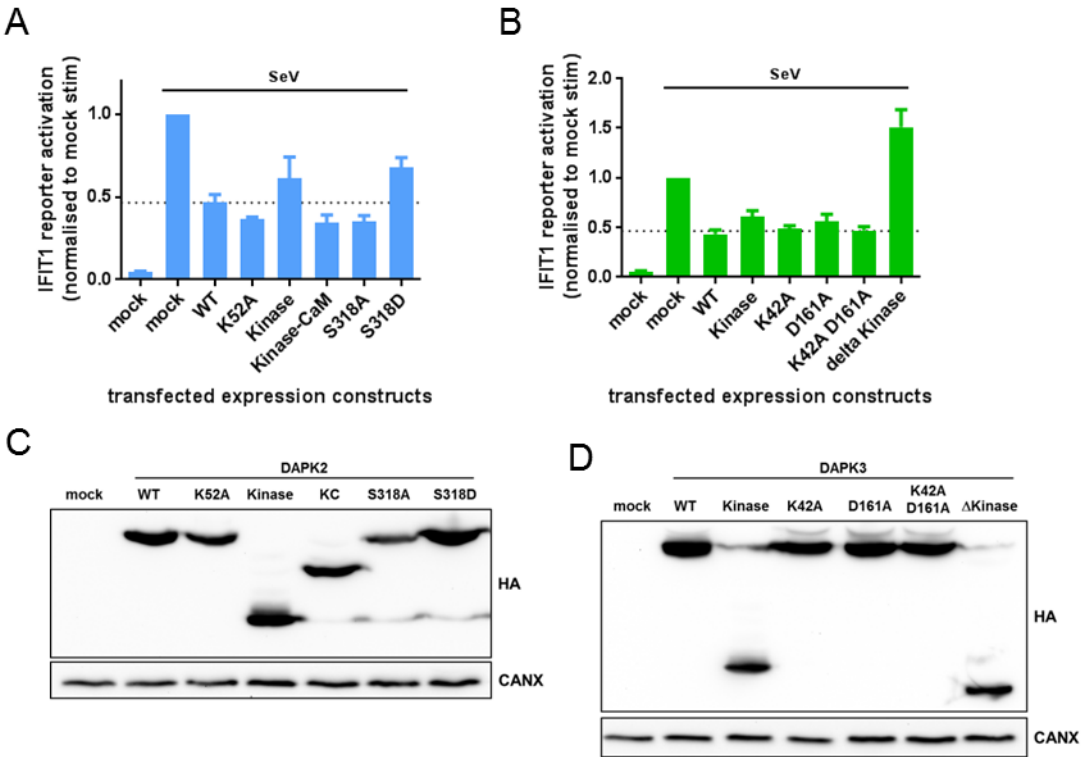

Figure 21 **Inhibition of RIG-I signalling by DAPK2 and DAPK3 is kinase-dependent**

IFIT1 reporter assay of 293T^{RIG-I} cells over-expressing DAPK2 **(A)** or DAPK3 **(B)** mutants. Cells were transfected with kinase mutants and stimulated by SeV (MOI 5) infection for 16h. Results show mean of four (DAPK2 WT, S318A, and S318D) or three (rest) independent experiments. Western Blot stains for HA-tag were performed to assess expression efficiency **(C, D)** and a representative result is shown.

Supposedly kinase-inactive DAPK2^{K52A} and DAPK3$^{K42A/D161A}$ inhibited IFIT1 promoter activity to the same extent as the full-length constructs. It is possible that these mutants retain kinase activity in over-expression experiments, similar to DAPK1$^{KCA\ K42A}$ for which auto-phosphorylation at S308 was observed when it was over-expressed in 293T^{RIG-I} cells (Figure 1C).

Nevertheless, the above results suggest that inhibition of RIG-I signalling by DAPK2 is kinase activity-dependent as a constitutively kinase-active mutant of DAPK2, DAPK2^{S318A}, conferred full inhibition of IFIT1 promoter activity, whereas a constitutively inactive mutant, DAPK2^{S318D}, lost this inhibitory function. Similarly, in case of DAPK3, its kinase domain alone acted like full-length DAPK3, but over-expression of a mutant lacking the kinase domain did not lead to RIG-I signalling inhibition. It has to be noted that the DAPK3$^{delta\ Kinase}$ construct is extremely small in comparison to full-length DAPK3. Hence, it remains to be examined whether inhibition of RIG-I signalling by DAPK3 really depends on DAPK3 kinase activity.

4.4.2 Activity of DAPK2 and DAPK3 is regulated upon initiation of antiviral signalling

As shown above in Figure 1, DAPK1 is subject to auto-phosphorylation at S308 which impacts its activity [251]. In fact, DAPK1 needs to be de-phosphorylated at S308 for full kinase activity and its activation status can be monitored by immune staining for p-DAPK1 S308 in Western Blotting. Not only did DAPK1 negatively regulate RIG-I upon over-expression, but it was also increasingly activated upon initiation of antiviral signalling ([199] and Figure 22). Therefore, it was proposed that DAPK1 is part of a negative feedback loop in which it is increasingly activated after initiation of antiviral signalling. DAPK1, being an inhibitor of RIG-I signalling, phosphorylates and deactivates RIG-I, providing a means of control of the antiviral response and preventing an overshooting immune response which could be detrimental for the host.

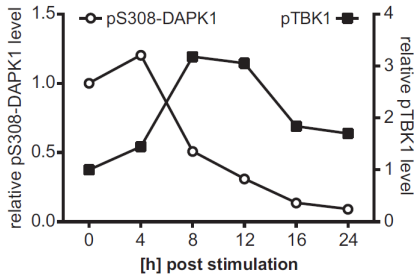

Figure 22 **DAPK1 activation after dsRNA stimulation**

A549 cells were stimulated with 5'ppp-dsRNA over a time course of 24h. Increasing RIG-I signalling activity is indicated by rising relative levels of p-TBK1. At the same time, relative p-DAPK1 S308 levels decrease steadily until hardly any p-DAPK1 is detected 24h after stimulation. Adapted from [199].

Experiments performed in this study identified DAPK2 and DAPK3 as negative regulators of RIG-I signalling. Moreover, their inhibitory function seemed to be kinase activity-dependent. These findings were similar to those previously obtained for DAPK1. Therefore, it was not unlikely that DAPK2 and DAPK3 activity might be regulated upon initiation of antiviral signalling. It was examined if activity of endogenous DAPK2 and DAPK3 changed upon initiation and progression of RIG-I-mediated antiviral signalling.

4.4.2.1 DAPK2 dimerises increasingly after SeV infection and initiation of RIG-I signalling

Analogous to DAPK1, DAPK2 is auto-phosphorylated at S318 which decreases kinase activity. Although there is an antibody available which supposedly detects p-DAPK2 S318 in ELISA analyses, it was not possible to obtain a specific signal for p-DAPK2 on Western Blot level using this antibody (data not shown). However, it is known that endogenous DAPK2 homodimerises and this dimerisation process was shown to be

especially efficient for constitutively kinase-active DAPK2 S318A [160], suggesting that DAPK2 dimerisation indicates increased DAPK2 activity. Furthermore, DAPK2 dimers were found to be extremely stable, allowing their detection even after denaturing SDS-PAGE [160].

DAPK2 over-expression did frequently result in a signal of higher apparent molecular weight whose size matched that of putative DAPK2 homodimers (Figure 26A). Remarkably, potential dimerisation was also observed for endogenous DAPK2, seemingly induced after virus infection (Figure 12A). To facilitate detection of DAPK2 dimers, chemical cross-linking of whole cell lysates from DAPK2 over-expressing 293T^{RIG-I} cells was employed. Indeed, in addition to DAPK2 monomers, dimers, trimers and higher molecular weight oligomers were observed after cross-linking (Figure 23A), which was especially efficient using a concentration of 1% paraformaldehyde.

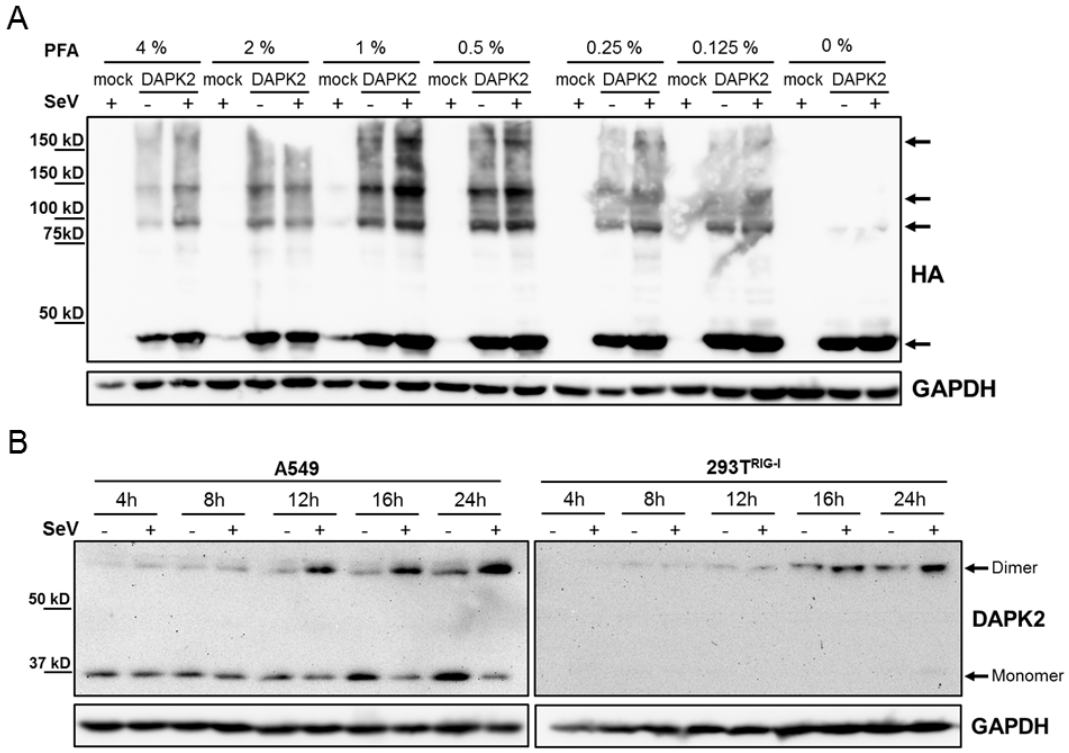

Figure 23 DAPK2 dimerisation

A) Western Blot analysis of dimer- and oligomerisation of over-expressed DAPK2 in 293T^{RIG-I} cells treated with increasing concentrations of paraformaldehyde (PFA). Arrows indicate DAPK2 monomers and oligomers. **B)** Western Blot analysis of DAPK2 dimerisation in A549 and 293T^{RIG-I} cells in a time course experiment. Cells were infected with SeV (MOI 5) and proteins were cross-linked at different time points after infection. A representative of three independent experiments is shown. Arrows indicate DAPK2 monomers and dimers.

This cross-linking approach was then used to detect dimerisation of endogenous DAPK2, and, in fact, an increasing amount of endogenous homodimerised DAPK2 was detected in A549 and 293T^{RIG-I} cells after SeV infection compared to unstimulated

controls in a time course experiment (Figure 23B). This suggests virus- or antiviral-signalling-dependent dimerisation of DAPK2 in A549 and 293T^{RIG-I} cells.

4.4.2.2 DAPK3 activating phosphorylation decreases in response to virus infection

Although DAPK3 has not been studied as extensively as DAPK1 and DAPK2 in regard to regulation of its kinase activity, it was reported that several residues of DAPK3 must be phosphorylated for full activity, one of them being threonine 265 (T265) [203] which sits in the kinase domain of DAPK3 (Figure 24A). In order to examine whether antiviral signalling caused changes in DAPK3 activity, DAPK3 activating phosphorylation at T265 in response to SeV infection was analysed in A549 cells using an antibody which specifically detects p-DAPK3 T265. In contrast to uninfected controls, in which p-DAPK3 T265 levels remained stable, prolonged infection with SeV lead to a decrease in p-DAPK3 T265 levels, whereas total DAPK3 levels were not changed (Figure 24B).

However, close examination and densitometric quantification of p-DAPK3 T265 levels in independent experiments revealed that DAPK3 phosphorylation was not always decreased to the same extent (Figure 24C, 1 and 2) and in some instances even increased over time (Figure 24C, 3). Nevertheless, virus infection ultimately resulted in significantly lower p-DAPK3 T265 levels compared to unstimulated controls at late time points in all experiments.

Taken together, activities of endogenous DAPK2 and DAPK3 were regulated upon initiation of antiviral signalling. DAPK2 dimerised increasingly after onset of RIG-I signalling, indicating increased activity. DAPK3, however, lost its activating phosphorylation at T265 over time after virus infection, suggesting decreased activity in response to RIG-I signalling initiation.

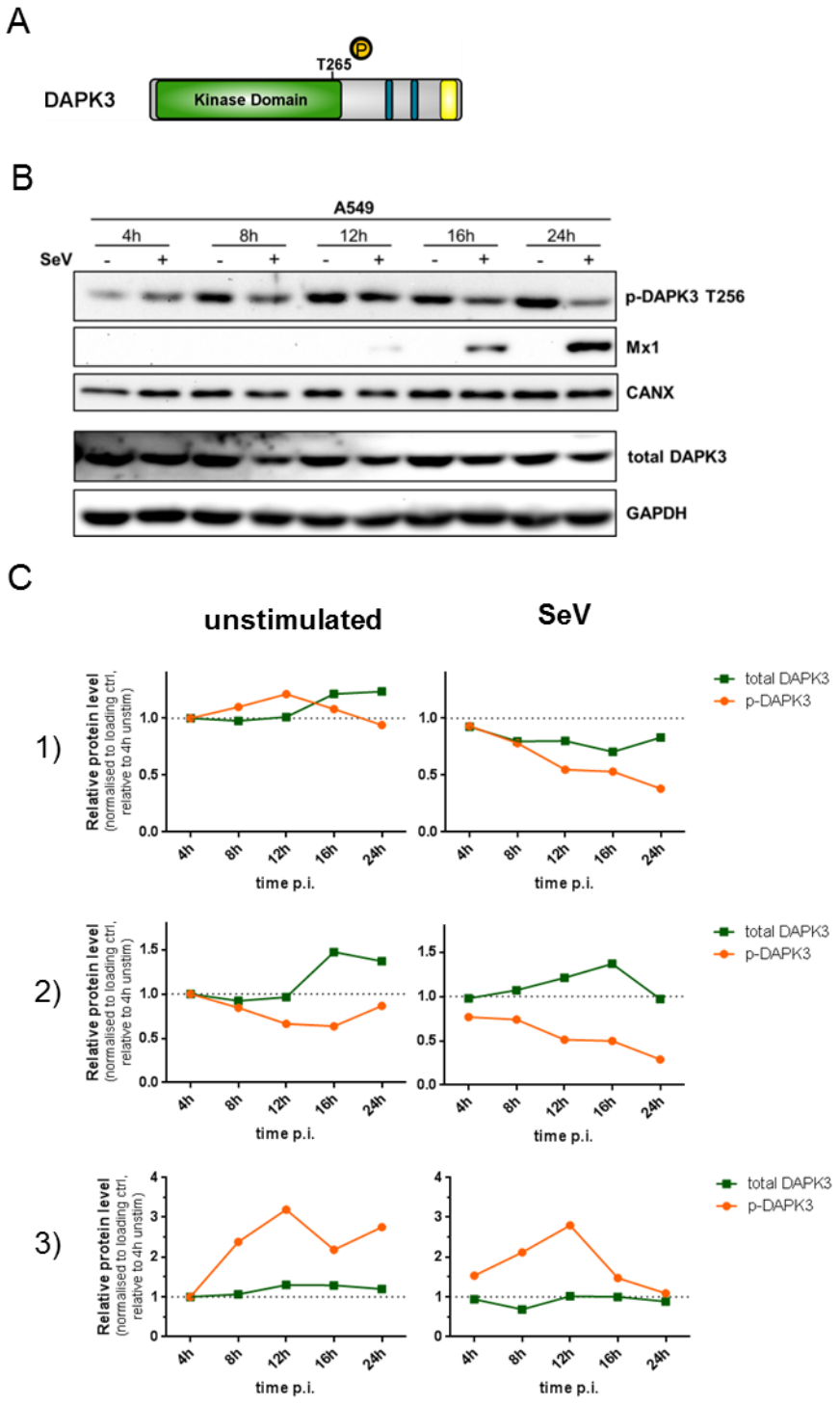

Figure 24 **DAPK3 activity is decreased in response to virus infection**

A) Overview of DAPK3. T265 is subject to phosphorylation which is necessary for full kinase activity. **B)** Western Blot analysis of p-DAPK3 T265 levels in a time course experiment in A549 cells. Cells were infected with SeV (MOI 5) and protein levels of p-DAPK3 T265, Mx1, total DAPK3 and loading controls were analysed after at different times after infection. A representative of three independent experiments is shown. **C)** Overview over DAPK3 phosphorylation at T265 and total DAPK3 protein levels after SeV infection in three independent experiments. Relative protein levels were measured by densitometry.

4.4.3 DAPK1 and DAPK2 interact with RIG-I and all DAPK family members phosphorylate RIG-I *in vitro*

It was shown that DAPK1 interacted with RIG-I when over-expressed in 293T^{RIG-I} cells and that DAPK1 phosphorylated RIG-I *in vitro*. Furthermore, phospho-mimetic mutations of DAPK1-targeted residues on RIG-I rendered RIG-I incapable of an initiation of antiviral signalling [199]. As the above results suggest an additional, possibly kinase-dependent inhibition of RIG-I signalling by DAPK family members DAPK2 and DAPK3, it was examined whether these interacted with RIG-I. DAPK family member DRAK1 was included in this analysis since it was just as capable of mediating RIG-I signalling inhibition as DAPK1, DAPK2, and DAPK3.

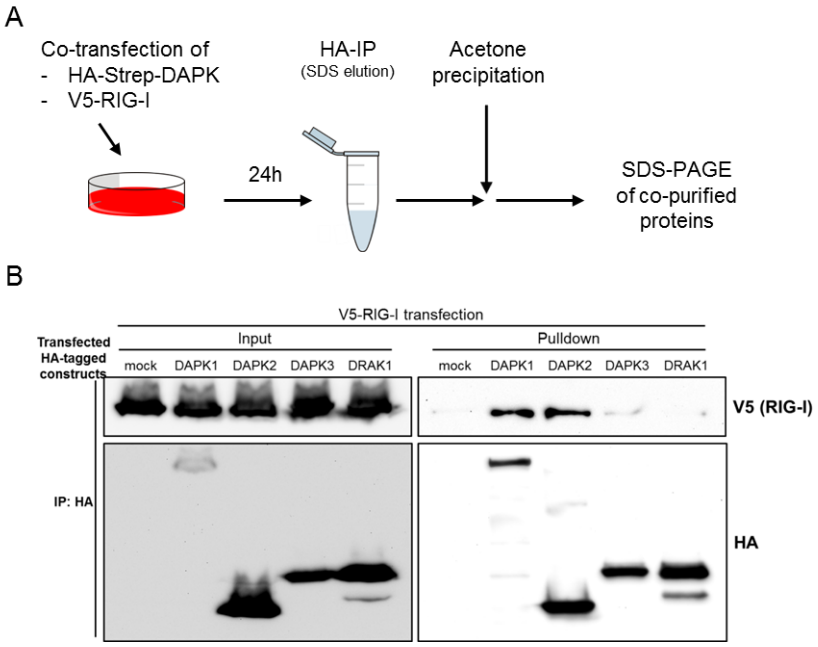

Figure 25 **RIG-I CoIP**

A) Experimental setup. 293T^{RIG-I} cells were co-transfected with HA-tagged DAPKs and V5-tagged RIG-I. Equal amounts of plasmid DNA were transfected. HA-tagged proteins were pulled down using anti-HA agarose beads. After overnight acetone precipitation, samples were analysed by SDS-PAGE. **B)** Western Blot analysis. V5 signal shows co-purified RIG-I. HA signal shows pulled down kinases. A representative result of five independent experiments is shown.

Interaction of DAPKs with RIG-I was examined in a co-immunoprecipitation assay in which DAPKs were co-transfected with RIG-I in 293T^{RIG-I} cells. DAPKs were purified from cell lysates and (co-)purified protein samples were analysed by Western Blot (Figure 25A).

DAPK1, DAPK2, DAPK3 and DRAK1 were efficiently pulled down by anti-HA immunoprecipitation, but RIG-I only co-purified with DAPK1 and DAPK2, and was not found in eluate from DAPK3 or DRAK1 pull-downs (Figure 25B). Thus, RIG-I strongly

interacts with DAPK1 and DAPK2, but might not or only transiently interact with DAPK3 or DRAK1.

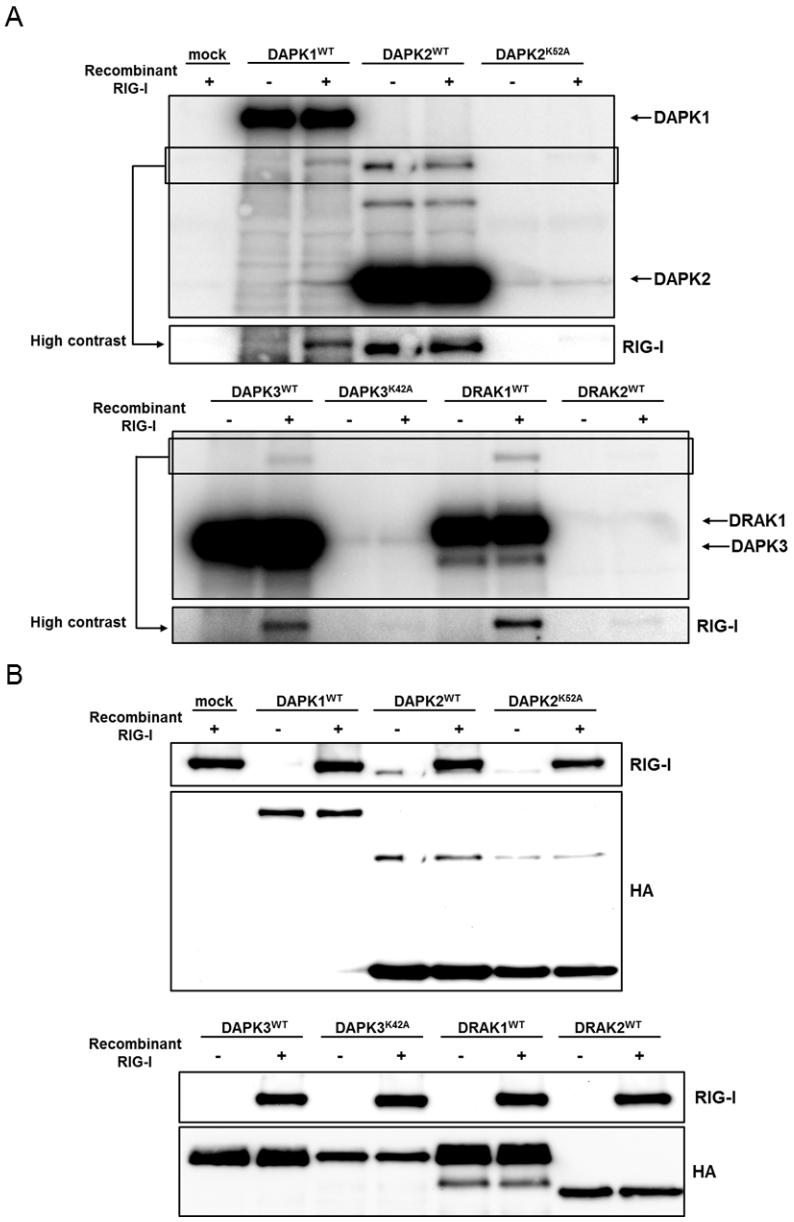

Figure 26 **In vitro phosphorylation of RIG-I by DAPKs**

For *in vitro* phosphorylation assays, Strep-tag-fused DAPKs or kinase-inactive mutants were over-expressed in 293T^{RIG-I} cells and purified using strep-tactin coated magnetic beads (compare Figure 25). Eluted kinases were incubated with 1µg of purified, recombinant RIG-I and ^{32}P-ATP and samples were analysed SDS-PAGE and Western Blot. Incorporation of ^{32}P-ATP was visualised by exposure of membranes on storage phosphor screens. **A)** Radioactive signal from phosphorylation reactions with or without RIG-I. **B)** Western Blot of membranes shown in A) stained for HA-tag and RIG-I. A representative of six independent experiments is shown. Arrows indicate auto-phosphorylated DAPKs.

Since DAPK1 was found to phosphorylate RIG-I *in vitro*, it was examined whether the same could be observed for the other DAPK family members. DRAK2 was analysed in addition to DAPK2, DAPK3, and DRAK1, because it behaved differently to DRAK1 when

over-expressed in 293T^{RIG-I} cells and did not confer inhibition of RIG-I signalling (Figure 14A).

RIG-I was phosphorylated in vitro by DAPK1, DAPK2, DAPK3, and DRAK1 (Figure 26A). In addition to RIG-I phosphorylation, auto-phosphorylation of WT DAPKs was detected as well. Kinase-inactive DAPK2^{K52A} and DAPK3^{K42A} did not show signal for auto-phosphorylation, nor did they phosphorylate RIG-I. Auto-phosphorylation signals of DAPK2 dimers (compare Figure 23A) were close to signals for phosphorylated RIG-I, which was, therefore, difficult to examine in some assays but clear in others, depending on the extent of DAPK2 dimerisation. Amounts of purified kinases and recombinant RIG-I were visualised by Western Blotting (Figure 26B). DRAK2 was neither auto-phosphorylated, nor did it phosphorylate RIG-I. As it was expressed in similar amounts to the other kinases, but no phosphorylation signals were observed in the respective samples, DRAK2 was apparently kinase-inactive when over-expressed in 293T^{RIG-I} cells, although the cloned coding sequence showed no non-silent deviation to that of a published reference [163].

The above findings show that although strong interaction of RIG-I was only observed for DAPK1 and DAPK2, all kinase-active DAPK family members phosphorylated RIG-I *in vitro*. The fact that DRAK2 was kinase-inactive when over-expressed might be the reason for its inability to inhibit IFIT1 promoter activity in previous analyses (Figure 14A).

4.4.4 DAPK family members interact

Although we detected no or only transient interaction of DAPK3 and DRAK1 with RIG-I, both kinases inhibited RIG-I signalling. As it was published that DAPKs interact [201], [216], it was conceivable that some DAPKs might not directly bind to RIG-I, but instead recruit other DAPK family members. By this indirect interaction with RIG-I, DAPK3 and DRAK1 might confer RIG-I signalling inhibition.

In order to find out if and how DAPKs interacted, *in vitro* kinase reactions containing pulled down DAPK2, DAPK3, and DRAK1 were subjected to mass spectrometry analyses. Earlier experiments analysing DAPK1 co-immunoprecipitations already showed that DAPK3, indeed, co-purified with DAPK1 and was, in fact, the second most abundant hit (Table 22).

Table 22 **Most abundant hits (5) of DAPK1 interactome obtained by mass spectrometry.**

Hit No.	Protein name	Gene name	Score
1	**Death-associated protein kinase 1**	DAPK1	32,68
2	Death-associated protein kinase 3	DAPK3	29,35
3	Hsp90 co-chaperone Cdc37	CDC37	27,43
4	Hypoxia-inducible factor 1-alpha inhibitor	HIF1AN	27,27
5	MAPK-interacting and spindle-stabilizing protein-like	MAPK1IP1L	26,56

HA-tagged DAPK1 was over-expressed in $293T^{RIG-I}$ cells and pulled down using anti-HA-tag beads. Immunoprecipitates were analysed by mass spectrometry (LC-MS/MS). Only the 5 most abundant detected proteins are displayed. A representative of three independent experiments is shown. The pulled down protein is indicated in bold, other DAPK family members are highlighted in red.

Importantly, interactome data for DAPK1 was obtained by using a different mass spectrometer and different means of data evaluation than for analyses concerning the other DAPK family members. This is the reason why obtained (arbitrary) scores from DAPK1 and DAPK2/DAPK3/DRAK1 analyses differ in magnitude. For DAPK2, DAPK3 and DRAK1 samples were taken from *in vitro* kinase assays. Thus, added recombinant RIG-I and CaM were among the most abundant hits obtained from those samples (table 23, table 24).

DAPK2 was found as a DAPK3-interacting protein among the most abundant hits in the DAPK3 interactome (table 23). Furthermore, DAPK2 and DAPK3 were found as DRAK1-interacting proteins among the most abundant hits in the DRAK1 interactome (table 24). No DAPK family member was found among the most abundant hits in the DAPK2 interactome. However, in agreement with a recent publication [226], DAPK2 interacted strongly with different proteins of the 14-3-3 family which represented 6 of the 14 most abundant DAPK2 interacting proteins (appendix, table 25). Conceivably, other DAPK family members are found in the DAPK2 interactome, especially since DAPK2 appeared in the DAPK3 interactome. However, in present experiments co-purification was apparently not as efficient as that for other interactors and did, consequently, not allow representation among the 14 most abundant hits.

Interestingly, the most abundant hit in the DAPK2 interactome (after recombinant RIG-I and CaM) was DDX3X, a RNA helicase which has been shown to be involved in RIG-I signalling. DDX3X was described to stimulate IRF3 activation by interaction with TBK1 [266], and to bind viral RNAs, associate with MAVS and enhance downstream signalling [267].

Table 23 **Overview of proteins identified in the DAPK2 and DAPK3 interactomes**

Hit No.	Protein name	Gene name	Score	Hit No.	Protein name	Gene name	Score
1	Probable ATP-dependent RNA helicase DDX58 (RIG-I)	DDX58	5001	1	Probable ATP-dependent RNA helicase DDX58 (RIG-I)	DDX58	5514
2	**Death-associated protein kinase 2**	DAPK2	2627	2	**Death-associated protein kinase 3**	DAPK3	2214
3	ATP-dependent RNA helicase DDX3X	DDX3X	2131	5	Calmodulin	CALM	899
4	Calmodulin	CALM	788	13	Death-associated protein kinase 2	DAPK2	170

Samples from in vitro kinase assays (Figure 26) were analysed by mass spectrometry (LC-MS/MS). Only the 14 most abundant detected proteins are displayed. A representative of two independent experiments is shown. The pulled down protein is indicated in bold, other DAPK family members are highlighted in red. For an overview of the 14 most abundant hits, refer to appendix, table 25.

Table 24 **Overview of proteins identified in the DRAK1 interactome**

Hit No.	Protein name	Gene name	Score	Hit No.	Protein name	Gene name	Score
1	Probable ATP-dependent RNA helicase DDX58 (RIG-I)	DDX58	5604	4	**Serine/threonine-protein kinase 17A**	ST17A	619
2	Keratin, type II cytoskeletal 1	K2C1	933	12	Death-associated protein kinase 3	DAPK3	69
3	Calmodulin	CALM	910	14	Death-associated protein kinase 2	DAPK2	49

Samples from in vitro kinase assays (Figure 26) were analysed by mass spectrometry (LC-MS/MS). Only the 14 most abundant detected proteins are displayed. A representative of two independent experiments is shown. The pulled down protein is indicated in bold, other DAPK family members are highlighted in red. For an overview of the 14 most abundant hits, refer to appendix, table 26.

Mass spectrometry analysis showed that DAPK family members did interact. Moreover, DAPK2 was found to interact with DDX3X. As DDX3X was shown to enhance the IFN response, regulation of DDX3X by DAPK2 could be another means by which DAPK2 controls the RIG-I signalling response.

4.5 DAPK1, DAPK2, and DAPK3 may interact but inhibit RIG-I signalling independently of each other

The above findings showed that, although an interaction with RIG-I could only be shown for DAPK1 and DAPK2, all DAPK family members phosphorylated RIG-I on specific residues. Additionally, the interactome obtained by mass spectrometry indicated that DAPKs interacted with each other, as most of the other kinase family members were found in the interacting protein fractions of a respective analysed kinase (table 21 - 24). In fact, interaction and cross-talk between DAPKs had been described before [201], [216].

Based on this knowledge, it was investigated whether DAPK1, DAPK2, and DAPK3, were dependent on each other with regard to their roles as inhibitors of RIG-I signalling.

4.5.1 Combined down-regulation of DAPK1 and DAPK3 results in an intermediate phenotype compared to effects on RIG-I signalling seen by single knockdown

Since DAPK2 protein levels were low in the examined cell types (Figure 12) and knockdown of DAPK2 had no effect on IFIT1 promoter activity (Figure 15C), a first approach examined possible interdependence between DAPK1 and DAPK3. Furthermore, as DAPK3 potently inhibited RIG-I signalling but showed no direct interaction with RIG-I in our biochemical assays, it was deemed feasible that DAPK3 might require DAPK1 to be directed towards RIG-I. In order to investigate a possible interdependence between both kinases, DAPK1 and DAPK3 were silenced in A549 and $293T^{RIG-I}$ cells either alone or in combination. Effects on RIG-I signalling were assessed by IFIT1 promoter reporter assay and quantification of IFNβ and IFIT1 mRNA levels.

In both A549 and $293T^{RIG-I}$ cells combined knockdown of DAPK1 and DAPK3 mostly resulted in an intermediate phenotype compared to single knockdown of each kinase as seen in IFIT1 promoter activity assays and qPCR analysis for IFNβ and IFIT1 mRNA (Figure 27A and C, compare to Figure 15A and D, and Figure 16A and B). Silencing efficiencies for both kinases were not as high when siRNAs were co-transfected, resulting in higher residual protein levels, especially in the case of DAPK1, in double knockdown samples compared to single knockdown (Figure 27B). This was also reflected on mRNA levels for DAPK1 and DAPK3 (Figure 27D). Similar to what was observed before (Figure 16C), DAPK2 mRNA levels were slightly increased in response to double knockdown of DAPK1 and DAPK3 in $293T^{RIG-I}$ cells.

Knockdown of genes using siRNAs is never 100% efficient. Furthermore, combined knockdown of DAPK1 and DAPK3 was even less efficient than single knockdown of each kinase and resulted in an intermediate phenotype which did not allow any conclusion as to whether DAPKs interdepend in their function as inhibitors of RIG-I signalling.

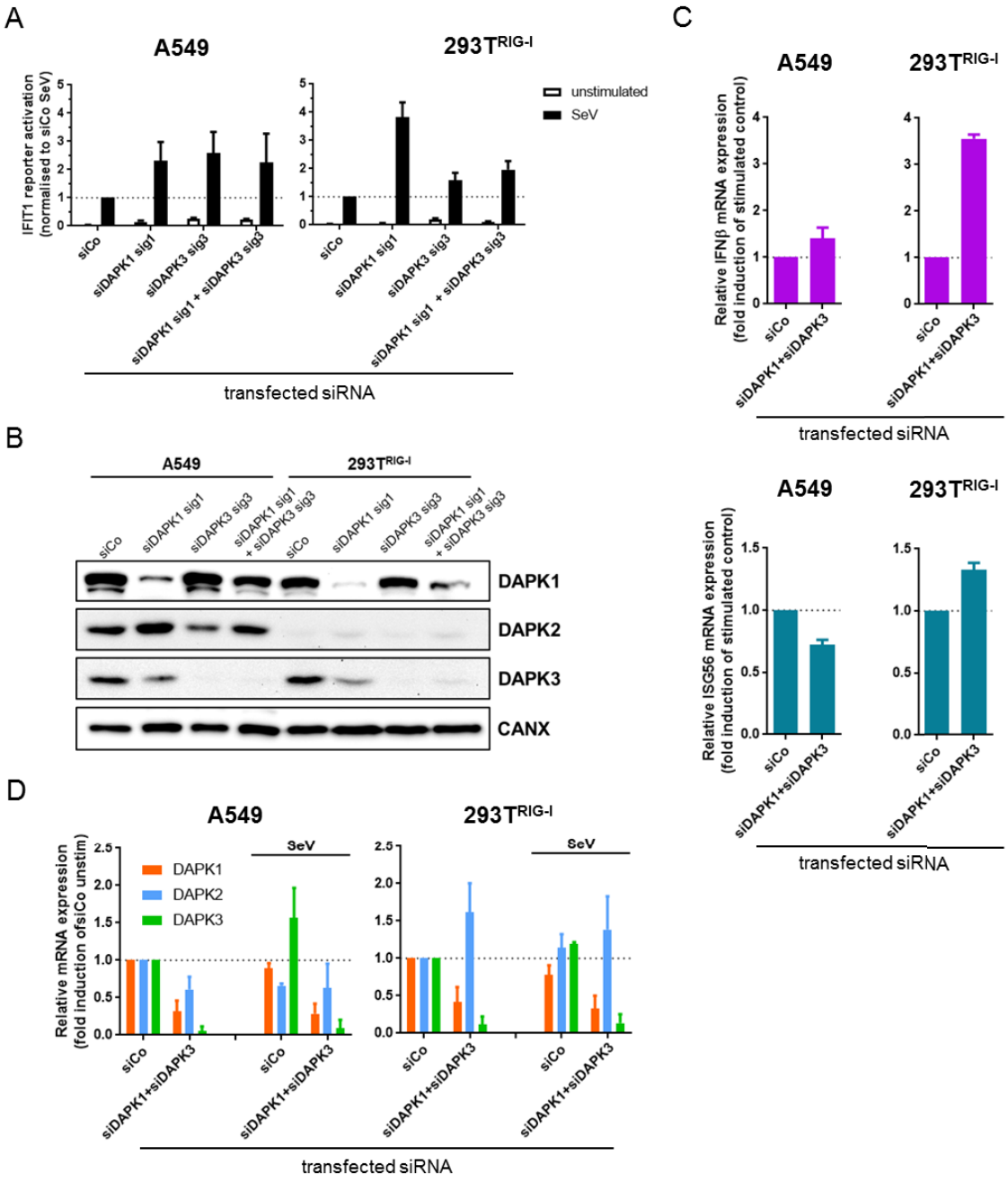

Figure 27 **Intermediate effect of combined DAPK1 and DAPK3 silencing**

For IFIT1 promoter reporter assays after silencing of DAPKs, siRNAs targeting the individual kinase were reverse transfected into A549 or 293T^{RIG-I} cells. 38h after siRNA transfection, reporter plasmids were transfected, and 48h after siRNA transfection cells were infected with SeV (MOI 5) for 16h. **A)** IFIT1 promoter activity after silencing of DAPK1 in A549 and 293T^{RIG-I} cells with corresponding Western Blots assessing silencing efficiency in **B)**. For qPCR analyses DAPK1 or DAPK3 were silenced for 48h in A549 or 293T^{RIG-I} cells. Cells were stimulated with SeV (MOI 5) for 16h before mRNA levels of DAPK1, DAPK2, DAPK3, IFNβ and IFIT1 were measured. **C)** IFNβ and IFIT1 mRNA levels after combined down-regulation of DAPK1 and DAPK3 in A549 and 293T^{RIG-I} cells. **D)** DAPK1, DAPK2, and DAPK3 mRNA in unstimulated and SeV infected A549 and 293T^{RIG-I} cells are shown. mRNA levels of target genes are normalised to GAPDH mRNA levels and shown as fold-induction of siRNA control. Results are the mean of two independent experiments.

4.5.2 Generation of stable DAPK knockout cell lines

In order to allow exact studies on the effects of individual DAPKs on RIG-I signalling and to find out how they might interact or depend on each other, a knockout approach was chosen. The CRISPR/Cas9 system was employed to deplete cells of endogenous DAPK expression. Loss of protein expression was indicative of successful knockout.

4.5.2.1 Stable knockout of DAPK1 does not facilitate RIG-I signalling in A549 or 293T^{RIG-I} cells

A549 cells will naturally engage in antiviral RIG-I-mediated signalling when infected with RNA viruses. On top of that, they express high endogenous levels of DAPK1 (Figure 12). Hence, as a first line of investigating whether knockout of DAPK1 would reproduce the increase in RIG-I signalling observed upon siRNA-mediated DAPK1 knockdown, DAPK1 was targeted using the CRISPR/Cas9 system. Four different small guide RNAs (sgRNAs) were tested and stably expressed in A549 cells by lentiviral transduction. Of those four sgRNAs, sgRNA 3 (crisp3) and 4 (crisp4) were most efficient in knocking down DAPK1 expression when assessed by Western Blotting in A549 bulks (Figure 28A). Since some cells of the transfected bulks retained DAPK1 expression which was unfavourable for further studies on DAPK interdependence, single cell DAPK1 knockout (KO) clones were generated and examined for DAPK1 expression.

Although DAPK1 was undetectable on protein level in all A549 single KO clones (Figure 28B) only one clone, 3.4, displayed a marked increase in IFIT1 promoter activity upon SeV stimulation (Figure 28C). Additionally, IFIT1 promoter activity was up to 3-fold different in unstimulated samples from different clones, suggesting that inter-clonal variation would result in significant changes in antiviral signalling in a single cell compared to bulk measurements.

In parallel to A549 cells, DAPK1 was knocked out in 293T^{RIG-I} cells since these are easily transfectable with expression plasmids, allowing not only re-constitution of DAPK1, but also expression of other DAPKs. Similar to what was observed in A549 cells, there was some leftover DAPK1 protein expression in 293T^{RIG-I} KO bulks after lentiviral transduction (Figure 29A). Thus, single cell KO clones were generated from sgRNA bulk 3 (crisp3) and 4 (crisp4), which were, again, displaying highest KO efficiency.

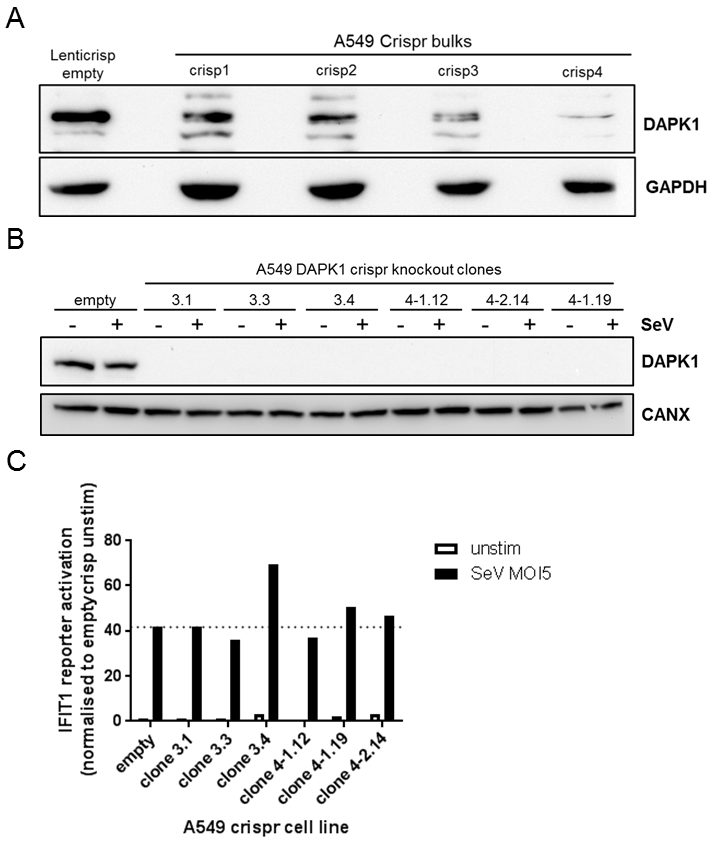

Figure 28 **A549 DAPK1 crispr knockout cell lines**

A) Western Blot for DAPK1 expression in A549 cells stably transfected with plasmids encoding Cas9 and DAPK1-targeting sgRNAs (crisp1-4). **B)** Western Blot for DAPK1 in A549 DAPK1 single cell knockout clones originating from sgRNA bulk 3 and 4. **C)** IFIT1 promoter reporter assay of A549 DAPK1 knockout clones stimulated with SeV (MOI 5) for 16h before lysis.

Although most 293T^{RIG-I} single cell DAPK1 KO clones showed no DAPK1 protein expression (Figure 29B and data not shown), the overall induction of IFIT1 promoter activity after SeV stimulation was similar to that seen for empty vector controls and WT 293T^{RIG-I} cells (Figure 29C). However, IFIT1 promoter activity in unstimulated samples differed significantly, demonstrating again that clonal expansion might change signalling capacity of individual clones dramatically.

Stable KO of DAPK1 in A549 and 293T^{RIG-I} cells did not reflect what had been observed for transient knockdown as there was no general increase in IFIT1 promoter activity in DAPK1-depleted cells.

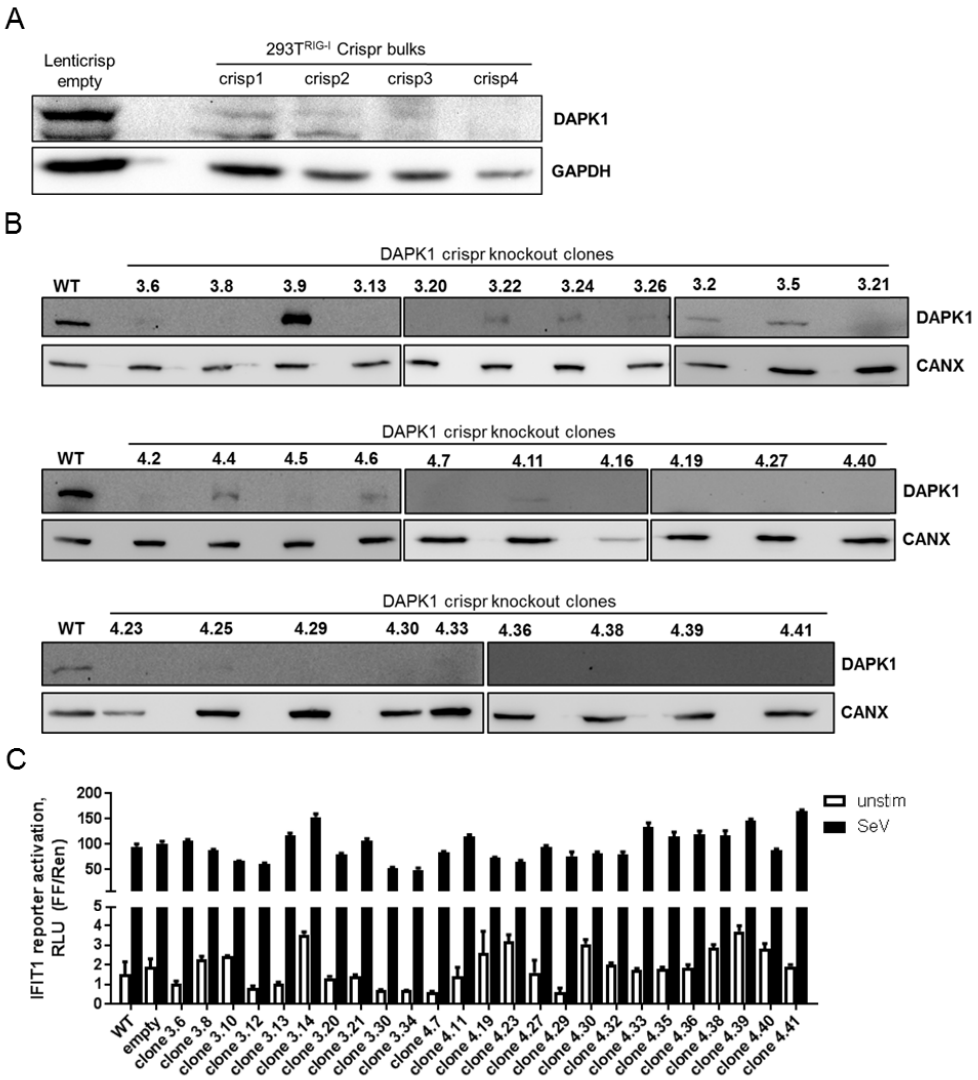

Figure 29 **293T^{RIG-I} DAPK1 crispr knockout cell lines**

A) Western Blot for DAPK1 expression in 293T^{RIG-I} cells stably transfected with plasmids encoding Cas9 and DAPK3-targeting sgRNAs (crisp1-4). **B)** Western Blot for DAPK1 in 293T^{RIG-I} DAPK3 single cell knockout clones originating from sgRNA bulk 3 and 4. **C)** IFIT1 promoter reporter assay of 293T^{RIG-I} DAPK1 knockout clones stimulated with SeV (MOI 5) for 16h before lysis. Error bars correspond to measurement of one biological replicate measured in triplicates.

4.5.2.2 Stable knockout of DAPK3 does not facilitate RIG-I signalling in A549 or 293T^{RIG-I} cells

DAPK3 protein was abundant in A549 and 293T^{RIG-I} cells and mRNA levels were even higher than those observed for DAPK1 (Figure 12). Knockdown of DAPK3 was accompanied by a marked increase in IFIT1 promoter activity. Therefore, it was investigated if DAPK3 KO would reproduce the stimulatory effect on RIG-I signalling observed upon siRNA-mediated knockdown in A549 and 293T^{RIG-I} cells.

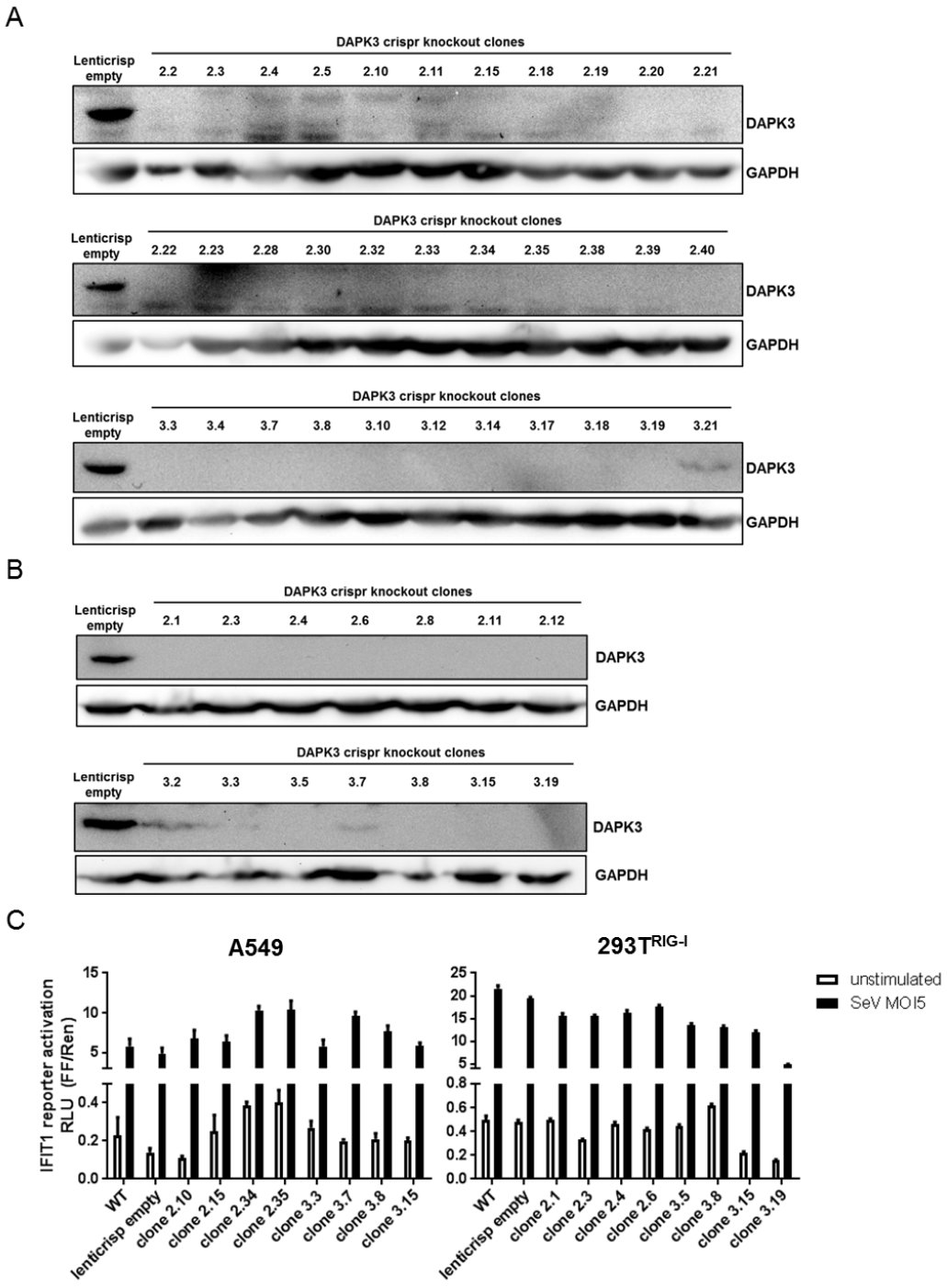

Figure 30 **DAPK3 crispr knockout cell lines**

Western Blot for DAPK3 expression in **(A)** A549 and **(B)** 293T^{RIG-I} single cell DAPK3 knockout clones. **C)** IFIT1 promoter reporter assay of A549 and 293T^{RIG-I} DAPK3 knockout clones stimulated with SeV (MOI 5) for 16h before lysis. Error bars correspond to measurement of one biological replicate measured in triplicates.

CRISPR/Cas9-mediated KO of DAPK3 in A549 cells using 4 different sgRNAs resulted in a strong decrease of DAPK3 protein levels with protein levels being lowest in sgRNA 2 (crisp2) and 3 (crisp3) samples (data not shown). Almost all generated A549 and 293T^{RIG-I} single cell DAPK3 KO clones did not express DAPK3 protein (Figure 30A and

32B), but, reminiscent of what had been observed for DAPK1 (Figure 28C and 31C), there was no marked increase in IFIT1 promoter activity in DAPK3 KO clones compared to empty plasmid transduced or WT control cells after SeV infection (Figure 30C). While a few A549 DAPK3 KO clones showed a minor increase in IFIT1 promoter activity, some 293T^{RIG-I} DAPK3 KO clones even displayed a reduced signalling response after stimulation.

Similar to what was observed for DAPK1, stable KO of DAPK3 in A549 and 293T^{RIG-I} cells did not yield comparable results to transient knockdown, as there were, if at all, only minor changes in RIG-I signalling activity in response to viral infection. Importantly, variability in IFIT1 reporter activity between individual single cell clones was substantial. Hence, inter-clonal variability could mask changes in RIG-I signalling caused by DAPK knockout.

4.5.2.3 Combined stable knockout of DAPK1 and DAPK3 has no effect on RIG-I signalling

Neither stable KO of DAPK1 nor DAPK3 alone had any effect on RIG-I signalling. Comparatively long time spans lay between lentiviral CRISPR/Cas9-transduction and functional assays since single cell clones were selected by antibiotic resistance and went through clonal expansion. Based on protein expression DAPK1 and DAPK3 were the two highest expressed members of DAPKs in A549 and 293T^{RIG-I} cells and it was known that they had similar functions in basic cellular processes such as cell death induction. Therefore, it was possible that stable KO of one DAPK was compensated for by up-regulation of another DAPK, an effect which would not be seen in the relatively short time span of a siRNA-silencing based reporter assay or qPCR experiment.

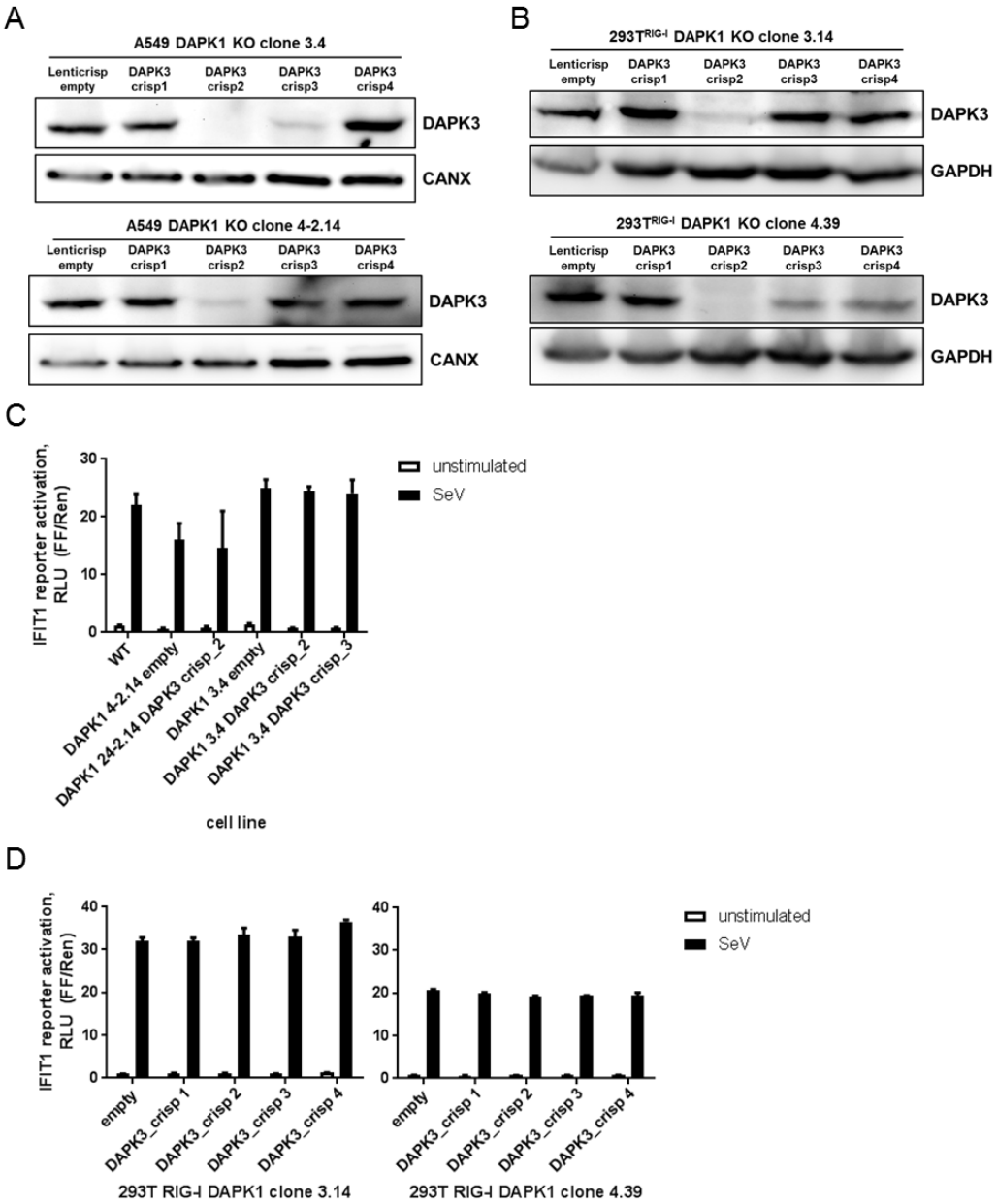

Figure 31 **DAPK1/DAPK3 crispr double knockout bulks**

Western Blots for DAPK3 expression in **A)** A549 and **B)** 293T^{RIG-I} DAPK1 knockout (KO) cell clones stably transfected with plasmids encoding Cas9 and DAPK3-targeting sgRNAs (crisp1-4). **C)** IFIT1 promoter reporter assay in A549 DAPK1/DAPK3 double knockout bulks in response to 16h of SeV (MOI 5) stimulation. **D)** IFIT1 promoter reporter assay in 293T^{RIG-I} DAPK1/DAPK3 double knockout bulks in response to 16h of SeV (MOI 5) stimulation. Error bars correspond to measurement of one biological replicate measured in triplicates.

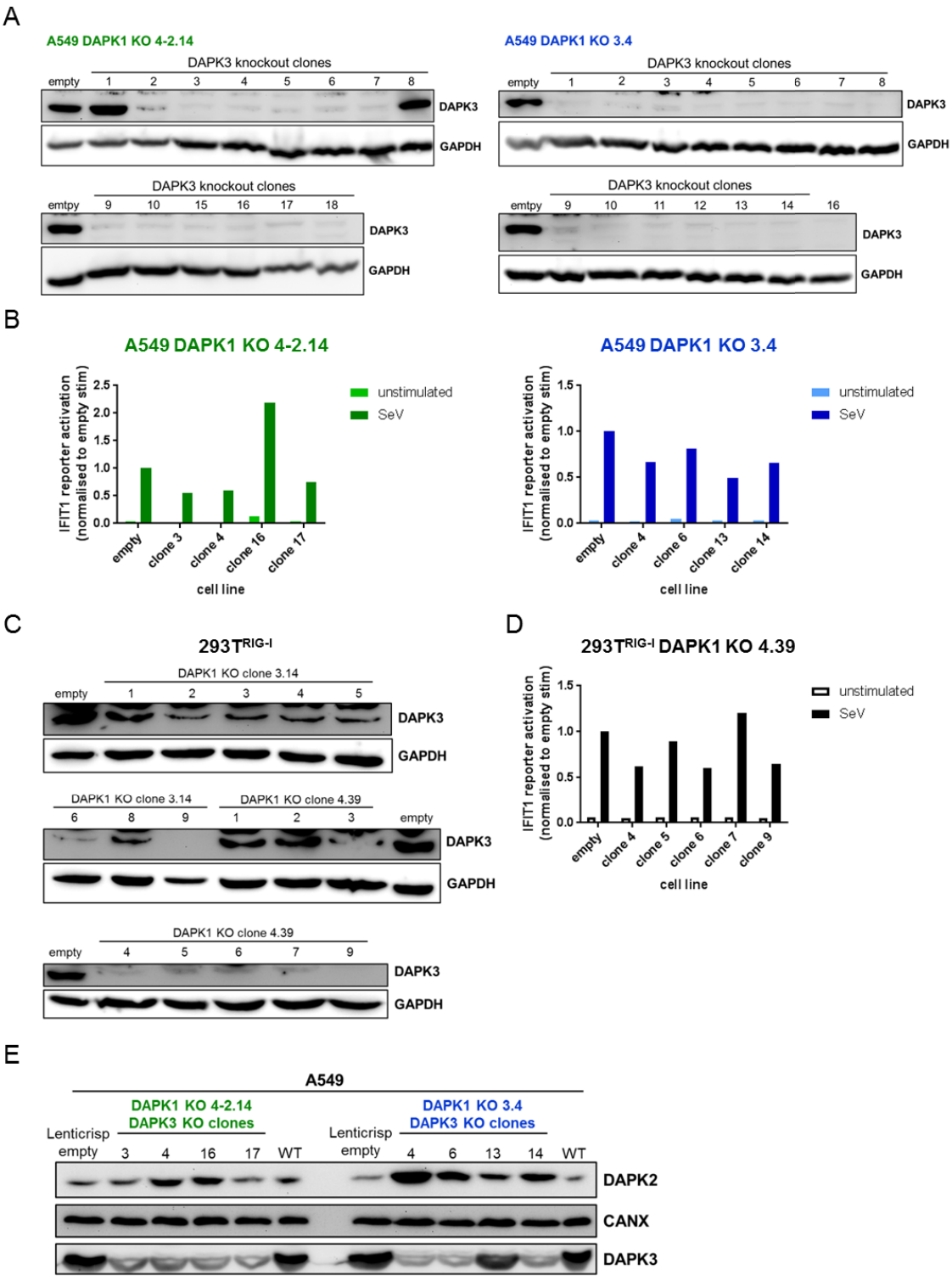

Figure 32 **DAPK1/DAPK3 crispr double knockout clones**

Western Blots for DAPK3 expression in **A)** A549 and **C)** 293T^{RIG-I} DAPK1/DAPK3 single cell knockout clones. IFIT1 promoter reporter assays in **B)** A549 and **D)** 293T^{RIG-I} DAPK1/DAPK3 double knockout clones (DKO) in response to SeV (MOI 5) infection for 16h. **E)** Western Blot for DAPK2 expression in A549 DAPK1/DAPK3 double knockout cell lines. Signals for DAPK3 in DAPK3 knockout clones are due to high background of the DAPK3 antibody as DAPK3 knockout had been previously established (compare Figure 30).

In order to avoid up-regulation of DAPK3 in DAPK1 stable KO lines and vice versa, DAPK1/DAPK3 double knockout (DKO) cell lines were created by stable expression of DAPK3 sgRNAs in existing DAPK1 KO clones. For this, two A549 and two 293T^{RIG-I} DAPK1 KO clones were chosen. DAPK3 protein levels were already strongly reduced in all A549 and 293T^{RIG-I} DAPK1-3 double knockout bulks expressing DAPK3 sgRNA 2 (crisp2) and in A549 double knockout bulks expressing DAPK3 sgRNA 3 (crisp3) (Figure 31A and 31B). When these DAPK1/DAPK3 DKO bulks were tested in IFIT1 promoter activity assays, however, no significant increase in reporter activity in response to SeV infection was observed (Figure 31C and 33D). Surprisingly, this did not change when DAPK1/DAPK3 DKO single cell clones were generated. When IFIT1 reporter activity in response to SeV infection was examined in those clones which did not express DAPK3 (Figure 32A and 32C), no marked increase in reporter activity was observed (Figure 32B and 32D). Interestingly, in comparison to WT and empty vector transduced cells, DAPK2 protein levels were increased in most A549 DAPK1/DAPK3 double knockout cell clones (Figure 32E).

Combined KO of DAPK1 and DAPK3 in A549 and 293T^{RIG-I} cells did not result in enhanced RIG-I signalling activity, other than indicated by previous transient knockdown experiments. In response to stable DAPK1 and DAPK3 KO, DAPK2 protein levels were elevated, indicative of compensatory effects initiated by combined loss of DAPK1 and DAPK3 expression.

4.5.2.4 Stable single knockout of DAPK2 or combined triple knockout of DAPK1, DAPK2, or DAPK3 has no effect on RIG-I signalling

Elevated DAPK2 levels in DAPK1/DAPK3 double knockout cell lines compared to WT cells suggested a compensatory mechanism of up-regulation in case cells were depleted of the other DAPK family members which might be the reason why there was no obvious effect on RIG-I signalling upon loss of DAPK1, DAPK3, or both.

Since DAPK2-targeting siRNAs were found to be toxic in combination with virus infection (data not shown), the CRISPR/Cas9 system was employed to generate stable DAPK2 KO cell lines. In parallel to WT A549 and 293T^{RIG-I} cells, DAPK2 was knocked out in previously established DAPK1/DAPK3 DKO clones. KO of DAPK2 in bulks generated by transduction with sgRNA 1 (crisp1) and 4 (crisp4) was highly efficient showing no residual DAPK2 protein (Figure 33A). IFIT1 promoter activity after SeV infection, however, remained unchanged in response to loss of DAPK2 in A549 (Figure 33C) and 293T^{RIG-I} (Figure 33D) WT and DAPK1/DAPK3/DAPK2 triple KO bulks.

In summary, the CRISPR/Cas9 system was successfully employed for the generation of DAPK knockout cell lines. However, neither single nor combined knockout of DAPK1, DAPK2, and DAPK3 had any impact on the induction of RIG-I signalling after virus infection.

4.5.3 DAPKs inhibit RIG-I signalling independently of each other

It was observed that only DAPK1 and DAPK2 interacted with RIG-I (Figure 25), although all DAPKs (except DRAK2) phosphorylated RIG-I *in vitro* and inhibited RIG-I signalling when they were over-expressed (Figure 13, Figure 14). Similar to what was previously observed [201], [216], an interaction between DAPKs was observed in the present study (interactome data, tables 1-3). Thus, it was possible that DAPK3 which did not interact with RIG-I, depended on DAPK1 expression in order to regulate RIG-I signalling. Similarly, RIG-I signalling inhibition of DAPK2 or DRAK1 could be mediated by interaction with other DAPK family members. In order to examine if and how DAPKs might interact to fulfil their role as negative regulators of RIG-I signalling, it was tested if DAPK1, DAPK2, and DAPK3 were capable of RIG-I signalling inhibition when cells were depleted of the other respective DAPK family members.

First, since DAPK1 and DAPK3 were the highest expressed DAPK family members in A549 and 293T^{RIG-I} cells (Figure 12), it was investigated whether DAPK1 depended on DAPK3 to confer inhibition of RIG-I signalling. To this end, DAPK3 was down-regulated

by siRNA-transfection in 293T^{RIG-I} cells and DAPK1 was over-expressed before SeV infection.

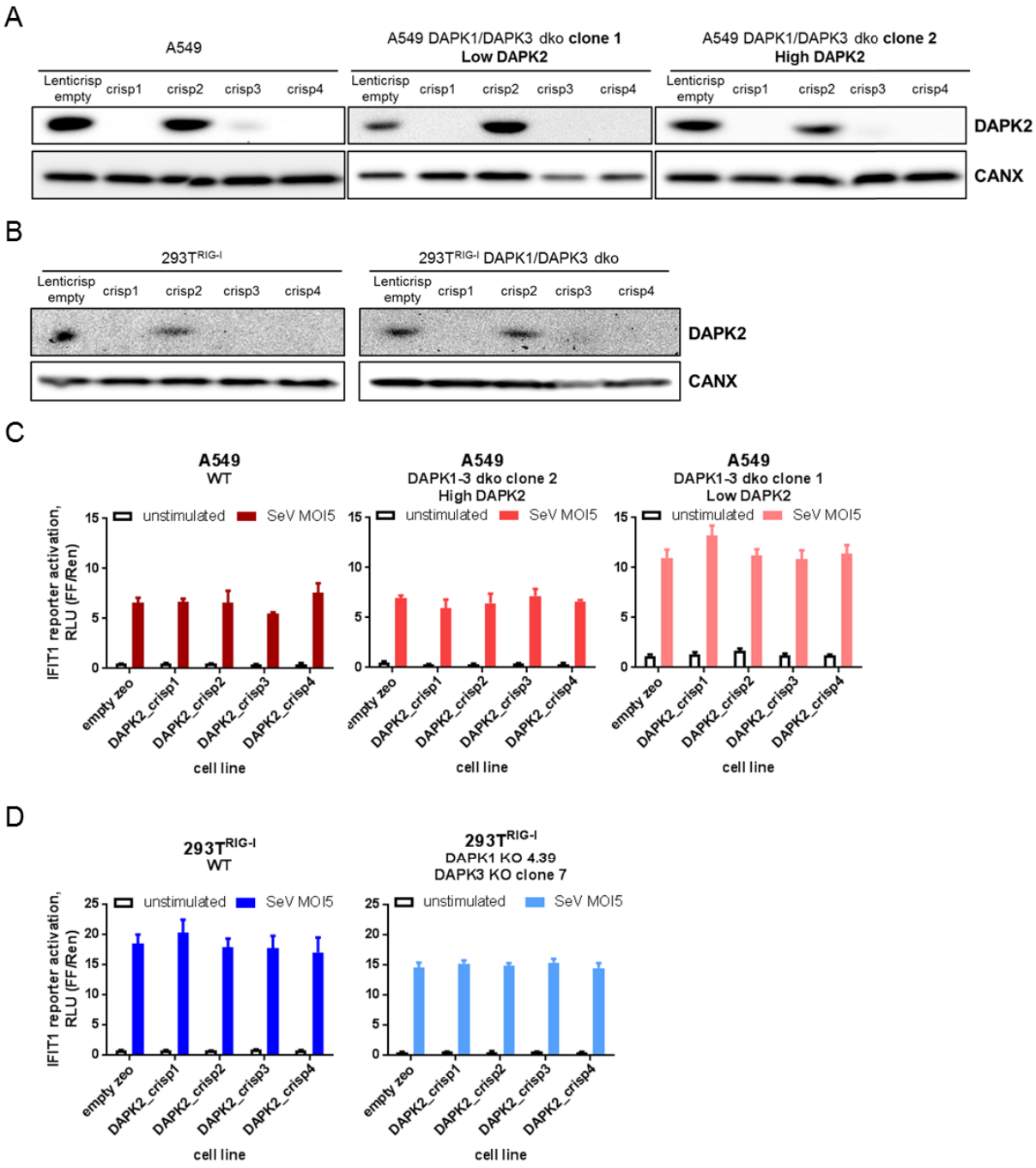

Figure 33 **DAPK2 crispr single knockout and DAPK1-2-3 triple knockout bulks**

Western Blots for DAPK2 expression in **A)** A549 and **B)** 293T^{RIG-I} WT and DAPK1/DAPK3 knockout cell clones stably transduced with plasmids encoding Cas9 and DAPK2-targeting sgRNAs (crisp1-4). **C)** IFIT1 promoter reporter assay in A549 WT and DAPK1/DAPK3 double knockout bulks in response to 16h of SeV (MOI 5) stimulation. **D)** IFIT1 promoter reporter assay in 293T^{RIG-I} WT and DAPK1/DAPK3 double knockout bulks in response to 16h of SeV (MOI 5) stimulation. Error bars represent the standard deviation of technical triplicates in one experiment.

Similarly to what was observed previously (Figure 15D), DAPK3 knockdown alone resulted in a ~3 fold increase in IFIT1 promoter activity (Figure 34A). DAPK1 over-expression reduced IFIT1 promoter activity in DAPK3 knockdown cells to the same extent (~65%) as in control siRNA-transfected cells, indicating that DAPK1 did not depend on high levels of DAPK3 to act as an inhibitor of RIG-I signalling.

As siRNA knockdown would always result in some residual protein being present after transfection, further DAPK over-expression experiments were performed in previously generated $293T^{RIG\text{-}I}$ DAPK1 and DAPK3 knockout cell clones. Interestingly, re-introduction of DAPK1 in DAPK1 knockout cell clones had the same inhibitory effect on IFIT1 promoter activity as in $293T^{RIG\text{-}I}$ empty vector control cells in about half of the clones, but resulted in no strong down-regulation of IFIT1 promoter activity in the rest of the clones (Figure 34B). This was probably due to remaining Cas9 activity in some clones, as DAPK1 was not detectable or only detected in small amounts on protein level in those clones (Figure 34C). Over-expression of DAPK3, however, was successful in all clones (Figure 34C) and resulted in a reduction of IFIT1 promoter activity similar to that observed in empty vector control cells (Figure 34B). Thus, DAPK3 apparently inhibited RIG-I signalling independently of DAPK1.

Along the same lines, DAPK1 and DAPK2 over-expression in $293T^{RIG\text{-}I}$ DAPK3 knockout clones resulted in a reduction of IFIT1 promoter activity similar to that observed for empty vector control cells (Figure 34D), indicating that DAPK1 and DAPK2 did not require DAPK3 expression to mediate inhibition of RIG-I signalling.

Importantly, over-expression of $DAPK3^{Kinase}$ and $DAPK3^{K42A}$ was not successful in most clones (Figure 34E) which was probably due to remaining Cas9 activity. Because of this, no conclusion as to whether these DAPK3 constructs depend on the expression of other DAPKs in order to fulfil their inhibitory role in RIG-I signalling could be drawn. Of note, strength of IFIT1 promoter activity, i.e. signalling induction, varied between DAPK3 knockout clones, emphasizing once again that high clonal variability might mask some of the effects caused by DAPK knockout.

Taken together, results from DAPK over-expression assays in DAPK knockout cell lines suggest that DAPK1, DAPK2, and DAPK3 do not interdepend in their function as negative regulators of RIG-I signalling. Additionally, re-constitution of kinase constructs harbouring the sgRNA-targeted sequence was impossible in most clones due to retained Cas9 activity after stable transduction and genomic integration.

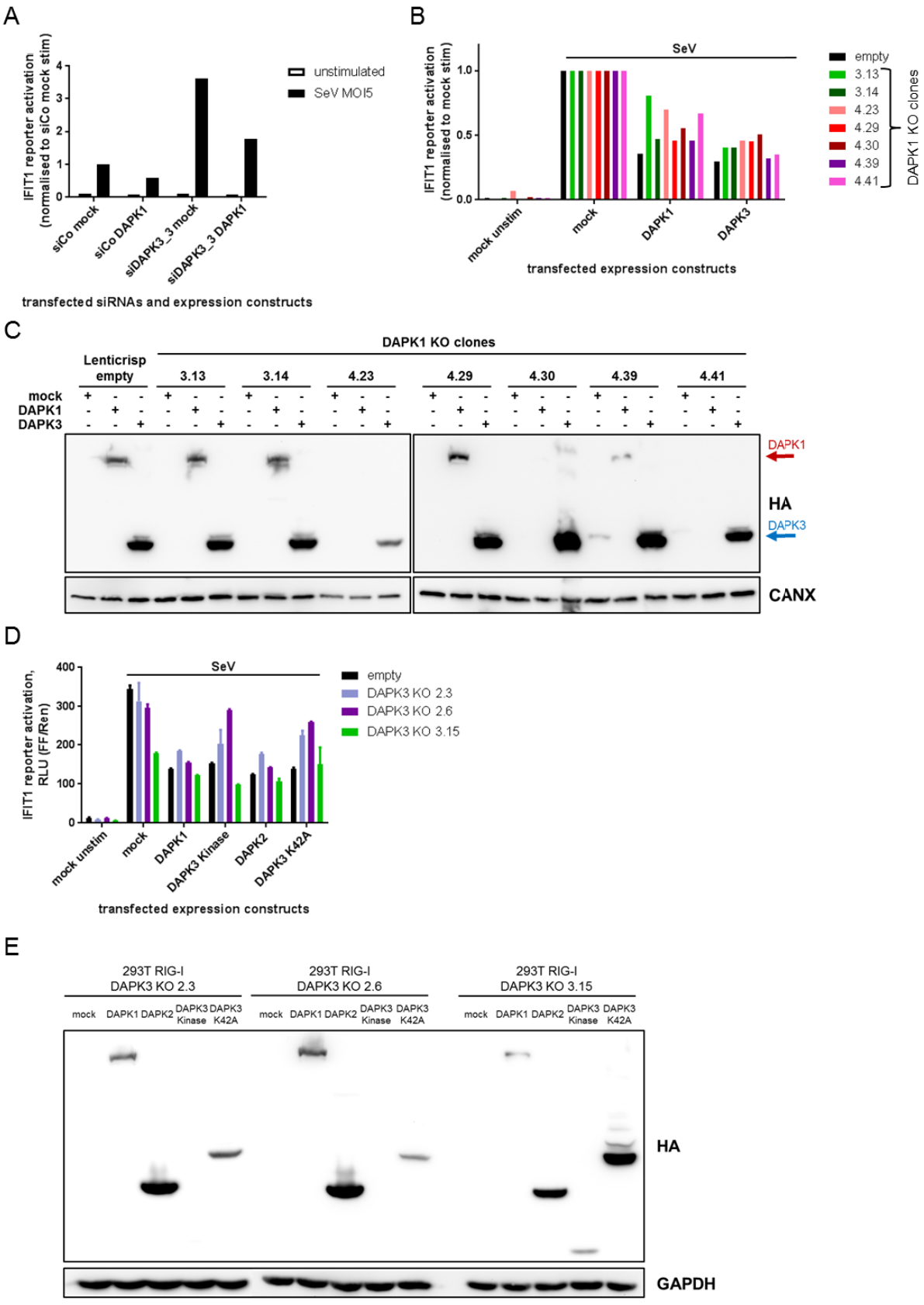

Figure 34 **DAPKs act independently of each other** (figure legend on the following page)

A) IFIT1 promoter reporter assay in 293T^{RIG-I} cells over-expressing DAPK1. Cells were either silenced with control or DAPK3-targeting siRNA for 48h before DAPK1 was over-expressed, and stimulated by SeV (MOI 5) infection for 16h before lysis. **B)** IFIT1 promoter reporter assay in 293T^{RIG-I} DAPK1 knockout clones over-expressing either DAPK1 or DAPK3 and stimulated with SeV (MOI 5) for 16h. **C)** Western Blot analysis for HA-tag expression corresponding to results shown in B). **D)** IFIT1 promoter reporter assay in 293T^{RIG-I} DAPK3 knockout clones over-expressing DAPK3 mutants, DAPK1, or DAPK2. Cells were infected with SeV (MOI 5) for 16h. Error bars correspond to one biological replicate measured in triplicates. **E)** Western Blot analysis for HA-tag expression corresponding to results shown in D).

4.6 DAPK1 and DAPK3 regulate the antiviral response to infection with different RNA viruses

Up to this point, experiments performed within the context of this study investigating the role of DAPKs in RIG-I signalling focused on assays which assessed the antiviral response based on promoter activity assays and qPCR analyses. It was unclear how endogenous DAPKs might control RIG-I signalling and regulate antiviral responses in actual virus infections. Therefore, we next examined how the replication cycles of different RNA viruses were influenced by expression of DAPKs. To this end, DAPK1 and DAPK3 were down-regulated by siRNA transfection and cells were infected with RNA viruses. Virus replication was assessed either through a luciferase reporter gene within the viral genome, or by flow cytometry analysis after staining for viral components. As DAPK2 protein levels were low and knockdown showed no effect or was even toxic in previous experiments, this kinase was not analysed in viral replication assays.

4.6.1 Down-regulation of DAPK1 or DAPK3 limits Rift Valley Fever Virus replication

In a first approach, in order to analyse how DAPK1 and DAPK3 might influence RNA virus replication in cell culture, both kinases were down-regulated by siRNA transfection in A549 cells. Cells were then infected with Rift Valley Fever Virus (RVFV) ΔNSs_Rluc and luciferase activity was measured (Figure 35A).

Down-regulation of DAPK1 resulted in 85% reduction in RVFV replication (in line with findings from [199]), DAPK3 down-regulation reduced RVFV to approximately 50% and combination of both siRNAs resulted in an intermediate phenotype (Figure 35B).

While single knockdown of DAPK1 was very efficient with no detectable protein on Western Blot level, some residual protein was detectable after single knockdown of DAPK3, and combination of both siRNAs was not as efficient as single knockdown, since more residual protein was detectable (Figure 35C). Interestingly, some counter-regulation of the kinases (which might occur in case of down-regulation of one DAPK family member) was observed as DAPK1 protein levels were increased in DAPK3-silenced cells and DAPK1 knockdown negatively influenced DAPK3 expression.

The observed inhibition of RIG-I signalling by DAPK1 and DAPK3 (section 4.2), therefore, was confirmed. Moreover, increased antiviral signalling upon silencing of DAPK1 and DAPK3 was directly reflected by significantly impaired replication of RVFV, with DAPK1 seemingly being a stronger effector in this setup.

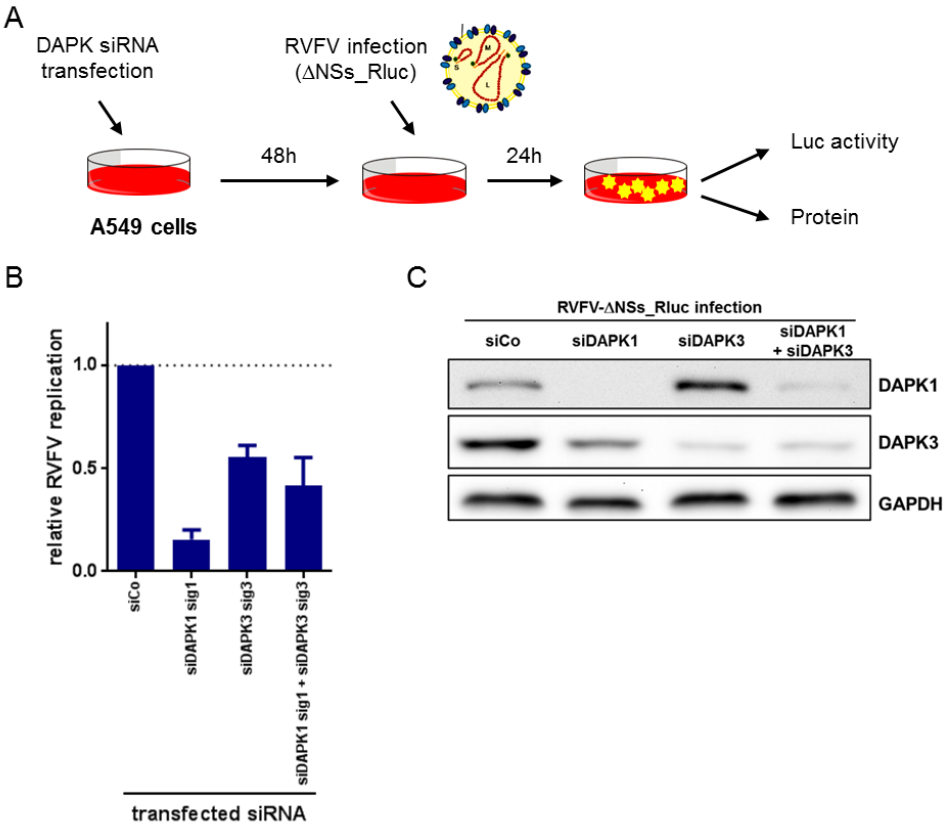

Figure 35 **Rift Valley Fever Virus replication in A549 cells silenced for DAPK1 and DAPK3**

A) Experimental setup. Virus particle adapted from CVR University of Glasgow. **B)** Luciferase assay of RVFV ΔNSs_Rluc replication. Relative renilla luciferase counts are shown. Results are mean of three independent experiments, each measured in triplicates. **C)** Western Blot assessing knockdown efficiency of DAPK1 and DAPK3 in the experiment shown in B). A representative of three independent experiments is shown.

4.6.2 Down-regulation of DAPK3 impairs influenza A virus replication

To complement data from RVFV infection with a different virus, DAPK1 and DAPK3-silenced in A549 cells were infected with influenza A (WSN/33) virus (FluA). In order to quantify viral replication FluA nucleoprotein (NP) was stained and cells were analysed by flow cytometry (Figure 36A). Interestingly, although knockdown efficiency for DAPK1 was high (Figure 36C), DAPK1 down-regulation had no effect on Influenza A virus replication in this experiment, whereas DAPK3 knockdown lead to about 75% reduction in the percentage of FluA infected cells (Figure 36B). In a repetition of the assay in which a higher overall infection rate was achieved, DAPK1 knock-down also impacted FluA replication (data not shown), similar to what we have published previously [199].

Targeting both DAPK1 and DAPK3 simultaneously resulted in an intermediate phenotype with around 50% reduction of FluA infected cells. In double knockdown settings, however, DAPK3 down-regulation was not as efficient as when it was targeted alone (Figure 36C).

It was shown that DAPK1 inhibited antiviral signalling and controlled virus replication in the context of FluA infection [199], even though this effect was not reproduced in the experiments shown here. Moreover, DAPK3 was found to be a novel potent inhibitor of antiviral signalling in the context of FluA infection and, accordingly, its knockdown profoundly decreased viral replication.

4.6.3 Down-regulation of DAPK1 and DAPK3 favours hepatitis C virus replication

Finally, it was examined how DAPK1 and DAPK3 silencing might influence hepatitis C virus (HCV) replication. We recently described DAPK1 as a negative regulator of RIG-I and could show that silencing of DAPK1 resulted in enhanced FluA replication [199]. Additionally, the present study showed that RVFV replication was increased in cells silenced for DAPK1 and DAPK3. We decided to assess if and how DAPK silencing would influence HCV replication since a recent study found an inhibitory role for DAPK1 in HCV replication. In the respective study, DAPK1 expression was up-regulated after IFNα treatment and promoted antiviral signalling by the mTOR pathway. Consequently, DAPK1 silencing enhanced HCV replication [268].

In order to examine if and how DAPK1 and DAPK3 silencing might influence HCV replication, both kinases were silenced in Huh7 Lunet cells which stably over-expressed HCV entry factor CD81 (Huh7 Lunet CD81^{high}) and were, therefore, susceptible to HCV

infection. *Renilla* luciferase-tagged HCV genotype 2a strain JCR2A was used for infection of cells and luciferase activity was measured at different time points post infection (Figure 37A). In a first approach, low luciferase counts indicated that HCV JCR2A replicated inefficiently in Huh7 Lunet CD81^{high} cells (Figure 37B). Furthermore, DAPK3 was not down-regulated by siRNA "siDAPK3_3" (Figure 28C). Nevertheless, silencing of DAPK1 even if it was not as efficient as in A549-based experiments (Figure 35 and Figure 36) resulted in increased HCV replication at 72h and 96h post infection. For a second approach, a different cell line was used, namely Huh7 Lunet CD81^{high} MAVS-GFP$_{NLS}$, which did not differ from the original Huh7 Lunet CD81^{high} functionally, but was found to support HCV JCR2A replication better than the previous cell line (data not shown). Luciferase counts were about 2-fold higher than in the initial assay, and, again, silencing of DAPK1 resulted in enhanced HCV replication starting at 48h after infection and continuing until the end of the time course, reaching an ~3-fold increase.

Interestingly, although there was an effect on HCV replication, DAPK1 down-regulation was not very efficient at early time points and virtually non-existent at late time points (Figure 37E) after infection. Silencing of DAPK3 resulted in an ~1.8-fold increase in HCV replication at 96h post infection, although overall silencing efficiency was equally low as observed for DAPK1. As a control, silencing of HCV host factor PI4Kα was included, whose down-regulation allowed no HCV replication (Figure 37D). Due to its size and tendency to form stable complexes, it was not possible to assess PI4Kα knockdown efficiency on Western Blot level.

In contrast to results from RVFV and FluA replication assays in which DAPK1 knockdown impaired viral replication, down-regulation of DAPK1 and DAPK3 favoured HCV JCR2A replication. This is in line with results presented by Liu et al. reporting an inhibitory role for DAPK1 in HCV replication [268]. Interestingly, Liu et al. used HCV genotype 1b for their experiments whereas we used a genotype 2a virus. Thus, DAPK1 seems to restrict replication of different genotypes of HCV. As the present study found an inhibitory role for DAPK1 and a potentially inhibitory role for DAPK3, experiments with a combined and more efficient knockdown might yield even more significant results. Furthermore, it is possible that DAPKs also regulate RIG-I signalling in liver cells. This function might simply be outweighed by the dependency of mTOR signalling in combating HCV replication.

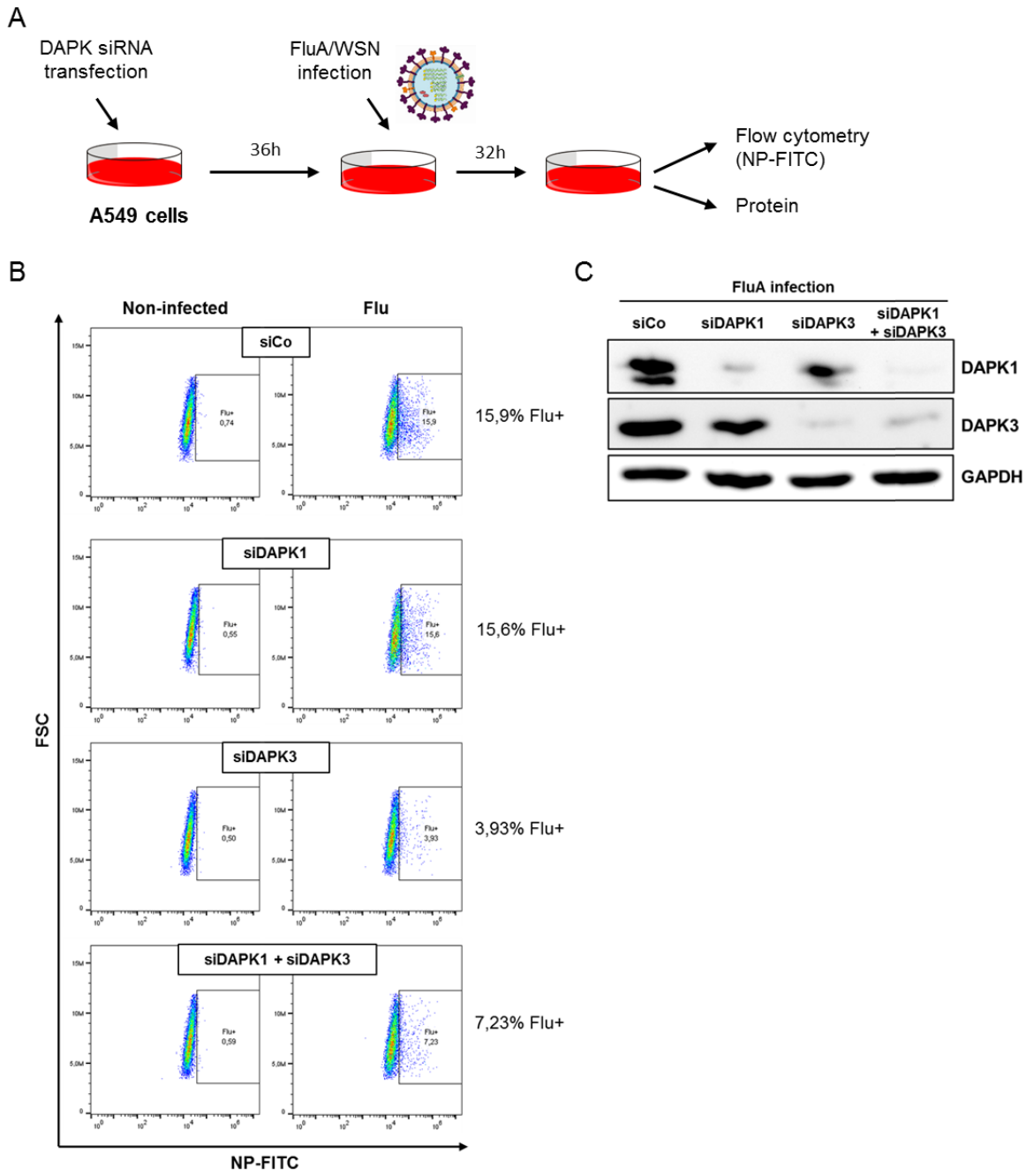

Figure 36 **Influenza A virus replication in A549 cells silenced for DAPK1 or DAPK3**

A) Experimental setup. Virus particle design by Vincent Racaniello (Columbia University) **B)** Flow cytometry analysis. DAPKs were silenced for 36h in A549 cells. Cells were infected with FluA (MOI 0.01) for 32h before analyses were performed. **C)** Western Blot analysis showing knockdown efficiencies for DAPK1 and DAPK3 in the experiment shown in B). Flow cytometry and Western Blot were performed in two independent replicates, one representative result is shown.

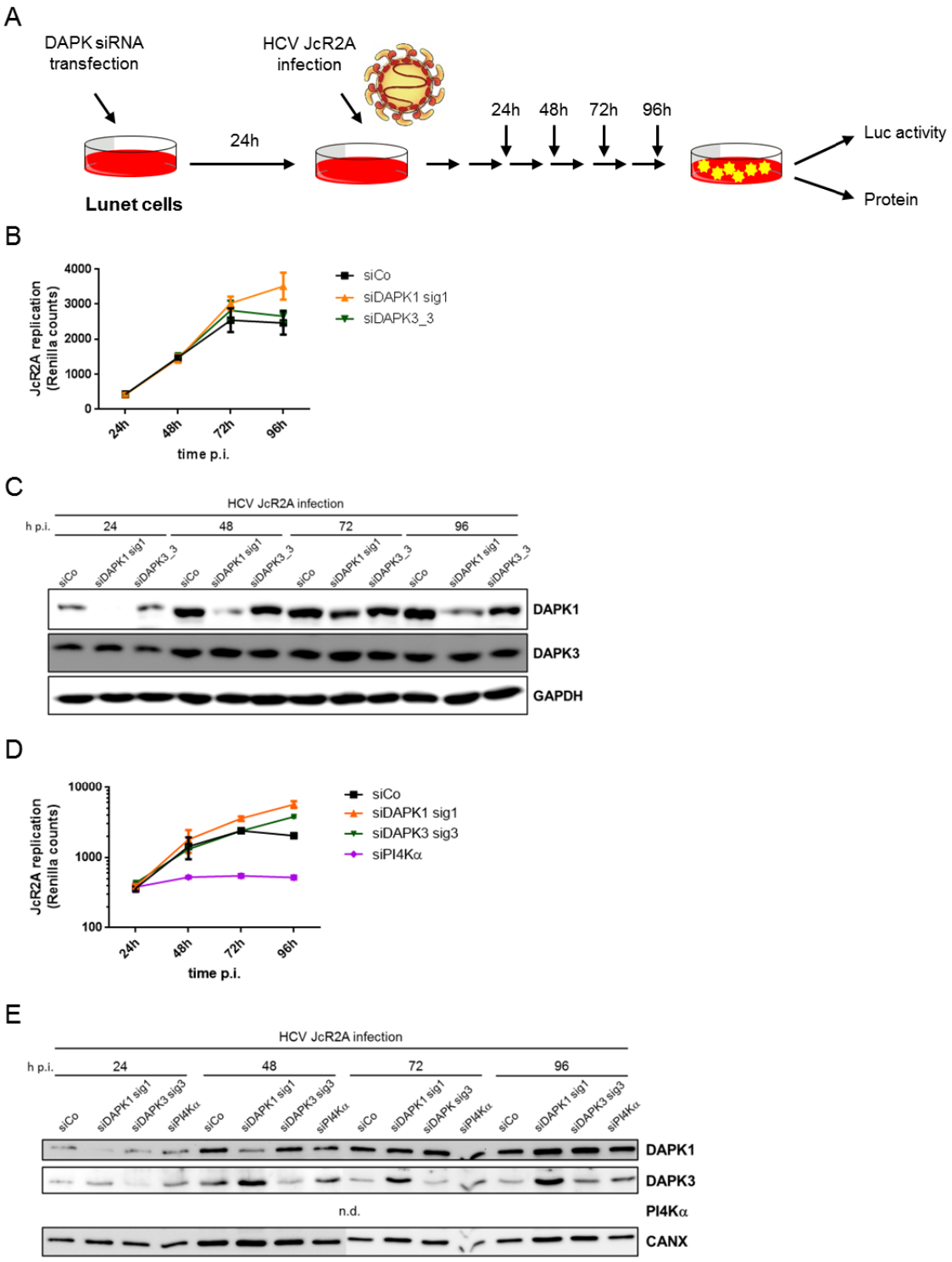

Figure 37 **Hepatitis C virus replication in Huh7 Lunet cells silenced for DAPK1 and DAPK3**

A) Experimental setup. HCV particle adapted from [269]. **B)** HCV replication measured by luciferase activity in Huh7 Lunet cells infected with HCV JCR2A (MOI 0.03) and lysed at indicated time points. **C)** Western Blot analysis for DAPK1 and DAPK3 silencing efficiency for data shown in B). **D)** HCV replication measured by luciferase activity in Huh7 Lunet cells infected with HCV JCR2A (MOI 0.03) and lysed at indicated time points. **E)** Western Blot analysis for DAPK1 and DAPK3 silencing efficiency for data shown in D). Luciferase activity for each condition and time points was measured in triplicates.

4.7 DAPK1, DAPK2, and DAPK3 inhibit MDA5-dependent antiviral signalling

Up to this point all analyses on the role of DAPKs in antiviral signalling were limited to RIG-I-dependent signalling, as over-expression experiments were performed in 293T cells over-expressing RIG-I, and SeV, whose replication intermediates are specifically recognised by RIG-I [270], was used to stimulate A549 cells. The question remained whether control of antiviral signalling by DAPKs was exclusively limited to an inhibition of RIG-I or if DAPKs would generally inhibit RLR signalling, including signalling initiated by MDA5. Besides RIG-I, MDA5 is the other main cytoplasmic receptor for dsRNA, i.e. viral replication intermediates. It was shown that in contrast to RIG-I, which mainly recognises short, 5'-triphosphorylated dsRNA, MDA5 favours the recognition of longer dsRNA, e.g. in the replication cycle of paramyxoviruses [38], [39].

In order to find out whether the three most closely related DAPKs, DAPK1, DAPK2, and DAPK3, inhibited MDA5-mediated signalling a cell line was established in which the RLR response to dsRNA was exclusively mediated by MDA5. To this end, the same 293T cells which had been used for the generation of the $293T^{RIG-I}$ cells employed in this study were stably transfected with MDA5 by lentiviral transduction. MDA5-over-expressing 293T cells expressed high amounts of MDA5, but no RIG-I (Figure 38A). This new cell line was termed $293T^{MDA5}$. Responsiveness of $293T^{MDA5}$ cells to dsRNA ligands was tested in the IFIT1 promoter activity assay. In contrast to $293T^{RIG-I}$ cells which dose-dependently induced IFIT1 promoter activity up to 23-fold when transfected with different concentrations of low molecular weight (LMW) poly(I:C), $293T^{MDA5}$ cells did not respond to this type of stimulation (Figure 38B).

Only when high molecular weight (HMW) poly(I:C) was transfected $293T^{MDA5}$ cells responded with a dose dependently increased activation of the IFIT1 promoter (Figure 38C), which is in line with previous findings regarding substrate specificity of RIG-I and MDA5 [271]. The average length of both poly(I:C) preparations was examined on a non-denaturing agarose gel. LMW poly(I:C) corresponded to a length of approximately 200 bp, whereas HMW poly(I:C) corresponded to a length of around 3-5 kb (Figure 38D). It has to be noted that $293T^{RIG-I}$ cells responded similarly to low and high molecular weight poly(I:C). Hence, HMW poly(I:C) was used to stimulated both $293T^{RIG-I}$ and $293T^{MDA5}$ cells over-expressing DAPK1, DAPK2, and DAPK3 in a direct comparison of both cell lines. DAPK1, DAPK2, and DAPK3, which had been found to be inhibitors of RIG-I-mediated signalling reduced IFIT1 promoter activity in $293T^{MDA5}$ cells to a similar extent (Figure 38E).

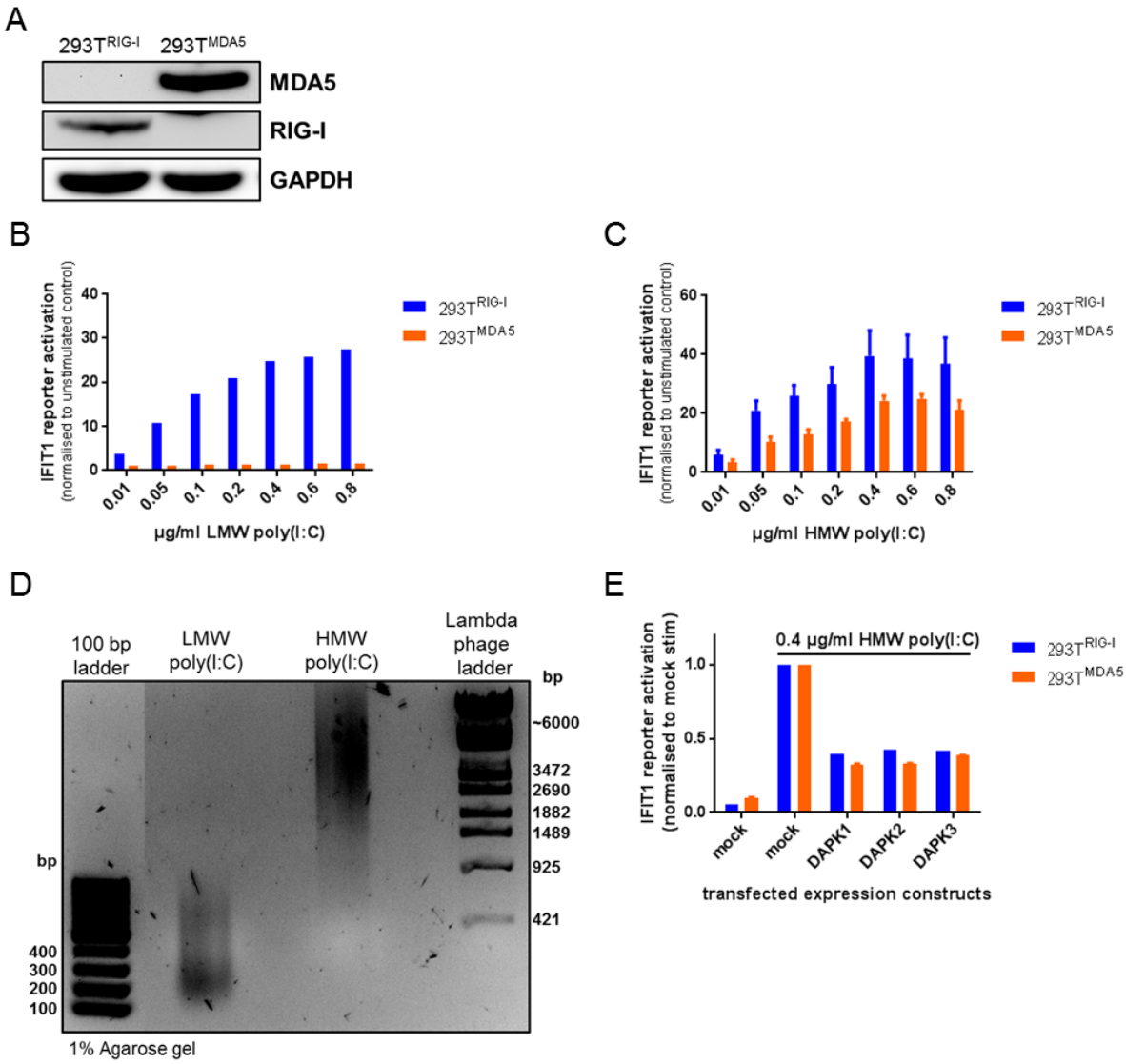

Figure 38 **DAPKs inhibit MDA5-dependent antiviral signalling**

A) Western Blot analysis of RIG-I and MDA5 expression in both 293T^{RIG-I} and 293T^{MDA5} cells. **B)** IFIT1 promoter reporter assay in 293T cells stably over-expressing RLRs in response to transfection of increasing amounts of low molecular weight (LMW) poly(I:C). **C)** IFIT1 promoter reporter assay in 293T cells stably over-expressing RLRs in response to transfection of increasing amounts of low molecular weight (HMW) poly(I:C). Mean of three independent experiments is shown. **D)** Agarose gel showing the average length of LMW and HMW poly(I:C). Two different DNA ladders are used to mark bp sizes. **E)** IFIT1 promoter reporter assay in 293T cells stably expressing RLRs and transiently over-expressing DAPKs. Cells were stimulated by transfection of the indicated amount of HMW poly(I:C). For 293T^{MDA5} cells the mean of two independent experiments is shown. For IFIT1 promoter reporter assays cells were stimulated for 16h before lysis.

As the original 293T cell line was not able to induce IFN signalling in response to poly(I:C) (data not shown and [249]), antiviral signalling initiated in 293T^{MDA5} cells was exclusively dependent on MDA5 activity. DAPK1, DAPK2, and DAPK3 inhibited IFIT1 promoter activity in 293T^{MDA5} cells to a similar extent as in 293T^{RIG-I} cells. This shows that DAPKs are capable of inhibiting not only RIG-I- but also MDA5-mediated antiviral signalling.

4.8 Inhibition of antiviral signalling by DAPKs is not limited to control of RLR activity

The three closest related members of the DAPK family, DAPK1, DAPK2, and DAPK3, are inhibitors of RIG-I signalling and we could show that in the case of DAPK1 this was achieved by direct, inhibitory phosphorylation of RIG-I. In order to examine whether the effect of DAPKs was solely carried out on the level of RIG-I activation, other means of stimulation which did not depend on active RIG-I were tested in $293T^{RIG\text{-}I}$ cells.

Interestingly, DAPKs were also capable to inhibit the signalling pathway when it was stimulated downstream of the effector molecule RIG-I. When $293T^{RIG\text{-}I}$ cells were stimulated by over-expression of the RIG-I CARD domains (RIG-I CA) or MAVS, which both strongly induce the signalling cascade but omit the activation step of RIG-I, signalling was strongly inhibited in DAPK1 over-expressing cells (Figure 39A). The same effect of DAPK1 expression was observed in cells stimulated by over-expression of a constitutively active form of IRF3 (IRF3 5D). Similarly, DAPK2 and DAPK3 over-expression inhibited IFIT1 promoter activity in cells stimulated either by over-expression of MAVS or IRF3 5D (Figure 39B). Furthermore, it was observed that the C-terminus of DAPK1 was able to inhibit RIG-I signalling in a kinase-independent fashion. Previous results obtained in our lab showed that a DAPK1 construct merely missing the kinase domain and the CaM domain, but containing the full C-terminus of the protein ($DAPK1^{\Delta KC}$), was able to inhibit IFIT1 promoter activity to a similar extent as full-length DAPK1 [249]. As this mutant was not able to phosphorylate RIG-I, another means of inhibition must take place when it was over-expressed. As mentioned above, Ankyrin repeats, which this mutant contained, can mediate protein-protein interaction.

As $293T^{RIG\text{-}I}$ cells expressed endogenous DAPK1, it was possible that via its Ankyrin repeats $DAPK1^{\Delta KC}$ recruited WT DAPK1 and thereby mediated RIG-I signalling inhibition. If this were true, dimerisation with WT DAPK1 could happen with any DAPK1 mutant containing the Ankyrin repeats domain. The newly established $293T^{RIG\text{-}I}$ DAPK1 knockout cell lines were employed to investigate if $DAPK1^{\Delta KC}$ would rely on endogenous DAPK1 to inhibit RIG-I signalling. When over-expressed in DAPK1 KO cells, $DAPK1^{\Delta KC}$ inhibited IFIT1 promoter activity to the same extent as in WT $293T^{RIG\text{-}I}$, indicating that it acted independently of endogenous DAPK1 (Figure 39C). It remains to be investigated if $DAPK1^{\Delta KC}$ requires other DAPK family members to confer its inhibitory function in RIG-I signalling. Interestingly, over-expression of full-length DAPK1 was not possible on some KO clones, probably because they expressed active Cas9 and N-terminal targeting sgRNA (Figure 39D).

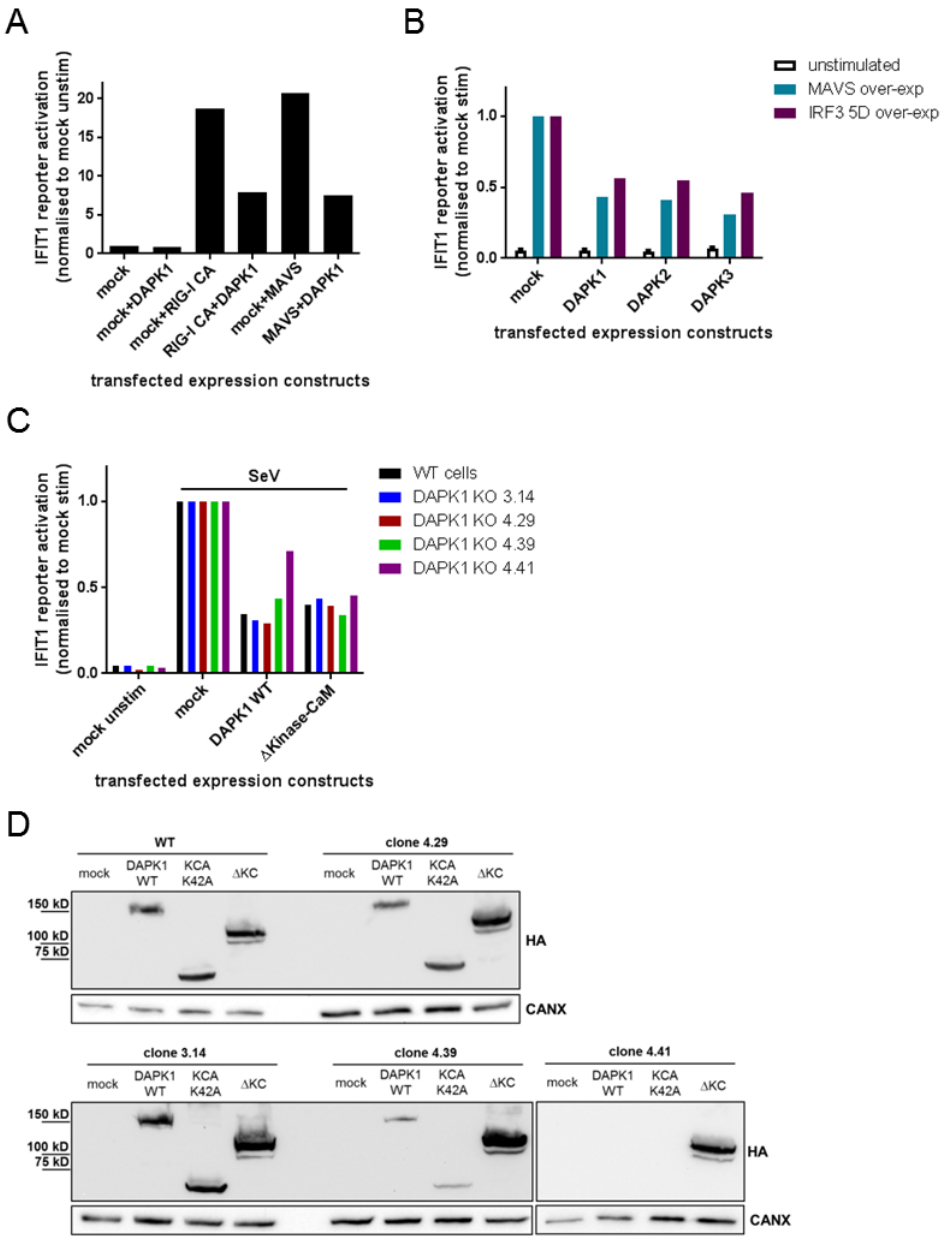

Figure 39 Inhibition of antiviral signalling by DAPKs is not limited to the level of RIG-I phosphorylation

A) IFIT1 promoter activity in 293T^{RIG-I} cells transfected with DAPK1 and stimulated by over-expression of constitutively active RIG-I (RIG-I CA) or MAVS for 16h. **B)** IFIT1 promoter activity in 293T^{RIG-I} cells transfected with DAPK1, DAPK2, or DAPK3 and stimulated by over-expression of MAVS or constitutively active IRF3 (IRF3 5D) for 16h. **C)** 293T^{RIG-I} with (WT) or without (DAPK1 KO) endogenous expression of DAPK1 were transfected with DAPK1^{WT}, DAPK1$^{KCA\ K42A}$ or DAPK1$^{\Delta KC}$ mutants. Cells were infected with SeV (MOI 5) for 16h before lysis. **D)** Western Blot of over-expression assay in C). Expression efficiency of transfected constructs was assessed by staining for HA-tag. Expression of DAPK1$^{KCA\ K42A}$ construct was included but not evaluated in IFIT1 promoter activity assay.

All three DAP kinases, DAPK1, DAPK2 and DAPK3, are capable to inhibit RLR signalling, not only by direct inhibition of RIG-I by inhibitory phosphorylation, but also downstream of the level of RLR receptors. In fact, DAPK1, DAPK2, and DAPK3 can seemingly modulate gene expression at the level or downstream of the transcription factor IRF3, as shown by their inhibitory effect when a constitutively active form of IRF3 was expressed. In case of DAPK1, this inhibition might be independent of its kinase activity, since a mutant lacking the kinase and CaM domain inhibited RIG-I signalling as efficiently as full-length DAPK1 and this was not due to dimerisation with endogenous DAPK1.

5 Discussion

Due to their role in death and survival signalling pathways, DAPKs have been of special interest ever since their discovery. Sure enough, the view on their function in the cell has since then expanded. Initially, the main function of all DAPK family members was thought to be that of mere inducers of apoptotic and autophagic cell death [161], [163], [164], [200], [207], [219], [228]. Since then, intensive research established that DAPKs are, actually, involved in the control of cell death and survival on different levels. They might, on the one hand, directly interact with p53 to induce apoptosis [226], [272], but can also facilitate cell survival, e.g. by promoting mTOR signalling [187], [227]. Furthermore, DAPKs control induction of inflammatory responses [197], [216] and are thought to be tumour suppressors [173]–[175], [220], [273].

RIG-I-like receptor-mediated antiviral signalling is crucial for an adequate induction of type I and type III interferons in response to recognition of cytosolic viral replication intermediates. Several post-translational modifications control RIG-I activity. Some of them are activating like TRIM25 and Riplet-mediated ubiquitinylation [122], [123], others are inhibiting like CARD phosphorylation by PKCα/β which also negatively regulates MDA5 activity [274].

The present study identified the DAPK family of serine/threonine kinases as negative regulators of RLR signalling. It had been established that DAPK1 regulates RIG-I activity in a negative feedback loop [199], a mechanism dependent on DAPK1 kinase activity, which our present results confirm and corroborate. Furthermore, this study describes the other members of the DAPK family as novel negative regulators of antiviral signalling with special emphasis on DAPK2 and DAPK3 regulation. Importantly, it was shown that control of RIG-I signalling by DAPKs happens independently of apoptosis and autophagy induction.

5.1 DAPK1 kinase-dependently inhibits RIG-I signalling

Using an siRNA-based screening approach, we identified DAPK1 as an inhibitor of RIG-I signalling [199]. A minimal construct comprising the DAPK1 kinase domain, CaM domain and Ankyrin repeats (DAPK1^{KCA}) was found to exert the same effect as full-length DAPK1, but lost its inhibitory potential when a small, N-terminal part of the kinase domain was deleted (DAPK1$^{\Delta 1\text{-}73}$, figure 9). As a critical lysine (K42) in the ATP acceptor site was deleted in DAPK1$^{\Delta 1\text{-}73}$ and this residue mediates phosphate transfer in phosphorylation reactions, failure of this mutant to inhibit RIG-I signalling indicated a

dependency on DAPK1 kinase activity (compare section 5.2.3) . Along those lines, constitutively active DAPK1$^{KCA\ S308A}$, a construct which mimics the active, de-phosphorylated state of DAPK1 [159], acted like DAPK1^{KCA}.

We previously established that Ankyrin repeats were necessary for the inhibitory function of DAPK1 in RIG-I signalling, as a construct comprising only the kinase and CaM domain (DAPK1^{KC}) was not able to confer RIG-I signalling inhibition [199]. Besides mediating protein-protein interactions, e.g. with MIB1 [194], DAPK1 Ankyrin repeats are targeted by kinases involved in growth factor signalling. These phosphorylation events inhibit DAPK1 kinase activity. Interestingly, we found that neither phospho-mimetic nor phospho-ablatant mutations of either S289 or Y491/Y492, targets of RSK and Src, respectively [188], [185], changed the ability of DAPK1^{KCA} to inhibit RIG-I signalling (figure 10). It is, therefore, unlikely that control of RIG-I by DAPK1 is linked to its role in growth factor signalling. However, DAPK1^{KCA} does not contain the C-terminal domain of DAPK1 which is targeted by growth factor-induced ERK. Phosphorylation of S735 increases DAPK1 activity which has been shown to negatively regulate ERK activity, promoting its retention in the nucleus [186]. Thus, activity of endogenous full-length DAPK1 might be regulated in response to growth factor signalling and thereby also influence RIG-I signalling.

Supporting an influence of cell growth and mitogenic signalling, we observed a strong influence of cell growth and division on DAPK1 expression levels, as we measured up to two-fold differences in protein expression in cells seeded at different densities (figure 10). Interestingly, DAPK1 expression was reversely regulated in the two examined epithelial cell types, 293T^{RIG-I} and A549 and it is not clear how control of DAPK1 expression differs between these two cell types. DAPK1 expression might in fact be influenced by ERK. It was shown that cell density dramatically influenced oscillations of ERK shuttling between nucleus and cytoplasm [275]. Moreover, DAPK1 mediates growth arrest in response to chemotherapeutic drugs [276], [277] and it is established that cell cycle progression depends on growth factor signalling. Not much is known about how DAPK1 expression is regulated in response to cues like epidermal growth factor (EGF) stimulation, but it is possible that there are feedback mechanisms which link DAPK1 expression to ERK activity, especially since DAPK1 activity is tightly controlled by growth factor signalling-related kinases. Our results emphasize that the outcome of assays analysing endogenous DAPK1 function might be strongly dependent on the number of cells seeded in an individual well, as well as variability in growth rates. Small differences in the number of seeded cells might, therefore, account for high variations of results from different biological replicates. This is in fact reflected in the comparatively high variation among silencing experiments performed throughout our study.

5.2 Extending the view to the DAPK family

Besides DAPK1, the DAPK family of protein kinases comprises four other members. DAPK2 and DAPK3 are closely related to DAPK1 and share high amino acid sequence homology in their respective kinase domain (figure 6 and appendix, figure 41). STK17A/DRAK1 and STK17B/DRAK2 are not as closely related to DAPK1 but amino acid sequences of their respective kinase domains are highly homologous (appendix, figure 41).

As the kinase domains of DAPKs are structurally similar, it is not surprising that DAPKs have common target proteins. DAPKs are phylogenetically related to MLCKs [278]. Therefore, all DAPKs may phosphorylate MLC [207], [279], [280] which induces cytoskeletal rearrangement, often accompanied by membrane blebbing. Interestingly, a common PEF/Y (PEF in DAPK1, DAPK2, DAPK3; PEY in DRAK1 and DRAK2) motif was identified which is critical for substrate recognition and interaction. It was shown that for DAPK1 this motif also mediates interaction with an autoinhibitory loop and is, therefore, crucial in regulating kinase activity [281]. Although DAPK N-terminal kinase domains are structurally similar, their C-terminal domains are very different (figure 6). This might provide means of differential regulation of DAPKs and explain reported substrate specificity. For example, only DAPK3 was shown to interact with and to phosphorylate STAT3 [282], and interaction with 14-3-3 proteins was only shown for DAPK2 [226]. Importantly, DAPKs have overlapping sets of target proteins, but can phosphorylate a common target at different residues, thereby influencing the targeted signalling pathway in different ways. This was shown, for example, in case of autophagy induction. Beclin1 is targeted by both DAPK1 and DAPK3 but is phosphorylated at different residues. In the case of DAPK1 this was shown to result in dissociation of Bcl2 family members from Beclin1 [170], while it is not fully understood how DAPK3-mediated phosphorylation of Beclin1 enhances autophagy induction [208]. Importantly, targeting of Beclin1 by DAPK3 seemed to be tissue-specific as this phosphorylation was shown to take place in skeletal muscle, but not in liver cells. Targeting different residues of the same protein by several kinases allows fine-tuning and exact regulation of a signalling pathway. Which DAPK targets a widely expressed effector protein in a certain context might depend on the tissue-specific expression of the kinase.

The present study examined roles and expression of DAPK family members in the context of viral infection. We previously described DAPK1 as a negative regulator of RIG-I [199]. As DAPKs often have similar targets, it was investigated whether the other members of the DAPK family influenced antiviral signalling as well. It was first addressed

how expression of the three most closely related DAPKs, DAPK1, DAPK2, and DAPK3, might differ in certain cell lines and tissues and if expression changed upon viral infection.

5.2.1 DAPK expression varies in different tissues and derived cell lines

DAPK gene expression data derived from the GTEx portal shows tissue-specific expression of DAPK1, DAPK2, and DAPK3 (figure 11), which is to a large extent reflected in cancer cell lines derived from these tissues (figure 12). Interestingly, while DAPK1 and DAPK2 expression varied substantially, DAPK3 mRNA and protein levels were similar in the analysed cell lines. This reflected DAPK3 gene expression data from patient samples in which, other than DAPK1 and DAPK2, DAPK3 was expressed in all analysed tissues (log10(RPKM) ~ 1). Importantly, expression of DAPK1, DAPK2, and DAPK3 seems to be especially high in tissues which frequently encounter viral infections and, therefore, rely on a well-regulated IFN response, such as the lung and the gastrointestinal tract. Thus, it is plausible that DAPKs might be involved in the control of antiviral signalling in these tissues and might indeed control RIG-I activity.

While virus infection resulted in slight changes in DAPK mRNA levels in the analysed cell types, protein levels remained largely unchanged. DAPK3 mRNA levels were increased in A549 and $293T^{RIG\text{-}I}$ cells in response to virus infection, which was frequently observed and is discussed in section 5.3. In Huh7 Lunet and HeLa cells, however, DAPK3 mRNA levels were slightly decreased after SeV infection. Interestingly, DAPK2 protein stains revealed a shift in signal size upon viral infection which corresponded to dimerised DAPK2 (implications of DAPK2 dimerisation are discussed in section 5.3). While this shift was clearly visible in A549 and Lunet cells, DAPK2 seemed to constitutively dimerise in $293T^{RIG\text{-}I}$ cells. As it was suggested that dimerisation of DAPK2 indicates increased activity [160], it remains to be determined how protein targets might be regulated by this seemingly highly active DAPK2 in $293T^{RIG\text{-}I}$ cells.

Interestingly, we found that expression of one DAPK might be influenced by expression of another DAPK family member as we observed that transfection of some siRNAs which, based on their seed sequence, were predicted to target only one DAPK family member, also diminished protein levels of another DAPK (figure 15). Therefore, it may be necessary to assess the expression of the most closely-related DAPK family members in addition that targeted by a siRNA before interpreting respective results.

5.2.2 DAPK2 and DAPK3 are negative regulators of RIG-I signalling

As we had established that, in addition to DAPK1, A549 and 293T^{RIG-I} cells also expressed DAPK2 and DAPK3 (figure 12), we now sought to determine whether these DAPK family members would also influence RIG-I signalling.

Moreover, the minimal construct DAPK1^{KCA} is similar to DAPK3 which harbours the N-terminal Kinase domain and a C-terminal Leucine zipper domain which, like the DAPK1^{KCA} Ankyrin repeats, mediates protein-protein interaction [218]. In that it contains the DAPK1 CaM domain, DAPK1^{KCA} is structurally related to DAPK2, which is, like DAPK1, a CaM-dependent kinase.

When over-expressed in 293T^{RIG-I} cells, both DAPK2 and DAPK3 dose-dependently inhibited antiviral signalling similarly to DAPK1 (figure 13). DAPK3 seemed to inhibit RIG-I signalling more efficiently than DAPK2 since four times more plasmid encoding DAPK2 was necessary to reach 50% reduction in IFIT1 promoter activity (50 ng DAPK3 vs 200 ng DAPK2). Due to the difference in size of encoding plasmid DNA and expressed protein, DAPK1 could not be directly compared to DAPK2 and DAPK3. For a direct comparison of efficiency, DAPK1, DAPK2, and DAPK3 expression would have to be monitored by gradient PAGE and Western Blot analysis. Furthermore, assessing IFIT1 promoter activity at different time points post infection could provide information as to how kinetics of RIG-I signalling inhibition might differ between DAPKs.

In addition to over-expression assays, we also chose to silence the DAPKs using specific siRNAs. Assessing changes in the antiviral response upon DAPK silencing, we further validated their roles as inhibitors of RIG-I signalling. Sure enough, silencing of DAPK3 increased IFIT1 promoter activity in response to RNA virus infection (figure 15). Additionally, IFNβ and IFIT1 mRNA levels were increased when DAPK3 was silenced prior to RNA virus infection (figure 16). As DAPK2 was expressed at much lower levels than DAPK1 and DAPK3 (figure 12), it was not surprising that knockdown of DAPK2 had no effect on the antiviral signalling response. However, it was observed that survival of cells silenced for DAPK2 and infected with SeV was significantly reduced with most cells detached and floating after 16h of infection. Knockdown of DAPK2 was shown to facilitate TRAIL-mediated apoptotic pathways by NFκB activation [227]. DAPK2 might inhibit apoptosis-promoting NFκB activation in response to SeV infection which would explain increased cell death in DAPK2-deficient SeV-infected cells.

Inhibition of antiviral signalling seems to be a conserved function amongst all DAPKs since DRAK1 inhibited RIG-I signalling to a similar extent as DAPK1 when over-

expressed in 293T^{RIG-I} cells (figure 14). Unexpectedly, despite harbouring the correct sequence compared to a reference sequence [163], DRAK2 was kinase inactive when over-expressed in 293T^{RIG-I} cells (figure 14) and also *in vitro* (figure 26) and did, consequently, not influence RIG-I signalling. Due to the limited expression of DRAKs in most tissues (appendix, figure 42), though, it remains debatable whether an inhibition of RIG-I signalling by DRAKs is physiologically relevant.

5.2.3 DAPKs kinase-dependently target RIG-I

It was established that truncation constructs of DAPK2 and DAPK3, mainly comprising the kinase domains, carried out inhibition of RIG-I signalling to the same extent as the respective full-length kinases (figure 21). Dependency on DAPK2 kinase activity was observed as DAPK2^{S318A} conferred signalling inhibition, DAPK2^{S318D} did not, which was in line with findings for DAPK1^{KCA} S308 mutants (figure 1). Also, DAPK2^{Kinase} did not inhibit IFIT1 promoter activity as efficiently as DAPK2$^{Kinase-CaM}$, likely reflecting decreased kinase activity upon loss of the CaM domain. Contrarily, earlier studies found increased kinase activity of a DAPK2 construct lacking the CaM domain [161], [283]. However, these earlier publications examined DAPK2 kinase activity in *in vitro* kinase and membrane blebbing assays only. Furthermore, DAPK2 constructs examined in these early studies lacked only the CaM domain while the complete C-terminal part of DAPK2 was deleted in the present study. Hence, it is possible that DAPK2 activity is regulated differently in a construct which only comprises the kinase domain in contrast to a construct containing kinase and CaM domain. As there are no reports about constitutively active or inactive mutants of DAPK3, it could not be validated that inhibition of RIG-I signalling by DAPK3 really depended on its kinase activity. As DAPK3 activity is differently regulated than activity of DAPK1 and DAPK2 (section 5.3), it is possible that kinase activity of DAPK3 is not as crucial for the control of RIG-I signalling as that of DAPK1 and DAPK2.

Substitution of K42/K52 with alanine creates DAPK mutants which are reportedly kinase dead [161], [164], [200]. This was reproducible in our in vitro phosphorylation assays (figure 26 and data not shown). However, supposedly kinase-inactive DAPK2^{K52A} and DAPK3^{K42A} (and DAPK3^{D161A} or DAPK3$^{K42A/D161A}$, respectively) constructs behaved like WT kinases when over-expressed and analysed in IFIT1 promoter reporter assays, although they were kinase-dead in *in vitro* phosphorylation assays (figure 26). Similarly, DAPK1$^{KCA\ K42A}$ did not rescue IFIT1 promoter reporter activity to the same extent as constitutively inactive DAPK1$^{KCA\ S308D}$ (figure 9).

Notably, it was reported for DAPK3 that K42A mutation only abrogated kinase activity when ATP concentrations were low (10-50 µM, typically used in *in vitro* assays), but retained kinase function under physiological ATP concentrations (5-10 mM) [284]. Additionally, Lee et al. reported that K42A mutation did not abrogate DAPK1-mediated Pin1 phosphorylation in cells [285], suggesting that the same might hold true for DAPK1. In line with this, we found the $DAPK1^{KCA\ K42A}$ construct to retain kinase activity in cells, as this construct auto-phosphorylated as efficiently as $DAPK1^{KCA}$ (figure 9). Thus, residual kinase activity of $DAPK1^{KCA\ K42A}$ might explain why this construct did not rescue RIG-I signalling inhibition similarly to the phospho-mimetic, constitutively inhibited $DAPK1^{KCA\ S308D}$ (figure 9). Analogously, it is likely that $DAPK2^{K52A}$ and $DAPK3^{K42A}$ (and D161 point mutations) are not kinase-dead under physiological ATP concentrations and retain kinase activity to some extent which allows them to influence RIG-I signalling when over-expressed in $293T^{RIG-I}$ cells.

In line with our cell-based assays, all DAPK family members were capable of RIG-I phosphorylation *in vitro*. Auto-phosphorylation signals were indicative of kinase activity and served as an internal control (figure 26). However, in binding assays, strong and reproducible interaction with RIG-I was only observed for DAPK1 and DAPK2 (figure 25). This does not necessarily indicate that RIG-I would not be a natural substrate of DAPK3 and DRAK1. In fact, due to the transient nature of kinase-substrate interactions co-immunoprecipitation experiments might not be an ideal approach to verify if a kinase interacts with a target protein. Instead, proximity ligation and FRET-based reporter systems have proved more successful in the identification of kinase targets [286], [287] and could be employed in order to examine whether DAPK3 and DRAK1 interact with RIG-I. Furthermore, also for DAPK1 and DAPK2, it remains to be determined if they require accessory proteins for an interaction with RIG-I or if they directly bind their target. Ultimately, as we identified T667 as a central residue phosphorylated by DAPK1 [199], it will be exciting to investigate if DAPK2 and DAPK3 phosphorylate the same or different residues on RIG-I.

5.3 Antiviral signalling influences DAPK2 and DAPK3 activity

We described DAPK1 to be part of a negative feedback loop. Upon activation of antiviral signalling, DAPK1 activity is increased and mediates a subsequent down-regulation of RIG-I signalling [199]. As an overshooting, prolonged immune response can be detrimental for the host, DAPK1 thereby ensures that an initial, strong IFN response finds a timely end.

Since DAPK2 and DAPK3 are closely related to DAPK1, we wondered whether activity of them, too, might be influenced by antiviral signalling.

Similar to activating dephosphorylation of S308 of DAPK1, dephosphorylation of S318 indicates increased DAPK2 activity [160]. As a DAPK2 p-S318-specific antibody did not give reliable signal in our hands, we decided to examine dimerisation of endogenous DAPK2 instead. Sure enough, we observed a shift of DAPK2 signal to a higher molecular weight (corresponding to the size of DAPK2 dimers) in Western Blot analyses of SeV-infected A549 and Huh7 Lunet cells (figure 12).

It has to be noted that it is still not entirely clear whether formation of DAPK2 dimers indicates increased or decreased kinase activity. Crystal structure analyses found murine DAPK2 dimers to be oriented in a way which does not allow substrate interaction [288]. Other than in the case of DAPK3, amino acid sequences of murine and human DAPK2 are highly homologous. However, since constitutively active DAPK2^{S318A} was shown to preferentially dimerise while non-active DAPK2^{S318D} does not, another group proposed that DAPK2 dimerisation is indicative of and necessary for DAPK2 activity [160]. Importantly, this group worked with human DAPK2 and included a variety of functional assays to show increased activity of DAPK2^{S318A}. We observed enhanced DAPK2 dimerisation over time in virus-infected cells as compared to non-infected controls, indicating that DAPK2 was increasingly activated in response to viral infection. Thus, DAPK2 might be involved in a similar negative feedback regulation as DAPK1. This might be especially relevant in tissues with high DAPK2 and low DAPK1 expression, such as the heart (figure 11).

In contrast to DAPK2 whose activity was likely up-regulated in response to viral infection, activity of DAPK3 seemed to decrease over time upon SeV infection (figure 24). While total DAPK3 protein levels remained stable over time, p-DAPK3 T265 levels decreased. It has to be stated that although phosphorylation of multiple residues of DAPK3 determines DAPK3 kinase activity and subcellular localisation [203], there are only two reports which state that especially T265 phosphorylation is needed for full DAPK3 activity [203], [204]. So far, DAPK3 T265 was found to be auto-phosphorylated as well as targeted by ROCK1 which caused stress fibre formation [284]. Importantly, the same publication also identified other residues, namely T180 and T225, whose phosphorylation was, in their hands, crucial for full DAPK3 activity. Unfortunately, no other antibody which might help identify activating phosphorylation of DAPK3 than the one detecting p-DAPK3 T265 is currently available. If T265 dephosphorylation truly indicates decreased DAPK3 activity, present findings indicate that DAPK3 activity is

reduced in response to viral infection, indicating that DAPK3 might be reversely controlled to DAPK2, given that dimerised DAPK2 is active. This seems counter-intuitive taking into account that DAPK3 mRNA levels were repeatedly up-regulated in virus-infected cells (figure 12 and 16). Also, DAPK3 was reported as an ISG in an earlier publication [205]. It is possible that dephosphorylation of DAPK3 T265 does not influence kinase activity. In this case, one would have to find other means of determining if and how active DAPK3 is in response to viral infection. As a matter of fact, the initial study which first described the kinase and its structure proposed that DAPK3 oligomerises and is trans-phosphorylated to attain full kinase activity [200]. A later study described that active DAPK3 forms trimers [201]. If active DAPK3 oligomerises in a similar way as DAPK2, a cross-linking approach or native PAGE could be employed to visualise DAPK3 oligomers, allowing observation of formation or dissociation of oligomers over time after viral infection.

If DAPK2 dimerisation indeed indicates enhanced activity, it seems, at this point, that DAPK2 is increasingly activated in response to viral infection, similar to what was observed for DAPK1. As DAPK2, like DAPK1, is an inhibitor of RIG-I signalling, this would imply DAPK2 is included in a similar negative feedback mechanism down-regulating an initial strong IFN response. Unlike for DAPK1 where dephosphorylation of S308 indicates activity, there is no definitive marker for the identification of active DAPK3. Until then, the results in this work indicate that DAPK3 activity might decrease when antiviral signalling is initiated, the implications of which are so far not clear.

5.4 It's not a question of life and death

The role of DAPKs in cell death induction has been studied extensively. The founding DAPK family member DAPK1 was first described as the main effector of IFNγ-induced cell death in HeLa cells [164]. Sure enough, DAPKs induce apoptosis by interaction with members of the p53 pathway [180], [205], [272]. Additionally, they promote autophagy induction by phosphorylation of Beclin1 [171], [208] or mTOR [228]. As we did not know how exactly DAPKs conferred inhibition of antiviral signalling, we decided to investigate if their inhibitory role in the RIG-I signalling pathway was dependent on their cell death-inducing properties. To this end, we inhibited apoptosis on the one hand, and either inhibited or triggered autophagy on the other hand, and examined how this would change RIG-I signalling.

We did observe that DAPK over-expression consistently resulted in a certain degree of cell death indicated by membrane blebbing and cell detachment. Consequently, PARP

cleavage was increased in cells over-expressing DAPKs (figure 18), indicating that, indeed, DAPKs promoted apoptosis in target cells. Pre- and co-treatment of cells with small molecule pan-caspase inhibitor Q-VD-OPh significantly reduced PARP cleavage, i.e. apoptosis induction, in response to DAPK expression. Importantly, there was no change their potency to inhibit RIG-I signalling when apoptosis was inhibited (figure 18). This indicated that negative regulation of RIG-I signalling conferred by DAPKs is not linked to their apoptosis-promoting function.

Interestingly, over-expression of DRAK1 hardly induced PARP cleavage. Even more strikingly, PARP cleavage induced by DRAK1 was not reduced by caspase inhibitor treatment. Although results based on DRAK1 over-expression are preliminary and require repetition, they suggest that the apoptosis-promoting function of DRAK1, at least in $293T^{RIG\text{-}I}$ cells, is limited. In fact, as DRAK1-induced PARP cleavage was low and not influenced by caspase inhibition, it is possible that instead of promoting apoptosis, DRAK1 actually induces autophagy. In fact, in the first publication describing DRAK1, conclusions regarding the cell death-promoting function of the kinase were based solely on phenotypic observations but included no mechanistic investigation as to how DRAK1 might induce apoptosis [163]. It is possible that DRAK1 over-expression rather promotes autophagy induction which either precedes or entails apoptotic cell death. Autophagy might also contribute to caspase-independent cell death, a mechanism which was first described in macrophages which died in response to lipopolysaccharide treatment in the presence of caspase inhibitors [289]. Moreover, DRAK1 is more closely related to DAPK2 than to DAPK1 or DAPK3 (appendix, figure 41). While the role of DAPK2 in apoptotic cell death is still debated [222], it has been repeatedly shown to influence the autophagic network [219], [221], [228]. Thus, if DRAK1 behaved similar to DAPK2, it would rather influence autophagic than apoptotic cell death. Up to this day neither DRAK1 nor DRAK2 have been examined in the context of autophagy induction.

In contrast, all three “classical” DAPKs, DAPK1, DAPK2, and DAPK3, have been described to induce autophagy, be it by phosphorylation of autophagy-promoting Beclin1 or by interfering with survival-promoting mTOR. By direct interaction of ATG12 and ATG5 with the CARD domains of RIG-I and MAVS, induction of autophagy inhibits RIG-I signalling in response to viral infections [290]. This mechanism probably prevents an overproduction of IFNs in response to viral infections, as $ATG5^{-/-}$ mouse embryonic fibroblasts produced extensive amounts of IFN and were resistant to vesicular stomatitis virus infection. If autophagy was induced upon DAPK expression, this could, therefore, result in an inhibition of RIG-I signalling.

Strikingly, none of the above-mentioned DAPKs induced autophagy when they were over-expressed in 293T^{RIG-I} cells as evidenced by LC3-I and –II levels remaining unchanged in comparison to mock transfected cells (figure 19). Pharmacological inhibition and induction of autophagy, however, was successful indicated by increased or decreased levels of LC3B-II, respectively. Torin-1 efficiently inhibited mTOR as assessed by p-S6K staining. Interestingly, DAPK1 and DAPK2 over-expression caused an increase in p-S6K levels compared to mock transfected cells. This indicated an increase in mTOR activity upon DAPK1 and DAPK2 over-expression, suggesting that the mTOR-stimulating functions of DAPK1 (and possibly DAPK2) predominated in 293T^{RIG-I} cells. If DAPK expression rather stimulated mTOR activity in 293T^{RIG-I} cells, this would explain the absence of autophagy in response to DAPK over-expression as mTOR activity usually restricts autophagy induction.

It was described before that the autophagic machinery was activated upon initiation of antiviral signalling and restricted IFN production. The present results indicate that this regulation does not take place in 293T^{RIG-I} cells as pharmacological autophagy induction did not inhibit the RIG-I signalling response. On the contrary, Spautin-1-mediated autophagy inhibition slightly reduced the antiviral signalling response. It is possible that excessive amounts of RIG-I, which is stably over-expressed in 293T^{RIG-I} cells, overwhelms the autophagic machinery rendering this way of regulation inefficient.

All in all, examinations of the cell death-promoting functions of DAPKs in the context of viral infection showed that although DAPKs induce apoptosis in transfected cells this does not account for their inhibitory effect on RIG-I signalling. Additionally, inhibition of RIG-I signalling by DAPKs was conferred independently of autophagy induction as DAPKs did not trigger type II cell death in the analysed cells, but strongly inhibited RIG-I signalling.

5.5 The role of DAPKs in RNA virus infection

The role of DAPKs as negative regulators of RIG-I signalling was confirmed in viral replication assays which highlighted the physiological relevance of our biological assays. In the present study only DAPK1 and DAPK3 were analysed and compared in viral replication assays as knockdown of DAPK2, probably due to low expression in examined cell lines, did not impact on IFIT1 promoter reporter activity.

Knockdown of DAPK1 and DAPK3 inhibited RVFV and FluAV replication (figure 37 and figure 38). Both viruses have been shown to specifically activate RIG-I which recognises the panhandle structure formed by complementary regions in their genomes [103], [104],

[111]. Combined knockdown of both kinases did not result in stronger suppression of viral replication, but rather resulted in an intermediate phenotype which ranged in between levels of single knockdown of either kinase. This was probably due to lower knockdown efficiency when both kinases were targeted, as indicated by remaining protein signal on Western Blot level. Interestingly, down-regulation of DAPK1 impacted RVFV replication to a much larger extent than knockdown of DAPK3. DAPK3, however, seemed to be more important than DAPK1 in controlling RIG-I signalling during FluAV replication, as only few virus-infected cells were detectable when it was silenced. Strikingly, in one experiment in our present study, knockdown of DAPK1 did not influence FluAV replication at all, whereas in earlier experiments knockdown of DAPK1 resulted in strong and reproducible inhibition of FluAV replication ([249] and [199]). The main differences between those previous and present results are that infection rates were much higher in earlier experiments (~80% infected cells in contrast to ~16%) and that a different siRNA targeting DAPK1 was used. It is possible that effects on FluAV replication mediated by DAPK1 are smaller than those mediated by DAPK3 and that the measurement window in the present experiments was too limited to show DAPK1-mediated effects. As DAPK3 was described to shuttle between cytoplasm and nucleus [202], [203] and FluAV replication happens in the nuclear compartment [291], it is possible that DAPK3 restricts the recognition of FluAV replication intermediates in the nucleus. This idea is especially intriguing since recent observations indicate that RIG-I might be present in the nuclear compartment and even recognise FluAV replication intermediates there (conference talk, unpublished research by the group of Friedemann Weber, Gießen University). Higher cytosolic concentrations of DAPK1, however, might restrict RIG-I after initial recognition of RVFV genomes. Also, it was previously shown that DAPK activity was changed upon viral infection. It is possible that DAPK1, DAPK2, and DAPK3 activity is regulated differently in response to certain RNA viruses. While infection with one virus might result in an increase in DAPK1 kinase activity, which benefits viral replication since it restricts RIG-I, another virus might cause up-regulation of DAPK3 and, therefore, react more sensitive when this kinase is down-regulated. Ultimately, it is not known if DAPKs influence other antiviral proteins and thereby specifically inhibit signalling in response to a certain virus.

In contrast to findings for RVFV and FluAV replication, silencing of DAPK1 and, to some extent, DAPK3, resulted in enhanced HCV JCR2A replication (figure 39). Generally, as HCV JCR2A replicated inefficiently in the examined Lunet CD81^{high} and Lunet CD81^{high} MAVS-GFP$_{NLS}$ (~10 fold increase in signal between the 24h and the 96h time point), the measurement window was quite small. However, HCV replication was clearly increased

when DAPK1 was knocked down, although DAPK1 protein levels recovered 72h after HCV infection. For down-regulation of DAPK3 only a slight increase in HCV replication was observed at 96h post infection. In light of our previous results it seems counterintuitive that DAPK knockdown should favour HCV replication. However, it should be noted that HCV permissive Huh7-derived cells are virtually deficient of interferon induction, meaning that the negative impact of DAPKs on the antiviral response might not play any role. Moreover, it was shown that pegylated IFNα suppresses HCV replication by an activation of DAPK1 which in turn activates mTOR [268]. Importantly, Liu et al. did not determine DAPK1 activity by staining for p-DAPK1 S308 but rather by examining phosphorylation of S735 which is targeted by ERK [186]. Also, their study provides no functional link between DAPK1 kinase activity and an increase in mTOR signalling, but merely shows an up-regulation of mTORc1 upon DAPK1 over-expression. Still, phenotypically, our results presented here support the notion of Liu et al. that DAPK1 might actually inhibit HCV replication. Of note, Liu et al. examined replication of HCV genotype 1b, whereas our JCR2A virus corresponds to genotype 2a. Therefore, DAPK1 apparently influences replication of HCV belonging to different genotypes.

Interestingly, hyper-methylation of the DAPK1 promoter was found to negatively influence therapy responses in chronic HCV genotype 4 infection and was prominent in hepatocellular carcinomas (HCC) caused by chronic HCV infection [292], [293], indicating that high DAPK1 expression might be favourable in the context of HCV infection. Still, it needs to be remembered that DAPK1 might actually promote tumour growth in cancers harbouring p53 mutations [189]. Hence, although high DAPK1 expression might first restrict HCV replication, it might be detrimental when p53 mutations occur in the course of HCC progression.

So far, it has not been investigated if DAPK2 or DAPK3 facilitate or restrict HCV replication. Present data indicate that DAPK3 might, similarly to DAPK1, negatively influence HCV (JCR2A) replication (figure 39). Assessing viral replication in cells where both kinases are down-regulated could contribute to better understanding of the role of DAPKs in HCV replication, since DAPK3 was up-regulated in cells silenced for DAPK1 (figure 39). This also suggests a counter-regulatory mechanism of DAPK expression which will be discussed in the following section.

5.6 DAPKs do not interdepend in their role as negative regulators of RIG-I signalling

5.6.1 Never alone? – Interaction of DAP kinases

We identified DAPKs as negative regulators of RIG-I signalling and found that all DAPK family members were capable of RIG-I phosphorylation. However, we only observed interaction with RIG-I for DAPK1 and DAPK2, but not for DAPK3 and DRAK1. It had been reported that DAPK1 and DAPK3 interacted [201] and that this interaction depended on a motif in their kinase domains termed the “basic loop”. As the basic loop found in DAPK1 and DAPK3, which comprises four arginine residues and is mostly conserved in DAPK2, except for a substitution of one arginine for glutamine (appendix figure 41). Thus, it is feasible that interaction of DAPK2 with both of the other kinases is mediated in a similar fashion.

We hypothesised that DAPK3/DRAK1 interacted with the other RIG-I-binding DAPKs and thereby mediated inhibition of RIG-I signalling. Hence, we decided to examine whether we could observe interaction between DAPK family members.

In line with the previous report on DAPK1-mediated regulation of DAPK3 [201], we did, in fact, find DAPK3 in the fraction of DAPK1 interacting proteins (table 21). When we analysed which proteins were pulled down with the other DAPK family members, we observed interaction between DAPK3 and DAPK2, and also between DRAK1 and DAPK2, as well as DAPK3 (table 23, table 24). We did not find DAPK1 in the interacting protein fractions of the other kinases, maybe because DAPK1 is a large protein and might be difficult to pull down alongside another, smaller protein. Furthermore, we only examined the 14 most enriched proteins and DAPK1 could be present among the less abundant proteins in DAPK2/DAPK3/DRAK1-interacting protein fractions.

Interestingly, we found a member of the antiviral signalling network, DDX3X, among the most abundant hits in the fraction of DAPK2-interacting proteins (table 23). This association of DDX3X with DAPK2 was also found by a different group which sought to determine DAPK2 interaction partners by coupling a proteomics approach with bimolecular fluorescence complementation [294]. DDX3X has been shown to bind viral RNAs and associate with MAVS, enhancing down-stream IFN production [267]. Furthermore, DDX3X interacts with TBK1, thereby increasing IRF3 activity [266]. It is tempting to speculate that, in addition to regulating RIG-I, DAPK2 might decrease DDX3X activity, which could result in an inhibition of antiviral signalling.

More advanced and more detailed proteomic analyses might shed further light on possible interactions between DAPKs and members of the antiviral RIG-I signalling pathways. Furthermore, it remains to be investigated if and how DAPK2 might influence the function of DDX3X in the RIG-I signalling pathway.

5.6.2 Stable knockout of DAPKs does not influence RIG-I signalling

We observed that DAPKs interacted and were frequently found to associate to another DAPK family member. It could, therefore, not be ruled out that effects on RIG-I signalling observed for DAPK2 and DAPK3 were actually mediated via an interaction with DAPK1 or vice versa.

In order to examine if inhibition of RIG-I signalling by DAPK1 depended on DAPK3, we employed a combined knockdown approach in which both, DAPK1 and DAPK3, were targeted simultaneously (figure 29). We excluded DAPK2, since it was expressed at very low levels in the examined cell lines. Therefore, it seemed unlikely effects on antiviral signalling observed for DAPK1 and DAPK3 were mediated by DAPK2. Interestingly, combined down-regulation of DAPK1 and DAPK3 resulted in an intermediate phenotype in terms of IFIT1 promoter activation and IFNβ/IFIT1 mRNA expression compared to what was observed when either kinase was targeted alone (figure 15 and figure 16). This was probably due to inefficient knockdown when both kinases were targeted simultaneously as especially DAPK1 protein levels were higher in the combined compared to the single knockdown samples. Thus, combined siRNA-mediated down-regulation of DAPK1 and DAPK3 did not yield conclusive results as to whether the observed inhibitory effect on RIG-I signalling was dependent on an interaction of both kinases.

In order to further investigate possible functional interactions between different DAPKs and their relevance in the regulation of RIG-I signalling a CRISPR/Cas9-mediated approach was chosen to stably deplete cells of DAPK expression.

DAPK1, DAPK3, and, eventually, DAPK2 were successfully knocked out in A549 and $293T^{RIG\text{-}I}$ cells (figure 31 to figure 34) as determined by undetectable levels of the respective DAPK protein in Western Blots. Knockout was not verified on DNA level except for a few DAPK1 knockout clones (data not shown), but even if some residual DAPK expression remained, it was less than achieved by siRNA-mediated knockdown. Surprisingly, IFIT1 promoter reporter assays of cells lacking either DAPK1, DAPK2, or DAPK3 did not resemble results obtained from transient siRNA-mediated silencing, as the antiviral response was virtually unaltered in cells lacking DAPK expression. We

observed that transfection of several siRNAs targeting different regions of the DAPK1 mRNA resulted in an increase in antiviral signalling. Therefore, we think it unlikely that the effect on RIG-I signalling seen upon DAPK1 silencing is due to off-target effects of the transfected siRNAs.

Knockout of DAPKs was achieved by lentiviral transduction of plasmids encoding Cas9 and sgRNAs and subsequent selection for antibiotic resistance. Furthermore, single cell knockouts were created by limiting dilution of knockout bulks. Growth of single cell colonies lasted several weeks until they could be tested for DAPK protein expression and IFIT1 promoter activation. Since DAPKs were shown to function in similar signalling pathways and often affect the same target proteins, it was initially assumed that down-regulation of one DAPK might trigger compensatory up-regulation of another kinase family member; especially since single cell clones were grown for several weeks and had plenty of time to adapt to DAPK loss. Indeed, compensatory up-regulation of DAPK2 was observed in most DAPK1/DAPK3 DKO single cell clones (figure 34). However, even when these cells were depleted of DAPK2, creating a DAPK1/DAPK2/DAPK3 triple knockout, no change in IFIT1 promoter activation was observed (figure 35). Nevertheless, it was shown that triple knockout of DAPK1, DAPK2, and DAPK3 is possible and that cells lacking all three kinases are viable.

It remains to be determined why stable DAPK knockout, in contrast to transient siRNA-mediated knockdown, has no effect on antiviral signalling induction.

As mentioned above, DAPKs are very important in the control of cell death and survival. DAPK1 was shown to be an important mediator of apoptosis. However, DAPK1 knockout mice have no defect in developmental apoptosis and grow normally [295] which either means that DAPK1 is dispensable for this type of apoptosis or that loss of DAPK1 is compensated for by another kinase. So far, DAPK2 and DAPK3 expression has not been analysed in DAPK1 knockout mice. Usually, the two remaining DAPK family members, DRAK1 and DRAK2, are expressed at low levels in tissues which do not belong to the blood-forming system. It is possible that combined loss of DAPK1, DAPK2, and DAPK3 results in an up-regulation of either DRAK1 or DRAK2, especially since these kinases have also been linked to apoptosis induction. Moreover, loss of one DAPK might not only result in compensatory up-regulation of another DAPK family member but might instead trigger up-regulation of a kinase which has hereto not been described to be able to take over DAPK functions.

5.6.3 Over-expression of DAPKs in knockout cell lines

Although single and combined knockout of DAPKs had no effect on antiviral signalling, generated KO cell lines were employed to determine effects of possible interaction between DAPKs upon over-expression. First results based on transient DAPK3 knockdown already suggested that DAPK1, when over-expressed in cells silenced for DAPK3, did not depend on DAPK3 to mediate inhibition of RIG-I signalling (figure 36). And indeed, when DAPK1 was expressed in DAPK3 KO clones, it efficiently inhibited IFIT1 promoter activation in response to SeV infection. Similarly, RIG-I signalling inhibition by DAPK2 did not depend on endogenous DAPK3 expression and DAPK3 inhibited RIG-I signalling when it was over-expressed in DAPK1 KO cells. Thus, the negative regulation of RIG-I signalling by DAPK1 did not depend on DAPK3 expression. Furthermore, DAPK2 inhibited RIG-I signalling independently of DAPK3 and the negative influence of DAPK3 on RIG-I signalling was not dependent on DAPK1. It remains to be examined if DAPK2 knockout influences the inhibitory function of DAPK1 and DAPK3 in RIG-I signalling, which is not likely as endogenous DAPK2 levels were very low in the examined cell types.

We previously observed that a DAPK1 construct lacking the kinase and CaM domain, $DAPK^{\Delta KC}$ inhibited RIG-I signalling in a similar way as full-length DAPK1 [249]. $DAPK^{\Delta KC}$ contains the DAPK1 Ankyrin repeats which were shown to mediate protein-protein interaction. Therefore, we hypothesised that $DAPK^{\Delta KC}$ conferred inhibition of RIG-I signalling by dimerisation with endogenous full-length DAPK1. However, over-expression of $DAPK1^{\Delta KC}$ in DAPK1 KO clones showed that this was not the case, since $DAPK1^{\Delta KC}$ inhibited RIG-I signalling to the same extent as in control cells (figure 39).

Unfortunately, reconstitution of full-length DAPKs was not possible in most of the single cell KO clones generated for the respective kinase if the transfected construct contained the sequence targeted by the stably expressed sgRNA (such as in the case of $DAPK3^{K42A}$, figure 34). This was probably due to remaining Cas9 activity which was integrated into target cell genomes alongside the sgRNA sequence during lentiviral transduction. Interestingly, Cas9 remained expressed even when selection antibiotics were withdrawn. Many DAPK KO clones were positive for FLAG-tag expression which the Cas9 was labelled with (data not shown).

In order to analyse how reconstituted DAPKs and mutants containing the sgRNA-targeted sequence behave in DAPK KO cells, one would have to introduce mutations into the sgRNA-targeted region in the expression construct. Alternatively, the Cas9 itself

could be targeted using a specific sgRNA and clones depleted of Cas9 expression could be selected.

In summary, results from over-expression assays in DAPK KO cells suggested that DAPK1, DAPK2, and DAPK3 do not interdepend in their function as negative regulators of RIG-I signalling. Moreover, DAPK1$^{\Delta KC}$ did not depend on endogenous DAPK1 for inhibition of RIG-I signalling. Implications of RIG-I signalling inhibition by DAPK1$^{\Delta KC}$ are discussed in the following section.

5.7 Control of antiviral signalling by DAPKs is not limited to negative regulation of RIG-I

The present study describes a kinase-dependent inhibitory role of not only the previously examined DAPK1 [199], but also DAPK2, DAPK3, and DRAK1 on RIG-I-mediated antiviral signalling. Remaining DAPK family member DRAK2 could not be analysed as it was kinase-inactive when over-expressed, although the cloned construct did not differ from a published sequence which was shown to be kinase active, albeit with reduced activity compared to DRAK1 [163].

We initially chose to over-express DAPKs in easy-to-transfect 293T cells. As the original 293T cell line expressed hardly any RIG-I, it did not induce signalling when it was stimulated with poly(I:C). Therefore, it was stably transduced with RIG-I (293T^{RIG-I}) and thereby made responsive to dsRNA stimulation [249]. Consequently, dsRNA was exclusively sensed by RIG-I in this cell line.

We stably introduced MDA5 into the original 293T cell line (293T^{MDA5}) in order to study whether DAPKs inhibited MDA5-mediated antiviral signalling.

5.7.1 DAPKs inhibit MDA5-mediated antiviral signalling

In line with previous reports stating that MDA5 predominantly recognises long dsRNA [271], only high molecular weight poly(I:C) (HMW poly(I:C), ~3-6 kb) activated antiviral signalling in 293T^{MDA5} cells while low molecular weight poly(I:C) (LMW poly(I:C), ~200 bp) did not. Thus, we used HMW poly(I:C) to stimulate DAPK over-expressing 293T^{MDA5} cells in order to find out if DAPK over-expression had an effect on MDA5-mediated signalling.

In a direct comparison with 293T^{RIG-I} cells, DAPKs inhibited MDA5-mediated antiviral signalling with similar efficiency (figure 30). As transfected poly(I:C) was exclusively

sensed by MDA5 in 293T^{MDA5} cells, we concluded that inhibition of antiviral signalling conferred by DAPKs is not limited to an inhibition of RIG-I.

PKCα/β inhibits RIG-I activity by negative phosphorylation of the RIG-I CARD domains [274], but has so far not been described to phosphorylate MDA5. Dephosphorylation by PP1α/β, however, has been shown to activate both RIG-I and MDA5 since it targets their highly homologous CARD domains [144]. Alignment of RIG-I and MDA5 shows that T667 in the Hel2 domain of RIG-I, which is phosphorylated by DAPK1, corresponds to S760 of MDA5. Being serine/threonine kinases, it can be speculated that DAPKs could also target S760. It remains to be determined whether a phosphorylation which might interfere with RNA-binding to RIG-I [199] will have the same effect when transferred onto the corresponding residue in MDA5.

Although DAPKs clearly inhibited MDA5-mediated antiviral signalling, it remains to be examined whether this is due to interaction with and direct phosphorylation of MDA5. As a matter of fact, results presented within this study indicate that DAPKs might also regulate antiviral signalling downstream of RNA-recognition by RLRs.

5.7.2 Inhibition of antiviral signalling by DAPKs downstream of RLRs

The RIG-I signalling cascade is not only activated upon dsRNA recognition, but also by over-expression of the RIG-I CARD (CA) domains [15], MAVS [296] or a constitutively active mutant of IRF3 called IRF3 5D [297]. Thus, it is possible to determine at which level a regulatory factor influences the signalling cascade. If a factor interferes with signalling at or above the level of IRF3 activation, no other stimulus than IRF3 5D over-expression should result in IFN induction.

Our group discovered that DAPK1 negatively regulates RIG-I activity, likely by direct inhibitory phosphorylation [199]. When we examined whether DAPK1 would also influence RIG-I signalling downstream of the step of dsRNA recognition, we saw that RIG-I signalling was still efficiently inhibited by DAPK1 if the pathway was stimulated by either RIG-I CA, MAVS or IRF3 5D over-expression (figure 41). Having observed striking similarities between the DAPK family members, we decided to further examine downstream pathway inhibition by DAPK2 and DAPK3. Similar to what we observed for DAPK1, MAVS- and IRF3 5D-mediated signalling induction was strongly inhibited by DAPK2 and DAPK3.

Moreover, we observed that DAPK1$^{\Delta KC}$ (which lacked kinase and CaM domain and was therefore incapable of RIG-I phosphorylation) inhibited antiviral signalling when it was

over-expressed in DAPK1 KO clones. As discussed above, DAPK1$^{\Delta KC}$ is unable to recruit endogenous DAPK1 (e.g. via its Ankyrin repeats) in these cells. Since DAPKs seem to interact via the basic loop in their kinase domains it is also unlikely that DAPK1$^{\Delta KC}$ recruits other DAPK family members. Still, it cannot be excluded that DAPKs interact with and recruit other kinases which may instead phosphorylate their targets. After all, antiviral signalling was unaffected by DAPK loss in triple KO bulks. It remains to be determined how DAPKs might inhibit RIG-I signalling downstream of IRF3 activation. DAPK1 was described to regulate Pin1 stability by interaction with its ROC-COR domain [285] which is present in DAPK1$^{\Delta KC}$. Once activated Pin1 marks IRF3 for degradation [136]. However, DAPK1-mediated Pin1 regulation was shown to be kinase-dependent and can, therefore, not be mediated by DAPK1$^{\Delta KC}$.

In summary, DAPKs seem to confer inhibition of RLR-mediated antiviral signalling not only on the level of RIG-I which, as it seems, is phosphorylated and inhibited by all DAPKs, but also downstream of RIG-I activation, maybe even on the level of IRF3 and IRF7 activation. One report describes DAPK1 as an IRF3/IRF7-interacting protein. However, contrary to what our group described, that report found DAPK1 to positively influence RIG-I signalling which is surprising given the fact that experiments were mainly performed in 293T cells [198], the same cell line our group used for DAPK1 over-expression assays. Moreover, Zhang et al. found DAPK1 functions in antiviral signalling to be kinase-independent. It is possible that DAPK1 kinase-independently modulates antiviral signalling downstream of RIG-I. Still, this does not explain the discrepancy between DAPK1 being solely inhibitory in assays performed in our group and results obtained by Zhang et al. As the present study showed that not only DAPK1, but also DAPK2 and DAPK3 controlled antiviral signalling, changes in DAPK1 functions might depend on DAPK2 and DAPK3 expression in the respective examined cell type. Furthermore, we showed that DAPK1 expression was influenced by cell growth. Thus, seeding cells at different densities might already heavily influence DAPK1 expression and function.

In summary, DAPK1 seems to possess kinase-independent properties which regulate antiviral signalling at the level of or downstream of the transcription factor IRF3. In addition to DAPK1, most other DAPK family members were found to inhibit RIG-I signalling in our present study. DAPK2, which dimerises and is potentially activated in response to viral infection, might be involved in a similar negative feedback loop as DAPK1. How DAPK3 regulates RIG-I signalling remains to be investigated. Similarly, it remains questionable if regulation of antiviral signalling by DRAKs is physiologically relevant since their expression is limited in most tissues. Importantly, DAPKs were found not only to regulate signalling on the level of RLR activation, but also as far downstream as on the level of IRF3-mediated gene transcription. Generated DAPK single and combined KO cell lines will help determine the exact mechanism of DAPK-mediated antiviral signalling regulation. Moreover, they might prove helpful in determining other functions of DAPKs and how their activity is controlled in cellular survival and death.

6 References

[1] J. C. Knight, 'Genomic modulators of the immune response', *Trends Genet.*, vol. 29, no. 2, pp. 74–83, Feb. 2013.

[2] J. T. Monteiro and B. Lepenies, 'Myeloid C-Type Lectin Receptors in Viral Recognition and Antiviral Immunity', *Viruses*, vol. 9, no. 3, Mar. 2017.

[3] S. Mariathasan and D. M. Monack, 'Inflammasome adaptors and sensors: intracellular regulators of infection and inflammation', *Nat. Rev. Immunol.*, vol. 7, no. 1, pp. 31–40, Jan. 2007.

[4] E. Hollenbach, M. Neumann, M. Vieth, A. Roessner, P. Malfertheiner, and M. Naumann, 'Inhibition of p38 MAP kinase- and RICK/NF-kappaB-signaling suppresses inflammatory bowel disease', *FASEB J. Off. Publ. Fed. Am. Soc. Exp. Biol.*, vol. 18, no. 13, pp. 1550–1552, Oct. 2004.

[5] D. Goubau, S. Deddouche, and C. Reis e Sousa, 'Cytosolic Sensing of Viruses', *Immunity*, vol. 38, no. 5, pp. 855–869, May 2013.

[6] V. Hornung *et al.*, 'AIM2 recognizes cytosolic dsDNA and forms a caspase-1-activating inflammasome with ASC', *Nature*, vol. 458, no. 7237, pp. 514–518, Mar. 2009.

[7] A. Ablasser *et al.*, 'cGAS produces a 2'-5'-linked cyclic dinucleotide second messenger that activates STING', *Nature*, vol. 498, no. 7454, pp. 380–384, Jun. 2013.

[8] L. Sun, J. Wu, F. Du, X. Chen, and Z. J. Chen, 'Cyclic GMP-AMP synthase is a cytosolic DNA sensor that activates the type I interferon pathway', *Science*, vol. 339, no. 6121, pp. 786–791, Feb. 2013.

[9] A. Takaoka *et al.*, 'DAI (DLM-1/ZBP1) is a cytosolic DNA sensor and an activator of innate immune response', *Nature*, vol. 448, no. 7152, pp. 501–505, Jul. 2007.

[10] M. H. Orzalli, N. A. DeLuca, and D. M. Knipe, 'Nuclear IFI16 induction of IRF-3 signaling during herpesviral infection and degradation of IFI16 by the viral ICP0 protein', *Proc. Natl. Acad. Sci. U. S. A.*, vol. 109, no. 44, pp. E3008-3017, Oct. 2012.

[11] N. Kerur *et al.*, 'IFI16 acts as a nuclear pathogen sensor to induce the inflammasome in response to Kaposi Sarcoma-associated herpesvirus infection', *Cell Host Microbe*, vol. 9, no. 5, pp. 363–375, May 2011.

[12] D. C. Rawling, A. S. Kohlway, D. Luo, S. C. Ding, and A. M. Pyle, 'The RIG-I ATPase core has evolved a functional requirement for allosteric stabilization by the Pincer domain', *Nucleic Acids Res.*, vol. 42, no. 18, pp. 11601–11611, Oct. 2014.

[13] A. M. Bruns and C. M. Horvath, 'LGP2 synergy with MDA5 in RLR-mediated RNA recognition and antiviral signaling', *Cytokine*, vol. 74, no. 2, pp. 198–206, Aug. 2015.

[14] A. Komuro and C. M. Horvath, 'RNA- and virus-independent inhibition of antiviral signaling by RNA helicase LGP2', *J. Virol.*, vol. 80, no. 24, pp. 12332–12342, Dec. 2006.

[15] M. Yoneyama *et al.*, 'The RNA helicase RIG-I has an essential function in double-stranded RNA-induced innate antiviral responses', *Nat. Immunol.*, vol. 5, no. 7, pp. 730–737, Jul. 2004.

[16] V. Hornung *et al.*, '5'-Triphosphate RNA is the ligand for RIG-I', *Science*, vol. 314, no. 5801, pp. 994–997, Nov. 2006.

[17] M. Schlee *et al.*, 'Recognition of 5' triphosphate by RIG-I helicase requires short blunt double-stranded RNA as contained in panhandle of negative-strand virus', *Immunity*, vol. 31, no. 1, pp. 25–34, Jul. 2009.

[18] A. Pichlmair *et al.*, 'RIG-I-mediated antiviral responses to single-stranded RNA bearing 5'-phosphates', *Science*, vol. 314, no. 5801, pp. 997–1001, Nov. 2006.

[19] M. Weber *et al.*, 'Incoming RNA Virus Nucleocapsids Containing a 5′-Triphosphorylated Genome Activate RIG-I and Antiviral Signaling', *Cell Host Microbe*, vol. 13, no. 3, pp. 336–346, Mar. 2013.

[20] H. Kato *et al.*, 'Differential roles of MDA5 and RIG-I helicases in the recognition of RNA viruses', *Nature*, vol. 441, no. 7089, pp. 101–105, May 2006.

[21] H. Kato *et al.*, 'Length-dependent recognition of double-stranded ribonucleic acids by retinoic acid-inducible gene-I and melanoma differentiation-associated gene 5', *J. Exp. Med.*, vol. 205, no. 7, pp. 1601–1610, Jul. 2008.

[22] M. Binder *et al.*, 'Molecular mechanism of signal perception and integration by the innate immune sensor retinoic acid-inducible gene-I (RIG-I)', *J. Biol. Chem.*, vol. 286, no. 31, pp. 27278–27287, Aug. 2011.

[23] D. Goubau *et al.*, 'Antiviral immunity via RIG-I-mediated recognition of RNA bearing 5'-diphosphates', *Nature*, vol. 514, no. 7522, pp. 372–375, Oct. 2014.

[24] J. R. Patel, A. Jain, Y. Chou, A. Baum, T. Ha, and A. García-Sastre, 'ATPase-driven oligomerization of RIG-I on RNA allows optimal activation of type-I interferon', *EMBO Rep.*, vol. 14, no. 9, pp. 780–787, Sep. 2013.

[25] C. Lässig *et al.*, 'ATP hydrolysis by the viral RNA sensor RIG-I prevents unintentional recognition of self-RNA', *eLife*, vol. 4, Nov. 2015.

[26] S. Cui *et al.*, 'The C-terminal regulatory domain is the RNA 5'-triphosphate sensor of RIG-I', *Mol. Cell*, vol. 29, no. 2, pp. 169–179, Feb. 2008.

[27] M. Yoneyama *et al.*, 'Shared and unique functions of the DExD/H-box helicases RIG-I, MDA5, and LGP2 in antiviral innate immunity', *J. Immunol. Baltim. Md 1950*, vol. 175, no. 5, pp. 2851–2858, Sep. 2005.
[28] D. Kang, R. V. Gopalkrishnan, Q. Wu, E. Jankowsky, A. M. Pyle, and P. B. Fisher, 'mda-5: An interferon-inducible putative RNA helicase with double-stranded RNA-dependent ATPase activity and melanoma growth-suppressive properties', *Proc. Natl. Acad. Sci. U. S. A.*, vol. 99, no. 2, pp. 637–642, Jan. 2002.
[29] J. S. Yount, T. M. Moran, and C. B. López, 'Cytokine-independent upregulation of MDA5 in viral infection', *J. Virol.*, vol. 81, no. 13, pp. 7316–7319, Jul. 2007.
[30] J. S. Yount, L. Gitlin, T. M. Moran, and C. B. López, 'MDA5 participates in the detection of paramyxovirus infection and is essential for the early activation of dendritic cells in response to Sendai Virus defective interfering particles', *J. Immunol. Baltim. Md 1950*, vol. 180, no. 7, pp. 4910–4918, Apr. 2008.
[31] Q. Feng *et al.*, 'MDA5 detects the double-stranded RNA replicative form in picornavirus-infected cells', *Cell Rep.*, vol. 2, no. 5, pp. 1187–1196, Nov. 2012.
[32] L. Gitlin *et al.*, 'Essential role of mda-5 in type I IFN responses to polyriboinosinic:polyribocytidylic acid and encephalomyocarditis picornavirus', *Proc. Natl. Acad. Sci. U. S. A.*, vol. 103, no. 22, pp. 8459–8464, May 2006.
[33] N. Grandvaux *et al.*, 'Sustained activation of interferon regulatory factor 3 during infection by paramyxoviruses requires MDA5', *J. Innate Immun.*, vol. 6, no. 5, pp. 650–662, Aug. 2014.
[34] A. Peisley *et al.*, 'Cooperative assembly and dynamic disassembly of MDA5 filaments for viral dsRNA recognition', *Proc. Natl. Acad. Sci. U. S. A.*, vol. 108, no. 52, pp. 21010–21015, Dec. 2011.
[35] I. C. Berke and Y. Modis, 'MDA5 cooperatively forms dimers and ATP-sensitive filaments upon binding double-stranded RNA', *EMBO J.*, vol. 31, no. 7, pp. 1714–1726, Apr. 2012.
[36] B. Wu *et al.*, 'Structural Basis for dsRNA Recognition, Filament Formation, and Antiviral Signal Activation by MDA5', *Cell*, vol. 152, no. 1–2, pp. 276–289, Jan. 2013.
[37] K. Takahasi *et al.*, 'Solution structures of cytosolic RNA sensor MDA5 and LGP2 C-terminal domains: identification of the RNA recognition loop in RIG-I-like receptors', *J. Biol. Chem.*, vol. 284, no. 26, pp. 17465–17474, Jun. 2009.
[38] K. Malathi, B. Dong, M. Gale, and R. H. Silverman, 'Small self-RNA generated by RNase L amplifies antiviral innate immunity', *Nature*, vol. 448, no. 7155, pp. 816–819, Aug. 2007.
[39] X. Li *et al.*, 'The RIG-I-like receptor LGP2 recognizes the termini of double-stranded RNA', *J. Biol. Chem.*, vol. 284, no. 20, pp. 13881–13891, May 2009.
[40] D. A. Pippig *et al.*, 'The regulatory domain of the RIG-I family ATPase LGP2 senses double-stranded RNA', *Nucleic Acids Res.*, vol. 37, no. 6, pp. 2014–2025, Apr. 2009.
[41] S. Rothenfusser *et al.*, 'The RNA helicase Lgp2 inhibits TLR-independent sensing of viral replication by retinoic acid-inducible gene-I', *J. Immunol. Baltim. Md 1950*, vol. 175, no. 8, pp. 5260–5268, Oct. 2005.
[42] T. Saito *et al.*, 'Regulation of innate antiviral defenses through a shared repressor domain in RIG-I and LGP2', *Proc. Natl. Acad. Sci. U. S. A.*, vol. 104, no. 2, pp. 582–587, Jan. 2007.
[43] T. Venkataraman *et al.*, 'Loss of DExD/H box RNA helicase LGP2 manifests disparate antiviral responses', *J. Immunol. Baltim. Md 1950*, vol. 178, no. 10, pp. 6444–6455, May 2007.
[44] T. Satoh *et al.*, 'LGP2 is a positive regulator of RIG-I- and MDA5-mediated antiviral responses', *Proc. Natl. Acad. Sci. U. S. A.*, vol. 107, no. 4, pp. 1512–1517, Jan. 2010.
[45] J.-P. Parisien *et al.*, 'A shared interface mediates paramyxovirus interference with antiviral RNA helicases MDA5 and LGP2', *J. Virol.*, vol. 83, no. 14, pp. 7252–7260, Jul. 2009.
[46] K. R. Rodriguez and C. M. Horvath, 'Paramyxovirus V protein interaction with the antiviral sensor LGP2 disrupts MDA5 signaling enhancement but is not relevant to LGP2-mediated RLR signaling inhibition', *J. Virol.*, vol. 88, no. 14, pp. 8180–8188, Jul. 2014.
[47] A. M. Bruns, G. P. Leser, R. A. Lamb, and C. M. Horvath, 'The innate immune sensor LGP2 activates antiviral signaling by regulating MDA5-RNA interaction and filament assembly', *Mol. Cell*, vol. 55, no. 5, pp. 771–781, Sep. 2014.
[48] E. Dixit *et al.*, 'Peroxisomes are signaling platforms for antiviral innate immunity', *Cell*, vol. 141, no. 4, pp. 668–681, May 2010.
[49] S. Bender, A. Reuter, F. Eberle, E. Einhorn, M. Binder, and R. Bartenschlager, 'Activation of Type I and III Interferon Response by Mitochondrial and Peroxisomal MAVS and Inhibition by Hepatitis C Virus', *PLoS Pathog.*, vol. 11, no. 11, p. e1005264, Nov. 2015.
[50] F. Hou, L. Sun, H. Zheng, B. Skaug, Q.-X. Jiang, and Z. J. Chen, 'MAVS forms functional prion-like aggregates to activate and propagate antiviral innate immune response', *Cell*, vol. 146, no. 3, pp. 448–461, Aug. 2011.
[51] H. Xu *et al.*, 'Structural basis for the prion-like MAVS filaments in antiviral innate immunity', *eLife*, vol. 3, p. e01489, Jan. 2014.
[52] B. Liu *et al.*, 'The ubiquitin E3 ligase TRIM31 promotes aggregation and activation of the signaling adaptor MAVS through Lys63-linked polyubiquitination', *Nat. Immunol.*, vol. 18, no. 2, pp. 214–224, Feb. 2017.
[53] S. K. Saha *et al.*, 'Regulation of antiviral responses by a direct and specific interaction between TRAF3 and Cardif', *EMBO J.*, vol. 25, no. 14, pp. 3257–3263, Jul. 2006.

[54] G. Oganesyan *et al.*, 'Critical role of TRAF3 in the Toll-like receptor-dependent and -independent antiviral response', *Nature*, vol. 439, no. 7073, pp. 208–211, Jan. 2006.
[55] R. Yoshida *et al.*, 'TRAF6 and MEKK1 play a pivotal role in the RIG-I-like helicase antiviral pathway', *J. Biol. Chem.*, vol. 283, no. 52, pp. 36211–36220, Dec. 2008.
[56] J. Ninomiya-Tsuji, K. Kishimoto, A. Hiyama, J. Inoue, Z. Cao, and K. Matsumoto, 'The kinase TAK1 can activate the NIK-I kappaB as well as the MAP kinase cascade in the IL-1 signalling pathway', *Nature*, vol. 398, no. 6724, pp. 252–256, Mar. 1999.
[57] N. Grandvaux *et al.*, 'Transcriptional profiling of interferon regulatory factor 3 target genes: direct involvement in the regulation of interferon-stimulated genes', *J. Virol.*, vol. 76, no. 11, pp. 5532–5539, Jun. 2002.
[58] K. Honda and T. Taniguchi, 'IRFs: master regulators of signalling by Toll-like receptors and cytosolic pattern-recognition receptors', *Nat. Rev. Immunol.*, vol. 6, no. 9, pp. 644–658, Sep. 2006.
[59] A. Isaacs and J. Lindenmann, 'Virus interference. I. The interferon', *Proc. R. Soc. Lond. B Biol. Sci.*, vol. 147, no. 927, pp. 258–267, Sep. 1957.
[60] F. W. Bazer, T. E. Spencer, and T. L. Ott, 'Interferon tau: a novel pregnancy recognition signal', *Am. J. Reprod. Immunol. N. Y. N 1989*, vol. 37, no. 6, pp. 412–420, Jun. 1997.
[61] R. M. Roberts, 'Conceptus interferons and maternal recognition of pregnancy', *Biol. Reprod.*, vol. 40, no. 3, pp. 449–452, Mar. 1989.
[62] A. J. Sadler and B. R. G. Williams, 'Interferon-inducible antiviral effectors', *Nat. Rev. Immunol.*, vol. 8, no. 7, pp. 559–568, Jul. 2008.
[63] L. F. Stancato, M. David, C. Carter-Su, A. C. Larner, and W. B. Pratt, 'Preassociation of STAT1 with STAT2 and STAT3 in separate signalling complexes prior to cytokine stimulation', *J. Biol. Chem.*, vol. 271, no. 8, pp. 4134–4137, Feb. 1996.
[64] D. E. Levy, D. S. Kessler, R. Pine, N. Reich, and J. E. Darnell, 'Interferon-induced nuclear factors that bind a shared promoter element correlate with positive and negative transcriptional control', *Genes Dev.*, vol. 2, no. 4, pp. 383–393, Apr. 1988.
[65] X. Tang *et al.*, 'Acetylation-dependent signal transduction for type I interferon receptor', *Cell*, vol. 131, no. 1, pp. 93–105, Oct. 2007.
[66] M. R. S. Rani and R. M. Ransohoff, 'Alternative and accessory pathways in the regulation of IFN-beta-mediated gene expression', *J. Interferon Cytokine Res. Off. J. Int. Soc. Interferon Cytokine Res.*, vol. 25, no. 12, pp. 788–798, Dec. 2005.
[67] R. E. Randall and S. Goodbourn, 'Interferons and viruses: an interplay between induction, signalling, antiviral responses and virus countermeasures', *J. Gen. Virol.*, vol. 89, no. 1, pp. 1–47, Jan. 2008.
[68] J. E. Pulverer *et al.*, 'Temporal and spatial resolution of type I and III interferon responses in vivo', *J. Virol.*, vol. 84, no. 17, pp. 8626–8638, Sep. 2010.
[69] S. G. Maher *et al.*, 'IFNalpha and IFNlambda differ in their antiproliferative effects and duration of JAK/STAT signaling activity', *Cancer Biol. Ther.*, vol. 7, no. 7, pp. 1109–1115, Jul. 2008.
[70] P. Sheppard *et al.*, 'IL-28, IL-29 and their class II cytokine receptor IL-28R', *Nat. Immunol.*, vol. 4, no. 1, pp. 63–68, Jan. 2003.
[71] S. V. Kotenko *et al.*, 'IFN-lambdas mediate antiviral protection through a distinct class II cytokine receptor complex', *Nat. Immunol.*, vol. 4, no. 1, pp. 69–77, Jan. 2003.
[72] C. Odendall *et al.*, 'Diverse intracellular pathogens activate Type III Interferon expression from peroxisomes', *Nat. Immunol.*, vol. 15, no. 8, pp. 717–726, Aug. 2014.
[73] L. Dumoutier, D. Lejeune, S. Hor, H. Fickenscher, and J.-C. Renauld, 'Cloning of a new type II cytokine receptor activating signal transducer and activator of transcription (STAT)1, STAT2 and STAT3', *Biochem. J.*, vol. 370, no. Pt 2, pp. 391–396, Mar. 2003.
[74] S. V. Kotenko and J. E. Durbin, 'Contribution of type III interferons to antiviral immunity: location, location, location', *J. Biol. Chem.*, vol. 292, no. 18, pp. 7295–7303, May 2017.
[75] H. M. Lazear, T. J. Nice, and M. S. Diamond, 'Interferon-λ: Immune Functions at Barrier Surfaces and Beyond', *Immunity*, vol. 43, no. 1, pp. 15–28, Jul. 2015.
[76] M. Mordstein *et al.*, 'Lambda interferon renders epithelial cells of the respiratory and gastrointestinal tracts resistant to viral infections', *J. Virol.*, vol. 84, no. 11, pp. 5670–5677, Jun. 2010.
[77] M. Mordstein *et al.*, 'Interferon-lambda contributes to innate immunity of mice against influenza A virus but not against hepatotropic viruses', *PLoS Pathog.*, vol. 4, no. 9, p. e1000151, Sep. 2008.
[78] B. Liu, S. Chen, Y. Guan, and L. Chen, 'Type III Interferon Induces Distinct SOCS1 Expression Pattern that Contributes to Delayed but Prolonged Activation of Jak/STAT Signaling Pathway: Implications for Treatment Non-Response in HCV Patients', *PloS One*, vol. 10, no. 7, p. e0133800, Jul. 2015.
[79] V. François-Newton *et al.*, 'USP18-based negative feedback control is induced by type I and type III interferons and specifically inactivates interferon α response', *PloS One*, vol. 6, no. 7, p. e22200, Jul. 2011.
[80] O. Haller, H. Arnheiter, J. Lindenmann, and I. Gresser, 'Host gene influences sensitivity to interferon action selectively for influenza virus', *Nature*, vol. 283, no. 5748, pp. 660–662, Feb. 1980.
[81] Z. Liu *et al.*, 'The interferon-inducible MxB protein inhibits HIV-1 infection', *Cell Host Microbe*, vol. 14, no. 4, pp. 398–410, Oct. 2013.
[82] G. Kochs and O. Haller, 'Interferon-induced human MxA GTPase blocks nuclear import of Thogoto virus nucleocapsids', *Proc. Natl. Acad. Sci. U. S. A.*, vol. 96, no. 5, pp. 2082–2086, Mar. 1999.

[83] S. Stertz *et al.*, 'Interferon-induced, antiviral human MxA protein localizes to a distinct subcompartment of the smooth endoplasmic reticulum', *J. Interferon Cytokine Res. Off. J. Int. Soc. Interferon Cytokine Res.*, vol. 26, no. 9, pp. 650–660, Sep. 2006.
[84] K. Turan, M. Mibayashi, K. Sugiyama, S. Saito, A. Numajiri, and K. Nagata, 'Nuclear MxA proteins form a complex with influenza virus NP and inhibit the transcription of the engineered influenza virus genome', *Nucleic Acids Res.*, vol. 32, no. 2, pp. 643–652, Jan. 2004.
[85] A. Hoenen, W. Liu, G. Kochs, A. A. Khromykh, and J. M. Mackenzie, 'West Nile virus-induced cytoplasmic membrane structures provide partial protection against the interferon-induced antiviral MxA protein', *J. Gen. Virol.*, vol. 88, no. Pt 11, pp. 3013–3017, Nov. 2007.
[86] M. Fernández, J. A. Quiroga, and V. Carreño, 'Hepatitis B virus downregulates the human interferon-inducible MxA promoter through direct interaction of precore/core proteins', *J. Gen. Virol.*, vol. 84, no. Pt 8, pp. 2073–2082, Aug. 2003.
[87] K. R. Loeb and A. L. Haas, 'The interferon-inducible 15-kDa ubiquitin homolog conjugates to intracellular proteins', *J. Biol. Chem.*, vol. 267, no. 11, pp. 7806–7813, Apr. 1992.
[88] D. Zhang and D.-E. Zhang, 'Interferon-stimulated gene 15 and the protein ISGylation system', *J. Interferon Cytokine Res. Off. J. Int. Soc. Interferon Cytokine Res.*, vol. 31, no. 1, pp. 119–130, Jan. 2011.
[89] M. P. Malakhov, O. A. Malakhova, K. I. Kim, K. J. Ritchie, and D.-E. Zhang, 'UBP43 (USP18) specifically removes ISG15 from conjugated proteins', *J. Biol. Chem.*, vol. 277, no. 12, pp. 9976–9981, Mar. 2002.
[90] G. Lu *et al.*, 'ISG15 enhances the innate antiviral response by inhibition of IRF-3 degradation', *Cell. Mol. Biol. Noisy--Gd. Fr.*, vol. 52, no. 1, pp. 29–41, May 2006.
[91] K.-I. Arimoto, H. Konishi, and K. Shimotohno, 'UbcH8 regulates ubiquitin and ISG15 conjugation to RIG-I', *Mol. Immunol.*, vol. 45, no. 4, pp. 1078–1084, Feb. 2008.
[92] J. D'Cunha, S. Ramanujam, R. J. Wagner, P. L. Witt, E. Knight, and E. C. Borden, 'In vitro and in vivo secretion of human ISG15, an IFN-induced immunomodulatory cytokine', *J. Immunol. Baltim. Md 1950*, vol. 157, no. 9, pp. 4100–4108, Nov. 1996.
[93] W. Yuan and R. M. Krug, 'Influenza B virus NS1 protein inhibits conjugation of the interferon (IFN)-induced ubiquitin-like ISG15 protein', *EMBO J.*, vol. 20, no. 3, pp. 362–371, Feb. 2001.
[94] H. A. Lindner, V. Lytvyn, H. Qi, P. Lachance, E. Ziomek, and R. Ménard, 'Selectivity in ISG15 and ubiquitin recognition by the SARS coronavirus papain-like protease', *Arch. Biochem. Biophys.*, vol. 466, no. 1, pp. 8–14, Oct. 2007.
[95] E. Meurs *et al.*, 'Molecular cloning and characterization of the human double-stranded RNA-activated protein kinase induced by interferon', *Cell*, vol. 62, no. 2, pp. 379–390, Jul. 1990.
[96] E. Slattery, N. Ghosh, H. Samanta, and P. Lengyel, 'Interferon, double-stranded RNA, and RNA degradation: activation of an endonuclease by (2'-5')An', *Proc. Natl. Acad. Sci. U. S. A.*, vol. 76, no. 10, pp. 4778–4782, Oct. 1979.
[97] M. H. Skiadopoulos *et al.*, 'Sendai Virus, a Murine Parainfluenza Virus Type 1, Replicates to a Level Similar to Human PIV1 in the Upper and Lower Respiratory Tract of African Green Monkeys and Chimpanzees', *Virology*, vol. 297, no. 1, pp. 153–160, Mai 2002.
[98] Y. Kimura *et al.*, 'Protection of mice against virulent virus infection by a temperature-sensitive mutant derived from an HVJ (Sendai virus) carrier culture', *Arch. Virol.*, vol. 61, no. 4, pp. 297–304, May 1979.
[99] D. Kolakofsky, 'Isolation and characterization of Sendai virus DI-RNAs', *Cell*, vol. 8, no. 4, pp. 547–555, Aug. 1976.
[100] M. Leppert and D. Kolakofsky, '5' Terminus of defective and nondefective Sendai viral genomes is ppp Ap', *J. Virol.*, vol. 25, no. 1, pp. 427–432, Jan. 1978.
[101] M. D. Johnston, 'The characteristics required for a Sendai virus preparation to induce high levels of interferon in human lymphoblastoid cells', *J. Gen. Virol.*, vol. 56, no. Pt 1, pp. 175–184, Sep. 1981.
[102] B. H. Bird, T. G. Ksiazek, S. T. Nichol, and N. J. Maclachlan, 'Rift Valley fever virus', *J. Am. Vet. Med. Assoc.*, vol. 234, no. 7, pp. 883–893, Apr. 2009.
[103] M. Weber *et al.*, 'Incoming RNA virus nucleocapsids containing a 5'-triphosphorylated genome activate RIG-I and antiviral signaling', *Cell Host Microbe*, vol. 13, no. 3, pp. 336–346, Mar. 2013.
[104] M. Habjan *et al.*, 'Processing of genome 5' termini as a strategy of negative-strand RNA viruses to avoid RIG-I-dependent interferon induction', *PloS One*, vol. 3, no. 4, p. e2032, Apr. 2008.
[105] G. Lorenzo *et al.*, 'Protection against Rift Valley fever virus infection in mice upon administration of interferon-inducing RNA transcripts from the FMDV genome', *Antiviral Res.*, vol. 109, pp. 64–67, Sep. 2014.
[106] M. Bouloy *et al.*, 'Genetic evidence for an interferon-antagonistic function of rift valley fever virus nonstructural protein NSs', *J. Virol.*, vol. 75, no. 3, pp. 1371–1377, Feb. 2001.
[107] N. Le May, S. Dubaele, L. Proietti De Santis, A. Billecocq, M. Bouloy, and J.-M. Egly, 'TFIIH transcription factor, a target for the Rift Valley hemorrhagic fever virus', *Cell*, vol. 116, no. 4, pp. 541–550, Feb. 2004.
[108] M. Habjan *et al.*, 'NSs protein of rift valley fever virus induces the specific degradation of the double-stranded RNA-dependent protein kinase', *J. Virol.*, vol. 83, no. 9, pp. 4365–4375, May 2009.
[109] T. Kuri, M. Habjan, N. Penski, and F. Weber, 'Species-independent bioassay for sensitive quantification of antiviral type I interferons', *Virol. J.*, vol. 7, p. 50, Feb. 2010.

[110] R. J. Webby and M. R. Sandbulte, 'Influenza vaccines', *Front. Biosci. J. Virtual Libr.*, vol. 13, pp. 4912–4924, May 2008.
[111] G. Liu, H.-S. Park, H.-M. Pyo, Q. Liu, and Y. Zhou, 'Influenza A Virus Panhandle Structure Is Directly Involved in RIG-I Activation and Interferon Induction', *J. Virol.*, vol. 89, no. 11, pp. 6067–6079, Jun. 2015.
[112] W. G. Davis *et al.*, 'The 3' untranslated regions of influenza genomic sequences are 5'PPP-independent ligands for RIG-I', *PloS One*, vol. 7, no. 3, p. e32661, Mar. 2012.
[113] M. U. Gack *et al.*, 'Influenza A virus NS1 targets the ubiquitin ligase TRIM25 to evade recognition by the host viral RNA sensor RIG-I', *Cell Host Microbe*, vol. 5, no. 5, pp. 439–449, May 2009.
[114] D. Marc, 'Influenza virus non-structural protein NS1: interferon antagonism and beyond', *J. Gen. Virol.*, vol. 95, no. Pt 12, pp. 2594–2611, Dec. 2014.
[115] P. W. Choppin, 'Replication of influenza virus in a continuous cell line: high yield of infective virus from cells inoculated at high multiplicity', *Virology*, vol. 39, no. 1, pp. 130–134, Sep. 1969.
[116] M. H. Heim and R. Thimme, 'Innate and adaptive immune responses in HCV infections', *J. Hepatol.*, vol. 61, no. 1 Suppl, pp. S14-25, Nov. 2014.
[117] X. Cao *et al.*, 'MDA5 plays a critical role in interferon response during hepatitis C virus infection', *J. Hepatol.*, vol. 62, no. 4, pp. 771–778, Apr. 2015.
[118] X.-D. Li, L. Sun, R. B. Seth, G. Pineda, and Z. J. Chen, 'Hepatitis C virus protease NS3/4A cleaves mitochondrial antiviral signaling protein off the mitochondria to evade innate immunity', *Proc. Natl. Acad. Sci. U. S. A.*, vol. 102, no. 49, pp. 17717–17722, Dec. 2005.
[119] G. Koutsoudakis *et al.*, 'Characterization of the early steps of hepatitis C virus infection by using luciferase reporter viruses', *J. Virol.*, vol. 80, no. 11, pp. 5308–5320, Jun. 2006.
[120] C. M. Pickart, 'Targeting of substrates to the 26S proteasome', *FASEB J. Off. Publ. Fed. Am. Soc. Exp. Biol.*, vol. 11, no. 13, pp. 1055–1066, Nov. 1997.
[121] B. Liu *et al.*, 'The ubiquitin E3 ligase TRIM31 promotes aggregation and activation of the signaling adaptor MAVS through Lys63-linked polyubiquitination', *Nat. Immunol.*, vol. 18, no. 2, pp. 214–224, Feb. 2017.
[122] M. U. Gack *et al.*, 'TRIM25 RING-finger E3 ubiquitin ligase is essential for RIG-I-mediated antiviral activity', *Nature*, vol. 446, no. 7138, pp. 916–920, Apr. 2007.
[123] H. Oshiumi, M. Matsumoto, S. Hatakeyama, and T. Seya, 'Riplet/RNF135, a RING finger protein, ubiquitinates RIG-I to promote interferon-beta induction during the early phase of viral infection', *J. Biol. Chem.*, vol. 284, no. 2, pp. 807–817, Jan. 2009.
[124] X. Lang, T. Tang, T. Jin, C. Ding, R. Zhou, and W. Jiang, 'TRIM65-catalized ubiquitination is essential for MDA5-mediated antiviral innate immunity', *J. Exp. Med.*, vol. 214, no. 2, pp. 459–473, Feb. 2017.
[125] K. Arimoto, H. Takahashi, T. Hishiki, H. Konishi, T. Fujita, and K. Shimotohno, 'Negative regulation of the RIG-I signaling by the ubiquitin ligase RNF125', *Proc. Natl. Acad. Sci. U. S. A.*, vol. 104, no. 18, pp. 7500–7505, May 2007.
[126] C. S. Friedman *et al.*, 'The tumour suppressor CYLD is a negative regulator of RIG-I-mediated antiviral response', *EMBO Rep.*, vol. 9, no. 9, pp. 930–936, Sep. 2008.
[127] J. Cui *et al.*, 'USP3 inhibits type I interferon signaling by deubiquitinating RIG-I-like receptors', *Cell Res.*, vol. 24, no. 4, pp. 400–416, Apr. 2014.
[128] E.-K. Pauli *et al.*, 'The ubiquitin-specific protease USP15 promotes RIG-I-mediated antiviral signaling by deubiquitylating TRIM25', *Sci. Signal.*, vol. 7, no. 307, p. ra3, Jan. 2014.
[129] H. Zhang *et al.*, 'Ubiquitin-specific Protease 15 Negatively Regulates Virus-induced Type I Interferon Signaling via Catalytically-dependent and -independent Mechanisms', *Sci. Rep.*, vol. 5, p. 11220, Jun. 2015.
[130] C. Castanier *et al.*, 'MAVS ubiquitination by the E3 ligase TRIM25 and degradation by the proteasome is involved in type I interferon production after activation of the antiviral RIG-I-like receptors', *BMC Biol.*, vol. 10, p. 44, May 2012.
[131] Y.-S. Yoo *et al.*, 'The mitochondrial ubiquitin ligase MARCH5 resolves MAVS aggregates during antiviral signalling', *Nat. Commun.*, vol. 6, p. 7910, Aug. 2015.
[132] H.-W. Chen, Y.-K. Yang, H. Xu, W.-W. Yang, Z.-H. Zhai, and D.-Y. Chen, 'Ring finger protein 166 potentiates RNA virus-induced interferon-β production via enhancing the ubiquitination of TRAF3 and TRAF6', *Sci. Rep.*, vol. 5, p. 14770, Oct. 2015.
[133] P.-H. Tseng, A. Matsuzawa, W. Zhang, T. Mino, D. A. A. Vignali, and M. Karin, 'Different modes of ubiquitination of the adaptor TRAF3 selectively activate the expression of type I interferons and proinflammatory cytokines', *Nat. Immunol.*, vol. 11, no. 1, pp. 70–75, Jan. 2010.
[134] A.-P. Mao *et al.*, 'Virus-triggered ubiquitination of TRAF3/6 by cIAP1/2 is essential for induction of interferon-beta (IFN-beta) and cellular antiviral response', *J. Biol. Chem.*, vol. 285, no. 13, pp. 9470–9476, Mar. 2010.
[135] S. Li, L. Wang, M. Berman, Y.-Y. Kong, and M. E. Dorf, 'Mapping a dynamic innate immunity protein interaction network regulating type I interferon production', *Immunity*, vol. 35, no. 3, pp. 426–440, Sep. 2011.
[136] T. Saitoh *et al.*, 'Negative regulation of interferon-regulatory factor 3-dependent innate antiviral response by the prolyl isomerase Pin1', *Nat. Immunol.*, vol. 7, no. 6, pp. 598–605, Jun. 2006.

[137] P. Wang, W. Zhao, K. Zhao, L. Zhang, and C. Gao, 'TRIM26 negatively regulates interferon-β production and antiviral response through polyubiquitination and degradation of nuclear IRF3', *PLoS Pathog.*, vol. 11, no. 3, p. e1004726, Mar. 2015.
[138] R. Higgs, J. Ní Gabhann, N. Ben Larbi, E. P. Breen, K. A. Fitzgerald, and C. A. Jefferies, 'The E3 ubiquitin ligase Ro52 negatively regulates IFN-beta production post-pathogen recognition by polyubiquitin-mediated degradation of IRF3', *J. Immunol. Baltim. Md 1950*, vol. 181, no. 3, pp. 1780–1786, Aug. 2008.
[139] K. Yang *et al.*, 'TRIM21 is essential to sustain IFN regulatory factor 3 activation during antiviral response', *J. Immunol. Baltim. Md 1950*, vol. 182, no. 6, pp. 3782–3792, Mar. 2009.
[140] R. Higgs *et al.*, 'Self protection from anti-viral responses--Ro52 promotes degradation of the transcription factor IRF7 downstream of the viral Toll-Like receptors', *PloS One*, vol. 5, no. 7, p. e11776, Jul. 2010.
[141] H.-X. Shi *et al.*, 'Positive regulation of interferon regulatory factor 3 activation by Herc5 via ISG15 modification', *Mol. Cell. Biol.*, vol. 30, no. 10, pp. 2424–2436, May 2010.
[142] S. M. Heaton, N. A. Borg, and V. M. Dixit, 'Ubiquitin in the activation and attenuation of innate antiviral immunity', *J. Exp. Med.*, vol. 213, no. 1, pp. 1–13, Jan. 2016.
[143] G. Manning, D. B. Whyte, R. Martinez, T. Hunter, and S. Sudarsanam, 'The Protein Kinase Complement of the Human Genome', *Science*, vol. 298, no. 5600, pp. 1912–1934, Dec. 2002.
[144] E. Wies *et al.*, 'Dephosphorylation of the RNA sensors RIG-I and MDA5 by the phosphatase PP1 is essential for innate immune signaling', *Immunity*, vol. 38, no. 3, pp. 437–449, Mar. 2013.
[145] N. P. Maharaj, E. Wies, A. Stoll, and M. U. Gack, 'Conventional protein kinase C-α (PKC-α) and PKC-β negatively regulate RIG-I antiviral signal transduction', *J. Virol.*, vol. 86, no. 3, pp. 1358–1371, Feb. 2012.
[146] Z. Sun, H. Ren, Y. Liu, J. L. Teeling, and J. Gu, 'Phosphorylation of RIG-I by Casein Kinase II Inhibits Its Antiviral Response', *J. Virol.*, vol. 85, no. 2, pp. 1036–1047, Jan. 2011.
[147] K. Takashima, H. Oshiumi, H. Takaki, M. Matsumoto, and T. Seya, 'RIOK3-mediated phosphorylation of MDA5 interferes with its assembly and attenuates the innate immune response', *Cell Rep.*, vol. 11, no. 2, pp. 192–200, Apr. 2015.
[148] S. Liu *et al.*, 'Phosphorylation of innate immune adaptor proteins MAVS, STING, and TRIF induces IRF3 activation', *Science*, vol. 347, no. 6227, p. aaa2630, Mar. 2015.
[149] C. Wen *et al.*, 'Identification of Tyrosine-9 of MAVS as Critical Target for Inducible Phosphorylation That Determines Activation', *PLOS ONE*, vol. 7, no. 7, p. e41687, Jul. 2012.
[150] D. Vitour *et al.*, 'Polo-like Kinase 1 (PLK1) Regulates Interferon (IFN) Induction by MAVS', *J. Biol. Chem.*, vol. 284, no. 33, pp. 21797–21809, Aug. 2009.
[151] Y. Zhou *et al.*, 'The kinase CK1ε controls the antiviral immune response by phosphorylating the signaling adaptor TRAF3', *Nat. Immunol.*, vol. 17, no. 4, pp. 397–405, Apr. 2016.
[152] S. Jiao *et al.*, 'The kinase MST4 limits inflammatory responses through direct phosphorylation of the adaptor TRAF6', *Nat. Immunol.*, vol. 16, no. 3, pp. 246–257, Mar. 2015.
[153] X. Ma *et al.*, 'Molecular basis of Tank-binding kinase 1 activation by transautophosphorylation', *Proc. Natl. Acad. Sci. U. S. A.*, vol. 109, no. 24, pp. 9378–9383, Jun. 2012.
[154] C.-Q. Lei, B. Zhong, Y. Zhang, J. Zhang, S. Wang, and H.-B. Shu, 'Glycogen synthase kinase 3β regulates IRF3 transcription factor-mediated antiviral response via activation of the kinase TBK1', *Immunity*, vol. 33, no. 6, pp. 878–889, Dec. 2010.
[155] X. Li *et al.*, 'The tyrosine kinase Src promotes phosphorylation of the kinase TBK1 to facilitate type I interferon production after viral infection', *Sci Signal*, vol. 10, no. 460, p. eaae0435, Jan. 2017.
[156] Y. Zhao *et al.*, 'PPM1B negatively regulates antiviral response via dephosphorylating TBK1', *Cell. Signal.*, vol. 24, no. 11, pp. 2197–2204, Nov. 2012.
[157] T. Shimada *et al.*, 'IKK-i, a novel lipopolysaccharide-inducible kinase that is related to IkappaB kinases', *Int. Immunol.*, vol. 11, no. 8, pp. 1357–1362, Aug. 1999.
[158] L. Long *et al.*, 'Recruitment of phosphatase PP2A by RACK1 adaptor protein deactivates transcription factor IRF3 and limits type I interferon signaling', *Immunity*, vol. 40, no. 4, pp. 515–529, Apr. 2014.
[159] G. Shohat *et al.*, 'The pro-apoptotic function of death-associated protein kinase is controlled by a unique inhibitory autophosphorylation-based mechanism', *J. Biol. Chem.*, vol. 276, no. 50, pp. 47460–47467, Dec. 2001.
[160] G. Shani *et al.*, 'Autophosphorylation restrains the apoptotic activity of DRP-1 kinase by controlling dimerization and calmodulin binding', *EMBO J.*, vol. 20, no. 5, pp. 1099–1113, Mar. 2001.
[161] T. Kawai *et al.*, 'Death-associated protein kinase 2 is a new calcium/calmodulin-dependent protein kinase that signals apoptosis through its catalytic activity', *Oncogene*, vol. 18, no. 23, pp. 3471–3480, Jun. 1999.
[162] J. Brognard, Y.-W. Zhang, L. A. Puto, and T. Hunter, 'Cancer-associated loss-of-function mutations implicate DAPK3 as a tumor-suppressing kinase', *Cancer Res.*, vol. 71, no. 8, pp. 3152–3161, Apr. 2011.
[163] H. Sanjo, T. Kawai, and S. Akira, 'DRAKs, novel serine/threonine kinases related to death-associated protein kinase that trigger apoptosis', *J. Biol. Chem.*, vol. 273, no. 44, pp. 29066–29071, Oct. 1998.

[164] L. P. Deiss, E. Feinstein, H. Berissi, O. Cohen, and A. Kimchi, 'Identification of a novel serine/threonine kinase and a novel 15-kD protein as potential mediators of the gamma interferon-induced cell death.', *Genes Dev.*, vol. 9, no. 1, pp. 15–30, Jan. 1995.
[165] P. Gade *et al.*, 'An IFN-γ-stimulated ATF6-C/EBP-β-signaling pathway critical for the expression of Death Associated Protein Kinase 1 and induction of autophagy', *Proc. Natl. Acad. Sci. U. S. A.*, vol. 109, no. 26, pp. 10316–10321, Jun. 2012.
[166] P. Gade, S. B. Manjegowda, S. C. Nallar, U. B. Maachani, A. S. Cross, and D. V. Kalvakolanu, 'Regulation of the death-associated protein kinase 1 expression and autophagy via ATF6 requires apoptosis signal-regulating kinase 1', *Mol. Cell. Biol.*, vol. 34, no. 21, pp. 4033–4048, Nov. 2014.
[167] C.-W. Jang, C.-H. Chen, C.-C. Chen, J. Chen, Y.-H. Su, and R.-H. Chen, 'TGF-beta induces apoptosis through Smad-mediated expression of DAP-kinase', *Nat. Cell Biol.*, vol. 4, no. 1, pp. 51–58, Jan. 2002.
[168] F. Llambi *et al.*, 'The dependence receptor UNC5H2 mediates apoptosis through DAP-kinase', *EMBO J.*, vol. 24, no. 6, pp. 1192–1201, Mar. 2005.
[169] C. Guenebeaud *et al.*, 'The dependence receptor UNC5H2/B triggers apoptosis via PP2A-mediated dephosphorylation of DAP kinase', *Mol. Cell*, vol. 40, no. 6, pp. 863–876, Dec. 2010.
[170] E. Zalckvar, H. Berissi, M. Eisenstein, and A. Kimchi, 'Phosphorylation of Beclin 1 by DAP-kinase promotes autophagy by weakening its interactions with Bcl-2 and Bcl-XL', *Autophagy*, vol. 5, no. 5, pp. 720–722, Jul. 2009.
[171] E. Zalckvar *et al.*, 'DAP-kinase-mediated phosphorylation on the BH3 domain of beclin 1 promotes dissociation of beclin 1 from Bcl-XL and induction of autophagy', *EMBO Rep.*, vol. 10, no. 3, pp. 285–292, Mar. 2009.
[172] A. Eisenberg-Lerner and A. Kimchi, 'PKD is a kinase of Vps34 that mediates ROS-induced autophagy downstream of DAPk', *Cell Death Differ.*, vol. 19, no. 5, pp. 788–797, May 2012.
[173] M. Sanchez-Cespedes *et al.*, 'Gene Promoter Hypermethylation in Tumors and Serum of Head and Neck Cancer Patients', *Cancer Res.*, vol. 60, no. 4, pp. 892–895, Feb. 2000.
[174] Y. Zhu *et al.*, 'Quantitative and correlation analysis of the DNA methylation and expression of DAPK in breast cancer', *PeerJ*, vol. 5, p. e3084, Mar. 2017.
[175] S. Zöchbauer-Müller, K. M. Fong, A. K. Virmani, J. Geradts, A. F. Gazdar, and J. D. Minna, 'Aberrant Promoter Methylation of Multiple Genes in Non-Small Cell Lung Cancers', *Cancer Res.*, vol. 61, no. 1, pp. 249–255, Jan. 2001.
[176] M. Krajnović, M. Radojković, R. Davidović, B. Dimitrijević, and K. Krtolica, 'Prognostic significance of epigenetic inactivation of p16, p15, MGMT and DAPK genes in follicular lymphoma', *Med. Oncol.*, vol. 30, no. 1, pp. 1–10, Mar. 2013.
[177] T. Raveh, G. Droguett, M. S. Horwitz, R. A. DePinho, and A. Kimchi, 'DAP kinase activates a p19ARF/p53-mediated apoptotic checkpoint to suppress oncogenic transformation', *Nat. Cell Biol.*, vol. 3, no. 1, pp. 1–7, Jan. 2001.
[178] B. Inbal *et al.*, 'DAP kinase links the control of apoptosis to metastasis', *Nature*, vol. 390, no. 6656, pp. 180–184, Nov. 1997.
[179] J.-C. Kuo, W.-J. Wang, C.-C. Yao, P.-R. Wu, and R.-H. Chen, 'The tumor suppressor DAPK inhibits cell motility by blocking the integrin-mediated polarity pathway', *J. Cell Biol.*, vol. 172, no. 4, pp. 619–631, Feb. 2006.
[180] L. Pei *et al.*, 'DAPK1-p53 interaction converges necrotic and apoptotic pathways of ischemic neuronal death', *J. Neurosci. Off. J. Soc. Neurosci.*, vol. 34, no. 19, pp. 6546–6556, May 2014.
[181] W. Tu *et al.*, 'DAPK1 interaction with NMDA receptor NR2B subunits mediates brain damage in stroke', *Cell*, vol. 140, no. 2, pp. 222–234, Jan. 2010.
[182] P.-R. Wu *et al.*, 'DAPK activates MARK1/2 to regulate microtubule assembly, neuronal differentiation, and tau toxicity', *Cell Death Differ.*, vol. 18, no. 9, pp. 1507–1520, Sep. 2011.
[183] B. M. Kim *et al.*, 'Death-associated protein kinase 1 has a critical role in aberrant tau protein regulation and function', *Cell Death Dis.*, vol. 5, p. e1237, May 2014.
[184] D.-X. Duan *et al.*, 'Phosphorylation of tau by death-associated protein kinase 1 antagonizes the kinase-induced cell apoptosis', *J. Alzheimers Dis. JAD*, vol. 37, no. 4, pp. 795–808, Jun. 2013.
[185] W.-J. Wang *et al.*, 'The Tumor Suppressor DAPK Is Reciprocally Regulated by Tyrosine Kinase Src and Phosphatase LAR', *Mol. Cell*, vol. 27, no. 5, pp. 701–716, Sep. 2007.
[186] C.-H. Chen *et al.*, 'Bidirectional signals transduced by DAPK-ERK interaction promote the apoptotic effect of DAPK', *EMBO J.*, vol. 24, no. 2, pp. 294–304, Jan. 2005.
[187] C. Stevens *et al.*, 'Peptide combinatorial libraries identify TSC2 as a death-associated protein kinase (DAPK) death domain-binding protein and reveal a stimulatory role for DAPK in mTORC1 signaling', *J. Biol. Chem.*, vol. 284, no. 1, pp. 334–344, Jan. 2009.
[188] R. Anjum, P. P. Roux, B. A. Ballif, S. P. Gygi, and J. Blenis, 'The tumor suppressor DAP kinase is a target of RSK-mediated survival signaling', *Curr. Biol. CB*, vol. 15, no. 19, pp. 1762–1767, Oct. 2005.
[189] J. Zhao *et al.*, 'Death-associated protein kinase 1 promotes growth of p53-mutant cancers', *J. Clin. Invest.*, vol. 125, no. 7, pp. 2707–2720, Jul. 2015.
[190] L. Bosgraaf and P. J. M. Van Haastert, 'Roc, a Ras/GTPase domain in complex proteins', *Biochim. Biophys. Acta*, vol. 1643, no. 1–3, pp. 5–10, Dec. 2003.
[191] R. Carlessi *et al.*, 'GTP binding to the ROC domain of DAP-kinase regulates its function through intramolecular signalling', *EMBO Rep.*, vol. 12, no. 9, pp. 917–923, Sep. 2011.

[192] A. Citri *et al.*, 'Hsp90 recognizes a common surface on client kinases', *J. Biol. Chem.*, vol. 281, no. 20, pp. 14361–14369, May 2006.
[193] L. Zhang, K. P. Nephew, and P. J. Gallagher, 'Regulation of death-associated protein kinase. Stabilization by HSP90 heterocomplexes', *J. Biol. Chem.*, vol. 282, no. 16, pp. 11795–11804, Apr. 2007.
[194] Y. Jin, E. K. Blue, S. Dixon, Z. Shao, and P. J. Gallagher, 'A death-associated protein kinase (DAPK)-interacting protein, DIP-1, is an E3 ubiquitin ligase that promotes tumor necrosis factor-induced apoptosis and regulates the cellular levels of DAPK', *J. Biol. Chem.*, vol. 277, no. 49, pp. 46980–46986, Dec. 2002.
[195] Y.-R. Lee, W.-C. Yuan, H.-C. Ho, C.-H. Chen, H.-M. Shih, and R.-H. Chen, 'The Cullin 3 substrate adaptor KLHL20 mediates DAPK ubiquitination to control interferon responses', *EMBO J.*, vol. 29, no. 10, pp. 1748–1761, May 2010.
[196] Y.-T. Chuang, L.-W. Fang, M.-H. Lin-Feng, R.-H. Chen, and M.-Z. Lai, 'The tumor suppressor death-associated protein kinase targets to TCR-stimulated NF-kappa B activation', *J. Immunol. Baltim. Md 1950*, vol. 180, no. 5, pp. 3238–3249, Mar. 2008.
[197] Y.-T. Chuang *et al.*, 'Tumor suppressor death-associated protein kinase is required for full IL-1β production', *Blood*, vol. 117, no. 3, pp. 960–970, Jan. 2011.
[198] J. Zhang, M.-M. Hu, H.-B. Shu, and S. Li, 'Death-associated protein kinase 1 is an IRF3/7-interacting protein that is involved in the cellular antiviral immune response', *Cell. Mol. Immunol.*, vol. 11, no. 3, pp. 245–252, Mai 2014.
[199] J. Willemsen *et al.*, 'Phosphorylation-Dependent Feedback Inhibition of RIG-I by DAPK1 Identified by Kinome-wide siRNA Screening', *Mol. Cell*, vol. 65, no. 3, p. 403–415.e8, Feb. 2017.
[200] T. Kawai, M. Matsumoto, K. Takeda, H. Sanjo, and S. Akira, 'ZIP kinase, a novel serine/threonine kinase which mediates apoptosis', *Mol. Cell. Biol.*, vol. 18, no. 3, pp. 1642–1651, Mar. 1998.
[201] G. Shani *et al.*, 'Death-associated protein kinase phosphorylates ZIP kinase, forming a unique kinase hierarchy to activate its cell death functions', *Mol. Cell. Biol.*, vol. 24, no. 19, pp. 8611–8626, Oct. 2004.
[202] D. H. Weitzel, J. Chambers, and T. A. J. Haystead, 'Phosphorylation-dependent control of ZIPK nuclear import is species specific', *Cell. Signal.*, vol. 23, no. 1, pp. 297–303, Jan. 2011.
[203] P. R. Graves, K. M. Winkfield, and T. A. J. Haystead, 'Regulation of zipper-interacting protein kinase activity in vitro and in vivo by multisite phosphorylation', *J. Biol. Chem.*, vol. 280, no. 10, pp. 9363–9374, Mar. 2005.
[204] N. Sato *et al.*, 'Phosphorylation of threonine-265 in Zipper-interacting protein kinase plays an important role in its activity and is induced by IL-6 family cytokines', *Immunol. Lett.*, vol. 103, no. 2, pp. 127–134, Mar. 2006.
[205] L. R. Burch, M. Scott, E. Pohler, D. Meek, and T. Hupp, 'Phage-peptide display identifies the interferon-responsive, death-activated protein kinase family as a novel modifier of MDM2 and p21WAF1', *J. Mol. Biol.*, vol. 337, no. 1, pp. 115–128, Mar. 2004.
[206] D. Kögel *et al.*, 'Dlk/ZIP kinase-induced apoptosis in human medulloblastoma cells: requirement of the mitochondrial apoptosis pathway', *Br. J. Cancer*, vol. 85, no. 11, pp. 1801–1808, Nov. 2001.
[207] H.-W. Tang, Y.-B. Wang, S.-L. Wang, M.-H. Wu, S.-Y. Lin, and G.-C. Chen, 'Atg1-mediated myosin II activation regulates autophagosome formation during starvation-induced autophagy', *EMBO J.*, vol. 30, no. 4, pp. 636–651, Feb. 2011.
[208] N. Fujiwara, T. Usui, T. Ohama, and K. Sato, 'Regulation of Beclin 1 Protein Phosphorylation and Autophagy by Protein Phosphatase 2A (PP2A) and Death-associated Protein Kinase 3 (DAPK3)', *J. Biol. Chem.*, vol. 291, no. 20, pp. 10858–10866, May 2016.
[209] U. Preuss, H. Bierbaum, P. Buchenau, and K. H. Scheidtmann, 'DAP-like kinase, a member of the death-associated protein kinase family, associates with centrosomes, centromers, and the contractile ring during mitosis', *Eur. J. Cell Biol.*, vol. 82, no. 9, pp. 447–459, Sep. 2003.
[210] W. Wu *et al.*, 'Zipper-interacting protein kinase interacts with human cell division cycle 14A phosphatase', *Mol. Med. Rep.*, vol. 11, no. 4, pp. 2775–2780, Apr. 2015.
[211] T. Agarwal, N. Annamalai, T. K. Maiti, and H. Arsad, 'Biophysical changes of ATP binding pocket may explain loss of kinase activity in mutant DAPK3 in cancer: A molecular dynamic simulation analysis', *Gene*, vol. 580, no. 1, pp. 17–25, Apr. 2016.
[212] T. P. Das *et al.*, 'Activation of AKT negatively regulates the pro-apoptotic function of death-associated protein kinase 3 (DAPK3) in prostate cancer', *Cancer Lett.*, vol. 377, no. 2, pp. 134–139, Jul. 2016.
[213] L. A. Puto, J. Brognard, and T. Hunter, 'Transcriptional Repressor DAXX Promotes Prostate Cancer Tumorigenicity via Suppression of Autophagy', *J. Biol. Chem.*, vol. 290, no. 25, pp. 15406–15420, Jun. 2015.
[214] S. Kake, T. Usui, T. Ohama, H. Yamawaki, and K. Sato, 'Death-associated protein kinase 3 controls the tumor progression of A549 cells through ERK MAPK/c-Myc signaling', *Oncol. Rep.*, vol. 37, no. 2, pp. 1100–1106, Feb. 2017.
[215] T. Usui, M. Okada, Y. Hara, and H. Yamawaki, 'Death-associated protein kinase 3 mediates vascular inflammation and development of hypertension in spontaneously hypertensive rats', *Hypertens. Dallas Tex 1979*, vol. 60, no. 4, pp. 1031–1039, Oct. 2012.

[216] R. Mukhopadhyay, P. S. Ray, A. Arif, A. K. Brady, M. Kinter, and P. L. Fox, 'DAPK-ZIPK-L13a axis constitutes a negative-feedback module regulating inflammatory gene expression', *Mol. Cell*, vol. 32, no. 3, pp. 371–382, Nov. 2008.
[217] B. Inbal, G. Shani, O. Cohen, J. L. Kissil, and A. Kimchi, 'Death-associated protein kinase-related protein 1, a novel serine/threonine kinase involved in apoptosis', *Mol. Cell. Biol.*, vol. 20, no. 3, pp. 1044–1054, Feb. 2000.
[218] Y. Shoval, H. Berissi, A. Kimchi, and S. Pietrokovski, 'New modularity of DAP-kinases: alternative splicing of the DRP-1 gene produces a ZIPk-like isoform', *PloS One*, vol. 6, no. 2, p. e17344, Mar. 2011.
[219] B. Inbal, S. Bialik, I. Sabanay, G. Shani, and A. Kimchi, 'DAP kinase and DRP-1 mediate membrane blebbing and the formation of autophagic vesicles during programmed cell death', *J. Cell Biol.*, vol. 157, no. 3, pp. 455–468, Apr. 2002.
[220] M. K. Tur *et al.*, 'Targeted restoration of down-regulated DAPK2 tumor suppressor activity induces apoptosis in Hodgkin lymphoma cells', *J. Immunother. Hagerstown Md 1997*, vol. 32, no. 5, pp. 431–441, Jun. 2009.
[221] H.-C. Chi *et al.*, 'Thyroid hormone suppresses hepatocarcinogenesis via DAPK2 and SQSTM1-dependent selective autophagy', *Autophagy*, vol. 12, no. 12, pp. 2271–2285, Dec. 2016.
[222] B. Geering, C. Stoeckle, S. Rozman, K. Oberson, C. Benarafa, and H.-U. Simon, 'DAPK2 positively regulates motility of neutrophils and eosinophils in response to intermediary chemoattractants', *J. Leukoc. Biol.*, vol. 95, no. 2, pp. 293–303, Feb. 2014.
[223] H. Li, G. Ray, B. H. Yoo, M. Erdogan, and K. V. Rosen, 'Down-regulation of death-associated protein kinase-2 is required for beta-catenin-induced anoikis resistance of malignant epithelial cells', *J. Biol. Chem.*, vol. 284, no. 4, pp. 2012–2022, Jan. 2009.
[224] K. Isshiki, T. Hirase, S. Matsuda, K. Miyamoto, A. Tsuji, and K. Yuasa, 'Death-associated protein kinase 2 mediates nocodazole-induced apoptosis through interaction with tubulin', *Biochem. Biophys. Res. Commun.*, vol. 468, no. 1–2, pp. 113–118, Dec. 2015.
[225] Y. Gilad, R. Shiloh, Y. Ber, S. Bialik, and A. Kimchi, 'Discovering protein-protein interactions within the programmed cell death network using a protein-fragment complementation screen', *Cell Rep.*, vol. 8, no. 3, pp. 909–921, Aug. 2014.
[226] K. Yuasa, R. Ota, S. Matsuda, K. Isshiki, M. Inoue, and A. Tsuji, 'Suppression of death-associated protein kinase 2 by interaction with 14-3-3 proteins', *Biochem. Biophys. Res. Commun.*, vol. 464, no. 1, pp. 70–75, Aug. 2015.
[227] C. R. Schlegel *et al.*, 'DAPK2 is a novel modulator of TRAIL-induced apoptosis', *Cell Death Differ.*, vol. 21, no. 11, pp. 1780–1791, Nov. 2014.
[228] Y. Ber, R. Shiloh, Y. Gilad, N. Degani, S. Bialik, and A. Kimchi, 'DAPK2 is a novel regulator of mTORC1 activity and autophagy', *Cell Death Differ.*, vol. 22, no. 3, pp. 465–475, Mar. 2015.
[229] P. Mao *et al.*, 'Serine/threonine kinase 17A is a novel p53 target gene and modulator of cisplatin toxicity and reactive oxygen species in testicular cancer cells', *J. Biol. Chem.*, vol. 286, no. 22, pp. 19381–19391, Jun. 2011.
[230] P. Mao *et al.*, 'Serine/threonine kinase 17A is a novel candidate for therapeutic targeting in glioblastoma', *PloS One*, vol. 8, no. 11, p. e81803, Nov. 2013.
[231] Y. Park *et al.*, 'Cytoplasmic DRAK1 overexpressed in head and neck cancers inhibits TGF-β1 tumor suppressor activity by binding to Smad3 to interrupt its complex formation with Smad4', *Oncogene*, vol. 34, no. 39, pp. 5037–5045, Sep. 2015.
[232] K.-M. Yang *et al.*, 'DRAK2 participates in a negative feedback loop to control TGF-β/Smads signaling by binding to type I TGF-β receptor', *Cell Rep.*, vol. 2, no. 5, pp. 1286–1299, Nov. 2012.
[233] T. L. Harris and M. A. McGargill, 'Drak2 Does Not Regulate TGF-β Signaling in T Cells', *PLOS ONE*, vol. 10, no. 5, p. e0123650, May 2015.
[234] M. L. Friedrich *et al.*, 'Modulation of DRAK2 autophosphorylation by antigen receptor signaling in primary lymphocytes', *J. Biol. Chem.*, vol. 282, no. 7, pp. 4573–4584, Feb. 2007.
[235] R. H. Newton, S. Leverrier, S. Srikanth, Y. Gwack, M. D. Cahalan, and C. M. Walsh, 'Protein kinase D orchestrates the activation of DRAK2 in response to TCR-induced Ca2+ influx and mitochondrial reactive oxygen generation', *J. Immunol. Baltim. Md 1950*, vol. 186, no. 2, pp. 940–950, Jan. 2011.
[236] S. Wang *et al.*, 'Drak2 contributes to West Nile virus entry into the brain and lethal encephalitis', *J. Immunol. Baltim. Md 1950*, vol. 181, no. 3, pp. 2084–2091, Aug. 2008.
[237] C. S. Schaumburg, M. Gatzka, C. M. Walsh, and T. E. Lane, 'DRAK2 regulates memory T cell responses following murine coronavirus infection', *Autoimmunity*, vol. 40, no. 7, pp. 483–488, Nov. 2007.
[238] Y. Fuchs and H. Steller, 'Live to die another way: modes of programmed cell death and the signals emanating from dying cells', *Nat. Rev. Mol. Cell Biol.*, vol. 16, no. 6, pp. 329–344, Jun. 2015.
[239] C. Holohan, S. Van Schaeybroeck, D. B. Longley, and P. G. Johnston, 'Cancer drug resistance: an evolving paradigm', *Nat. Rev. Cancer*, vol. 13, no. 10, pp. 714–726, Oct. 2013.
[240] Y. A. Lazebnik, S. H. Kaufmann, S. Desnoyers, G. G. Poirier, and W. C. Earnshaw, 'Cleavage of poly(ADP-ribose) polymerase by a proteinase with properties like ICE', *Nature*, vol. 371, no. 6495, pp. 346–347, Sep. 1994.

[241] M. Tewari *et al.*, 'Yama/CPP32 beta, a mammalian homolog of CED-3, is a CrmA-inhibitable protease that cleaves the death substrate poly(ADP-ribose) polymerase', *Cell*, vol. 81, no. 5, pp. 801–809, Jun. 1995.
[242] V. Schreiber, F. Dantzer, J.-C. Ame, and G. de Murcia, 'Poly(ADP-ribose): novel functions for an old molecule', *Nat. Rev. Mol. Cell Biol.*, vol. 7, no. 7, pp. 517–528, Jul. 2006.
[243] M. Li *et al.*, 'Suppression of lysosome function induces autophagy via a feedback down-regulation of MTOR complex 1 (MTORC1) activity', *J. Biol. Chem.*, vol. 288, no. 50, pp. 35769–35780, Dec. 2013.
[244] S. Shao *et al.*, 'Spautin-1, a novel autophagy inhibitor, enhances imatinib-induced apoptosis in chronic myeloid leukemia', *Int. J. Oncol.*, vol. 44, no. 5, pp. 1661–1668, May 2014.
[245] N. Fujita, T. Itoh, H. Omori, M. Fukuda, T. Noda, and T. Yoshimori, 'The Atg16L complex specifies the site of LC3 lipidation for membrane biogenesis in autophagy', *Mol. Biol. Cell*, vol. 19, no. 5, pp. 2092–2100, May 2008.
[246] G. Mariño, M. Niso-Santano, E. H. Baehrecke, and G. Kroemer, 'Self-consumption: the interplay of autophagy and apoptosis', *Nat. Rev. Mol. Cell Biol.*, vol. 15, no. 2, pp. 81–94, Feb. 2014.
[247] J. Schindelin *et al.*, 'Fiji: an open-source platform for biological-image analysis', *Nat. Methods*, vol. 9, no. 7, pp. 676–682, Jul. 2012.
[248] M. W. Pfaffl, 'A new mathematical model for relative quantification in real-time RT–PCR', *Nucleic Acids Res.*, vol. 29, no. 9, p. e45, May 2001.
[249] J. Willemsen, 'High Throughput Screening Approach to Identify and Characterize Novel Kinases in the Antiviral RIG-I Signaling Pathway', Ruperto-Carola University of Heidelberg, Heidelberg, 2015.
[250] M. Jinek, K. Chylinski, I. Fonfara, M. Hauer, J. A. Doudna, and E. Charpentier, 'A programmable dual-RNA-guided DNA endonuclease in adaptive bacterial immunity', *Science*, vol. 337, no. 6096, pp. 816–821, Aug. 2012.
[251] G. Shohat *et al.*, 'The Pro-apoptotic Function of Death-associated Protein Kinase Is Controlled by a Unique Inhibitory Autophosphorylation-based Mechanism', *J. Biol. Chem.*, vol. 276, no. 50, pp. 47460–47467, Dec. 2001.
[252] J. Li, A. Mahajan, and M.-D. Tsai, 'Ankyrin repeat: a unique motif mediating protein-protein interactions', *Biochemistry (Mosc.)*, vol. 45, no. 51, pp. 15168–15178, Dec. 2006.
[253] S. Aland, H. Hatzikirou, J. Lowengrub, and A. Voigt, 'A Mechanistic Collective Cell Model for Epithelial Colony Growth and Contact Inhibition', *Biophys. J.*, vol. 109, no. 7, pp. 1347–1357, Oct. 2015.
[254] T. M. Caserta, A. N. Smith, A. D. Gultice, M. A. Reedy, and T. L. Brown, 'Q-VD-OPh, a broad spectrum caspase inhibitor with potent antiapoptotic properties', *Apoptosis Int. J. Program. Cell Death*, vol. 8, no. 4, pp. 345–352, Aug. 2003.
[255] S. An and K. A. Knox, 'Ligation of CD40 rescues Ramos-Burkitt lymphoma B cells from calcium ionophore- and antigen receptor-triggered apoptosis by inhibiting activation of the cysteine protease CPP32/Yama and cleavage of its substrate PARP', *FEBS Lett.*, vol. 386, no. 2–3, pp. 115–122, May 1996.
[256] T. Tamaoki, H. Nomoto, I. Takahashi, Y. Kato, M. Morimoto, and F. Tomita, 'Staurosporine, a potent inhibitor of phospholipid/Ca++dependent protein kinase', *Biochem. Biophys. Res. Commun.*, vol. 135, no. 2, pp. 397–402, Mar. 1986.
[257] H. J. Chae *et al.*, 'Molecular mechanism of staurosporine-induced apoptosis in osteoblasts', *Pharmacol. Res.*, vol. 42, no. 4, pp. 373–381, Oct. 2000.
[258] H. M. Sobell, 'Actinomycin and DNA transcription', *Proc. Natl. Acad. Sci. U. S. A.*, vol. 82, no. 16, pp. 5328–5331, Aug. 1985.
[259] R. W. Hyman and N. Davidson, 'Kinetics of the in vitro inhibition of transcription by actinomycin', *J. Mol. Biol.*, vol. 50, no. 2, pp. 421–438, Jun. 1970.
[260] B. Harrison *et al.*, 'DAPK-1 binding to a linear peptide motif in MAP1B stimulates autophagy and membrane blebbing', *J. Biol. Chem.*, vol. 283, no. 15, pp. 9999–10014, Apr. 2008.
[261] Z. Tallóczy, H. W. Virgin, and B. Levine, 'PKR-dependent autophagic degradation of herpes simplex virus type 1', *Autophagy*, vol. 2, no. 1, pp. 24–29, Mar. 2006.
[262] F. Takeshita, K. Kobiyama, A. Miyawaki, N. Jounai, and K. Okuda, 'The non-canonical role of Atg family members as suppressors of innate antiviral immune signaling', *Autophagy*, vol. 4, no. 1, pp. 67–69, Jan. 2008.
[263] M. C. Tal and A. Iwasaki, 'Autophagic control of RLR signaling', *Autophagy*, vol. 5, no. 5, pp. 749–750, Jul. 2009.
[264] C. H. Jung, S.-H. Ro, J. Cao, N. M. Otto, and D.-H. Kim, 'mTOR regulation of autophagy', *FEBS Lett.*, vol. 584, no. 7, pp. 1287–1295, Apr. 2010.
[265] G. Shohat *et al.*, 'The pro-apoptotic function of death-associated protein kinase is controlled by a unique inhibitory autophosphorylation-based mechanism', *J. Biol. Chem.*, vol. 276, no. 50, pp. 47460–47467, Dec. 2001.
[266] D. Soulat *et al.*, 'The DEAD-box helicase DDX3X is a critical component of the TANK-binding kinase 1-dependent innate immune response', *EMBO J.*, vol. 27, no. 15, pp. 2135–2146, Aug. 2008.
[267] H. Oshiumi, K. Sakai, M. Matsumoto, and T. Seya, 'DEAD/H BOX 3 (DDX3) helicase binds the RIG-I adaptor IPS-1 to up-regulate IFN-beta-inducing potential', *Eur. J. Immunol.*, vol. 40, no. 4, pp. 940–948, Apr. 2010.

[268] W.-L. Liu *et al.*, 'Pegylated IFN-α suppresses hepatitis C virus by promoting the DAPK-mTOR pathway', *Proc. Natl. Acad. Sci. U. S. A.*, vol. 113, no. 51, pp. 14799–14804, Dec. 2016.
[269] R. Thimme, M. Binder, and R. Bartenschlager, 'Failure of innate and adaptive immune responses in controlling hepatitis C virus infection', *FEMS Microbiol. Rev.*, vol. 36, no. 3, pp. 663–683, May 2012.
[270] J. Melchjorsen *et al.*, 'Activation of Innate Defense against a Paramyxovirus Is Mediated by RIG-I and TLR7 and TLR8 in a Cell-Type-Specific Manner', *J. Virol.*, vol. 79, no. 20, pp. 12944–12951, Oct. 2005.
[271] H. Kato *et al.*, 'Length-dependent recognition of double-stranded ribonucleic acids by retinoic acid-inducible gene-I and melanoma differentiation-associated gene 5', *J. Exp. Med.*, vol. 205, no. 7, pp. 1601–1610, Jul. 2008.
[272] T. Raveh, G. Droguett, M. S. Horwitz, R. A. DePinho, and A. Kimchi, 'DAP kinase activates a p19ARF/p53-mediated apoptotic checkpoint to suppress oncogenic transformation', *Nat. Cell Biol.*, vol. 3, no. 1, pp. 1–7, Jan. 2001.
[273] J. Bi *et al.*, 'Downregulation of ZIP kinase is associated with tumor invasion, metastasis and poor prognosis in gastric cancer', *Int. J. Cancer*, vol. 124, no. 7, pp. 1587–1593, Apr. 2009.
[274] N. P. Maharaj, E. Wies, A. Stoll, and M. U. Gack, 'Conventional protein kinase C-α (PKC-α) and PKC-β negatively regulate RIG-I antiviral signal transduction', *J. Virol.*, vol. 86, no. 3, pp. 1358–1371, Feb. 2012.
[275] H. Shankaran *et al.*, 'Rapid and sustained nuclear-cytoplasmic ERK oscillations induced by epidermal growth factor', *Mol. Syst. Biol.*, vol. 5, p. 332, Jan. 2009.
[276] B. Wu, H. Yao, S. Wang, and R. Xu, 'DAPK1 modulates a curcumin-induced G2/M arrest and apoptosis by regulating STAT3, NF-κB, and caspase-3 activation', *Biochem. Biophys. Res. Commun.*, vol. 434, no. 1, pp. 75–80, Apr. 2013.
[277] D. H. A. Ishak *et al.*, 'A bismuth diethyldithiocarbamate compound promotes apoptosis in HepG2 carcinoma, cell cycle arrest and inhibits cell invasion through modulation of the NF-κB activation pathway', *J. Inorg. Biochem.*, vol. 130, pp. 38–51, Jan. 2014.
[278] K. Temmerman, B. Simon, and M. Wilmanns, 'Structural and functional diversity in the activity and regulation of DAPK-related protein kinases', *FEBS J.*, vol. 280, no. 21, pp. 5533–5550, Nov. 2013.
[279] S. Bialik, A. R. Bresnick, and A. Kimchi, 'DAP-kinase-mediated morphological changes are localization dependent and involve myosin-II phosphorylation', *Cell Death Differ.*, vol. 11, no. 6, pp. 631–644, Feb. 2004.
[280] B. Geering, C. Stoeckle, S. Rozman, K. Oberson, C. Benarafa, and H.-U. Simon, 'DAPK2 positively regulates motility of neutrophils and eosinophils in response to intermediary chemoattractants', *J. Leukoc. Biol.*, vol. 95, no. 2, pp. 293–303, Feb. 2014.
[281] K. Temmerman *et al.*, 'A PEF/Y Substrate Recognition and Signature Motif Plays a Critical Role in DAPK-Related Kinase Activity', *Chem. Biol.*, vol. 21, no. 2, pp. 264–273, Feb. 2014.
[282] N. Sato *et al.*, 'Physical and functional interactions between STAT3 and ZIP kinase', *Int. Immunol.*, vol. 17, no. 12, pp. 1543–1552, Dec. 2005.
[283] B. Inbal, G. Shani, O. Cohen, J. L. Kissil, and A. Kimchi, 'Death-associated protein kinase-related protein 1, a novel serine/threonine kinase involved in apoptosis', *Mol. Cell. Biol.*, vol. 20, no. 3, pp. 1044–1054, Feb. 2000.
[284] L. Hagerty *et al.*, 'ROCK1 phosphorylates and activates zipper-interacting protein kinase', *J. Biol. Chem.*, vol. 282, no. 7, pp. 4884–4893, Feb. 2007.
[285] T. H. Lee *et al.*, 'Death Associated Protein Kinase 1 Phosphorylates Pin1 and Inhibits its Prolyl Isomerase Activity and Cellular Function', *Mol. Cell*, vol. 42, no. 2, pp. 147–159, Apr. 2011.
[286] D. Jurkiewicz, K. Michalec, K. Skowronek, and K. A. Nałęcz, 'Tight junction protein ZO-1 controls organic cation/carnitine transporter OCTN2 (SLC22A5) in a protein kinase C-dependent way', *Biochim. Biophys. Acta*, vol. 1864, no. 5, pp. 797–805, May 2017.
[287] R. F. Sommese and S. Sivaramakrishnan, 'Substrate Affinity Differentially Influences Protein Kinase C Regulation and Inhibitor Potency', *J. Biol. Chem.*, vol. 291, no. 42, pp. 21963–21970, Oct. 2016.
[288] A. K. Patel, R. P. Yadav, V. Majava, I. Kursula, and P. Kursula, 'Structure of the dimeric autoinhibited conformation of DAPK2, a pro-apoptotic protein kinase', *J. Mol. Biol.*, vol. 409, no. 3, pp. 369–383, Jun. 2011.
[289] Y. Xu, S. O. Kim, Y. Li, and J. Han, 'Autophagy contributes to caspase-independent macrophage cell death', *J. Biol. Chem.*, vol. 281, no. 28, pp. 19179–19187, Jul. 2006.
[290] N. Jounai *et al.*, 'The Atg5 Atg12 conjugate associates with innate antiviral immune responses', *Proc. Natl. Acad. Sci. U. S. A.*, vol. 104, no. 35, pp. 14050–14055, Aug. 2007.
[291] M. Lukarska *et al.*, 'Structural basis of an essential interaction between influenza polymerase and Pol II CTD', *Nature*, vol. 541, no. 7635, pp. 117–121, 05 2017.
[292] A.-R. N. Zekri *et al.*, 'Methylation of multiple genes in hepatitis C virus associated hepatocellular carcinoma', *J. Adv. Res.*, vol. 5, no. 1, pp. 27–40, Jan. 2014.
[293] A.-R. N Zekri *et al.*, 'Promotor methylation: does it affect response to therapy in chronic hepatitis C (G4) or fibrosis?', *Ann. Hepatol.*, vol. 13, no. 5, pp. 518–524, Oct. 2014.
[294] B. Geering *et al.*, 'Identification of Novel Death-Associated Protein Kinase 2 Interaction Partners by Proteomic Screening Coupled with Bimolecular Fluorescence Complementation', *Mol. Cell. Biol.*, vol. 36, no. 1, pp. 132–143, Jan. 2016.

[295] D. Gozuacik *et al.*, 'DAP-kinase is a mediator of endoplasmic reticulum stress-induced caspase activation and autophagic cell death', *Cell Death Differ.*, vol. 15, no. 12, pp. 1875–1886, Dec. 2008.
[296] R. B. Seth, L. Sun, C.-K. Ea, and Z. J. Chen, 'Identification and Characterization of MAVS, a Mitochondrial Antiviral Signaling Protein that Activates NF-κB and IRF3', *Cell*, vol. 122, no. 5, pp. 669–682, Sep. 2005.
[297] R. Lin, Y. Mamane, and J. Hiscott, 'Structural and Functional Analysis of Interferon Regulatory Factor 3: Localization of the Transactivation and Autoinhibitory Domains', *Mol. Cell. Biol.*, vol. 19, no. 4, pp. 2465–2474, Apr. 1999.

7 Presentations and Publications

7.1 Poster presentations

I. **Annual Meeting of the Society for Virology**
Bochum, Germany (2015)

"The role of DAPK1 in the RIG-I signalling pathway"
J. Wolanski, J. Willemsen, N. Baur, C. Hübner, O. Wicht, M. Binder

II. **Annual Meeting of the German Society for Cell Biology**
Cologne, Germany (2015)

"The role of DAPK1 in the RIG-I signalling pathway"
J. Wolanski, J. Willemsen, N. Baur, C. Hübner, O. Wicht, M. Binder

III. **Annual Meeting of the Society for Virology**
Marburg, Germany (2017)

"DAPK family members are negative regulators of RIG-I signalling"
J. Wolanski, J. Willemsen, M. Binder

7.2 Publications

Willemsen J., Wicht O., **Wolanski J.C**., Baur N., Bastian S., Haas D.A., Matula P., Knapp B., Meyniel-Schicklin L., Wang C., Bartenschlager R., Lohmann V., Rohr K., Erfle H., Kaderali L., Marcotrigiano J., Pichlmair A., Binder M.

"Phosphorylation-Dependent Feedback Inhibition of RIG-I by DAPK1 Identified by Kinome-wide siRNA Screening."

Mol Cell. 2017 Feb 2; 65(3):403-415.e8. doi: 10.1016/j.molcel.2016.12.021.
Epub 2017 Jan 26.

8 Appendix

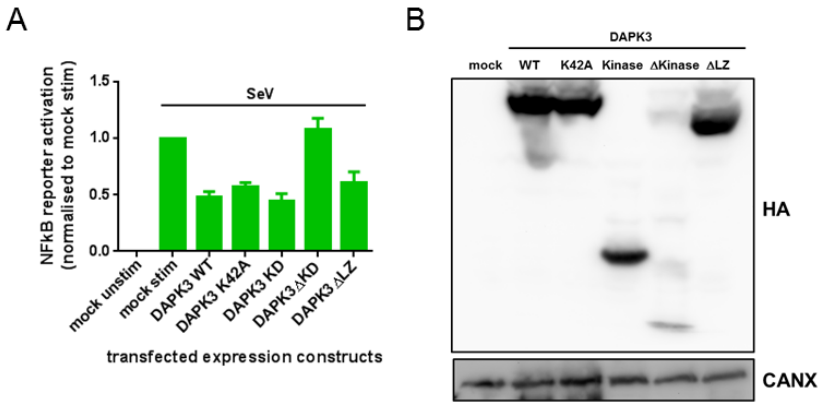

Figure 40 **A minimal DAPK3 construct, DAPK3^{Kinase}, inhibits NFκB activation**

A) IFIT1 reporter assay. DAPK3 constructs were over-expressed in 293T^{RIG-I} cells and cells were stimulated by SeV (MOI 5) infection. Error bars correspond to three independent biological replicates. **B)** Western Blot analysis for assay performed in A). A representative of three independent biological replicates is shown.

Table 25 **Most abundant hits (14) of DAPK2 and DAPK3 interactomes obtained by mass spectrometry.**

Hit No.	Protein name	Gene name	Score	Hit No.	Protein name	Gene name	Score
1	Probable ATP-dependent RNA helicase DDX58 (RIG-I)	DDX58	5001	1	Probable ATP-dependent RNA helicase DDX58 (RIG-I)	DDX58	5514
2	**Death-associated protein kinase 2**	DAPK2	2627	2	**Death-associated protein kinase 3**	DAPK3	2214
3	ATP-dependent RNA helicase DDX3X	DDX3X	2131	3	Keratin, type II cytoskeletal 1	K2C1	1317
4	Calmodulin	CALM	788	4	Keratin, type I cytoskeletal 9	K1C9	1153
5	Heat shock 70 kDa protein 1A	HS71A	639	5	Calmodulin	CALM	899
6	14-3-3 protein epsilon	1433E	569	6	Heat shock protein HSP 90-beta	HS90B	566
7	Serum albumin	ALBU	445	7	Heat shock protein HSP 90-alpha	HS90A	475
8	14-3-3 protein theta	1433T	254	8	Serum albumin	ALBU	440
9	14-3-3 protein zeta/delta	1433Z	246	9	Keratin, type II cytoskeletal 2 epidermal	K22E	408
10	14-3-3 protein eta	1433F	230	10	Keratin, type I cytoskeletal 10	K1C10	376
11	14-3-3 protein gamma	1433G	205	11	Pyruvate carboxylase, mitochondrial	PYC	290
12	14-3-3 protein beta/alpha	1433B	149	12	Heat shock 70 kDa protein 1A	HS71A	276
13	NADH dehydrogenase [ubiquinone] 1 alpha subcomplex subunit 8	NDUA8	94	13	Death-associated protein kinase 2	DAPK2	170
14	Apolipoprotein A-I	APOA1	90	14	Apolipoprotein A-I	APOA1	83

Samples from in vitro kinase assays (figure 26) were analysed by mass spectrometry (LC-MS/MS). Only the 14 most abundant detected proteins are displayed. A representative of two independent experiments is shown. The pulled down protein is indicated in bold, other DAPK family members are highlighted in red.

Table 26 Most abundant hits (14) of DRAK1 interactome obtained by mass spectrometry.

Hit No.	Protein name	Gene name	Score	Hit No.	Protein name	Gene name	Score
1	Probable ATP-dependent RNA helicase DDX58 (RIG-I)	DDX58	5604	8	Heat shock 70 kDa protein 1A	HS71A	466
2	Keratin, type II cytoskeletal 1	K2C1	933	9	Keratin, type II cytoskeletal 2 epidermal	K22E	411
3	Calmodulin	CALM	910	10	Pyruvate carboxylase, mitochondrial	PYC	322
4	**Serine/threonine-protein kinase 17A**	ST17A	619	11	Pyrroline-5-carboxylate reductase 2	P5CR2	110
5	Keratin, type I cytoskeletal 10	K1C10	589	12	Death-associated protein kinase 3	DAPK3	69
6	Keratin, type I cytoskeletal 9	K1C9	529	13	Apolipoprotein A-I	APOA1	67
7	Serum albumin	ALBU	467	14	Death-associated protein kinase 2	DAPK2	49

Samples from in vitro kinase assays (figure 26) were analysed by mass spectrometry (LC-MS/MS). Only the 14 most abundant detected proteins are displayed. A representative of two independent experiments is shown. The pulled down protein is indicated in bold, other DAPK family members are highlighted in red.

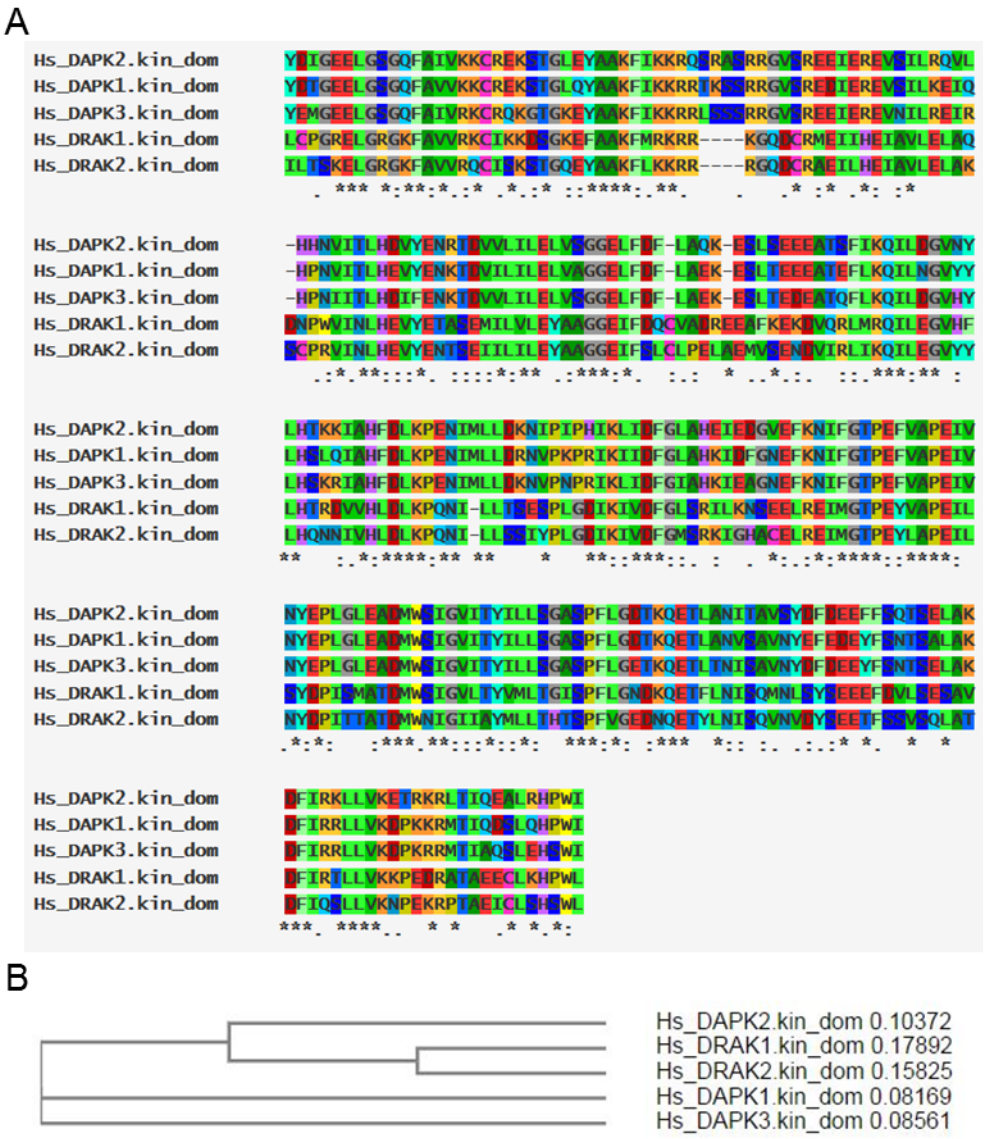

Figure 41 Similarities and differences of DAPKs

A) and B) were generated using the KinBase online tools (http://www.kinase.com/kinbase)

A) Kinase domain alignment of DAPK family members. Amino acids are colour-coded. Kinase domains of DAPK1, DAPK2, and DAPK3 are highly homologous, while DRAK1 and DRAK2 are more distantly related to them, but highly homologous to each other. **B)** Phylogenetic tree corresponding to alignment in A.

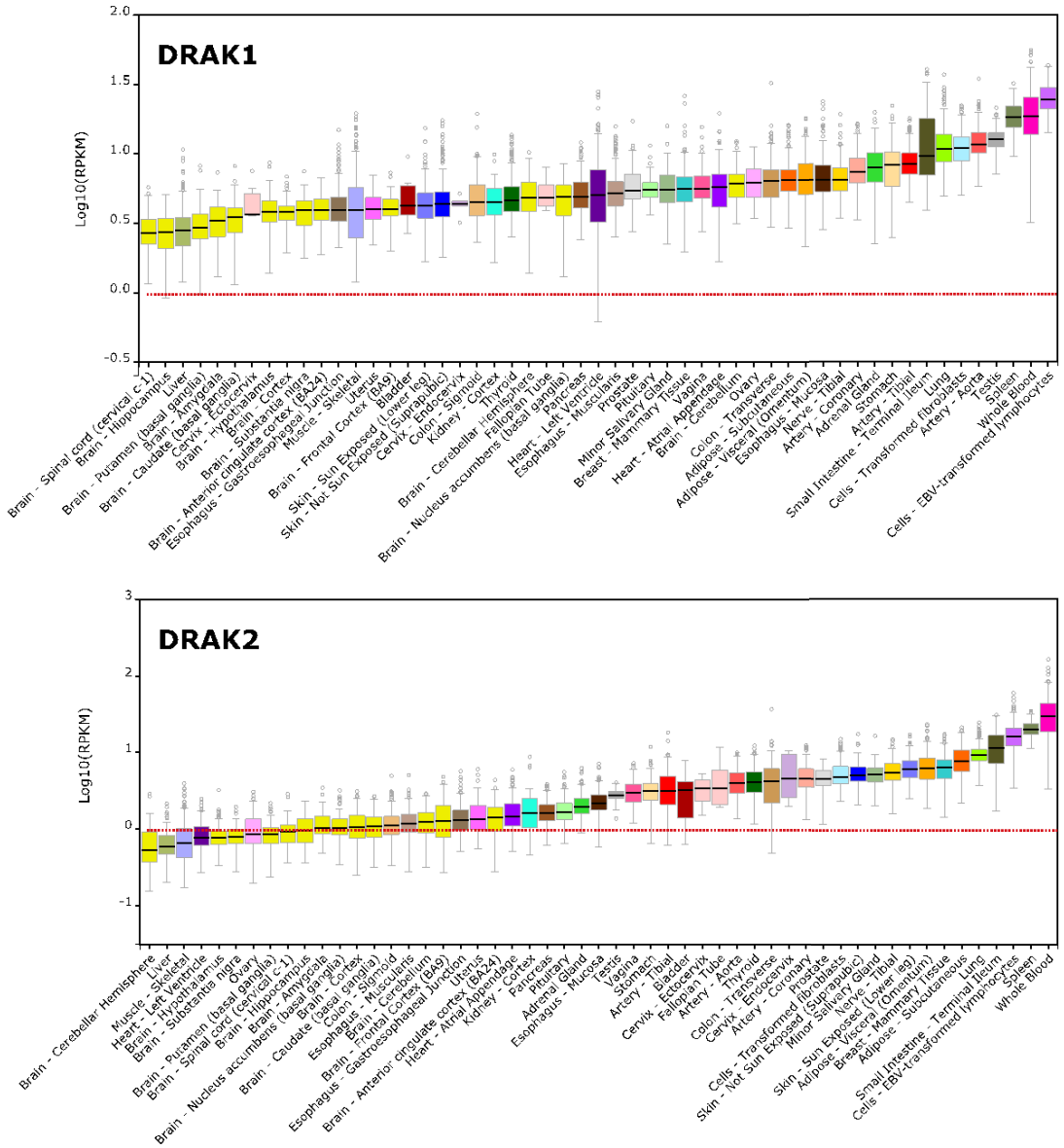

Figure 42 **Tissue-specific expression of DRAK1 and DRAK2**

Overview of DRAK1 and DRAK2 expression in different tissues from patient samples. Gene expression is shown in Reads Per Kilobase of transcript per Million mapped reads (RPKM) and dashed lines indicate a Log10(RPKM) of zero. Displayed data were obtained from the GTEx Portal (gtexportal.org, GTEx Analysis Release V6p, dbGaP Accession phs000424.v6.p1) on 06/13/17.